New Frontiers in X-ray Spectroscopy of FeZSM-5

Grensverleggend onderzoek betreffende Röntgenspectroscopie van FeZSM-5

(met een samenvatting in het Nederlands)

Proefschrift

ter verkrijging van de graad van doctor aan de Universiteit Utrecht
op gezag van de Rector Magnificus, Prof. Dr. W. H. Gispen, ingevolge
het besluit van het College voor Promoties in het openbaar te verdedigen
op maandag 4 april 2005 des middags te 2:30 uur

door

Willem Matthijs Heijboer

geboren op 5 juni 1977, te Tholen

promotoren: Prof. dr. ir. D.C. Koningsberger
Faculteit Scheikunde, Universiteit Utrecht

Prof. dr. ir. B.M. Weckhuysen
Faculteit Scheikunde, Universiteit Utrecht

copromotor: Dr. F.M.F. de Groot
Faculteit Scheikunde, Universiteit Utrecht

Het in dit proefschrift beschreven onderzoek werd mede mogelijk gemaakt met financiële steun van de Nederlandse Organisatie voor Wetenschappelijk Onderzoek (NWO)

Want er is geschreven: Ik zal de wijsheid der wijzen doen vergaan,
en het verstand der verstandigen zal Ik te niet maken.
Waar is de wijze? Waar is de schriftgeleerde? Waar is de onderzoeker dezer eeuw?
Heeft God de wijsheid dezer wereld niet dwaas gemaakt?
Want nademaal, in de wijsheid Gods, de wereld God niet heeft gekend door de wijsheid,
zo heeft het Gode behaagd, door de dwaasheid der prediking, zalig te maken, die geloven;

1 Korinthe 1: 19-21

For it is written, I will destroy the wisdom of the wise,
and will bring to nothing the understanding of the prudent.
Where is the wise? where is the scribe? where is the disputer of this world?
hath not God made foolish the wisdom of this world?
For after that in the wisdom of God the world by wisdom knew not God,
it pleased God by the foolishness of preaching to save them that believe.

1 Corinthians 1: 19-21

ISBN 90336 0585 6

Opmaak en omslag audiovisuele dienst, Faculteit Scheikunde, Universiteit Utrecht

Uitgave in samenwerking met Uitgeverij De Banier BV, Utrecht

Contents

1

General Introduction

Abstract

The concept of heterogeneous catalysis and catalyst characterization is introduced. In addition, the role of *in situ* X-ray absorption and emission spectroscopy in catalyst characterization is discussed and the advantage of novel X-ray spectroscopic techniques is demonstrated.

1.1. Catalysis and Catalyst Characterization

Our modern society would be completely different without catalysis. It is a key concept in both the production of useful chemicals and materials, and in the prevention and destruction of unwanted byproducts and waste.

The start and end of a chemical reaction is governed by thermodynamics. That means that the energy of the reactants and the products is fixed. The way in between, the kinetics, can be steered by a catalyst. Such a substance enhances the rate of reaction by choosing an energy-favored reaction path, but without being affected itself.

Usually, catalysis is divided into three fields: heterogeneous, homogeneous and biocatalysis.[1] The latter group comprises for instance – immobilized – cells and enzymes. In homogeneous catalysis, often, large molecules or aggregates containing transition metal centers are employed, besides the more traditional acid/base catalysts. Solid catalysts, both bulk materials and supported active phases, form the class of heterogeneous catalysts. Either porous or crystalline support materials are used to anchor active particles or clusters consisting of metals, metal oxides, metal sulfides, metal carbides and metal nitrides. The catalysts studied in this research, FeZSM-5, are heterogeneous systems.

In daily life structure and function are strongly correlated. Objects that should move are equipped with wheels and so on. Our – very limited – knowledge of nature teaches us that things are intentional rather than coincidental. Also for a catalyst the same principle holds: you need a certain design to be able to perform a certain action. To understand the relation between the activity and the structure you should know how the active component looks. Using this connection it opens the possibility to tune the properties of a catalyst. From this viewpoint, catalyst characterization is of decisive importance.

Catalyst characterization can be carried out on different levels. By naked eye we can, for example, observe macroscopic properties like the millimeter range-size, shape or color of extrudates. To look inside such a cluster of particles or crystallites, on the mesoscopic scale, one can use tools like a microscope and sorption of probe molecules. That provides for instance a picture of the distribution between 'empty' and 'filled' space within a catalyst, in the range from microns down to nanometers. Since the basic action of a catalyst is determined by its elemental composition and structure, we favor characterization techniques that perceive the atomic level. In this way, we can image molecules, atoms within – molecular – structures, bonding between atoms, and – electronic – phenomena inside the atom. Several characterization techniques will be discussed below. This study concerns techniques within the class of 'X-ray spectroscopy'.

1.2. Probing catalysts on the atomic level using photons

1.2.1. Electromagnetic radiation and catalyst characterisation

Photons with certain energy interfere with matter, being absorbed, scattered or diffracted. The classification of electromagnetic radiation into different regions according to its frequency and wavelength is summarized in Figure 1. The type of interactions with matter depends on the energy of the photons and is indicated in the figure too.

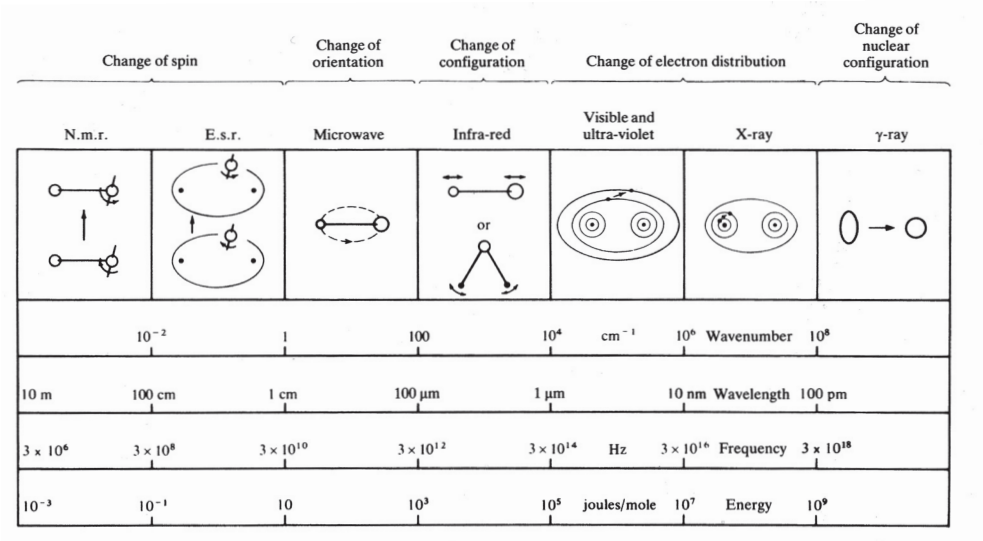

Figure 1: The electromagnetic spectrum divided in the spectral regions, and the corresponding interactions with matter. Figure adapted from reference 2.

Techniques that are frequently used in catalyst characterisation are[3,4] I) Magnetic resonance techniques, using microwave and radio wave radiation. Either the spin state of an electron is probed in the case of Electron Spin Resonance (ESR), or the spin state of a nucleus in the case of Nuclear Magnetic Resonance (NMR). The use is limited to systems that posses at least one unpaired spin (ESR) or to the accessible nuclei (NMR). II) Vibrational spectroscopies like Infrared spectroscopy (IR) and Raman spectroscopy (RS), probe vibrations and as such are sensitive to functional groups of atoms and particular bonds between atoms. III) In the Electronic spectroscopy, UV-VIS, non-core electrons as d-electrons of transition metals and electrons involved in bonding are temporarily elevated to an excited state. The corresponding transitions give information about atoms or groups present in the catalyst. The next class of techniques, IV) X-ray based spectroscopies and X-ray diffraction (XRD), goes further down in the used wavelength and reaches the dimensions of molecules and atoms, thus directly probing the atomic level. We distinguish

X-ray absorption spectroscopy (XAS) and X-ray photoelectron spectroscopy (XPS). XPS provides information on the electronic state of an element and indirectly on the nature of its bonding to other elements. The experimental conditions of this technique limit somehow its applicability, since the detection of electrons requires, in general, vacuum conditions. XAS is discussed in detail below. Finally, we consider in this brief overview of techniques V) Mössbauer spectroscopy (MS). Although, Mössbauer has its potential as an atomic probe for iron-containing catalysts, there are some drawbacks. The technique is only sensitive to the ^{57}Fe isotope (natural abundance ~ 2 %) so that catalysts with a low loading of iron need to be enriched with the appropriate isotope. For highly dispersed particles the spectra become more informative at cryogenic temperatures, due to an increase of the detectable fraction and a split up of spectral features. Monitoring catalytic phenomena by Mössbauer measurements of catalysts under realistic reaction conditions, that is *in situ*, is complicated because most information obtainable at low temperatures is lost. In addition, the relatively long acquisition time of a spectrum (up to hours) makes time-resolved studies difficult.

1.2.2. X-ray spectroscopy in absorption and emission mode

X-ray spectroscopy makes use of photons that are absorbed at energies above the binding energy of core levels through the photoelectric effect.[5] In this way the technique probes the local electronic, structural and magnetic properties of matter. Information can be obtained on the nature of the absorber element (element specific), its chemical and oxidation state, local geometry and the number, type and distance of neighbors. Important characteristics of the technique are that it applies to any element (other than H and He) and works at low concentrations. In most cases, it has minimal sample requirements for measurements, and is suitable for investigations at elevated temperatures and in the presence of gasses. In contrast to XRD the technique does not require long-range order and hence amorphous samples and solutions can be measured too. The acquisition time of a spectrum depending on the measurement configuration and sample concentration is usually in the order of minutes. The difficulty in discrimination of contributions that originate from the same element, but which is present in different situations, is a major concern. For this purpose site selective X-ray absorption techniques are under development. In the following paragraph, we discuss the principles of X-ray spectroscopy and the power for catalyst characterization of X-ray absorption, X-ray emission and a combination of both.

1.2.3. Basics of X-ray spectroscopy

The absorption of X-ray light (XAS) by matter follows the general description for spectroscopic phenomena, that is Lambert-Beer's Law:

$$I = I_0 e^{-\mu \cdot x} \qquad (1)$$

where I_0 is the intensity of the incident beam, $\mu(E)$ the X-ray absorption coefficient,

x the sample thickness and I the intensity of the transmitted beam. The absorption coefficient is strongly related to the X-ray energy E, the atomic number Z, the density ρ and the atomic mass A in the following way:

$$\mu \sim \rho \cdot Z^4 / A \cdot E^3 \qquad (2)$$

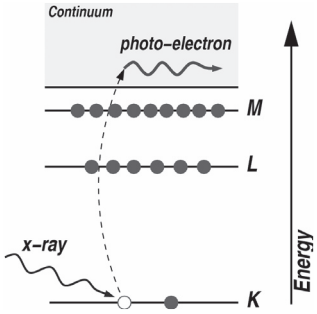

Figure 2: X-ray absorption: creation of photo-electron and core hole.

When the incident X-ray has an energy E equal to that of the binding energy of a core level electron E_0, the core electron is ejected to an empty state above the Fermi level, the continuum, see Figure 2. At this particular energy a sharp rise in the absorption spectrum can be observed, that is called the absorption edge. The energy position is dependent on the element (atomic number) and its shell (atomic orbital). The values are tabulated. The ejected core electron is transformed into a photoelectron that, using the excess of energy $E - E_0$ as kinetic energy, will scatter as a wave with the neighboring atoms (resulting in a fine structure around the atomic absorption in the extended part of the absorption spectrum, see below).

The formal description that forms the basis of X-ray absorption is given by the Fermi Golden Rule that states the transition probability W between a system in its initial state Φ_i and final state Φ_f is given by:

$$W_{fi} \propto \sum_q \left| \left\langle \Phi_f \left| \hat{e}_q \cdot r \right| \Phi_i \right\rangle \right|^2 \delta_{E_f - E_i - \hbar\omega} \qquad (3)$$

The initial and final state wave functions are built from an electron part and a photon part. The photon part of the wave function takes care of the annihilation of a photon in the X-ray absorption process. The delta function takes care of the energy conservation. A transition takes place if the energy of the final state equals the energy of the initial state plus the X-ray energy. The squared matrix element gives the transition rate.

According to formula 1 and 2 the penetration depth of X-rays is determined by their energy and the medium.[6] In Figure 3 the dependence of i) the attenuation in FeZSM-5 (ρ = 0.5 g/cm^3, Si/Al = 17 and Fe/Al = 1) and ii) the transmission through 1 cm of air is given as a function of the photon energy. The attenuation length is defined as the depth into the material measured along the surface normal where the intensity of X-rays falls to 1/e of its value at the surface. The penetration of X-rays in the catalyst material, reported on the left axis, steadily increases with the photon energy. The trend is hampered at certain energy positions that correspond to the absorption edges of the elements present in FeZSM-5, as indicated in the figure. In this study most investigations concern the state of iron because this is the active component. Thus, the majority of the X-ray absorption experiments were performed on the Fe L and K edge at respectively 707 / 720 and 7112 eV.

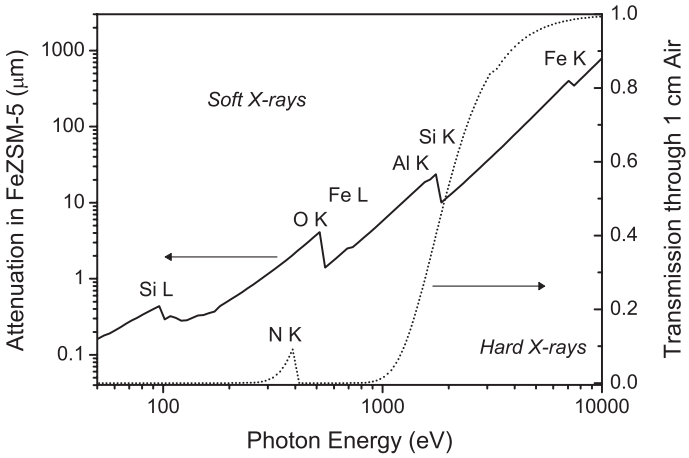

Figure 3: X-ray attenuation length in FeZSM-5 (solid line, left axis) and transmission through 1 cm air at normal pressure and room temperature (dotted line, right axis). X-ray light with energy below 1 keV usually is called 'soft' and above 'hard'.

On the right axis of Figure 3 the transmission of X-rays through 1 cm of air is depicted for a situation at normal pressure and at room temperature. Around the photon energy of 1 keV a sharp rise of the transmission is observed. Before almost no light is able to pass through. Based on this distinct difference in X-ray absorption by air usually a division is made into the so-called 'soft' and 'hard' X-rays, indicating respectively the energy range below 1 keV and above 3 keV. In between the soft and hard domains, X-rays are called 'tender'. The practical implications for doing X-ray absorption in the soft X-ray regime are numerous and will be discussed below.

1.3. Developments in X-ray spectroscopy

1.3.1. Soft X-ray absorption spectroscopy

In the X-ray absorption process at the Fe L edge electrons from the second core level (n = 2) are removed, analogous to Figure 2. In the Fe L edge three regions can be distinguished: the L_1 edge and the combined $L_{2,3}$ spectral shape, which correspond respectively to the creation of a core hole in a 2s and a 2p orbital. In our studies we use the excitation of 2p electrons. According to the dipole selection rules ($\Delta l = \pm 1$) promotion occurs to unoccupied 3d and 4s orbitals. The 2p core hole has a very strong coupling between its S = 1/2 spin- and L = 1 orbital states, which creates a splitting into a J = 3/2 and a J = 1/2 state, respectively the L_3 and the L_2 edge. Figure 4 shows typical $L_{2,3}$ spectra, for two iron oxides, and one can see that the L_2 edge is positioned around 720 eV, while the L_3 edge starts at 707 eV. In addition, one can observe that the L_3 and L_2 edges have significant fine structure. This is caused by the fact that the 2p core hole and valence shell 3d-holes strongly overlap with each other. The contribution of the continuum excitations (to 4s levels and higher) is visible in the spectra as an increase in the baseline.

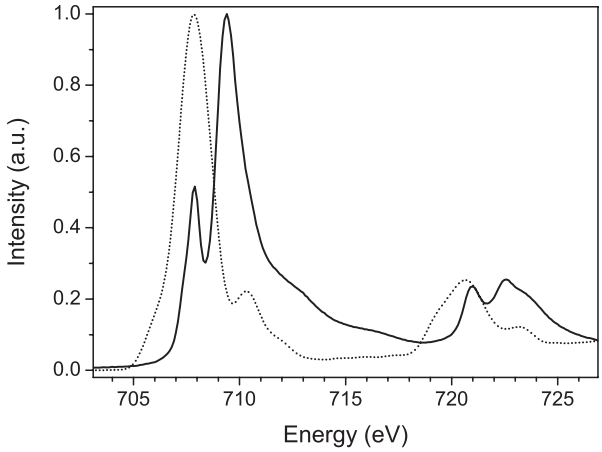

Figure 4: Experimental Fe $L_{2,3}$ edge X-ray absorption spectra of the iron oxides α-Fe_2O_3, hematite (solid, Fe^{III} in octahedral oxygen coordination), and Fe_2SiO_4, fayalite (dot, Fe^{II} in octahedral oxygen coordination).

The overlap of the 2p and 3d wave functions creates the so-called multiplet effect. It is, as yet, not feasible to treat the multiplet effect explicitly within ab-initio programs and a semi-empirical charge transfer multiplet (CTM) has been developed to simulate the $L_{2,3}$ spectral shapes of transition metals.[7,8]

The relaxation of the exited core hole occurs via a re-filling by an electron from a higher level. The energy difference between the two levels can be released in two ways: either via the emission of an X-ray photon (fluorescent decay) or by the promotion of another electron to the continuum (Auger effect). Both processes take place together, but the probability for Auger emission is higher for absorption edges at lower energy (or for low Z). This process is followed by a cascade of decays and induces a flux of electrons with a low kinetic energy and, linked to that, a limited pathway through a solid (according to the so-called universal curve). Only the electrons near to the surface have sufficient energy to escape. The detection of electrons (total electron yield, TEY) is proportional to the X-ray absorption. Because of the small energy the escape depth is ca. 5 nm, which makes soft XAS to be a surface sensitive technique.

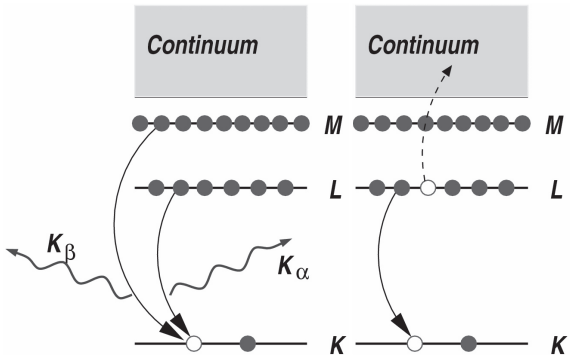

Figure 5: Relaxation of a core hole via fluorescent decay (left) or Auger effect (right).

We already noticed from Figure 3 (right axis) that in the soft X-ray region the transmission of photons from the incident beam through air at 1 bar is less than 1 cm. Therefore, the detection of secondary electrons with an even lower energy usually takes place in ultra high vacuum. This is for instance the case for surface science studies using XPS. However, in catalysis research the study of materials under realistic conditions is highly desirable. Knop-Gericke and coworkers successfully bridged the 'pressure gap' by developing a XAS detector system that is suitable for in situ XAS investigations in the soft energy range 250 eV ≤ hν ≤ 1000 eV.[9-11] Figure 6 displays a schematic drawing of this detector system.

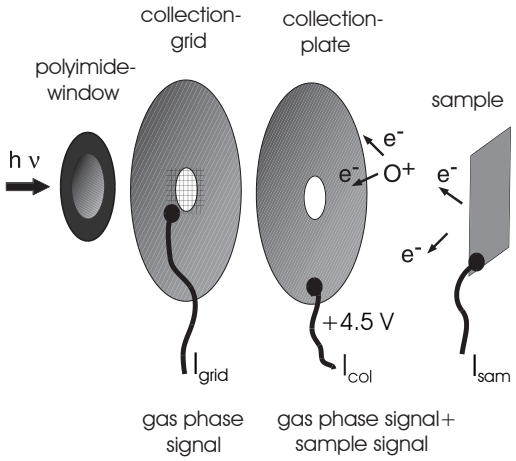

Figure 6: Detection scheme for in situ soft XAS. The synchrotron radiation enters the reaction cell by passing the X-ray window from the left. The detection (TEY) setup consists of two collector plates. Auger and secondary electrons from the sample are multiplied by interaction with the gas phase and detected by the plate on the right. On the second grid, which is shielded from the sample, the gas phase signal is measured. Picture kindly provided by Axel Knop-Gericke.

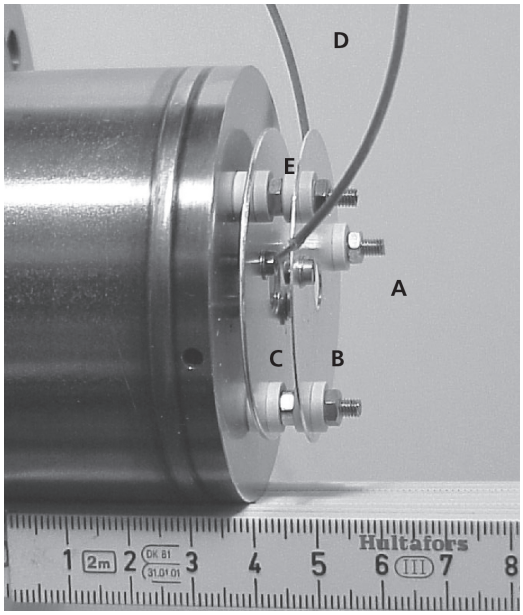

Figure 7: Photograph of the detection system for *in situ* soft XAS. The ruler gives the dimensions in cm. The synchrotron radiation enters the reaction cell from the left at the position indicated by (A). The collection plate right (B) detects the Auger and secondary electrons from the sample and gas phase together. On the second grid (C), only the gas phase signal is measured. (D) shows signal wires and (E) ceramic spacers. Photo by Axel Knop-Gericke.

In Figure 7 a photograph of the detection setup is shown. The ruler gives an impression of the dimensions. The position of the sample, which is mounted on a heating stage, is just in front of the collection plate on the right. So the path length of the soft X-rays in the reaction cell is approximately 2 cm. The maximum pressure in the cell should not exceed 10 mbar to avoid too much gas phase absorption of the emitted electrons. The use of mass flow controllers enables to flush the cell with a defined gas flow. The sample can easily be heated to temperatures of about 500 °C. The – catalytic – results obtained under the conditions during soft XAS experiments turned out to be in good agreement with reaction under ambient conditions in the laboratory.[10] We used this setup for the study of the redox behavior of overexchanged Fe/ZSM-5. The results are presented in chapters 3 and 4. They serve as an example of catalyst characterization using excitation at the L edge to probe the valence and geometry of transition metals in an accurate and fast way. Besides, the K edge of low Z scatters as oxygen is in the same energy region, and therefore, the 1s absorption can also be measured.

1.3.2. X-ray Magnetic Circular Dichroism

The magnetic properties of catalytic materials that contain transition metal ions can be investigated by ESR or Mössbauer spectroscopy. An emerging technique based on X-ray spectroscopy to probe magnetic information of heterogeneous catalysts is X-ray Magnetic Circular Dichroism (X-MCD).[12] In general MCD makes use of the polarization of light. When in optical spectroscopy the orientation of a colored sample is varied with respect to the polarization direction of light one observes a different color since a different part of the light is absorbed by the sample. From this phenomenon the term 'dichroism' (= two-coloredness) is derived, meaning the polarization dependence of the absorption spectrum. 'Normal' synchrotron X-rays have a linear polarization, which implies that the direction of the magnetic vector is perpendicular to the propagation plane of the electromagnetic wave in both dimensions (up and down). As soon as the balance between left and right polarized is changed a net polarization into one direction is induced that causes the (circular) rotating propagation of the wave.[13,14]

In an X-MCD experiment the difference is measured in the absorption of left- and right-circularly polarized X-rays by a magnetized sample. The X-MCD spectrum is given by the (L-polarized minus R-polarized) Fe L edge XAS spectra. Information on the amount and nature of magnetic Fe species can be obtained as well as the oxidation state of iron. By means of charge transfer multiplet simulations the X-MCD spectrum of the various possible iron species can be calculated. The measurement conditions needed for X-MCD (4 K in vacuum) are intrinsically not compatible with in situ catalysis. Nevertheless, because of the important additional information that can be obtained, X-MCD could become an interesting new tool for catalyst characterization. We present a X-MCD study on 0.3 wt % FeZSM-5 zeolites in chapter 5.

1.3.3. Hard X-ray absorption spectroscopy

In the X-ray absorption process at the Fe K edge electrons from the 1s core level are promoted to empty states above the Fermi level, i.e. 4p orbitals. Figure 8 shows a representative Fe K edge XAS spectrum, of a FeZSM-5 sample. One can divide a Fe K edge spectrum into three regions: the pre edge feature, the absorption edge and the extended fine structure.

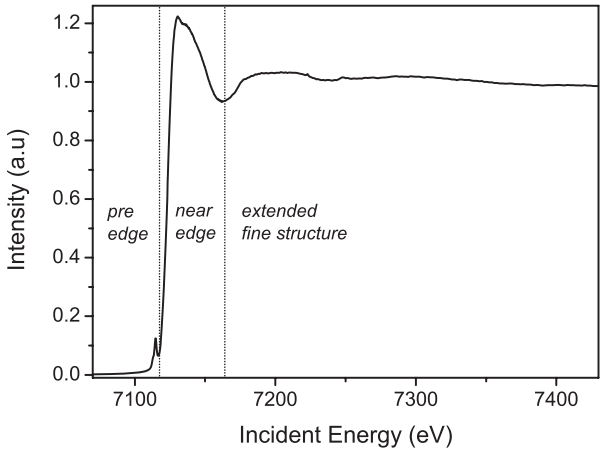

Figure 8: Experimental Fe K edge X-ray absorption spectrum of FeZSM-5 (framework-substituted sample, as synthesized, measured in air and at room temperature). In the spectrum the three distinct regions are indicated: pre-edge feature, near edge structure and extended fine structure.

Several eV before the absorption edge some weak features may be present that originate from dipole forbidden 1s to 3d transitions. The integrated intensity of the pre-edge (peak area) is correlated to the symmetry of the absorbing atom, while its weighted energy position (centroid) depends on the valence. Thus, the detailed analysis of the pre-edge can provide information on the symmetry and valence of 3d metals, as we will show below.

The second region in a XAS spectrum is named the X-ray Absorption Near Edge Structure, XANES. Sometimes in the literature the acronym NEXAFS, Near Edge X-ray Absorption Fine Structure, is used. The near-edge spectral shape reflects the density of states, DOS. This implies that multiple scattering processes of the created photoelectron lasting over long distances (up to 7.5 Å) play an important role. XANES contains mainly information about the electronic properties and the local geometry of the absorbing atom. Nowadays, Density Functional Theory (DFT) programs, for example FEFF8[15] and PARATEC,[16] can calculate the X-ray absorption spectral shape with a close agreement.

The Extended X-ray Absorption Fine Structure, EXAFS, starts at ~ 50 eV above the edge. This region is dominated by single scattering events of the outgoing electron on the neighboring atoms. The X-ray absorption coefficient, $\mu(E)$, is proportional to the probability of photoelectric absorption (via Fermi's Golden Rule). This transition probability is a function of the interference process between absorber- and neighbor- waves and modulates the signal so that a fine structure is observed. The oscillating part of the

absorption coefficient, the EXAFS function χ, is isolated and treated in the data analysis, yielding information about the local atomic structure around the absorber.

Hard X-ray Emission – K Fluorescence

The energetic ground state for Fe before X-ray absorption is given by the electron configuration [Ar]$3d^n$, where n = 6 or 5 for respectively divalent and trivalent Fe atoms. The state after K edge X-ray absorption is an iron atom with a core hole in the 1s orbital. The relaxation of this excited state mainly proceeds via the fluorescent decay of an electron from a 2p or 3p level, respectively resulting in a final state $2p^53d^n$ or $3p^53d^n$. Subsequently, these states undergo a further relaxation by emission of low energy X-ray photons or via Auger decay (this will not be considered here). Figure 9 shows a simplified energy scheme for the relaxation of a 1s core hole via K fluorescence.[17]

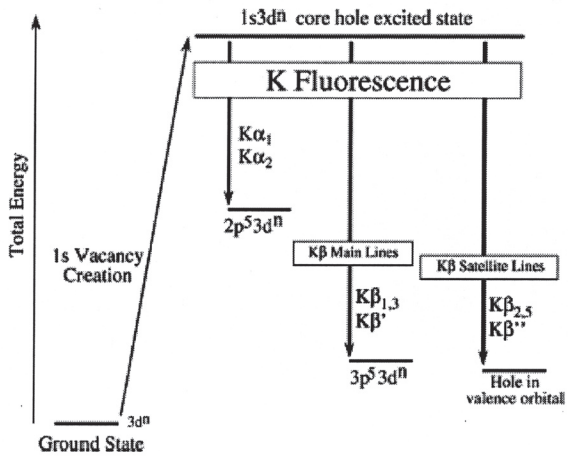

Figure 9: Simplified energy scheme for K fluorescence emission. The different radiative decay channels of the 1s vacancy give rise to the K fluorescence spectrum. The continuum electron that occurs after 1s photo-ionization is neglected in the intermediate and final states. Atomic configurations are used for simplicity. Figure adapted from ref 15.

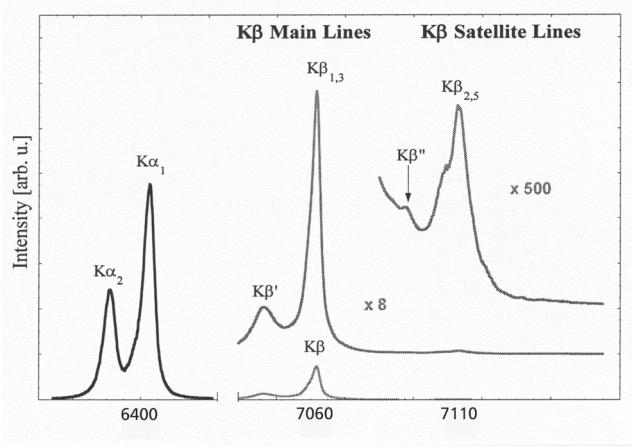

Figure 10: Fe K fluorescence emission spectrum: intensity versus fluorescence photon energy. The Kβ main lines and Kβ satellite lines are enlarged for comparison with the Kα lines, which are most intense. Figure adapted from ref 15.

The decay of electrons from discrete energy levels to fill a core hole gives rise to well defined, intense emission lines. The energy position of these peaks (broadening of the lines is due to the splitting of final states) is as follows, relative intensity in % between brackets: $K\alpha_2$ = 6390.8 eV (50), $K\alpha_1$ = 6403.8 eV (100) and $K\beta_{1,3}$ =7058.0 eV (17). Figure 10 shows a representative X-ray emission spectrum displaying the main peaks, their energy position and relative intensity.

Hard X-ray absorption measurements

The X-ray absorption (coefficient) of a material can be determined experimentally in two ways: i) directly by measuring the amount of initial X-ray light that is transmitted (or absorbed) through the sample and ii) indirectly by detecting the amount of fluorescent X-ray light that is emitted by the sample (Figure 12). The interaction of X-ray photons with a certain element strongly decreases with increasing energy (according to formula 2) and therefore the decline in the X-ray intensity upon transmission trough a zeolite is ascribable to the absorbance by iron (the absorber at that energy), while otherwise mainly low Z scatters are present. So for measuring X-ray absorption in the transmission mode formula 1 can be rewritten as follows:

$$\mu(E) \cdot x = - \ln (I_T / I_0) \qquad (3)$$

where I_0 is the intensity of the incident X-ray beam and I_T is the intensity of the beam after transmitting the sample.

Since the emission of X-ray fluorescence is occurring upon the refilling of the deep core hole, its detection is an indirect way to probe the X-ray absorption according to:

$$I_F \propto \mu_A / (\mu_A + \mu_B) \qquad (4)$$

where I_F is the fluorescence yield signal, μ_A the absorption coefficient of the absorber and μ_B the background absorption.

The measurement of the X-ray absorption is easier in a transmission setup and can be used for sufficiently concentrated samples. Fluorescence detection is particularly suitable for investigations of samples with low concentration of the element of interest. Since the emitted fluorescence – in the particular energy window of the detector – originates from the absorption process a 'pure' signal of the absorber is collected. However, too concentrated samples induce self-absorption or saturation effects and the relation between the measured intensity and the absorption coefficient is no longer linear. In the case of transmission experiments the sample should be diluted with an inert material like boron nitride; for fluorescence detection this can be applied too, but for non-diluted samples one can switch also to the use of transmission XAS.

Experimental setup and practical challenges

The high energy of hard X-ray photons enables passing through a zeolite sample of

almost one-millimeter thickness (Figure 3) and consequently measurements in transmission mode. Besides, the transmission through air lasts for a much longer distance compared to soft X-rays, up to 20 cm, even at normal pressure. Therefore, X-ray absorption measurements under realistic conditions are possible, often denoted with the adjective *in situ*. In our department an *in situ* XAS cell was constructed for measurements of – catalytic – samples at non-ambient conditions as elevated temperatures and reaction-like gas atmospheres. In the past years we encountered a special problem regarding the measurement of samples containing a very low concentration of iron, below 1 wt %. Although fluorescence yield XAS is the appropriate way to measure, the signal was completely disturbed by scattered light. Since the interior of the *in situ* cell initially just exposed the stainless steel where it was made from, already a tiny amount of scattering from the incident beam caused a huge amount of fluorescence. The application of a gold coating of ~ 40 μm thickness solved the problem. In Figure 11 we show detailed photographs of the in situ XAS cell, which is suitable for X-ray absorption measurements both in transmission and in fluorescence detection mode.[18-20]

In Figures 13 and 14 we show photographs of the setups for X-ray absorption measurements using respectively standard transmission/fluorescence detection and a high-resolution detection system. The specific technical details of the latter setup are also described in literature.[21]

Where in the normal detection setup for transmission and fluorescence XAS measurements the distances between the beamline elements and the cell are in the order of centimeters no additional action is required to prevent the total absorption by air of X-ray photons (either incident, transmitted or emitted). Because of the Rowland circle conditions, the distance between the sample and the monochromator crystals (B in Figure 13) is approximately one meter. The detector (C in Figure 13) is positioned just below the sample and a large bag filled with He is placed in between the sample and detector on one side and the crystals on the other side.

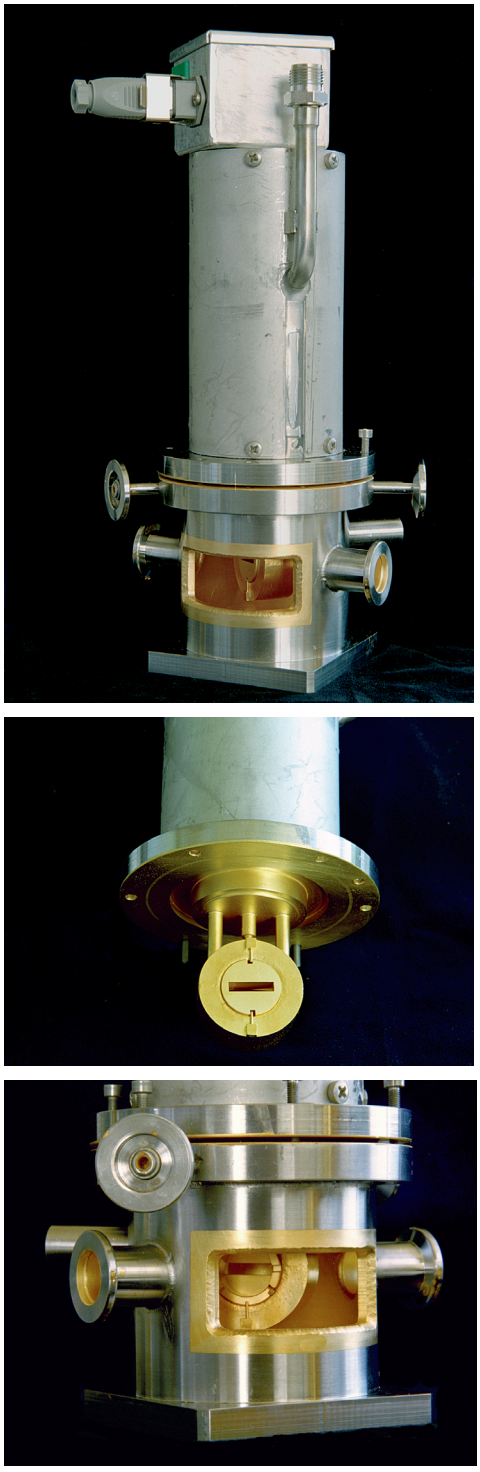

Figure 11: Photographs of a cell used for *in situ* XAS measurements, developed at Utrecht University.

(top) The upper part of the cell accommodates tubes for cooling liquid nitrogen, and connections for a furnace and a thermocouple. On top a reservoir for liquid nitrigen can be placed. The reaction chamber usually is at ambient pressure and can be flushed with gases. The outside of the cell is double-walled and water-cooled. The interior of the reaction chamber including the cylinder and sample holder are coated with a thin layer of gold.

(middle) Close-up of the hollow cylinder used for cooling/heating (-196 < T < 500 °C) of the reaction cell and the sample. In the center of the cylinder the replaceable sample holder is mounted, equipped with a slit (3 x 12 mm) for a pressed sample wafer.

(bottom) View on the reaction chamber. In the transmission mode the X-ray light enters at the left flange, passes the sample in a straight line and leaves the cell through the right flange. In fluorescence detection (actually depicted here) the sample is placed at an angle to the incoming beam. The fluorescent radiation emitted by the sample leaves the cell perpendicular to the direction of the incident beam, through the large window in front. Both the entrance flanges and fluorescence window are sealed by kapton.

Photos by Marjan Versluijs-Helder, Utrecht University.

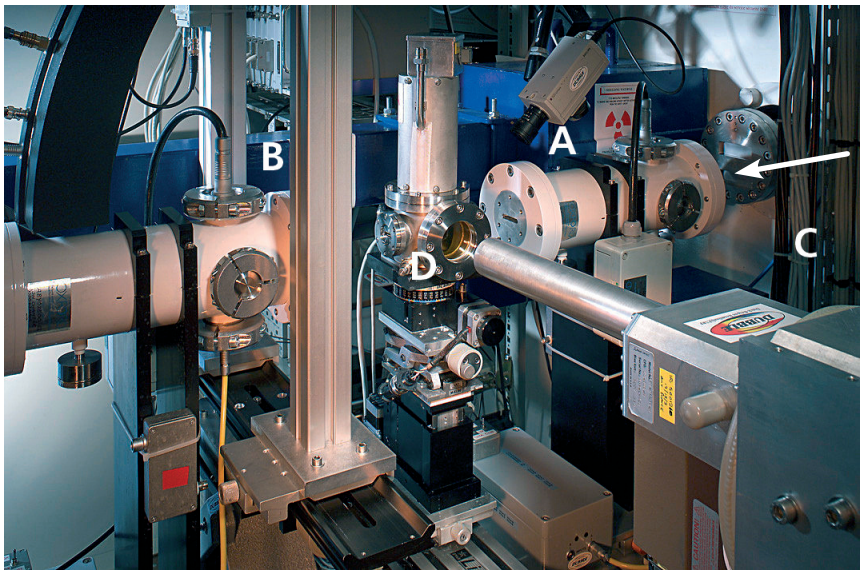

Figure 12: Photograph of a beam line for XAS measurements. In the transmission mode one uses two ionization chambers to measure the initial, I_0, (A) and final intensity, I_T (B). In the fluorescence mode, the intensity I_F is measured by the standard fluorescence detector (C), that is placed perpendicular to the direction of the X-ray beam (←), in front of a large fluorescence window of the *in situ* cell (D). Photo DUBBLE beam line at ESRF by Daniel Michon, ARTECHNIQUE GRENOBLE.

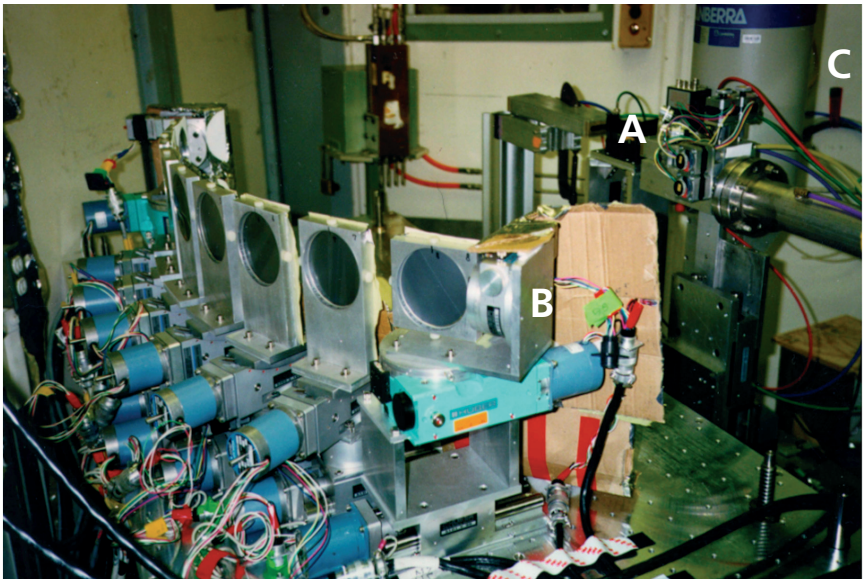

Figure 13: Photograph of a high-resolution fluorescence crystal array spectrometer, using six spherically bent Ge(620) crystals to collect the Fe Kβ region with ~ 1.0 eV resolution. Each individual analyzer crystal is oriented as such that the assembly forms a set of Rowland circles. During measurements a large bag filled with helium is placed between the sample (A), the crystals (B) and the solid-state detector (C). Photo BioCAT beam line at APS by Pieter Glatzel.

Selective methods – combining absorption and emission

The energy of the fluorescent photon is equal to the difference between the energy levels of the core orbital and the higher orbital from which the core hole is filled. In particular the energy of the 3p level depends on the state of the absorbing transition metal. Through that connection the photon energy of 3p to 1s decay (Kβ emission) reflects the valence and spin state of iron, visible as a 'chemical shift' of the maximum of the $K\beta_{1,3}$ peak (Figure 10). In a normal X-ray absorption experiment the measured signal reflects the averaged contribution of all species present in the sample. The absorption coefficient of a certain species within the range of species of the same element can only be determined when one makes use of this chemical sensitivity of fluorescence detection. This is challenging because of the relatively small chemical shift. The energy window for standard (solid-state) fluorescence detection is 50-100 eV and therefore is inadequate for selective XAS. The recent introduction of high-resolution fluorescence spectrometers enabled the selective measurement of very close emission peaks. This class of detectors utilizes a set of crystals that select X-rays with a very narrow energy range, based on Bragg reflection. It is possible to measure Fe fluorescence with ~ 1.0 eV resolution at either the Kα or the Kβ region, depending on the type of crystals used. The potential of such a detection setup is nicely illustrated by the site selective EXAFS study of Prussian Blue, the coloring agent in ink. This compound, with the chemical formula $Fe_4[Fe(CN)_6]_3$, contains high-spin Fe^{3+} and (Fe–N bond) and low-spin Fe^{2+} (Fe–C bond) in the ratio 4:3 and the local coordination of each species could be determined seperately.[22]

In our research we used the mentioned high-resolution fluorescence detection setup (Figure 13) for the acquisition of high quality XANES spectra. In chapter 6 we show that high-resolution spectra offer the opportunity to probe quantitatively the local coordination of iron, and besides its oxidation state. For that purpose the pre-edge spectral shape was analyzed in detail. In particular for iron in a centrosymmetric symmetry the pre-edge is small. However, when the symmetry around the absorbing atom changes from centrosymmetric symmetry (O_h) to non-centrosymmetric symmetry (T_d) a mixing of 4p and 3d orbitals takes place. In this way p-character is added to the d-band and as a consequence the pre-edge intensity is enhanced. We make use of a relationship between the integrated intensity of the pre-edge and the symmetry of iron, which was established from extensive studies on iron minerals. The energy position of the pre-edge centroid on its turn reflects the iron valence.[23] For the determination of these characteristics, that suitably describe the state of iron, a precise measurement of the pre-edge is crucial.

We combine for the study of FeZSM-5 catalysts i) the use of *in situ* investigations, ii) the comparison with well-defined, stable reference materials (minerals) with iii) sophisticated detection setups for X-ray spectroscopy measurements.

1.4. The thesis

This thesis 'New Frontiers in X-ray Spectroscopy of FeZSM-5' intends to contribute to the application of novel X-ray spectroscopic techniques in the study of heterogeneous catalysts as well as to the understanding of the structure and function of FeZSM-5 zeolites. In what follows, we give an outline of the research described in this thesis.

Chapter 2 presents a review on the preparation and characterization of FeZSM-5 catalyst materials. We summarize the recent literature with respect to the different synthesis and activation procedures, and also try to relate the preparation methods to the iron species that are formed as well as to structures, which are proposed to be active in NO_x/N_2O removal and selective oxidation.

In **Chapter 3** '*In situ* soft X-ray absorption of overexchanged Fe/ZSM-5' we demonstrate the use of *in situ* soft X-ray absorption spectroscopy (XAS) in catalyst characterization to study structural and electronic properties. The Fe redox behavior in overexchanged Fe/ZSM-5, prepared by chemical vapor deposition of $FeCl_3$, was followed in time as a function of (heat) treatment and gas atmosphere. Experimental data are supported and explained by charge-transfer multiplet calculations. New information on the geometry and valence of the iron sites is obtained. *In situ* soft XAS proves to be an accurate method to determine the average valence of transition metals during oxidation/reduction cycles.

In **Chapter 4** 'Redox behaviour of overexchanged Fe/ZSM-5 zeolites studied with *in situ* soft X-ray absorption spectroscopy' we utilize the abovementioned technique to compare different Fe/ZSM-5 samples. Thanks to the ability to determine accurately the average valence of iron on a one-minute timescale, we explore how the severity of the calcination treatments of overexchanged Fe/ZSM-5 influences its reduction-oxidation behaviour. The so-called 'mildly calcined' samples show a high flexibility in the Fe valence that depends on the conditions and furthermore have a strong tendency to auto-reduce in He atmosphere.

Chapter 5 deals with the combination of soft X-ray absorption and Magnetic Circular Dichroism (X-MCD). We investigate of framework-substituted FeZSM-5 samples with a low iron loading that could not be measured with the *in situ* soft XAS technique. We do not perform dynamic measurements now, but focus on the additional information that is provided by looking to the magnetic properties of FeZSM-5.

Chapter 6 'Kβ-detected XANES of Framework-Substituted FeZSM-5 Zeolites' introduces a selective X-ray absorption technique. Kβ-detected XANES is distinct from 'normal' X-ray Absorption Near Edge Structure with respect to the way of detection. Just a part of the released fluorescence induced by the absorption process is selected, i.e. on the maximum of the Kβ emission, resulting in a higher sensitivity to the electronic states of Fe. The pre-edge region of the Kβ-detected XANES spectra can be isolated more precisely so that detailed information on the local coordination and oxidation state of an absorbing transition metal can be obtained. A quantitative analysis of Fe K pre-edge spectra is used to study the activation of framework-substituted FeZSM-5 zeolites.

In **Chapter 7** we discuss the possibility of an alternative interpretation of EXAFS data on overexchanged Fe/ZSM-5. We show that this technique is able to detect both Fe–Fe and Fe–Al(Si) scattering. This new analysis procedure has implications for the picture that we have about the molecular structure of the various species present in Fe/ZSM-5. The findings from this chapter are used for the investigation of EXAFS data on framework-subsituted FeZSM-5 in the next **Chapter 8** 'An EXAFS study on the steaming of low loaded FeZSM-5: from framework Fe to oligomeric Fe clusters'. This study demonstrates the profit of selective hard XAS for the measurement of good quality EXAFS data for low-loaded samples. We combine the results of the two previous chapters 6 and 7 to obtain more insight in the processes that take place and the structures that are formed during the several activation treatments of framework-substituted FeZSM-5 zeolites.

Lastly, in the 'Summary' we sum up the main findings of the research reported in the body of this thesis.

References

(1) R. A. van Santen, P. W. N. M. van Leeuwen, J. A. Moulijn, B. A. Averill (Eds.), Catalysis, an Integrated Approach, Second, Revised and Enlarged Edition, Elsevier, Amsterdam, **1999**.

(2) Banwell, C. N. and E. M. McCash, (Eds.), Fundamentals of Molecular Spectroscopy, McGraw-Hill Publishing Company, Maidenhead, Berkshire, England, **1994**, 123-144.

(3) Niemantsverdriet, J. W., Spectroscopy in Catalysis - An Introduction, Wiley-VCH, Weinheim, **1993**.

(4) Weckhuysen, B. M., in B.M. Weckhuysen (Ed.), In-situ Spectroscopy of Catalysts, American Scientific Publishers, Stevenson Ranch, CA, USA, **2004**, 1-11.

(5) Koningsberger, D. C. and Prins, R., (Eds.), X-ray Absorption: Principles, Applications, Techniques of EXAFS, SEXAFS and XANES, John Wiley, New York, **1988**.

(6) For the calculation of X-ray interactions with matter we used the web interface of the Center for X-ray Optics at Lawrence Berkely National Laboratory, see http://www.cxro.lbl.gov.

(7) de Groot, F. M. F., *J. Electr. Spectr. Rel. Phen.*, **1994**, *67,* 529-622.

(8) de Groot, F. M. F., *Coord. Chem. Rev.*, **2005**, *249,* 31-63.

(9) Knop-Gericke, A.; Havecker, M.; Schedel-Niedrig, T. and Schlogl, R., *Top. Catal.*, **2000**, *10,* 187-198.

(10) Knop-Gericke, A.; Havecker, M.; Schedel-Niedrig, T. and Schlogl, R., *Catal. Lett.*, **2000**, *66,* 215-220.

(11) Knop-Gericke, A.; De Groot, F. M. F.; Van Bokhoven, J. A. and Ressler, T., in B.M. Weckhuysen (Ed.), In-situ Spectroscopy of Catalysts, American Scientific Publishers, Stevenson Ranch, CA, USA, **2004**, 107-121.

(12) Funk, T.; Deb, A.; George, S. J.; Wang, H. and Cramer, S. P., *Coord. Chem. Rev.*, **2005**, *249,* 3-30.

(13) Goedkoop, J. B., Ph.D. thesis, Catholic University Nijmegen (1989), 7-36.

(14) Vogel, J., Ph.D. thesis, Catholic University Nijmegen (1994), 3-25.

(15) Rehr, J. J. and Ankudinov, A. L., *Coord. Chem. Rev.*, **2005**, *249,* 131-140.
(16) Taillefumier, M.; Cabaret, D.; Flank, A.-M. and Mauri, F., *Phys. Rev. B*, **2002**, *66,* 195107.
(17) Glatzel, P. and Bergmann, U., *Coord. Chem. Rev.*, **2005**, *249,* 65-95.
(18) Kampers, F. W. H.; Maas, T. M. J.; Vangrondelle, J.; Brinkgreve, P. and Koningsberger, D. C., *Rev. Sci. Instr.*, **1989**, *60,* 2635-2638.
(19) Vaarkamp, M.; Mojet, B. L.; Kappers, M. J.; Miller, J. T. and Koningsberger, D. C., *J. Phys. Chem.*, **1995**, *99,* 16067-16075.
(20) Van Bokhoven, J. A.; Ressler, T.; De Groot, F. M. F. and Knop-Gericke, A., in B.M. Weckhuysen (Ed.), In-situ Spectroscopy of Catalysts, American Scientific Publishers, Stevenson Ranch, CA, USA, **2004**, 123-144.
(21) Bergmann, U. and Cramer, S. P., *SPIE Proc.*, **1998**, *3448,* 198-209.
(22) Glatzel, P.; Jacquamet, L.; Bergmann, U.; de Groot, F. M. F. and Cramer, S. P., *Inorg. Chem.*, **2002**, *41,* 3121-3127.
(23) Wilke, M.; Farges, F.; Petit, P. E.; Brown, G. E. and Martin, F., *Am. Miner.*, **2001**, *86,* 714-730.

2

Preparation and characterization of FeZSM-5

Abstract

In this chapter a review is presented on the preparation and characterization of FeZSM-5 catalyst materials. The recent literature is summarized with respect to the synthesis and activation procedures applied. An attempt is also made to relate the preparation methods to the iron species formed as well as to the structures proposed to be active in NO_x/N_2O removal and selective oxidation. We restricted this survey to the open literature till the end of 2004.

2.1. Introduction

Zeolites are crystalline microporous solids based on a network of silicon, oxygen and aluminum atoms.[1] Applications of zeolites include ion exchange from waste water streams and the selective sorption of small molecules out of gas flows.[2] The framework of zeolites consists of SiO_4 tetrahedrons that are interconnected via oxygen bridges and together form a more-dimensional structure. The way the building blocks are linked to each other determines the ordered structure that is formed. Since there are many possibilities, various zeolite structures exist – featured by a unique three-letter code.[3] The differences between the types concern the size and shape of the channels and cavities. A common way to indicate the dimension of a pore is the number of oxygen (or silicon) atoms that are part of it. Figure 1 depicts the crystalline framework of the zeolite type MFI (or ZSM-5) along the different orientation axes. Its structure contains two types of 10-membered ring channels, straight and sinusoidal, of 5.5 Å diameter size.

In addition to silicon other positively charged atoms can be build in the zeolite structure. The incorporation of such a 'heteroatom' in the framework (isomorphous substitution) implies the replacement of a Si^{4+} ion by for instance Al^{3+} without affecting the local structure (morphology) of the zeolite.[4] The replacement of Si^{4+} ions by trivalent ions introduces negative charge in the framework. The charge is compensated by the inclusion of non-framework cations like Na^+, which are widely available during the synthesis, in the intra-crystalline volume of the zeolite. Through ion exchange other cations can be associated to the framework, like, NH_4^+ and Ca^{2+}. The MFI-type zeolite that contains Al is most abundant and usually called ZSM-5 (Zeolite Synthesis Mobil Five, after the inventors at that company). The incorporation of aluminum in the zeolite structure is extensively used, also in other zeolite topologies, to introduce Brønsted acidity: in the case of H^+ as a charge-compensating ion a bridging OH-group is formed.

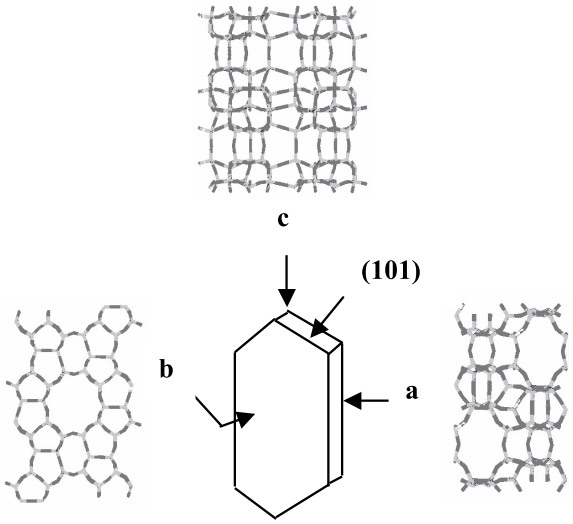

Figure 1: A scheme of the crystal structure of MFI (TPA-synthesis). The crystal faces and dimensions along with the corresponding framework projections are indicated. Dark sticks represent bridging O atoms and light sticks Si atoms in tetrahedral framework positions.
Figure kindly provided by Isabel Díaz.[1]

In the thesis we focus on the X-ray spectroscopic study of Fe-containing MFI-type zeolites. This class of catalysts is used for the breakdown of harmful nitrogen oxides.[5] N_2O and NO_x (*i.e.* NO and NO_2) are formed during combustion processes in the presence of air and in the production of chemicals. A main source of NO_x is exhaust emission from engines; N_2O is abundantly released in the production of nitric acid. N_2O, laughing gas, is a problem because of its behavior as a strong greenhouse gas, approximately 300 times more effective than CO_2. NO_x contributes to environmental pollutions as acid rain and smog. A recently discovered, peculiar ability of FeZSM-5 is the selective oxidation of hydrocarbons using N_2O as an oxygen source instead of O_2.[6] In Table 1 an overview is given of the main reactions that are catalyzed by FeZSM-5 catalysts materials.

The main aspects concerning the preparation and characterization of FeZSM-5 materials are discussed in this chapter. Iron can be introduced into ZSM-5 in two different ways. Firstly, Fe ions can be introduced during the zeolite synthesis, resulting in the formation of what we call 'Fe *in* ZSM-5'. In the synthesis preparation route Fe is isomorphously substituting for some silicon atoms in the zeolite framework. Secondly, an existing ZSM-5 structure can be loaded with Fe by post-synthesis treatments, yielding 'Fe *on* ZSM-5'. We summarized the preparation of FeZSM-5 in Figure 2. For each preparation route we indicated in the scheme the major parameters that influence the characteristics of the FeZSM-5 material. For hydrothermally synthesized FeZSM-5 the Si, Al and Fe content and relative amount depend on the composition of the synthesis gel. The nature and distribution of the Fe species that are formed strongly depend on the activation treatments that are applied after the synthesis step. For post-synthesis prepared FeZSM-5 materials the parent ZSM-5 structure determines the Si/Al ratio. The extent of Fe loading is based on the route that is chosen. Three post-synthesis routes are indicated: aqueous ion exchange (AIE), solid-state ion exchange (SSIE) and chemical vapor deposition (CVD). Again, the activation treatments are supposed to have a large influence on the Fe species finally present.

Table 1: Overview of main reactions catalyzed by FeZSM-5 catalyst materials.

reaction	reactant	product	redox agent	ref
selective catalytic reduction				
	NO	N_2	HC / NH_3 / CO	7-11
	N_2O	N_2	HC / NH_3 / CO	12-14
direct decomposition				
	N_2O	N_2	–	15-20
selective oxidation				
	C_6H_6	C_6H_5OH	N_2O	21-24
	CH_4	CH_3OH	N_2O	25-27
alkane conversion				
	CH_4	C_nH_n	–	28-30

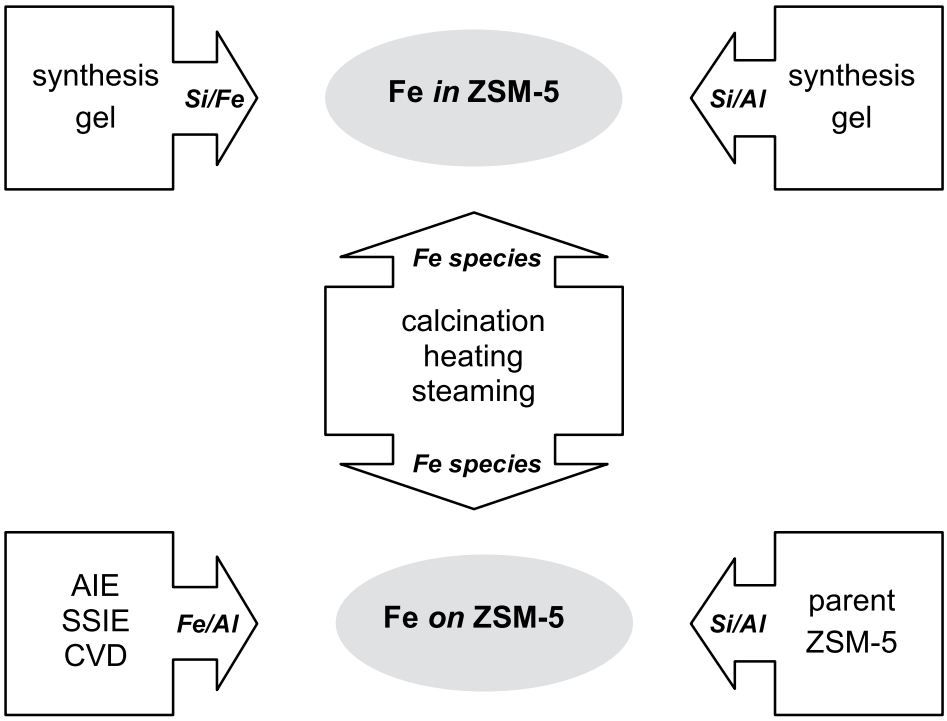

Figure 2: Scheme of the preparation of FeZSM-5 catalyst materials. Hydrothermally synthesized FeZSM-5 is indicated as 'Fe *in* ZSM-5' and post-synthesis prepared FeZSM-5 zeolites as 'Fe *on* ZSM-5'. Block arrows point to the various parameters that influence the final composition of the FeZSM-5 catalyst

To discriminate between the different FeZSM-5 catalyst materials prepared through the various routes we adopt the following nomenclature throughout the thesis:

- FeZSM-5, framework-substituted samples (synthesis)
- Fe-ZSM-5, ion-exchanged samples (post-synthesis)
- Fe/ZSM-5, chemical vapor deposited samples (post-synthesis)

In this chapter we will show that the study of FeZSM-5 is an excellent example to illustrate common difficulties in catalysis research. Firstly, we discuss various aspects of existing synthesis routes. In the last decade many efforts have been made to develop reproducible preparation routes for active FeZSM-5 catalysts. Differences in the preparation affect a catalyst's activity and selectivity. Most probably, these parameters depend on differences in the structure of the active species. Therefore, besides the determination of activity also the structure should be examined. We demonstrate in the last part of the chapter that the result of catalyst characterization may also depend on the sensitivity of the technique used.

2.2. Preparation methods

2.2.1. Hydrothermal synthesis

The use of the hydrothermal synthesis method aims at the inclusion of iron at zeolite framework positions during the synthesis step. In this method a gel, prepared by adding a mixture of silica source, organic template and sodium hydroxide to an aqueous solution with iron and aluminum, is heated in an autoclave for several days yielding a crystalline zeolite material. Ratnasamy and Kumar reviewed in 1991 the subject of framework incorporation of iron in zeolites during synthesis.[31] They also described some proven recipes for the synthesis of some ferrisilicate analogs of zeolites. The extensive study of FeZSM-5 became a hit in the late nineties and in many cases the experimental procedures refer to this study although variations from it have emerged. In most of the present studies the FeZSM-5 zeolites are prepared by hydrothermal synthesis analogous to the procedure described below.[32] The synthesis mixture (in the case of FeZSM-5 with Si/Al = 36 and Si/Fe = 152) contains tetraethylorthosilicate (TEOS), tetrapropylammonium hydroxide (TPAOH, ~20% in water), iron nitrate nonahydrated ($Fe(NO)_3 \cdot 9H_2O$), aluminum nitrate nonahydrated ($Al(NO)_3 \cdot 9H_2O$), and sodium hydroxide (NaOH) in the following nominal molar ratios: H_2O/Si = 45, TPAOH/Si = 0.1–0.3, NaOH/Si = 0–0.2, Si/Al = 36, and Si/Fe = 152. In a typical synthesis one adds the silica source (TEOS) to the organic template (TPAOH) and sodium hydroxide while stirring. Drops of this solution are added to a mixture of iron and aluminum nitrates dissolved in water. The final solution is transferred to a stainless steel autoclave lined with Teflon and kept in a static air oven at 175 °C for 5 days. The crystalline material is separated by filtration and washed with water until the latter is free of nitrate. In the absence of NaOH in the synthesis gel one may increase the template concentration to reach the optimum pH. In the literature, differences are reported for zeolites prepared under static and rotating conditions during the synthesis.[33]

Table 2 shows selected studies concerning the preparation of FeZSM-5 by the hydrothermal synthesis method. These as-synthesized samples are calcined in air at 550 °C for 10 h to remove the template. In this template removal step (the first calcination) sometimes a lower temperature ramp and an anaerobic gas environment is used to prevent too much heat formation during the combustion of the organic structure-directing agent. The template free samples are converted into the H-form by exchange with an ammonium nitrate solution (NH_4NO_3) and subsequent calcination in air at 550 °C for 5 h. Usually, in a final step the catalysts are due to an activation treatment, for instance steaming at high temperature for several hours (p_{H_2O} = 100 - 500 mbar, T = 550 - 700 °C, t = 3 - 5 h).

2.2.2. Post synthesis

Three different routes can be distinguished for the post-synthesis preparation of FeZSM-5 zeolites: i) aqueous ion exchange (AIE), ii) solid-state ion exchange (SSIE) and iii) chemical vapor deposition (CVD), also called sublimation.

Aqueous ion exchange

The preparation of Fe-ZSM-5 by ion exchange in aqueous solution would have been an attractive route because of its relatively simple experimental conditions provided that the redox chemistry of iron in water would not be so complicated. Feng and Hall initiated a lot of research by their proposal to prepare Fe-ZSM-5 using an iron(II) oxalate solution under exclusion of air.[34,35] Their procedure, however, turned out to be not reproducible, but dependent on the history of the zeolite.

It should be mentioned that the focus of many studies is on the preparation of so-called 'overexchanged' samples, which contains iron, as charge compensating ion, in a Fe/Al ratio above 0.5 (assuming to be a Fe^{2+} ion). For the preparation of samples below this value it still might be possible to employ ion exchange in aqueous media.

Table 3 shows selected studies concerning the preparation of Fe-ZSM-5 by aqueous ion exchange. The iron source varies from $FeCl_3$ and $FeNO_3$ for Fe^{III} to $FeSO_4$, $FeCl_2$ and FeC_2O_4 for Fe^{II} salts. The starting material for the ion exchange is a Na^+ or NH_4^+ form of the zeolite. H/ZSM-5 is rarely used, while the affinity of the cation exchange positions for H^+ is higher and thus leads to a lower exchange degree for iron cations. Furthermore, monovalent cations can be exchanged more easily into a zeolite than di- or trivalent cations because the positive charge of multivalent cations has to be balanced by spatially separated negative charges of the zeolite matrix. Therefore formation of oxo-ions or hydroxo-ions as $Fe(OH)^+$ is favoured. The exchange degree is in this way also determined by the pH of the solution where at low pH (complexes of) Fe ions have to compete with protons. As soon as the pH becomes above neutrality the formation of hydroxylated Fe-species plays a role and precipitation of $Fe(OH)_2$, FeO(OH) and $Fe(OH)_3$ may occur. A difficulty is that $Fe(OH)^+$ can exist only in a narrow pH region and only in equilibrium with Fe^{2+} and/or $Fe(OH)_2$. Another problem is the control of the pH and as such the presence of $Fe(OH)^+$ species in the zeolite channel.

In general, it is stated that exchange from solutions containing Fe^{2+} is more efficient than from Fe^{3+}. A possibility to stabilize Fe^{II} is to start from iron(II) salts under oxygen free conditions like an inert nitrogen atmosphere, or to use of methanol as a solvent instead of water. The addition of reducing agents was reported to be not successful, at least in the case of using oxalate since that was blocking the zeolite pore.[36]

Solid-state ion exchange

Preparation of Fe-ZSM-5 by solid-state ion exchange involves the heating of a mixture of the zeolite and an appropriate amount of the iron precursor. Table 4 shows selected studies concerning the preparation of Fe-ZSM-5 by solid-state ion exchange. Mostly, the parent zeolite is in the acidic form. As a precursor are used: $FeCl_3$, $FeCl_2$ ($\cdot 4H_2O$), $FeSO_4 \cdot 7H_2O$ and Fe_2O_3. The ion exchange reaction with $FeCl_3$ takes place at 310 °C, i.e. the sublimation temperature of this iron salt. For the other precursors the ion exchange temperature is 550 °C. The gas atmosphere is varying between the different studies. In some cases exposure to air and moisture is prevented, where others perform the reaction in air. However, for Fe/Al ratios > 0.2 the formation of iron oxide phases, Fe_{Ox} and/or Fe_2O_3, seems unavoidable.

Usually the catalyst is washed and calcined before the use in the catalytic reaction.

A recent development in solid-state ion exchange of ZSM-5 is, besides the introduction of Fe, the anchoring of Al species onto an existing zeolite. The post-synthesis introduction of Al can either be done prior to or simultaneously with the Fe exchange. The aluminum sources used are respectively trimethylaluminum, Me_3Al,[23] and aluminum chloride, $AlCl_3$.[37] In both cases, the additional loading of Al influences positively the activity for N_2O decomposition.

Chemical vapor deposition

The chemical vapor deposition method makes use of the sublimation of a $FeCl_3$ precursor into the zeolite pores, followed by a thermal treatment required to obtain the active catalyst.*[38] Sachtler and coworkers[39] developed this method to be able to prepare reproducible 'overexchanged' FeZSM-5. Attempts to achieve overexchange by other post-synthesis methods mostly resulted in the formation of iron oxide phases on the outside of the zeolite crystals. The stabilization of the excess of iron on the cation exchange positions becomes possible when the iron is present in a (monovalent) complex.

For the CVD-preparation of FeZSM-5 the starting material is the acidic form of ZSM-5, H/ZSM-5, which in general is prepared from a Na/ZSM-5 *via* aqueous ion exchange of a dilute ammonia solution (NH_4NO_3) and calcination in O_2 flow. Reactors with a special design are used that allow a separate loading of the calcined H/ZSM-5 and the $FeCl_3$ precursor, for instance an U-shaped reactor with a porous frit in each of the legs. The loading of the anhydrous $FeCl_3$ in the reactor takes place in a glove bag under N_2. The sublimation of $FeCl_3$ is performed in Ar at 320 °C. A NaOH solution can be used to absorb HCl from the outlet gas to determine the degree of iron exchange. After a certain time, the color of the zeolite bed becomes uniformly yellow and the sample is removed and washed with (doubly deionized) H_2O. After drying in air, the catalyst is calcined for 2 h in flowing O_2 at 600 °C.

In Table 5 an overview is given of selected studies concerning the preparation of Fe/ZSM-5 by chemical vapor deposition of $FeCl_3$. The temperature used for the sublimation reaction is in all studies close to the vaporization temperature, 310 °C. At this temperature $FeCl_3$ is present in the gas phase as a dimer. In one study also a sublimation temperature of 700 °C is used since the precursor is then present as a monomer.[40] In all cases, the carrier of the vaporized iron chloride is an inert gas: Ar, He or N_2. The usual Si/Al ratio of the parent ZSM-5 is in the range from 10 to 20. The preparation of 'overexchanged' Fe/ZSM-5 by definition yields a Fe/Al > 0.5 and in most cases this ratio is close to unity, which – depending on the Si/Al ratio – corresponds to an iron loading of 3 to 5 wt %.

Washing with deionized water is an important step in the preparation. The iron complex is then converted from a chlorine iron complex to an oxo- or hydroxo complex.

* A real CVD process does not require an additional (thermal) step to obtain the active catalyst material. According reference 38 the preparation of Fe/ZSM-5 via sublimation should be denoted as gas phase impregnation - decomposition, GPI-D.

Although this part of the preparation procedure is often not well described, it turned out that better washing resulted in less aggregation of iron during the next calcination step.[9,41] No washing causes the formation of Fe_2O_3 at the exterior of the zeolite crystals. Residues of chlorine, which is more volatile, are supposed to enhance the mobility of the formed iron species in the zeolite channel and hence the agglomeration into large iron oxide particles at the external surface.

Sometimes the washing step is omitted and next to the sublimation procedure a heating treatment is carried out to convert the chlorine iron species in oxo iron species. Usually the best results in terms of activity and stability are obtained when a washing step is applied, followed by calcination or another heating treatment.

2.2.3. Activation

We define activation treatment, as the treatment that is applied to an existing zeolite accessible by molecules/reactants, in other words it does not anymore contain a template in its pore system. We describe generally the treatments i) calcination, ii) steaming, and iii) heating in vacuo or in helium.

Calcination

Calcination means heating in a flow of oxygen or air. This treatment is often performed as a stabilization step in catalyst preparation before reaction. Water and hydroxyl groups are modified into sites with an oxo-character. Sometimes, calcination is applied to convert other groups. For instance, in solid-state ion exchanged Fe-ZSM5 samples iron chloride species are transformed into iron oxo sites. We like to distinguish calcination from the elimination of a synthesis template from a zeolite pore system, which we specify as template removal.

Normally, the calcination temperature is equal to or higher than the reaction temperature. From Tables 1 to 4 we can deduce that the usually applied calcination temperature ranges from 500 to 600 °C. In all cases, the gas environment contains O_2, either present in a pure flow, as diluted with helium or N_2, or as part of a stream of air. The heating rate varies between the different studies, from very low, 0.5 °C/min, to high, 10 °C/min. For post-synthesis prepared FeZSM-5 zeolites, the combination of the parameters used in the treatment has a significant influence on the nature of the resulting species.[9,10,41,42] In general, the utilization of milder conditions prevents the formation of agglomerates. A high oxygen concentration, a high heating rate, high temperature and a long duration of the treatment favor the formation of ultimately stable iron oxide phases. A crucial aspect is the removal of adsorbed water from the zeolite channels, which is a slow process but important in view of the tendency of isolated sites to form clustered iron species.[42] Also for hydrothermally synthesized FeZSM-5 calcination may have an impact on the structure of the framework. Especially in the case of zeolites in their H-form water may promote the formation of extraframework species, both from Fe and Al lattice atoms.[43] It is known that calcination in an ammonia stream limits the formation of extraframework Al species.[44]

Steam treatment

The hydrolysis of oxo-bonds by water is a well-known process, and even not limited to inorganic chemistry. In zeolite chemistry the high temperature treatment of molecular sieves with water containing streams is often indicated as steaming. Steam treatments are in particular used for the activation of framework-substituted FeZSM-5 samples. The incorporation of elements that have a deviant atomic radius or charge induces a local stress on the zeolite framework. The weakened bonds are liable to an attack and are more easily broken so that the heteroatom might migrate to extraframework positions. The extraframework iron species are better accessible, have a higher flexibility in coordination by oxygen and thus are supposed to be more active in oxygen transfer reactions. As such the results of a steam treatment are welcome, however, the process is difficult to control and hence in the end one may obtain extensive clustering of iron. Therefore, the anchoring of extracted species is important and the presence of Al sites may play here a decisive role.[23,45,46]

The conditions applied during steam treatment are summarized in Table 2 for framework-substituted FeZSM-5. Usually temperatures around 600 °C are employed and the water partial pressure is in the range from 200 to 500 mbar. The duration of the treatment differ strongly, from 3 to 5 h. Summarizing the influences of the various parameters, one may state that in general the severity of the steam treatment increases with a higher temperature and a higher water concentration, the presence of O_2 in the stream and with a decreasing flow rate.

For post-synthesis prepared FeZSM-5 samples also a beneficial effect of steaming is reported in several studies.[18,47] This increased activity is not necessarily related to the formation of more active species, but rather can be originating from the formation of mesoporosity.[48-50] Certainly for samples with a high iron concentration the blocking of pores is a limiting factor as proven by diffusion studies[51] and this restraint may be cancelled partially by steaming.

Heat treatment

Thermal activation in an inert medium or in vacuum is another route to destabilize the zeolite framework with the intention to make heteroatoms free. A similar effect than in the case of steaming is observed.[15,52-54] The thermal extraction of iron from the zeolite framework requires significantly higher temperatures when compared to other activation treatments, i.e. 1050 °C. Usually the sample is heated in a helium flow.

The absence of water has some advantages. First of all, the mobility of the extracted atoms is much less since hydration makes atoms much more mobile. Hence, for high temperature helium activation the probability for clustering is lower and extraframework species with a lower degree of nuclearity might be formed, in a more homogeneous distribution. One can speculate about the different sensitivity to thermal activation of iron an aluminum atoms and the possible preferential removal of the larger iron atom. Most probably, the iron species formed by this method expose unsaturated oxygen coordination.[55]

TABLE 2: Literature survey of FeZSM-5 catalysts prepared by the hydrothermal synthesis method [a]

Si/Al	Si/Fe	Fe wt %	Synthesis T (°C)	Synthesis t (h)	Template Removal T (°C)	Template Removal ramp (°C/min)	Template Removal t (h)	Template Removal gas	Calcination [b] T (°C)	Calcination ramp (°C/min)	Calcination t (h)	Calcination gas	Treatments T (°C)	Treatments t (h)	Treatments gas (mbar)	R	CT	Main identified species	ref
31	125	0.67	175	120	550		10	air	550		5	air	600	5	300 H_2O	BtoP	EPR	- dispersed EF Fe - Oh Fe clusters not active	32
																N_2O		- S: various EF Fe	56,57
37	360	0.25	190	120	520		2	N_2	520	2	2.5	dry air	600 550	5 4	300 200 H_2O		XAS	- TR + C: distortion zeolite - S: extraction part Td F Fe	58
28.0 19.5 300 14.1 12.5 37.0 28.0 28.0		0.003 0.005 below 0.018 0.020 0.041 0.120 0.200														BtoP	ESR	- C + S: active EF Fe - no clear relation H^+ and activity - H-form induces Fe transfer position, Na-form not	43,59,60
25 42 36		0.1 0.02 0.007	171	48	600		5	air	550		5	N_2	550 1050	3 4	310 H_2O He	N_2O	TPD IR	- $Fe_2 + H^+$: $[Fe_2O_2H^+]$. - HT He: enhanced activity	17,61
		0.55 below 0.51 0.550 0.024	175	120	550	1	8	N_2	550	0	4	O_2 / N_2	700	3	200 O_2 + 100 H_2O	BtoP	IR	- S: EF Fe–Al–O - PSI Al: improved activity	23
		0.007 –.210 below	104	85	120 550	0.5	3 16	air air	550				600	5	300 - 500 H_2O	BtoP	TPR EPR IR	- S: reducible Fe_2O_3 units - main part = Fe_2 complexes	22
54 >500		2.2 2.2			350 550	3 5	2 5	air air								BtoP		- ps Oh Fe_1 active = minor fraction	24
		0.006 0.03 0.05 0.065 0.18 0.53							500				650		500 H_2O	BtoP		- conv. N_2O: sharp increase with conc. Fe up to 0.3 wt% - prod. P through maximum	62,15

[a] A list of abbreviations is given at the end of the chapter, [b] after ion exchange to H-form of template removed sample

TABLE 3: Literature survey of Fe-ZSM-5 catalysts prepared by aqueous ion exchange [a]

ZSM-5	Si/Al	Fe/Al	Fe wt %	Fe source	Conc (M)	T (ºC)	t (h)	pH	Atmos-phere	CT	Calcination T (ºC)	Calcination t (h)	Calcination gas	Main identified species	ref
Na	21.85	0.01 0.02 0.03 0.04		$Fe(NO_3)_3$	0.05	RT	0 1 4 12			EPR				- Fe_2O_3 and 'complex Fe-O-Fe particles (most probably $[HO-Fe^{3+}-O-Fe^{3+}-OH]^{2+}$)	63
NH_4	15	6	16	$Fe(NO_3)_3$ $FeCl_3$		90	8							- some formation of Fe_2O_3	64
Na	14.2 14.6 23.0 14.2 14.6	029 0.11 0.21 0.52 0.50		$FeSO_4 \cdot 7H_2O$ $FeC_2O_4 \cdot 2H_2O$			48	6.8-7.0	N_2	TPR				- using Fe(II)sulfate instead of Fe(II)oxalate: lower Fe/Al ratio, lower Fe loading, but also less formation of Fe_2O_3	39
Na	11.9		2.9	$FeSO_4$ $Fe(NO_3)_3$		50		5.5-7.0	N_2 impr.					- impregnated sample: almost inactive due to Fe_2O_3	65
H	11.7	0.8		$FeSO_4$	0.0015	50	20		N_2		500	12	air		14,66-68
Na	12			FeC_2O_4		RT	24	6.5-7.5	N_2					- not reproducible for different parent ZSM-5	34
Na	12			FeC_2O_4		RT	24	5.5-7.0	N_2					- species depend on history zeolite	35
NH_4	15.7	0.11 0.15 0.33	0.54 0.73 1.86	$Fe(NO_3)_3$		RT RT 80	48	3.0-3.5	air		550 r10	8	air	- nuclearity Fe species is higher in Fe-ZSM-5 than on Fe-BEA and -FER	69
Na	11.9		3.4 1.8 1.0	$FeSO_4 \cdot 7H_2O$	0.0245 0.0129 0.0072	70	12				500	3	air		70
NH_4	12.5	0.0005 0.0015 0.015 0.14	0.002 0.01 0.1 1.0	$Fe_2NH_4(SO_4)_2 \cdot 6H_2O$	0 - - -	RT	0 24 24 24				550 r5	4	air	- IE samples: good initial activity compared to HT-synthesized samples	24
Na and NH_4	33	0.27	0.71 0.75 1.5	$Fe(NO_3)_3$ $Fe(NO_3)_3$ FeC_2O_4		RT RT RT	 24	5-6	Ar N_2 / CH_3OH N_2					- both samples: Fe_4O_4, Fe_{Ox} nanoclusters, no reduction below Fe^{II} - last sample: mostly Fe_2O_3	71

H	15 25		1.2, 2.35, 3.5 0.5, 1.0, 1.5, 2.1	$FeCl_3$	6.25 mg Fe / 1 cc H_2O			impr.	ESR	500			- amount low-coord. Fe^{III} cations below Fe/Al ~ 0.15 - rest aggregates in ESR-invisible species or in Fe_2O_3	72
NH_4	10	0.5	1.4 1.9	$FeCl_2$	0.05	RT	24		better AIE	ESR				- presence Td Fe^{3+} - some aggregation to Fe_2O_3	73-77
Na	26	0.8/1.3 0.4/0.7 0.4/0.7 0.2/0.3 <0.05		FeC_2O_4 $C_{12}H_{14}FeO_{12}$ $FeSO_4$ (in 0.1 M citric acid)	sat. sol. 0.02 0.1	RT	24	5-6 5 7 7	 TPA N_2H_4	 IR				- FeC_2O_4 blocks pores, - W: rest FeC_2O_4 into Fe_2O_3 - mostly H^+ on cation sites - 2nd IE: H^+ removed and prec. neutral [Fe}] in pores - prec. $[Fe(N_2H_4)_2(SO_4)]$	36,41
NH_4	37	0.57	1.4	$Fe(NO_3)_3$	0.0003	RT	15			UV TEM				- majority inactive Fe_2O_3	12
Na	11.9	0.40 0.24 0.15 0.10 0.05		$FeSO_4 \cdot 7H_2O$		50	20		N_2	TPR	500	3	air	- Fe/Al 0.15 more reducible Fe species - low TPR-peak related to N_2O treatment, activity : active site probably Fe_2	78
NH_4	11.3	0.36	2.3	$FeSO_4$		80	24		air	TPR	550	5		- add. impr. with 0.15 wt % Pd: 50% Fe attached to Al sites and 50% forms Fe_2O_3	13,79

[a] A list of abbreviations is given at the end of the chapter.

TABLE 4: Literature survey of Fe-ZSM-5 catalysts prepared by solid state ion exchange [a]

Si/Al [b]	Fe/Al	Fe wt%	Fe source	Preparation T (°C)	ramp (°C/min)	t (h)	gas	W t/nL	Calcination T (°C)	ramp (°C/min)	t (h)	gas	R	CT	Main identified species	ref
25	0.33 0.66 1.00		$FeCl_3$	310										XAS	- Fe_1 associated with F Al	80
25	0.14 0.19 0.37 0.56 0.85 0.96	0.49 0.67 1.26 1.94 2.61 2.86	$FeCl_3$	310	0.2 5	4	He							XAS	- Fe/Al < 0.19: almost all in $[Fe(OH)_2]^+$ form - Fe/Al to 0.56: exchanged for H^+ - higher loading: Fe_{Ox} particles	81 20
20	0.30 0.40 0.55	1.37 1.82 2.50	$FeCl_2$	550	0.2 5	24	Ar	2	550		4	O_2	N_2O NOx red	ESR IR	- dist. Td Fe_1 - overexchanged samples: presence Fe_2- and Fe_N-clusters	82
12.5	0.14	1	Fe_2O_3	550	5	12	O_2						BtoP		- fast deactivation	24
11.7 [c] 11.3 11.4 [d]	0.775 0.757 0.842		$FeCl_2{\cdot}4H_2O$	550	3	6	air		500		1	He	NO/C_3H_8 N_2O/C_3H_8		- starting samples NH_4-form: most active, also on Fe content basis	83
11.4 [d]	0.007 0.125 0.25 0.75		$FeCl_2{\cdot}4H_2O$	550	3	6	air		500		1	He	NO/C_3H_8 N_2O/C_3H_8		- Fe/Al < 0.5: increase activity with Fe loading - Fe/Al = 0.25: some Fe_2O_3 present	84
11.4 [d]	0.25 0.5 1.35 0.25 0.5 1.35	1.84 3.71 10.01 1.84 3.71 10.01	$FeSO_4{\cdot}7H_2O$	400	50	1- 24 1-5	vac air		600 600		1 1	N_2 N_2	N_2O		- Fe/Al > 0.5: traces Fe_2O_3 - vacuum and air preparation: no activity difference, both most active - Fe/Al = 1.35: pore blocking due to precipitation	85
14	1.48	8.7	$FeCl_3{\cdot}6H_2O$	300		1	N_2	no							- no W: excess Fe left in zeolite	9

[a] A list of abbreviations is given at the end of the chapter, [b] parent ZSM-5 in all cases: H-ZSM-5, [c] parent zeolite in Na-form, [d] parent zeolite in NH_4-form

TABLE 5: Literature survey of Fe/ZSM-5* catalysts prepared by sublimation of $FeCl_3$ [a]

Si/Al [b]	Fe/Al	Fe wt %	sublimation T (°C)	t (h)	gas	W t/nL	calcination T (°C)	ramp (°C/min)	t (h)	gas	R	CT	Main identified species	ref
10.7	1		320		Ar		600		2	O_2	NO/i-C_4H_{10}	TPR	- Fe_2 -complexes	39,82
14.2	1												- some Fe_2O_3 on ext. surf.	
23.0	1													
17.2	1.0		330	0.5	He	1	550	5	3	O_2	NO/i-C_4H_{10}	XAS	- W + C: Fe_2 -complexes	7,42,8
17.2	1.0		330	0.5	He	1	200	0.5		He		Möss	- C: determines Fe-clustering into	6,87
							550	0.5	3	He/O_2		TEM	FeOOH and Fe_2O_3 on ext. surf.	
11	0.69	3.9	320	3	He	p	600		5	air	NO/NH_3	TPR	- cations at locations are active	40
	0.51	2.9	700	1	He	p	600		5	air			- amount of different iron oxides	
	0.67	3.8	320	0.5	He	p	600		5	air			depends on treatment and loading	
	0.80	4.5	320	3	He	p	600		5	air				
14	0.92	5.4	300	1	N_2	1	600	5	1	air	NO/i-C_4H_{10}	XAS	- Fe_1 species active = minority	9
14	0.88	5.2	300	1	N_2	1	600	10	1	air		Möss	- significant part present in Fe_{Ox}	
14	0.90	5.3	300	1	N_2	1	600	0.5	1	air		TEM		
14	0.84	5.0	300	1	N_2	10	600	0.5	1	air		TPR		
40	1.13	2.6	300	1	N_2	1	600	5	1	air				
19.4	0.97	3.68	300		N_2	2*2.5	550	2	3	He/O_2	N_2O	XAS	- C: heterogeneous system	10,88
19.4	0.97	3.68	300		N_2	2*2.5	700		3	He/O_2	BtoP	Möss	- HT: neutral Fe_{Ox} react with H^+ to	
19.4	0.97	3.68	300		N_2	2*2.5	700		3	He/O_2/ H_2O	NO/i-C_4H_{10}	TEM UV-Vis NMR	charge compensating Fe sites - S: same as HT but more - treatments cause dealumination	
15	0.8	4.5	320	2	He		600		2	O_2	NO/i-C_4H_{10}	XAS	- ZSM-5-20: Fe_2-complexes	89,90
20	1	3.6	320	2	He	no	600		2	O_2		UV-Vis	- other samples: hematite	
20	1	3.6	320	2	He		600		2	O_2			- W: important, otherwise Fe_2O_3	
20	1	3.6	320	2	He		450		2	He			- C in He instead of O_2: Fe_3O_4-like clusters	
11.75	1.06		320		Ar		600		2	O_2	NO/i-C_4H_{10}	EPR	- dist Td Fe_1: activity assumed	91
													- poisoned by SO_2	
14	1	5.0	320		Ar		600		2	O_2	N_2O/CO	UV-Vis TEM	- majority Fe_N: oligonuclear $Fe_x^{3+}O_y$ clusters	12
11.65	0.9	5.2	320		Ar		500		2	O_2	NO/i-C_4H_{10}	ESR TPR	- 2nd sublimation: H^+ , activity , stability , dist. Td Fe^{3+} , Fe_2O_3 -less dealumination in wet streams	92
	1.2	7.1												

[a] A list of abbreviations is given at the end of the chapter, [b] parent ZSM-5 in all cases: H-ZSM-5

2.3. Characterization studies

The characterization of the molecular structure of the active site in FeZSM-5 catalysts is complicated by the presence of various phases. In the previous paragraph we noticed that different preparation routes might lead to the formation of different species. In addition, the sensitivity to detect a certain species varies between the characterization techniques applied. The identification of the structures requires the accurate determination of key characteristics as the oxidation state and the local coordination. In Table 6 we summarize the different techniques (as briefly discussed in the previous chapter) used for the study of FeZSM-5 together with the information obtained on the valence, symmetry and type of neighbors.

Table 6. Characterization techniques for Fe speciation in FeZSM-5 catalyst materials and the information typically provided.

technique	valence			symmetry	neighbors	quantitative	*in situ*
	0	2	3				
ESR	–	±	+	+	+	+	+
IR	–	±	±	+	±	–	+
RS	–	±	±	+	±	–	+
UV-VIS	–	+	+	+	±	+	+
XRD	–	–	–	–	–	–	+
XPS	+	+	+	–	+	+	–
soft XAS	+	+	+	+	±	±	±
XMCD	+	+	+	+	±	±	–
XANES	+	+	+	+	±	±	+
EXAFS	+	+	+	+	+	±	+
MS	+	+	+	±	–	±	±
VM	+	+	+	±	–	–	–
TPR-TPO	±	±	±	–	–	+	–

From Table 6 we can conclude that no single characterization technique is able to provide a final answer for the structure of the Fe site(s) in FeZSM-5 catalysts. Moreover, one can make a distinction to the strict classification as presented above. Techniques that provide typical features for certain species may not be sensitive at all to other species, for example ESR is informative on the non-integer spin Fe^{III} structures, but tells little about the abundance of Fe^{II}, which is ESR silent. Furthermore, in spectroscopy the relative intensity of certain spectral contributions may depend on transition permission rather than on existence. Therefore, quantification remains difficult. Also the measurement of an average of several contributions may be complicating, which is a particular problem of X-ray absorption techniques.

Main issues in the characterization of FeZSM-5 are reducibility, local Fe environment, nuclearity of the Fe species and the structural changes observed during treatments and reactions. Qualified candidates for their characterization are X-ray based spectroscopic

techniques. Therefore, in line with the scope of this thesis, special attention will be paid to the outcome of FeZSM-5 catalysts characterization using X-ray spectroscopic techniques.

In most of the studies on the preparation of FeZSM-5 (Tables 2 to 5) also an effort is made to identify the species existing within the catalyst. Several publications are entirely devoted to characterization. According to literature, the main identified species present in FeZSM-5 can be classified as follows (models depicted in Figure 3):

- single framework Fe sites, Fe_F (framework)
- isolated, single extraframework Fe sites, Fe_1 (mononuclear)
- oxo-bridged extraframework Fe centers, Fe_2 (binuclear)
- chain-like structures of extraframework Fe, Fe_N (oligomeric)
- aggregates of extraframework Fe inside zeolite crystals, $Fe_{Ox,IN}$
- agglomerated extraframework Fe on the external surface, $Fe_{Ox,OUT}$

In what follows, we will discuss more in detail the different molecular structures.

Framework Fe, Fe_F

FeZSM-5 prepared via the hydrothermal synthesis method should contain exclusively iron in zeolite framework positions, isomorphously substituting for silicon atoms. That implies that single iron atoms are well incorporated in the zeolite structure, are isolated, and in a tetrahedral surrounding of oxygen. The next-nearest neighbor atoms are silicon (or aluminum) atoms. The characterization techniques that display typical spectral features for Fe_F (correctly speaking for Fe^{III} in T_d) and which are most widely used to prove its presence are EPR[93-95], Mössbauer[57,96,97] and XANES.[46,98,99]

Mononuclear Fe, Fe_1

The second type of single, isolated Fe sites can be found in extraframework positions and is called 'mononuclear'. At the cationic positions associated to the zeolite lattice H^+ is replaced by Fe ions and a chemical bond to zeolite oxygen atoms is effectuated. Probably the local surrounding by oxygen for iron in extraframework positions will deviate from a perfect symmetry. The occurrence of Fe_1 sites as Fe^{III} in T_d symmetry (besides in O_h symmetry) complicates the spectroscopic discrimination from Fe_F species. Mössbauer spectroscopy in principle should be able to distinguish a perfect tetraeder (singlet) from one that is slightly distorted (doublet). However, the proximity of other framework iron atoms in case of a higher Fe loading may induce similar spectral features.[33] Also for EPR caution is recommended regarding the exclusive assignment of certain g-values to the presence of one particular species.[100] Even though EXAFS can provide detailed information on the local structure of materials it will be difficult to distinguish thus resembling sites. One can imagine that extraframework Fe_1 sites might be easier to reduce than framework Fe_F.

Binuclear Fe, Fe_2

Sachtler and coworkers proposed a binuclear oxygen bridged complex as the major active ingredient of Fe/ZSM-5 prepared by chemical vapor deposition of $FeCl_3$.[39] A similar structure was reported before for copper containing ZSM-5 and the analogy with biological

structures that also were able to perform oxygen transfer reaction was attractive. Arguments in favor of such iron oxo centers were the Fe/Al ratio of 1, indicating that the positive charge of iron was balanced partially by extraframework oxygen of a complex. In addition it was possible to carry out CO oxidations, in essence to be reduced through loss of oxygen. A fraction up to 20 % was subject to reduction from Fe^{3+} to Fe^{2+} by the thermal release of O_2 upon mere heating in helium (often indicated by autoreduction) to 600 °C.[101]

In the past years numerous articles appeared on the identification of binuclear complexes by spectroscopic techniques and chemical probe reactions.[7-9,36,42,82,86,88,89,102-104] EXAFS studies have had a leading position for the characterization of these complexes. The detection of Fe–Fe scattering, at a similar distance (R ~ 3.0 Å) and with a coordination number close to unity, strongly supported the hypothesis of Fe_2 sites. The structural – and functional – resemblance with the active site of forms of MMO (the enzyme methane monooxygenase) was striking.[15] Also Mössbauer studies supported the existence of binuclear iron complexes.[15,42]

Initially the presence of Fe_2 sites was supposed just for overexchanged Fe/ZSM-5 prepared by the sublimation technique. However, the formation of these complexes is also assumed to occur upon activation treatments of FeZSM-5 prepared by other routes.[17,105,106] In contrast, the assumption that Fe_2 sites are the only or most abundant species present in FeZSM-5 samples is no longer supported in part of the recent literature.[50,93,104,107]

Oligomeric Fe, Fe_N

The formation of multinuclear iron species larger than binuclear ones has also been reported.[42,50,56] EXAFS, Mössbauer and UV-Vis experiments indicate that oligimeric species are formed as chains in the zeolite channels. This iron species is distinguished from binuclear species since the iron atoms are not necessarily close to aluminum sites (Fe/Al > 1) as well as from iron oxide like phases because some reducibility is observed. It is suggested that oligomers may contribute to N_2O decomposition albeit with a low reaction rate, but are not capable to oxidize hydrocarbons or even CO.[53]

Intrazeolitic agglomerated Fe, $Fe_{Ox,IN}$

Within the zeolite structure small agglomerated iron phases can be formed that are less easy to reduce. The size of these Fe_{Ox} particles is up to 2 nm and they cannot be observed by TEM. Their formation most likely is induced by severe activation treatments like calcination or steaming. Steaming creates voids and larger pores that may accommodate such particles. Intrazeolitic Fe_{Ox} is distinct from oligomeric Fe_N with respect to the extent of Fe–Fe coordination, in other words its iron oxide-like nature is more pronounced. The images in Figures 3d and 3e give the impression that the conversion of Fe_N into Fe_{Ox} is feasible.

Zeolite surface Fe crystallites, $Fe_{Ox,OUT}$

Small particles of Fe_3O_4, FeO(OH) and Fe_2O_3, are observed on the external zeolite surface of several FeZSM-5 materials. Provided the particles formed are large enough iron

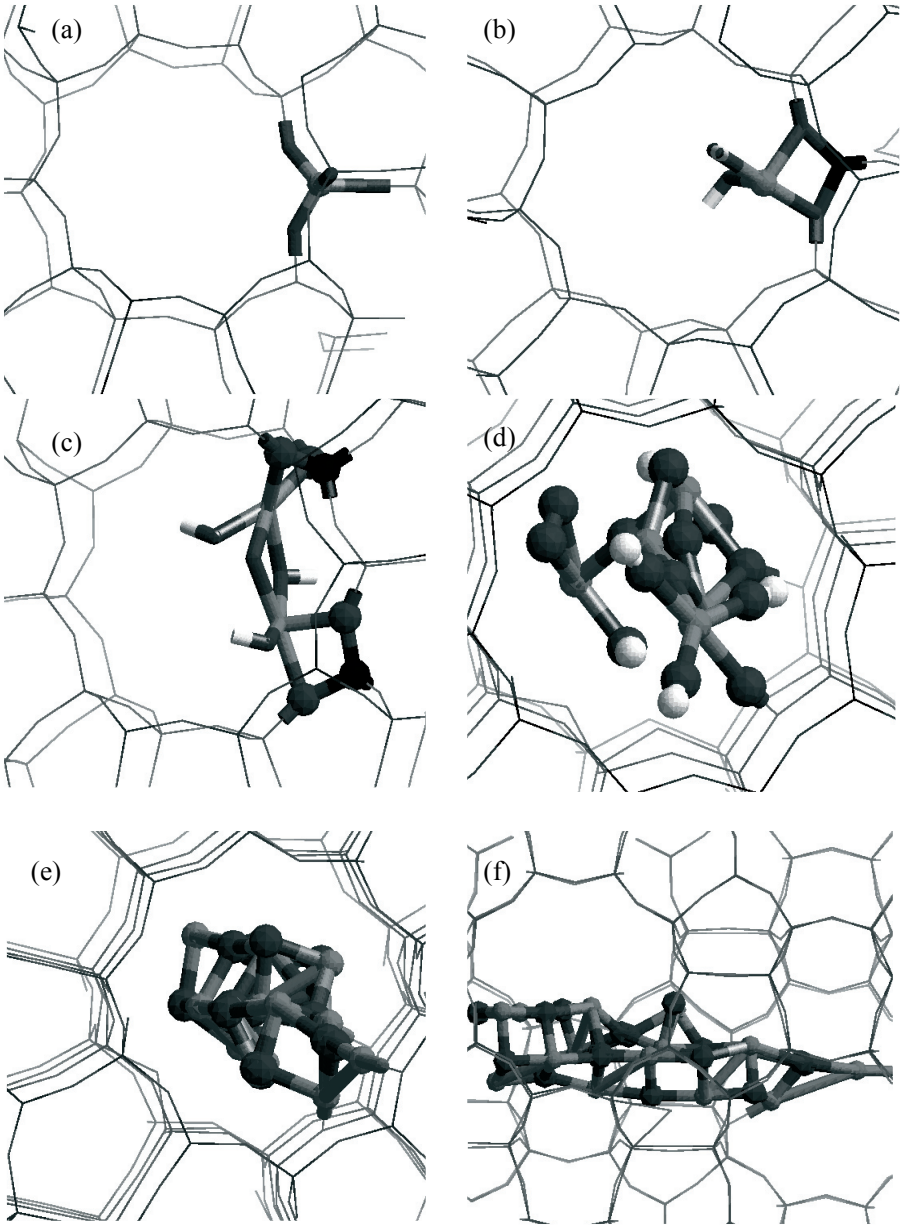

Figure 3: Models of possible molecular structures for sites present in FeZSM-5 catalyst materials, created by Cerius^{2}.[101] The ZSM-5 zeolite framework is represented by thin lines, Fe by gray balls/sticks, Al by black balls, O by dark gray balls/sticks and H by white balls/sticks. (a) framework Fe_F (b) mononuclear Fe_1 (c) binuclear Fe_2 (d) oligomeric Fe_N (e) $Fe_{Ox,IN}$: small iron oxide like agglomerate inside the straight channel of ZSM-5 (f) $Fe_{Ox,IN}$: side view of (e); growth inside the perpendicularly oriented sinusoidal channels is also possible, as well as on the external surface of the zeolite crystal resulting in $Fe_{Ox,OUT}$.

oxide phases can be easily detected by XRD and TEM, in particular when combined with EDX or EELS. Also EXAFS and Mössbauer are able to detect for instance Fe_2O_3 if a significant fraction is present.

Fe_{Ox} originates for instance from that part of the iron precursor that is not well anchored during the preparation stage of post-synthesis FeZSM-5 samples and subsequently is converted upon calcination. Some preparation routes yield more iron oxide like species than others; especially ion exchange from aqueous solutions is a notorious method (Table 3). Also severe conditions applied in activation treatments like calcination and steaming promote the forming of Fe_{Ox}. Besides such phases represent inactive iron they most likely harm the activity by blocking of zeolite pores thus making active sites inaccessible.

2.4. Conclusion

On the basis of a review of the literature concerning the preparation and characterization of FeZSM-5 materials we encountered various difficulties that are universal for catalysis research. In the first place, a large variety exists in the way to prepare an active catalyst material. Each route has its pros and cons. Here, no conclusive answer can be presented about what is the most preferable synthesis procedure for FeZSM-5 zeolites. Nevertheless, we try to generalize some of our observations.

It is evident from the literature survey that it seems impossible at present to prepare a FeZSM-5 sample that contains exclusively one active iron species. On the other hand, the formation of presumed inactive iron oxide-like phases, Fe_{Ox} and Fe_2O_3, should be limited. Their presence not only implies that the available iron is not completely used (although it is cheap), moreover, their attendance hinders the characterization of the active species (being a spectator) and obstructs the catalytic activity (causing blocking and/or side-reactions). Factors that favor the formation of iron oxide are the application of severe treatments (hard calcination and steaming) and conditions (high heating ramp, temperature, oxygen and water concentration). In addition, for post-synthesis preparation routes the careful washing may enhance the formation of stable iron-oxo species, the anchoring of species to the zeolite framework and the removal of excess of iron precursor; all matters that limit the chance to form oxides.

On the other hand, no long-term stable FeZSM-5 catalyst will be obtained without the use of proper activation treatments, including heating. In particular for hydrothermally synthesized FeZSM-5 few activity is observed if no activation step is carried out, since the as-made form possesses iron in hardly accessible and flexible zeolite framework positions.

The choice of the preparation method may be inspired by the desired amount of iron in the sample and the intended nature of the formed species. Although it should be realized that the kind and distribution of the iron species not only varies with the initial synthesis route but also are strongly correlated with the subsequent activation treatments. Taking this into account the preparation of Fe/ZSM-5 via chemical vapor deposition might be slightly advantageous as this route is most reproducible, yields the best ratio between active and non-active iron, gains the highest absolute amount of iron per volume zeolite and finally does not require relatively harsh activation treatments.

The second statement based on the literature survey may be that the rationalization of the various influences on the final FeZSM-5 sample is a challenging task and requires a systematic approach with an emphasis on careful characterization. It has become clear that no single technique is able to provide the answer on the nature of the active site. Especially, the presence of multiple species and the issue of different detection sensitivity towards those various species are complicating. Nevertheless, we are inclined to say that characterization techniques that are based on X-ray spectroscopy are amongst the most powerful ones, in particular if a combination of them is employed.

List of Abbreviations

AIE	aqueous ion exchange
B	benzene
BtoP	selective oxidation of benzene to phenol using N_2O
C	calcination
CT	characterization technique
CVD	chemical vapor deposition
EF	extraframework
ESR	electron spin resonance
EXAFS	extended X-ray absorption fine structure
F	framework
Fe_F	single framework Fe site
Fe_1	isolated, single extraframework Fe site
Fe_2	oxo-bridged extraframework Fe center
Fe_N	chain-like structure of extraframework Fe
$Fe_{Ox,IN}$	aggregated of extraframework Fe inside zeolite crystals
$Fe_{Ox,OUT}$	agglomerated extraframework Fe on the external surface
HT He	heat treatment in He
IR	infrared spectroscopy
MFI	zeolite type Mobil Five
MS	Mössbauer spectroscopy
NO_x	nitrogen oxides
NO/C_3H_8	selective catalytic reduction of NO by propane
O_h	octahedral symmetry
ps	pseudo
P	phenol
PSI	post-synthesis introduction
red	reduction
R	reaction
RS	Raman spectroscopy
S	steam treatment
Soft XAS	soft X-ray absorption spectroscopy
T_d	tetrahedral symmetry
TPR-TPO	temperature programmed reduction-oxidation
SSIE	solid state ion exchange
UV-VIS	ultra violet-visible spectroscopy
VM	voltametric methods
W	washing
XANES	X-ray absorption near edge structure
XMCD	X-ray magnetic circular dichroism
XPS	X-ray photoelectron spectroscopy
XRD	X-ray diffraction
ZSM-5	Al-containing MFI

References

(1) Díaz, I.; Kokkoli, E.; Terasaki, O. and Tsapatsis, M., *Chem. Mat.*, **2004**, *16,* 5226-5232.

(2) Behrens, P., in B. Cornils, W. A. Hermann, R. Schlögl, and C.-H. Wong (Eds.), Catalysis from A to Z – A Concise Encylopedia, Wiley-VCH, Weinheim, **2000**.

(3) Flanigen, E. M., in H. van Bekkum, E. M. Flanigen, P. A. Jacobs, and J. C. Jansen (Eds.), Introduction to Zeolite Science and Practice, Elsevier, Amsterdam, **2001**.

(4) Thomas, J. M. and Thomas, W. J., Principles and Practice of Heterogeneous Catalysis, Wiley-VCH, Weinheim, **1997**.

(5) Kapteijn, F.; Rodriguez Mirasol, J. and Moulijn, J. A., *Appl. Catal. B,* **1996**, *9,* 25-64.

(6) Panov, G. I., *Cattech,* **2000**, *4,* 18-32.

(7) Battiston, A. A.; Bitter, J. H. and Koningsberger, D. C., *J. Catal.,* **2003**, *218,* 163-177.

(8) Chen, H. Y.; Voskoboinikov, T. and Sachtler, W. M. H., *J. Catal.,* **1998**, *180,* 171-183.

(9) Heinrich, F.; Schmidt, C.; Loffler, E.; Menzel, M. and Grünert, W., *J. Catal.,* **2002**, *212,* 157-172.

(10) Zhu, Q.; van Teeffelen, R. M.; van Santen, R. A. and Hensen, E. J. M., *J. Catal.*, **2004**, *221,* 575-583.

(11) Lobree, L. J.; Hwang, I.-C.; Reimer, J. A. and Bell, A. T., *Catal. Lett.,* **1999**, *63,* 233-240.

(12) Pérez-Ramírez., J.; Santhosh Kumar, M. and Brückner, A., *J. Catal.,* **2004**, 13-27.

(13) Van Den Brink, R. W.; Booneveld, S.; Pels, J. R.; Bakker, D. F. and Verhaak, M., *Appl. Catal. B,* **2001**, *32,* 73-81.

(14) Yamada, K.; Kondo, S. and Segawa, K., *Micropor. Mesopor. Mater.*, **2000**, *35-6,* 227-234.

(15) Dubkov, K. A.; Ovanesyan, N. S.; Shteinman, A. A.; Starokon, E. V. and Panov, G. I., *J. Catal.*, **2002**, *207,* 341-352.

(16) Pirngruber, G. D., *J. Catal.*, **2003**, *219,* 456-463.

(17) Kiwi-Minsker, L.; Bulushev, D. A. and Renken, A., *J. Catal.*, **2003**, *219,* 273-285.

(18) Perez-Ramirez, J.; Kapteijn, F.; Groen, J. C.; Domenech, A.; Mul, G. and Moulijn, J. A., *J. Catal.*, **2003**, *214,* 33-45.

(19) El-Malki, E. M.; Van Santen, R. A. and Sachtler, W. M. H., *Micropor. Mesopor. Mater.*, **2000**, *35-6,* 235-244.

(20) Wood, B. R.; Reimer, J. A. and Bell, A. G., *J. Catal.*, **2002**, *209,* 151-158.

(21) Dubkov, K. A.; Sobolev, V. I.; Talsi, E. P.; Rodkin, M. A.; Watkins, N. H.; Shteinman, A. A. and Panov, G. I., *J. Mol. Catal. A*, **1997**, *123,* 155-161.

(22) Meloni, D.; Monaci, R.; Solinas, V.; Berlier, G.; Bordiga, S.; Rossetti, I.; Oliva, C. and Forni, L., *J. Catal.*, **2003**, *214,* 169-178.

(23) Hensen, E. J. M.; Zhu, Q. and van Santen, R. A., *J. Catal.*, **2003**, *220,* 260-264.

(24) Perathoner, S.; Pino, F.; Centi, G.; Giordano, G.; Katovic, A. and Nagy, J. B., *Top. Catal.*, **2003**, *23,* 125-136.

(25) Kucherov, A. V.; Nissenbaum, V. D.; Kucherova, T. N. and Kustov, L. M., *Kinet. Katal.*, **2002**, *43,* 711-723.

(26) Panov, G. I.; Sobolev, V. I.; Dubkov, K. A.; Parmon, V. N.; Ovanesyan, N. S.; Shilov, A. E. and Shteinman, A. A., *Reac. Kin. Catal. Lett.*, **1997**, *61,* 251-258.

(27) Wood, B. R.; Reimer, J. A.; Bell, A. T.; Janicke, M. T. and Ott, K. C., *J. Catal.*, **2004**, *225,* 300-306.
(28) Weckhuysen, B. M.; Wang, D. J.; Rosynek, M. P. and Lunsford, J. H., *Angew. Chem. Int. Ed.*, **1997**, *36,* 2374-2376.
(29) Weckhuysen, B. M.; Wang, D. J.; Rosynek, M. P. and Lunsford, J. H., *J. Catal.*, **1998**, *175,* 338-346.
(30) Weckhuysen, B. M.; Wang, D. J.; Rosynek, M. P. and Lunsford, J. H., *J. Catal.*, **1998**, *175,* 347-351.
(31) Ratnasamy, P. and Kumar, R., *Catal. Today*, **1991**, *9,* 329-416.
(32) Ribera, A.; Arends, I. W. C. E.; De Vries, S.; Perez-Ramirez, J. and Sheldon, R. A.,*J. Catal.*, **2000**, *195,* 287-297.
(33) Taboada, J. B.; Overweg, A. R.; Craje, M. W. J.; Arends, I. W. C. E.; Mul, G. and Kraan, A. M. v. d., *Micropor. Mesopor. Mater.*, **2004**, *75,* 237-246.
(34) Feng, X. B. and Hall, W. K., *J. Catal.*, **1997**, *166,* 368-376.
(35) Hall, W. K.; Feng, X. B.; Dumesic, J. and Watwe, R., *Catal. Lett.*, **1998**, *52,* 13-19.
(36) Marturano, P.; Kogelbauer, A. and Prins, R., *J. Catal.*, **2000**, *190,* 460-468.
(37) Sun, K. Q.; Zhang, H. D.; Xia, H.; Lian, Y. X.; Li, Y.; Feng, Z. C.; Ying, P. L. and Li, C., *Chem. Comm.*, **2004**, 2480-2481.
(38) Serp, P.; Kalck, P. and Feurer, R., *Chem. Rev.*, **2002**, *102,* 3085-3128.
(39) Chen, H. Y. and Sachtler, W. M. H., *Catal. Today*, **1998**, *42,* 73-83.
(40) Krishna, K.; Seijger, G. B. F.; van den Bleek, C. M.; Makkee, M.; Mul, G. and Calis, H. P. A., *Catal. Lett.*, **2003**, *86,* 121-132.
(41) Marturano, P.; Kogelbauer, A. and Prins, R., *Stud. Surf. Sci. Catal.*, **1999**, *125,* 619-625.
(42) Battiston, A. A.; Bitter, J. H.; De Groot, F. M. F.; Overweg, A. R.; Stephan, O.; Van Bokhoven, J. A.; Kooyman, P. J.; Van Der Spek, C.; Vanko, G. and Koningsberger, D. C., *J. Catal.*, **2003**, *213,* 251-271.
(43) Kubanek, P.; Wichterlova, B. and Sobalik, Z., *J. Catal.*, **2002**, *211,* 109-118.
(44) van Bokhoven, J. A.; Koningsberger, D. C.; Kunkeler, P.; van Bekkum, H. and Kentgens, A. P. M., *J. Am. Chem. Soc.*, **2000**, *122,* 12842-12847.
(45) Berlier, G.; Zecchina, A.; Spoto, G.; Ricchiardi, G.; Bordiga, S. and Lamberti, C., *J. Catal.*, **2003**, ***215,*** 264-270.
(46) Heijboer, W. M.; Glatzel, P.; Sawant, K. R.; Lobo, R. F.; Bergmann, U.; Barrea, R. A.; Koningsberger, D. C.; Weckhuysen, B. M. and de Groot, F. M. F., *J. Phys. Chem. B*, **2004**, *108,* 10002-10011.
(47) Hensen, E. J. M.; Zhu, Q.; Hendrix, M.; Overweg, A. R.; Kooyman, P. J.; Sychev, M. V. and van Santen, R. A., *J. Catal.*, **2004**, *221,* 560-574.
(48) Selli, E.; Isernia, A. and Forni, L., *Phys. Chem. Chem. Phys.*, **2000**, *2,* 3301-3305.
(49) Perez-Ramirez, J.; Kapteijn, F.; Mul, G. and Moulijn, J. A., *Chem. Comm.*, **2001**, 693-694.
(50) Jia, J. F.; Pillai, K. S. and Sachtler, W. M. H., *J. Catal.*, **2004**, *221,* 119-126.
(51) Bitter, J. H.; Battiston, A. A.; van Donk, S.; de Jong, K. P. and Koningsberger, D. C.,*Micropor. Mesopor. Mater.*, **2003**, *64,* 175-184.

(52) Berlier, G.; Spoto, G.; Bordiga, S.; Ricchiardi, G.; Fisicaro, P.; Zecchina, A.; Rossetti, I.; Selli, E.; Forni, L.; Giamello, E. and Lamberti, C., *J. Catal.*, **2002**, ***208,*** 64-82.

(53) Yuranov, I.; Bulushev, D. A.; Renken, A. and Kiwi-Minsker, L., *J. Catal.*, **2004**, *227,* 138-147.

(54) Roy, P. K. and Pirngruber, G. D., *J. Catal.*, **2004**, *227,* 164-174.

(55) Berlier, G.; Ricchiardi, G.; Bordiga, S. and Zecchina, A., *J. Catal.*, **2005**, *229,* 127-135.

(56) Pérez-Ramírez., J.; Mul, G.; Kapteijn, F.; Moulijn, J. A.; Overweg, A. R.; Doménech, A.; Ribera, A. and Arends, I. W. C. E., *J. Catal.*, **2002**, 113-126.

(57) Overweg, A. R.; Craje, M. W. J.; van der Kraan, A. M.; Arends, I.; Ribera, A. and Sheldon, R. A., *J. Catal.*, **2004**, *223,* 262-270.

(58) Heijboer, W. M.; Glatzel, P.; Sawant, K. R.; Lobo, R. F.; Bergmann, U.; Barrea, R. A.; Koningsberger, D. C.; Weckhuysen, B. M. and de Groot, F. M. F., *J. Phys. Chem. B*, **2004**, *108,* 10002-10011.

(59) Wichterlova, B.; Sobalik, Z. and Dedecek, J., *Appl. Catal. B*, **2003**, *41,* 97-114.

(60) Wichterlova, B., *Top. Catal.*, **2004**, *28,* 131-140.

(61) Bulushev, D. A.; Kiwi-Minsker, L. and Renken, A., *J. Catal.*, **2004**, *222,* 389-396.

(62) Pirutko, L. V.; Chernyavsky, V. S.; Uriarte, A. K. and Panov, G. I., *Appl. Catal. A*, **2002**, *227,* 143-157.

(63) Cik, G.; Hubinova, M.; Sersen, F. and Brezova, V., *Collect. Czech. Chem. Commun.*, **2002**, *67,* 1743-1759.

(64) Brabec, L.; Jeschke, M.; Klik, R.; Novakova, J.; Kubelkova, L. and Meusinger, J., *Appl. Catal. A*, **1998**, *170,* 105-116.

(65) Kameoka, S.; Yuzaki, K.; Takeda, T.; Tanaka, S.; Ito, S.; Miyadera, T. and Kunimori, K., *Phys. Chem. Chem. Phys.*, **2001**, *3,* 256-260.

(66) Pophal, C.; Yogo, T.; Yamada, K. and Segawa, K., *Appl. Catal. B*, **1998**, *16,* 177-186.

(67) Pophal, C.; Yogo, T.; Tanabe, K. and Segawa, K., *Catal. Lett.*, **1997**, *44,* 271-274.

(68) Yamada, K.; Pophal, C. and Segawa, K., *Micropor. Mesopor. Mater.*, **1998**, *21,* 549-555.

(69) Guzman-Vargas, A.; Delahay, G. and Coq, B., *Appl. Catal. B*, **2003**, *42,* 369-379.

(70) Chaki, T.; Arai, M.; Ebina, T. and Shimokawabe, M., *J. Catal.*, **2003**, *218,* 220-226.

(71) Joyner, R. and Stockenhuber, M., *J. Phys. Chem. B,* **1999**, *103,* 5963-5976.

(72) Kucherov, A. V. and Shelef, M., *J. Catal.*, **2000**, *195,* 106-112.

(73) Long, R. Q. and Yang, R. T., *J. Am. Chem. Soc.*, **1999**, *121,* 5595-5596.

(74) Long, R. Q. and Yang, R. T., *J. Catal.*, **2001**, *198,* 20-28.

(75) Long, R. Q. and Yang, R. T., *J. Catal.*, **2000**, *194,* 80-90.

(76) Long, R. Q. and Yang, R. T., *J. Catal.*, **1999**, *188,* 332-339.

(77) Long, R. Q. and Yang, R. T., *Catal. Lett.*, **2001**, *74,* 201-205.

(78) Yoshida, M.; Nobukawa, T.; Ito, S. I.; Tomishige, K. and Kunimori, K., *J. Catal.*, **2004**, *223,* 454-464.

(79) van den Brink, R. W.; Booneveld, S.; Verhaak, M. and de Bruijn, F. A., *Catal. Today*, **2002**, *75,* 227-232.

(80) Choi, S. H.; Wood, B. R.; Ryder, J. A. and Bell, A. T., *J. Phys. Chem. B*, **2003**, *107,* 11843-11851.

(81) Lobree, L. J.; Hwang, I. C.; Reimer, J. A. and Bell, A. T., *J. Catal.*, **1999**, *186,* 242-253.
(82) El-Malki, E. M.; Van Santen, R. A. and Sachtler, W. M. H., *J. Catal.*, **2000**, *196,* 212-223.
(83) Kogel, M.; Sandoval, V. H.; Schwieger, W.; Tissler, A. and Turek, T., *Catal. Lett.*, **1998**, *51,* 23-25.
(84) Kogel, M.; Monnig, R.; Schwieger, W.; Tissler, A. and Turek, T., *J. Catal.*, **1999**, *182,* 470-478.
(85) Rauscher, M.; Kesore, K.; Monnig, R.; Schwieger, W.; Tissler, A. and Turek, T., *Appl. Catal. A*, **1999**, *184,* 249-256.
(86) Battiston, A. A.; Bitter, J. H.; Heijboer, W. M.; De Groot, F. M. F. and Koningsberger, D. C., *J. Catal.*, **2003**, *215,* 279-293.
(87) Battiston, A. A.; Bitter, J. H. and Koningsberger, D. C., *Catal. Lett.*, **2000**, *66,* 75-79.
(88) Hensen, E. J. M.; Zhu, Q.; Hendrix, M. M. R. M.; Overweg, A. R.; Kooyman, P. J.; Sychev, M. V. and van Santen, R. A., *J. Catal.*, **2004**, *221,* 560-574.
(89) Marturano, P.; Drozdova, L.; Pirngruber, G. D.; Kogelbauer, A. and Prins, R., *Phys. Chem. Chem. Phys.*, **2001**, *3,* 5585-5595.
(90) Marturano, P.; Drozdova, L.; Kogelbauer, A. and Prins, R., *J. Catal.*, **2000**, *192,* 236-247.
(91) Decyk, P.; Kim, D. K. and Woo, S. I., *J. Catal.*, **2001**, *203,* 369-374.
(92) Lee, H. T. and Rhee, H. K., *Catal. Lett.*, **1999**, *61,* 71-76.
(93) Santhosh Kumar, M.; Schwidder, M.; Grünert, W. and Brückner, A., *J. Catal.*, **2004**, *227,* 384-397.
(94) Fejes, P.; Lazar, K.; Marsi, I.; Rockenbauer, A.; Korecz, L.; Nagy, J. B.; Perathoner, S. and Centi, G., ***Appl. Catal. A***, **2003**, ***252,*** 75-90.
(95) Ferretti, A. M.; Forni, L.; Oliva, C. and Ponti, A., *Res. Chem. Intermed.*, **2002**, *28,* 101-116.
(96) Lazar, K.; Kotasthane, A. N. and Fejes, P., *Catal. Lett.*, **1999**, *57,* 171-177.
(97) Ovanesyan, N. S.; Shteinman, A. A.; Dubkov, K. A.; Sobolev, V. I. and Panov, G. I., *Kinet. Katal.*, **1998**, *39,* 792-797.
(98) Hensen, E.; Zhu, Q. J.; Liu, P. H.; Chao, K. J. and van Santen, R., *J. Catal.*, **2004**, *226,* 466-470.
(99) Bordiga, S.; Buzzoni, R.; Geobaldo, F.; Lamberti, C.; Giamello, E.; Zecchina, A.; Leofanti, G.; Petrini, G.; Tozzola, G. and Vlaic, G., *J. Catal.*, **1996**, *158,* 486-501.
(100) Goldfarb, D.; Bernardo, M.; Strohmaier, K. G.; Vaughan, D. E. W. and Thomann, H., *J. Am. Chem. Soc.*, **1994**, *116,* 6344-6353.
(101) Voskoboinikov, T. V.; Chen, H. Y. and Sachtler, W. M. H., *Appl. Catal. B*, **1998**, *19,* 279-287.
(102) Chen, H. Y.; Voskoboinikov, T. and Sachtler, W. M. H., *Catal. Today*, **1999**, *54,* 483-494.
(103) Pirngruber, G. D.; Roy, P. K. and Weiher, N., *J. Phys. Chem. B*, **2004**, *108,* 13746-13754.
(104) Pillai, K. S.; Jia, J. F. and Sachtler, W. M. H., *Appl. Catal. A*, **2004**, *264,* 133-139.
(105) Pirngruber, G. D.; Luechinger, M.; Roy, P. K.; Cecchetto, A. and Smirniotis, P., *J. Catal.*, **2004**, *224,* 429-440.
(106) chapter 8 of this thesis.
(107) chapter 7 of this thesis.

3

In situ soft X-ray absorption of overexchanged Fe/ZSM-5

Based on: W. M. Heijboer, A. A. Battiston, A. Knop-Gericke, M. Hävecker, R. Mayer, H. Bluhm, R. Schlögl, B. M. Weckhuysen, D. C. Koningsberger and F. M. F. de Groot, *J. Phys. Chem. B*, 2003, **107**, 13069 – 13075

Abstract

In situ soft X-ray absorption spectroscopy (XAS) has been applied to study the redox behavior of overexchanged Fe/ZSM-5. The Fe $L_{2,3}$ XAS and oxygen K spectral shapes of the Fe/ZSM-5 surface have been measured during heat treatments and reduction/oxidation cycles. Charge-transfer multiplet calculations provide a detailed understanding of the $L_{2,3}$ spectra of iron in Fe/ZSM-5. The oxidized form of Fe/ZSM-5 contains Fe^{III} ions in an octahedral surrounding, with a total crystal field splitting of ~ 1.0 eV. This value is significantly smaller than that for Fe_2O_3, which is indicative of a much weaker Fe–O bonding. The reduced form of Fe/ZSM-5 has Fe^{II} ions in a tetrahedral oxygen surrounding. The Fe $L_{2,3}$ spectra show that iron in calcined Fe/ZSM-5 is reduced in 15 min to an average valence state of 2.65, under 10 mbar of pure helium at room temperature. This value has a relative uncertainty on the order of 0.01. Heating in helium up to 350 °C under the same pressure further reduces the iron valence to 2.15. The oxygen K edge spectra show that the autoreduction is accompanied by a loss of molecular oxygen and water. Reoxidation with 5 % O_2 in helium yields a valence of > 2.90 after 10 min.

3.1. Introduction

Photons in the soft X-ray range (100-1000 eV) are suitable probes for the electronic structure of a reacting catalyst surface. Because of the use of the electron-yield detection mode, the X-ray absorption signal is surface sensitive. *In situ* soft X-ray absorption spectroscopy (XAS) has been introduced by Knop-Gericke and co-workers.[1-3] For example, by measuring the Cu $L_{2,3}$ edge of the surface and the oxygen K spectra for the surface and the gas phase, a new form of weakly bound oxygen was discovered that only exists under the reaction conditions and can be correlated with the selective oxidation reaction.

Fe/ZSM-5 is a catalyst that can be used for a variety of reactions, depending on the iron loading, preparation method, thermal treatment, and activation procedure. For example, low-loaded, isomorphously substituted Fe/ZSM-5, after steaming at 550 °C, is very active in the decomposition of N_2O to nitrogen and oxygen and the subsequent direct oxidation of benzene to phenol.[4,5] Overexchanged Fe/ZSM-5 with a high iron loading (up to 5 wt %) is an effective catalyst for the selective catalytic reduction of NO_x using hydrocarbons.[6,7] The amount of iron present in the catalyst can be tuned by the manner of preparation. In general, the substitution of iron in the framework of ZSM-5 results in a maximum iron loading of 1 wt %. By introducing iron in extra framework positions (for example, via ion exchange or sublimation), a higher loading is possible. The sensitivity of iron species toward washing, calcination, steaming, reduction, and oxidation treatments is different for different locations within the zeolite. Battiston and co-workers[8] extensively investigated the molecular structures of the different Fe species obtained after the different steps in the preparation procedure, using the sublimation of $FeCl_3$. In addition, a severe calcination procedure (heating rate of 5 °C/min), as used in the literature, leads to binuclear Fe centers to some larger iron oligomers inside the zeolite channels. In addition, one finds the formation of iron oxide clusters on the outside of the ZSM-5 crystals. By applying a mild calcination (a heating rate of 0.5 °C/min) the amount of binuclear Fe species seems to account for ~ 80 % of the total iron amount. The binuclear Fe species are believed to be the catalytic active centers for the reduction of NO_x.[9] A precise characterization of the iron phases in Fe/ZSM-5 is complicated, particularly without the use of *in situ* studies. The presence of catalytic inactive Fe species (spectators) complicates the identification of the active Fe phase.

Garten and co-workers showed that the iron in zeolite Y exhibits autoreduction upon heating and evacuation.[10] Several other authors confirmed the autoreduction ability of iron in Fe/ZSM-5[11-14] and, generally, the sensitivity toward the autoreduction of metal oxide complexes.[15,16] Battiston and co-workers[9] studied the autoreduction behavior of the Fe/ZSM-5 catalyst that was prepared via the mild calcination route with Fe K edge XAFS. The authors observed that the binuclear Fe species present could be reduced in helium at 350 °C to an average Fe valence of ~ 2.4. In this paper, we applied *in situ* soft XAS to further determine the structural and electronic properties of the Fe species present in Fe/ZSM-5.

We will demonstrate that Fe $L_{2,3}$ XAS is a valuable technique that can be applied under *in situ* conditions and allows for a precise determination of the valence of iron. We will study

the oxidation and reduction behavior of the Fe sites in Fe/ZSM-5 and determine the iron valence under various conditions. By simulating the experimental spectral shape, detailed information about the coordination of Fe can be obtained. We will measure the valence of iron in Fe/ZSM-5 in a helium atmosphere at room temperature and during heating to 350 °C with a time resolution of ~ 1 min. In addition, the detection of the oxygen K edge of the gas phase will be used to check the development of the presence of water and molecular oxygen. In the following chapter, we will present a more extensive study on Fe/ZSM-5 that has been prepared via mild calcination. This additional study will show that the application of *in situ* soft X-ray spectroscopy can give relevant information about the catalytic active Fe sites.

3.2. Experimental Section

3.2.1. Catalyst Preparation and Characterization

Fe/ZSM-5 was prepared via the $FeCl_3$ sublimation method proposed by Chen and Sachtler.[17] NH_4/ZSM-5 (Si/Al = 17), obtained from Zeolyst, was converted to the H^+ form by calcination in O_2 at 550 °C for 3 h. The calcined H/ZSM-5 (1.0 g) was flushed overnight in a helium flow (40 mL/min) at 300 °C. Then, 0.31 g of anhydrous $FeCl_3$ (98 %, Acros Organics) was loaded and the sublimation exchange procedure was performed at 330 °C for 30 min. After sublimation, the sample was washed in 1000 mL of doubly deionized H_2O for 30 min, dried overnight in air at 70 °C, and calcined for 3 h in flowing O_2 at 550 °C.

The HCl formed during the $FeCl_3$ reaction with the Brønsted acid sites of the H/ZSM-5 was absorbed in a NaOH solution, and acid-base titration of the remaining OH^- in the solution was used to quantify the amount of HCl released during the $FeCl_3$ exchange. The ratio between the HCl produced during the sublimation reaction and the H^+ sites that are theoretically present in the support, by assuming $Al/H^+ = 1$, was used to calculate the H^+ removal efficiency, according to the reaction $Fe_2Cl_6 + 2\ H^+ \rightarrow 2\ HCl + [Fe_2Cl_4]^{2+}$.

Details about the sample preparation were described earlier by Battiston et al.[18] Almost all Brønsted acid sites were removed from the H/ZSM-5, considering that the H^+ removal efficiency value of 0.98. Inductively coupled plasma (ICP) analysis was performed to determine the Si/Al ratio (Si/Al = 17.0) and the iron loading (Fe/Al = 0.97) of the starting Fe/ZSM-5 sample. This implies that the Fe wt % is 4.71. The sample was heated under flowing oxygen at a rate of 120 mL/min in a tubular oven, using a temperature ramp of 5 °C/min, and calcined at 550 °C for 3 h. The crystalline fingerprint of the zeolite support was monitored after each synthesis step using XRD. On the basis of these measurements, lattice damage or significant formation of large iron oxide particles could be excluded. X-ray absorption experiments were conducted to investigate the valence of iron and the nature of the evolving gases during various chemical and heat treatments. The Fe/ZSM-5 samples that are described in Table 1 will be used.

Table 1: Fe/ZSM-5 samples used in the measurements

sample	measurement conditions	catalyst pretreatment
Fe/ZSM-5-A	Fe/ZSM-5 under 5% O_2 in helium (reoxidized)	calcination ramp of 5 °C/min
Fe/ZSM-5-B	Fe/ZSM-5 under 5% H_2 in helium (reduced)	calcination ramp of 5 °C/min
Fe/ZSM-5-C	Fe/ZSM-5 under 5% H_2 in helium (reduced)	calcination ramp of 0.5 °C/min

3.2.2. *In situ* Soft X-ray Absorption Spectroscopy

The soft X-ray absorption spectra of the Fe $L_{2,3}$ edge (700-730 eV) and the oxygen K edge (525-550 eV) were measured at BESSY (Berlin), using beamlines U49/2-PGM-1 and UE56/2-PGM-1. The spectral resolution of the monochromators was ~ 0.2 eV. The instrumentation for *in situ* low-energy XAS experiments has been developed by Knop-Gericke and co-workers and is described in detail elsewhere.[1-3] We used a stainless-steel *in situ* cell in which the powdered zeolite sample was fixed in a sample holder. The flow rates of helium and of 5 % O_2 in helium was 100 mL/min, of which approximately half entered the *in situ* cell. A homemade gas-mixing system regulated the flow, and the total pressure was ~ 10 mbar during the experiments. The temperature was increased from room temperature to the reaction temperature of 350 °C, using a ramp rate of 5 °C /min.

The X-ray absorption spectral shape is measured with two collector plates that detect the ionized gas that is due to the created electrons in the X-ray absorption process and the subsequent nonradiative decay of the core hole, i.e., ionized-gas conversion total electron yield, with a probing depth of ~ 4 nm.[19] One detector measures the gas phase, while a second detector (close to the sample surface) detects both the gas phase and surface signal, where 'surface' is defined here as the top 4 nm of the sample. The surface signal can be revealed through subtraction of the gas-phase signal. The energy scale was calibrated with the O peak position of O_2[20] and the Fe peak position of Fe_2O_3.[21] After background subtraction, all spectra were normalized to 1.0, because yield methods in X-ray absorption only scale with the absorption cross section but are not capable of measuring the absolute absorption cross sections.

3.3. Results

3.3.1. The Fe $L_{2,3}$ spectra

The Fe 2p X-ray absorption spectral shape has peaks at ~ 712 eV for the L_3 edge and 725 eV for the L_2 edge, where the energy splitting is given by the 2p spin-orbit coupling. Figure 1 compares the Fe $L_{2,3}$ spectrum of Fe/ZSM-5-A with that of Fe_2O_3. The Fe_2O_3 spectrum is identical to the spectra published in literature.[21-24] These references also include the $L_{2,3}$ X-ray absorption spectra of FeO, Fe_3O_4, and other iron oxides. The spectra of both Fe/ZSM-5-A and Fe_2O_3 have been analyzed with the charge-transfer multiplet (CTM) program.[25-28] The Fe $L_{2,3}$ spectrum of Fe_2O_3 is used as a reference and the spectrum shown is measured at the same beamline, to compare the experimental resolution. It corresponds well to the theoretical curve that has been calculated using a ground-state description of the Fe^{III} site given with two configurations, respectively $3d^5$ and $3d^6\underline{L}$. The $\underline{L}$ denotes a ligand hole, i.e., a hole on the O neighbors that surround the Fe atom under consideration. Within the CTM model, the ground state is defined by several parameters, as given in Table 2. The first two columns respectively show the ionic value of the cubic crystal field (10 Dq(ion)) and the charge-transfer energy (Δ), which defines the energy difference between the $3d^5$ and $3d^6\underline{L}$ configurations. These configurations are split by multiplet effects and spin-orbit couplings, for which we use the atomic values.[27] The third and fourth columns contain the mixing terms for E_g and T_{2g} hopping, respectively. E_g hopping implies that an electron is moved from an oxygen orbital to a metal E_g orbital. In an octahedral crystal field, E_g hopping is approximately twice as strong as T_{2g} hopping, as is confirmed from the experiments and from density functional calculations.[27] The fifth and sixth columns give the local geometry and site symmetry of the iron site, respectively.

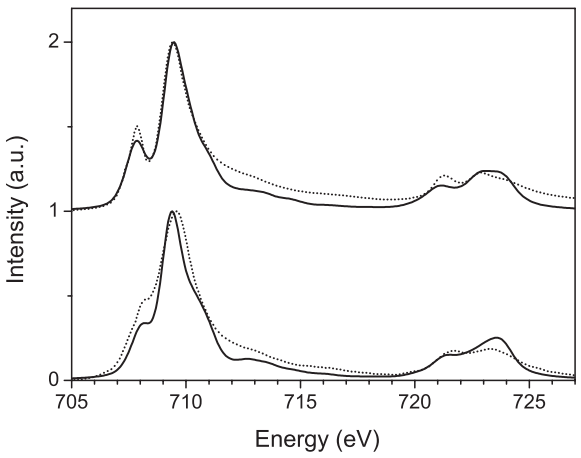

Figure 1: Charge-transfer multiplet (CTM) simulations (solid lines) compared with the experimental spectra (dotted lines) of Fe_2O_3 (top spectra) and Fe/ZSM-5-A (bottom spectra).

Table 2: Charge-transfer parameters[a] as used in the simulations of the Fe $L_{2,3}$ spectra

	10 Dq (ion)	charge-transfer energy, Δ	$T(E_g)$	$T(T_{2g})$	symmetry	geometry
Fe_2O_3	1.1	3	2	1	$^6A_1$	octahedral
Fe/ZSM-5-A	0.7	3	2	1	$^6A_1$	octahedral
Fe/ZSM-5-C	-1.0	4	1	2	^5E	tetrahedral

[a] All numerical values are given in electron volts (eV)

The spectral shape of Fe/ZSM-5-A can be explained well from the same configurations, although with a reduced ionic crystal field splitting of 0.7 eV. The mixing of the $3d^5$ and $3d^6\underline{L}$ configurations adds an additional 0.3-0.4 eV to the overall splitting between the E_g and T_{2g} states. This implies that the overall crystal-field splitting is 1.4 eV for Fe_2O_3 and 1.0 eV for Fe/ZSM-5-A. The reduced crystal-field splitting is particularly evident in the first peak, which is reduced in intensity and shifted closer to the main peak. The CTM analysis shows that Fe/ZSM-5-A is indeed completely oxidized to a trivalent state, within an octahedral surrounding. It is noted that this Fe/ZSM-5-A sample is reoxidized after first being reduced. The fact that the crystal-field splitting of Fe/ZSM-5-A is considerably smaller than that for Fe_2O_3 suggests (on average) less bonding between Fe and its six O neighbors. Depending on the particular model used, these six O neighbors may belong to the zeolite framework, hydroxyl groups, adsorbed water, and bridging O atoms.

Both Fe_2O_3 and Fe/ZSM-5-A have a $^6A_1$ ground state that has all the spin-up electrons filled, ($t_{2g}^3e_g^2${up}) and all the spin-down states empty. This special characteristic makes the spectrum rather insensitive to small geometric distortions. This implies that the geometric symmetry can be determined as octahedral-like, but small distortions will not be detectable.

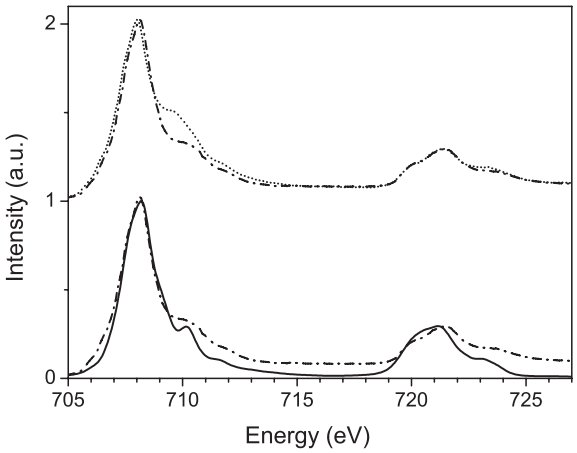

Figure 2: (Top) Experimental spectra of Fe/ZSM-5-C (dashed-dotted line) and Fe/ZSM-5-B (dotted line). (Bottom) CTM simulation (solid line) compared with the experimental spectrum of Fe/ZSM-5-C (dashed-dotted line).

Figure 2 shows the Fe/ZSM-5-B and Fe/ZSM-5-C spectra in comparison with an Fe^{II} simulation for tetrahedral symmetry. A CTM calculation has been used, with the parameters as given in Table 1. The ionic crystal-field splitting is -1.0 eV, where the negative sign implies that the energy ordering of the T_{2g} and E_g orbitals is reversed with, for a tetrahedral crystal field, the T_{2g} antibonding states at higher energy, because of their larger interaction with the neighboring O atoms. An ionic crystal field of -1.3 implies a total crystal-field splitting of approximately -1.3 eV. The ground state has ^5E symmetry, which implies that the sixth 3d electron occupies an e_g orbital. Figure 2 shows that a good agreement with the spectrum has been obtained. The top portion of the figure shows a comparison of the spectrum of Fe/ZSM-5-B (dashed-dotted line) with that of Fe/ZSM-5-C (dotted line). The bottom portion of the figure shows a comparison of the spectrum of the Fe/ZSM-5-C sample (the dashed-dotted line) with the theoretical spectrum (solid line). The Fe/ZSM-5-B sample is expected to contain some 20 nm-size Fe_2O_3 particles on the outside of the zeolite crystal, which prevents the sample from being completely reduced to the divalent state.[9] The Fe/ZSM-5-C sample has been completely reduced, as is shown by the good agreement between the simulation and the experiment. The valence of Fe/ZSM-5-B is simulated by addition of the experimental spectra of Fe/ZSM-5-A and Fe/ZSM-5-C, yielding a value of 2.16. Disregarding the estimated maximum systematic error of 5 %, this value has a relative uncertainty on the order of 0.01. This high accuracy is possible because the 'reference spectra' of Fe/ZSM-5-A and Fe/ZSM-5-C are very closely related to the actual spectra of the Fe/ZSM-5 system at various temperatures and gas conditions. This strong similarity allows for a smaller error bar, with respect to the general methods that have been derived, for example, by Van Aken and Liebscher.[21] In this paper, which involves iron oxide minerals, several detailed analysis procedures are compared, and it is found that, for a wide range of iron oxide minerals, good estimates could be made of the oxidation state from peak fitting (with an error of < 0.04) and reference spectra fitting (with an error of < 0.02). Given the similarity of the reference compounds, this allows for an uncertainty on the order of 0.01 for the Fe/ZSM-5 systems.

We conducted extensive searches for a possible octahedral ground-state situation; however, none of the reasonable descriptions of the ground state came close to describing the Fe 2p X-ray absorption spectral shape. In particular, the octahedral complexes do give a systematically larger value for the splitting between the L_3 and L_2 structures. This rules out an octahedral surrounding for Fe^{II} and implies that the sixth electron indeed occupies an e_g orbital. There can be, and most likely will be, symmetry distortions from a pure tetrahedral surrounding. If these symmetry distortions are small, their effect on the spectral shape also will be small. In addition, in the likely case that there will be a range of different distortions, the only expected effect is a broadening of the spectral shape. In conclusion, it can be stated that octahedral Fe^{III} sites in oxidized Fe/ZSM-5 change to tetrahedral Fe^{II} sites in reduced Fe/ZSM-5. Later in this chapter, we will show that this is a reversible process.

3.3.2. Autoreduction in helium

Each Fe $L_{2,3}$ spectrum can be considered as a linear combination of the reference spectra of Fe/ZSM-5-A and Fe/ZSM-5-C. To accelerate the measurement time to 50 s, we have not measured the entire $L_{2,3}$ spectrum, but rather only the L_3 edge. Figure 3 compares the two reference spectra for this energy range, i.e., the Fe L_3 spectra of Fe/ZSM-5-A and Fe/ZSM-5-C. In principle, each measured spectrum can be simulated from the addition of the Fe^{II} and Fe^{III} spectra. It has been checked in detail that this procedure can accurately be replaced by a procedure for which one measures the intensities at the peak positions for Fe^{II} (707.9 eV) and Fe^{III} (709.5 eV) and scales the intensity ratio to the theoretical curves. In other words, the ratio between the two peaks at the given energies can be considered as a measure for the average oxidation number. By analyzing the spectra as such, we were able to monitor the mean valence of the iron present in Fe/ZSM-5 during treatments at temperatures in the range of 25-350 °C and with gas flows of helium and O_2. The relative uncertainty in the effective valence of iron, estimated from the addition of spectra, is ~ 0.02. Fast Fe L_3 measurements with intervals of 50 s were taken in the energy range of 702.5-714.5 eV. Periodically, we recorded the complete Fe $L_{2,3}$ spectral shape to check potential variations in the background.

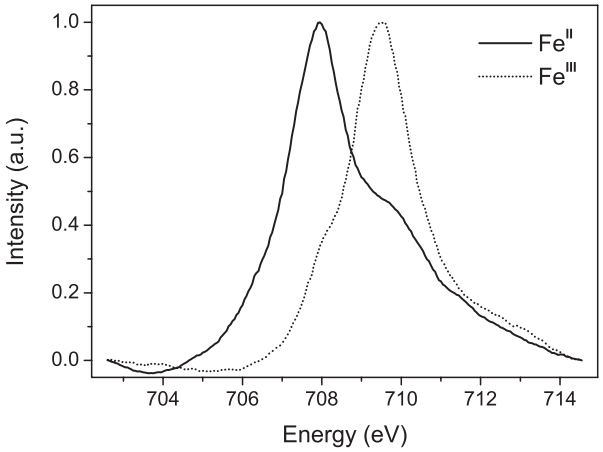

Figure 3: Fe L_3 X-ray absorption spectra of Fe/ZSM-5-A (dotted line, Fe^{III}) and Fe/ZSM-5-C (solid line, Fe^{II}) as used in the fast valence determination method.

Figure 4 shows the variation of the average valence state under the oxidation, with 5 % O_2 in helium, of calcined Fe/ZSM-5 at room temperature and a pressure of 2 mbar. The oxidized form is subsequently exposed to helium for 2 h. The valence of the Fe/ZSM-5-A sample under 5 % O_2 in helium at room temperature first shows an oxidation to a valence of 2.94 ± 0.01 and remains constant at this value for 50 min. At t = 90 min, we switch to pure helium, after which time the sample is reduced in 15 min to a minimum valence of 2.64, followed by a slight reoxidation to a value of ~ 2.68 after 200 min. Figure 4 shows that, even at room temperature, the Fe/ZSM-5 system is subject to significant autoreduction. A possible explanation of the reoxidation from 2.65 to 2.68 is a slight reoxidation that is due

to O_2 that comes from the bulk. As previously mentioned, soft X-ray absorption measures only the top 4 nm of the sample, and the autoreduction can be expected to be faster at the surface than in the bulk. This observation indicates a very dynamic local valence that will be considered further in the discussion below. Next, we have investigated the difference between the X-ray irradiated portion of the sample and a fresh spot. The valence of the spot that was irradiated for 200 min is 2.68, and a fresh spot had an average valence of 2.49. Apparently, an irradiated area has a higher mean valence. This is not obvious, because the temperature effect of the irradiation will tend to decrease the valence, as will be discussed below. Apparently, the temperature effect is not important and the ionizing effect of the X-ray tends to reoxidize the Fe sites. A re-reduction effect of irradiation on the valence state is observed for almost-trivalent iron at high temperatures. In that case, the change to a nonirradiated spot displays a lower valence state. It can be concluded that, upon irradiation, the average valence state of iron changes faster to its equilibrium state than a nonirradiated portion of the sample.

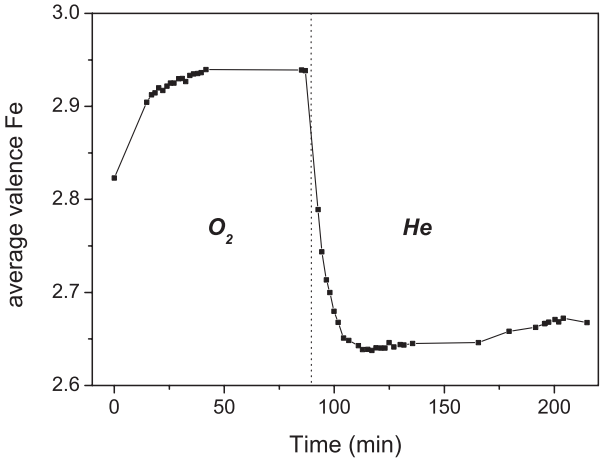

Figure 4: Oxidation in an O_2 atmosphere, followed by autoreduction in helium, of iron in Fe/ZSM-5-A samples at room temperature.

To investigate the stability of the iron phase that is present at the zeolite surface at the reaction temperature for the deNO_x reaction, 350 °C, we recorded Fe L_3 spectra while heating the Fe/ZSM-5 from 25 °C to 350 °C, at a rate of 5 °C /min, at 2 mbar of helium. The result is shown in Figure 5. During heating from room temperature to 350 °C, the mean valence is reduced from 2.49 to 2.16. The starting valence is 2.49, because we used a nonirradiated starting position of the sample, as discussed previously. The gap between t = 70 min and t = 100 min is related to a re-injection of electrons into the storage ring. After reaching the final temperature of 350 °C, we again observe a slight reoxidation. As discussed previously, a likely explanation is the reoxidation of the surface Fe^{II} sites with O_2 that comes from the bulk (in other words, the equilibration between the valence at the surface and in the bulk). Reoxidation in 5 % O_2 in helium at 350 °C yields an Fe valence of > 2.90 after 10 min, demonstrating that the autoreduction of iron in Fe/ZSM-5 is a fast, reversible process.

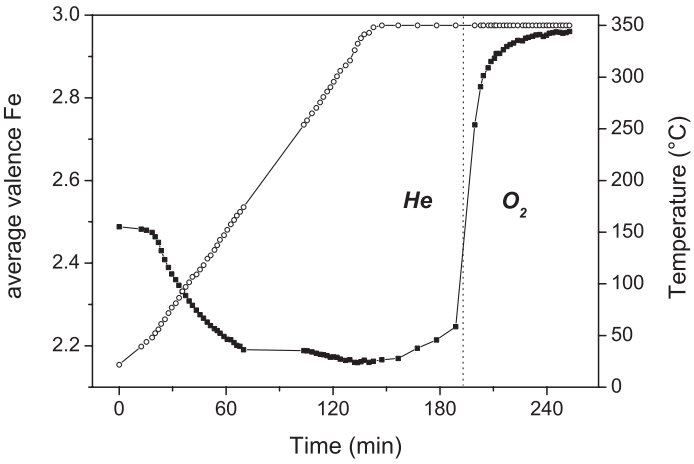

Figure 5: Progressed autoreduction, in helium, of iron in Fe/ZSM-5; conditions were heating from 20 °C to 350 °C, followed by reoxidation in an O_2 atmosphere at 350 °C. (■) average valence of the Fe ion and (O) temperature.

3.3.3. The oxygen K edge spectra

The *in situ* cell and detection setup allows for the simultaneous measurement of the sample and gas-phase signal. This is not important for the Fe L edge, because there is no gas-phase iron. However, it opens the possibility to measure the gas-phase and surface signal of the oxygen K edge at 530 eV. We also measured, during the heat treatment in helium (shown in Figure 5), the oxygen K edge spectrum of the gas phase above the catalyst surface. In Figure 6, we show the results of the oxygen K edge spectra of the gas phase at different temperatures, while flushing the cell with purified helium. Figure 7 shows that the first peak (530.8 eV) can be assigned to molecular oxygen (O_2).[29] The second peak in Figure 6 belongs to the three-peak feature of water. Figure 7 shows the full water spectrum with peaks at 533.7, 535.7, and 536.9 eV. For clarity, in Figure 6, only the first of the H_2O peaks is shown, where we have checked that the ratio between the three peaks is the same for all temperatures and spectra measured.

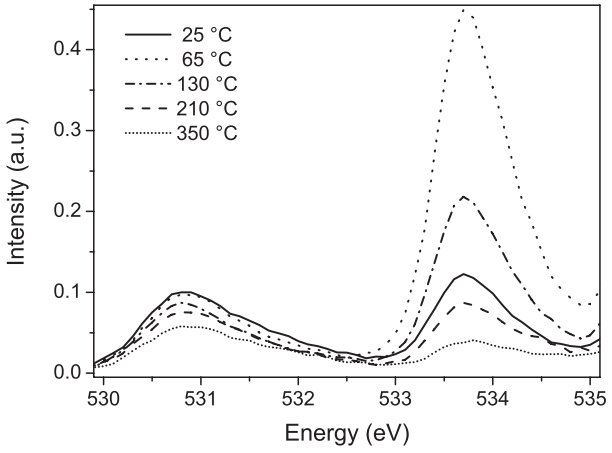

Figure 6: Evolution of the O K-edges during autoreduction in helium at selected tem-peratures in the range of 25-350 °C.

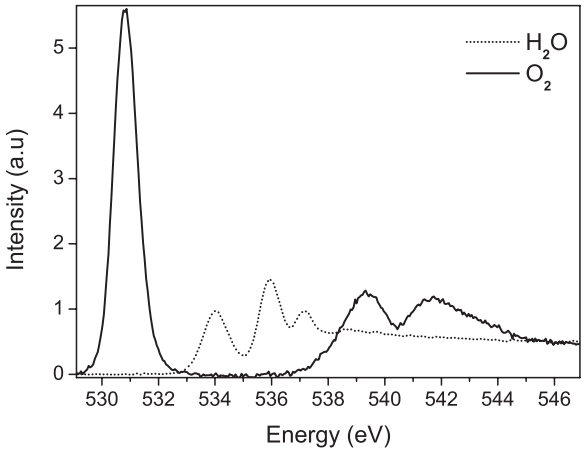

Figure 7: O 1s X-ray absorption for molecular oxygen (solid line) and water (dotted line). Gas-phase oxygen and water reference spectra have been replotted from the COREX database.[25]

Figure 8 summarizes the results in a graph that represents the trends in O_2 and H_2O evolution during heating of Fe/ZSM-5 in helium. The presence of the O_2 peak at room temperature indicates the release of O_2 from the zeolite already at this temperature. The peak decreases with the temperature. Comparison of this figure with the iron valence (Figures 4 and 5) shows that this formation of O_2 is proceeding simultaneously with the autoreduction process of iron. To probe the amount of oxygen and water formed qualitatively, we have defined the intensity integral for O_2 for the photon-energy range of 530.0-532.9 eV and H_2O for 533.0-535.2 eV. Figure 8 shows that the autoreduction of iron in helium is accompanied by the release to the gas phase of O_2 and H_2O over the entire temperature range of 25-350 °C. The signal that is due to water reaches a maximum intensity at a temperature of 75 °C and, at higher temperatures, decreases in intensity. The release of O_2 slowly decreases from 25 °C to higher temperatures. It is noted that, in addition to the water produced during the iron autoreduction process, it is likely that another contribution for water release can be attributed to physisorbed water that comes from the surface and out of the channels of the zeolite upon heating.

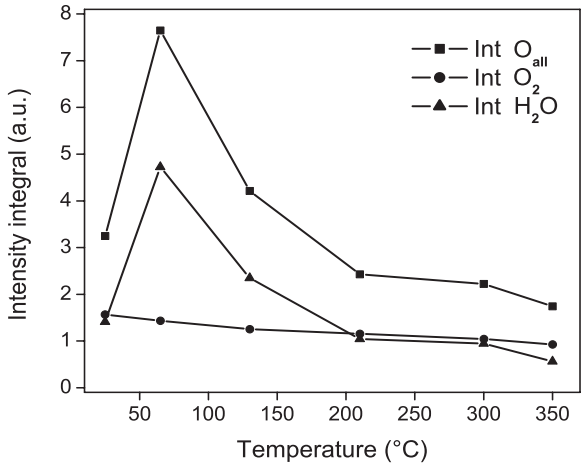

Figure 8: Trends in the O_2 and H_2O evolution during the heating of Fe/ZSM-5 in helium.

3.4. Discussion

In the calcination procedure (using a temperature ramp of 5 °C /min), agglomeration of the binuclear Fe complexes toward inactive oxide/hydroxide clusters is significant.[8] Thus, some of the iron is present in the form of iron oxide clusters instead of binuclear clusters. The iron in the iron oxide clusters is octahedral Fe^{III} and also the binuclear complexes contain octahedral Fe^{III}. Figure 9a shows a possible structure for the binuclear complexes in overexchanged Fe/ZSM-5 in air at room temperature, based on the structures derived by Battiston and co-workers.[9] It shows the binuclear complexes (cylinders and balls) within the ZSM-5 zeolite framework (thin lines), looking parallel to the 10-membered pores. The Fe atoms are bound to two O atoms of the zeolite framework neighboring an Al atom. In addition, they are connected via two hydroxo bridges to each other. Further bonding exists to a hydroxide group and to a water molecule. This yields two sixfold-coordinated sites. Figure 9a and b have been created with Cerius[2], using an optimization of the binuclear complexes with universal force field (UFF) parameters.[30] The zeolite lattice has been fixed and only the nonframework O, H, and Fe atoms were optimized. The two Al positions were chosen at a distance similar to the average Al–Al distance within ZSM-5 for a Si/Al ratio of 17. Both Fe atoms in the structure are octahedrally surrounded, where the bottom Fe atom has a significantly distorted octahedron. The Fe–Fe distance is 3.05 Å in this structure, in agreement with the structure as derived from *in situ* extended X-ray absorption fine structure (EXAFS) analysis.[9] For many Al–Al distances that allowed the formation of binuclear centers, the iron distances were constantly similar to this value.

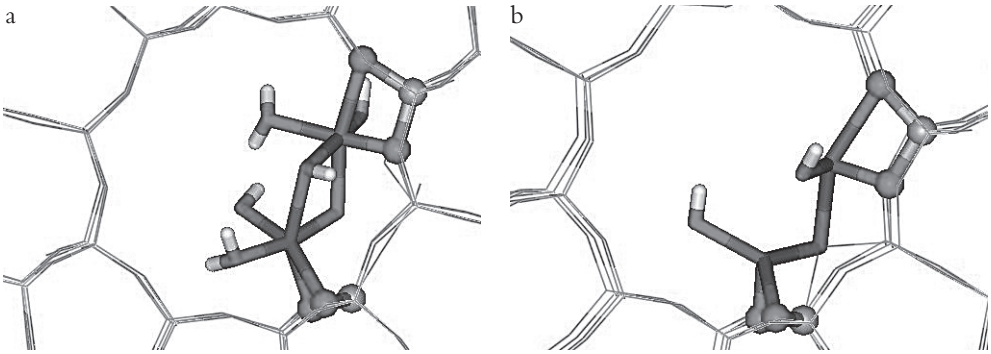

Figure 9: Models of possible structures for Fe/ZSM-5 (a) at room temperature in air and (b) in helium at 350 °C. The binuclear center is highlighted within the ZSM-5 zeolite framework (thin lines), Fe (dark sticks) and Al (light balls). O is indicated in gray (as gray lines in the framework and gray sticks/balls in the binuclear center), H is represented as white sticks, and Si is represented as black lines.

Treatment in helium at room temperature reduces the valence state of Fe from 2.94 to 2.65 for the irradiated portion of the sample and to 2.49 for the nonirradiated portion. First, this implies that the X-rays affect the reduction significantly, a fact that must be kept in mind while performing (soft) X-ray experiments on sensitive materials. The average valence of ~ 2.5 implies that, of the binuclear centers, on average, one Fe is reduced to Fe^{II}, and the other remains Fe^{III}. It could also indicate that some of the binuclear complexes are more reactive than others (for example, because of the depth at which they are located within the channels or due to the anchoring site, i.e., the position of the Al binding atoms within the zeolite). Spectral shape analysis showed that the Fe^{II} site is (distorted) tetrahedral, which suggests the presence of binuclear centers that consist of a combination of octahedral Fe^{III} with tetrahedral Fe^{II}. The change from six to four neighbors implies that the Fe^{III} sites will have to lose water molecules. The analysis of the hard X-ray data in references 8 and 9 suggested that, at lower temperatures, the number of neighbors is reduced faster than the change of the iron valance. This observation is further confirmed by the fact that the water loss is highest at ~ 60 °C. It can be concluded that a large amount of loosely bound water escapes from the zeolite at temperatures < 100 °C and some of this water originates from the binuclear iron sites.

Heating in helium to 350 °C leads to a further reduction of Fe to an average valence of 2.16. This number is lower than the average valence of 2.4 that has been determined from hard X-ray absorption near edge structure (XANES) analysis. This difference is probably due to the difference in probing depth (5 nm for the soft X-ray L edges versus several μm for the hard X-ray K edge. An average valence of very close to 2.0 implies that most of the iron is present in (binuclear) sites that consist of (two) tetrahedral Fe^{II} sites (in other words, the removal of two O neighbors from each Fe atom). Figure 9b shows a possible structure of the two tetrahedral sites. Starting with Figure 9a, the two bridging hydroxide groups lose water, where the bridging between the Fe atoms is modified to a free O atom and a framework O atom. In addition, the two water molecules are lost, followed by the loss of the bridging free O atom. This creates two Fe tetrahedral sites bridged only by a framework O atom. Note that, in the force field calculation also, this bridging framework O atom was optimized, as can be observed in Figure 9b. The Fe–Fe distance of this cluster is 3.00 Å, which confirms the trend that was determined from EXAFS.[9] The loss of oxygen and water is confirmed by the gas-phase oxygen signal. This observation implies that Fe^{II} sites are spatially close together, because they share a framework O atom. As we show in chapter 4, a reoxidation can readily restore the bridging O atom between these close Fe^{II} sites. Reoxidation in O_2 creates two octahedral Fe^{III} sites within a matter of minutes.

3.5. Conclusions

Charge-transfer multiplet calculations provide a detailed theoretical understanding of the $L_{2,3}$ spectra of iron in Fe/ZSM-5. The oxidized form of Fe/ZSM-5 has iron in an octahedral surrounding, with a total crystal-field splitting of ~ 1.0 eV, which is considerably less than that of bulk Fe_2O_3. This indicates much weaker Fe–O bonding. The reduced form of Fe/ZSM-5 has a tetrahedral surrounding of oxygen.

The Fe^{II} and Fe^{III} L_3 X-ray absorption spectra allow for an accurate determination of the valence under various conditions. The Fe species in Fe/ZSM-5 undergo autoreduction to a valence of 2.68 in helium at room temperature. During heating to 350 °C, the valence is further reduced to 2.16. The introduction of oxygen causes fast reoxidation of the system to almost-pure Fe^{III}.

We have shown that *in situ* soft X-ray absorption provides an additional tool to determine the oxidation/reduction behavior of Fe/ZSM-5. It yields new information on the geometry and valence of the Fe sites and it provides an accurate method to determine the average iron valence during oxidation/reduction cycles.

References

1. Knop-Gericke, A.; Hävecker, M.; Neisius, T.; Schedel-Niedrig, T. *Nucl. Instrum. Methods Phys. Res., Sect. A* **1998**, *406*, (2), 311-322.
2. Hävecker, M.; Knop-Gericke, A.; Schedel-Niedrig, T. *Appl. Surf. Sci.* **1999**, *142*, 438-442.
3. Knop-Gericke, A.; Hävecker, M.; Schedel-Niedrig, T.; Schlögl, R. *Top. Catal.* **2000**, *10*, 187-198.
4. Panov, G. I.; Uriarte, A. K.; Rodkin, M. A.; Sobolev, V. I. *Catal. Today* **1998**, *41*, 365-385.
5. Ribera, A.; Arends, I.; De Vries, S.; Perez-Ramirez, J.; Sheldon, R. A. *J. Catal.* **2000**, *195*, 287-297.
6. Chen, H. Y.; Voskoboinikov, T.; Sachtler, W. M. H. *J. Catal.* **1998**, *180*, 171-183.
7. Wang, X.; Chen, H. Y.; Sachtler, W. M. H. *J. Catal.* **2001**, *197*, 281-291.
8. Battiston, A. A.; Bitter, J. H.; de Groot, F. M. F.; Overweg, A. R.; Stephan, O.; van Bokhoven, J. A.; Kooyman, P. J.; van der Spek, C.; Vankó, G.; Koningsberger, D. C. *J. Catal.* **2003**, *213*, 251.
9. Battiston, A. A.; Bitter, J. H.; de Groot, F. M. F.; Heijboer, W. M.; Koningsberger, D. C. *J. Catal.* **2003**, *215*, 279.
10. Garten, R. L.; Delglass, W. N.; Boudart, M. *J. Catal.* **1970**, *18*, 90-107.
11. Lobree, L. J.; Hwang, I. C.; Reimer, J. A.; Bell, A. T. *J. Catal.* **1999**, *186*, 242-253.
12. Joyner, R.; Stockenhuber, M. *J. Phys. Chem. B* **1999**, *103*, 5963-5976.
13. Pérez-Ramírez, J.; Mul, G.; Kapteijn, F.; Moulijn, J. A.; Overweg, A. R.; Doménech, A.; Ribera, A.; Arends, I. W. C. E. *J. Catal.* **2002**, *207*, 113-126.
14. Marturano, P.; Drozdova, L.; Pirngruber, G. D.; Kogelbauer, A.; Prins, R. *Phys. Chem. Chem. Phys.* **2001**, *3*, 5585-5595.
15. Nováková, J.; Kubelková, L.; Wichterlová, B.; Juška, T.; Dolejšek, Z. *Zeolites* **1982**, *2*, 17-22.

16. Jacobs, P. A. *Stud. Surf. Sci. Catal.* **1986**, *29*, 357-414.
17. Chen, H. Y.; Sachtler, W. M. H. *Catal. Today* **1998**, *42*, 73-83.
18. Battiston, A. A.; Bitter, J. H.; Koningsberger, D. C. *Catal. Lett.* **2000**, *66*, 75-79.
19. Abbate, M.; Goedkoop, J. B.; De Groot, F. M. F.; Grioni, M.; Fuggle, J. C.; Hofmann, S.; Petersen, H.; Sacchi, M. *Surf. Interface Anal.* **1992**, *18*, 65-69.
20. Outka, D. A.; Madix, R. J.; Stöhr, J. *Surf. Sci.* **1985**, *164*, 235.
21. Van Aken, P. A.; Liebscher, B. *Phys. Chem. Miner.* **2002**, *29*, 188-200.
22. Crocombette, J. P.; Pollak, M.; Jollet, F.; Thromat, N.; Gautier-Soyer, M. *Phys. Rev. B* **1995**, *52*, 3143-3150.
23. Kuiper, P.; Searle, B. G.; Rudolf, P.; Tjeng, L. H.; Chen, C. T. *Phys. Rev. Lett.* **1993**, *70*, 1549-1552.
24. Colliex, C.; Manoubi, T.; Ortiz, C. *Phys. Rev. B* **1991**, *44*, 11402-11411.
25. de Groot, F. M. F.; Fuggle, J. C.; Thole, B. T.; Sawatzky, G. A. *Phys. Rev. B* **1990**, *41*, 928.
26. de Groot, F. M. F.; Fuggle, J. C.; Thole, B. T.; Sawatzky, G. A. *Phys. Rev. B* **1990**, *42*, 5459.
27. de Groot, F. M. F. *J. Electron. Spectrosc. Relat. Phenom.* **1994**, *67*, 529-622.
28. de Groot, F.M.F. *Chem. Rev.* **2001**, *101*, 1779-1808.
29. Hitchcock, A. P.; Stöhr, J. *J. Chem. Phys.* **1987**, *87*, 3253-3255.
30. Cerius^2 is a modeling and simulation software package, created by Molecular Simulations, Inc. (MSI), which is now Accelrys. See http://www.accelrys.com/cerius2/.

4

Redox behavior of overexchanged Fe/ZSM-5 zeolites studied with *in situ* soft X-ray absorption spectroscopy

Based on: W. M. Heijboer, A. A. Battiston, A. Knop-Gericke, M. Hävecker, H. Bluhm, B. M. Weckhuysen, D. C. Koningsberger and F. M. F. de Groot, *Phys. Chem. Chem. Phys.*, 2003, **5**, 4484 - 4491

Abstract

The oxidation and reduction behavior of calcined overexchanged Fe/ZSM-5 has been studied using *in situ* soft X-ray by measuring the average iron valence under helium, oxygen and deNOx conditions between room temperature and 350 °C absorption (under 2 mbar pressure and with a probing depth of ~ 4 nm). The results show that Fe/ZSM-5 is an extremely flexible redox system. The calcination procedure (severe calcination: heating rate 5 °C/min, as normally used in the literature; mild calcination: heating rate 0.5 °C/min) is proven to be important to optimise the reducibility of iron. Upon a mild calcination Fe/ZSM-5 has an average valence of 2.9 under O_2 (5 % in helium), of 2.5 under pure helium at room temperature, and of 2.1 under pure helium at 350 °C. Upon a severe calcination Fe/ZSM-5 shows higher average valences, in agreement with the assumption that part of the iron in this sample is positioned in small iron oxide nanoparticles at the outer surface of the zeolite crystals. During heating in helium, the valence reaches a minimum value before slightly rising again (reoxidation) when the temperature is kept constant. It is also found that the X-ray irradiation is able to affect the average valence by values up to 0.10. This study confirms that iron in overexchanged Fe/ZSM-5 consists dominantly of highly reactive iron complexes, where the iron is (distorted) octahedral Fe^{III} in the oxidized state. The implications for the reaction mechanism for the N_2O decomposition and the nature of the α-oxygen sites are discussed, in relation to recent developments in the understanding of iron non-heme enzymes.

4.1. Introduction

Over the past years, Fe containing ZSM-5 has been the subject of an extensive body of research. ZSM-5 with an iron loading below 1 wt % is an active catalyst for the decomposition of N_2O[1,2] and for the selective oxidation of hydrocarbons, for example benzene to phenol, using N_2O as oxidant.[3,4] Overexchanged Fe/ZSM-5, with an iron loading up to around 5 wt %, is an effective catalyst for the reduction of nitrogen oxides in the presence of excess oxygen, the Hydro-Carbon assisted Selective Catalytic Reduction (HC-SCR) of NO.[5,6]

Recently, much attention has been paid to the identification and characterization of the active iron phases in FeZSM-5. A complex factor in the discussions is the large diversity of the studied FeZSM-5 materials. A variety of synthesis and activation routes are used and there are qualitative differences in the Si/Al ratio, iron loading, parent ZSM-5 materials and iron precursors.

The activation of framework-substituted FeZSM-5 is performed by calcination *in vacuo* or by steaming at high temperature. During these procedures, different Fe-containing species are formed.[4,7] These species vary from isolated extraframework Fe oxo-ions (Fe_1), binuclear oxo-iron complexes (Fe_2) and oligonuclear oxo-iron complexes (Fe_N) located in the zeolite channels, to larger iron-oxide nanoparticles whether or not located on the external surface of the zeolite (FeO_x or Fe_2O_3). These FeO_x nanoparticles have been shown to be inactive. The selective oxidation properties of FeZSM-5 are indeed ascribed to dispersed Fe-containing species in the zeolite channels. According to Panov and co-workers steam treatments cause the formation of extraframework binuclear iron species by extraction of iron from the zeolite matrix into the micropores. Upon reaction with nitrous oxide these iron centres are believed to generate a particularly reactive oxygen species.[3] This species, so-called α-oxygen, is believed to be capable of the oxidation of benzene to phenol, already at room temperature. Sachtler and co-workers have performed a number of isotopic exchange studies on Fe/ZSM-5.[8,9] They have shown that Fe/ZSM-5, previously reduced at temperatures above 500 °C and reoxidized by N_2O, exchanges oxygen very rapidly at 250 °C. This oxygen exchange involves fairly isolated oxygen atoms as can be inferred from the R^1 mechanism, resulting in the production of $^{18}O^{16}O$ oxygen molecules. The authors speculate that Fe^{III} first needs to be reduced to Fe^{II}, where these Fe^{II} sites are brought into a situation of coordinative unsaturation. Reaction with N_2O then possibly creates mononuclear $[Fe{=}O]^{2+}$ sites or diamond core $[Fe_2O_2]^{2+}$ sites as possible "α-oxygen" sites. These speculations are partly originating from recent developments in iron non-heme enzymes, where such diamond core sites play a crucial role. An important route to create active oxygen species in iron non-heme enzymes can be written as:

$$Fe^{II} \xrightarrow{O_2} Fe^{II}O_2 \xrightarrow{H^+,e^-} Fe^{III}OOH \xrightarrow[OH^\bullet]{} Fe^{IV}{=}O$$

This and related routes are the subject of much research and evidence for such reaction schemes in iron non-heme enzymes and their model compound analogues is building up quickly.[10-13] In relation with Fe/ZSM-5, it should be mentioned that in both

systems the $Fe^{IV}=O$ state seems to be generated from a starting situation containing reduced Fe^{II}, i.e. the $Fe^{IV}=O$ state does not seem to be directly obtainable from a Fe^{III} state.

In general, substitution of Fe in the framework of ZSM-5 results in a maximum iron loading of 1 wt %. By introducing iron in extraframework positions by post-synthesis methods, on the contrary, a higher iron loading is possible, with either ion exchange or sublimation. Binuclear Fe oxo/hydroxo species located at the Brønsted sites position of the framework have been proposed to be the active phase also in Fe/ZSM-5 prepared by the sublimation of anhydrous $FeCl_3$.[5] Iron species are sensitive towards washing, calcination, steaming, reduction and oxidation treatments. In particular, Fe-binuclear complexes can undergo agglomeration during calcination, finally resulting in the formation of inactive goethite and hematite crystals on the external surface of the zeolite. It has been demonstrated in a previous study by our group[14] that the agglomeration of iron in Fe/ZSM-5 can be controlled by adequately tuning the conditions applied during calcination. As such, Fe/ZSM-5 with an estimated amount of binuclear Fe species higher than 70 % can be obtained by applying a mild calcination procedure, using a moderate temperature ramp (heating rate 0.5 °C/min) and a high specific gas flow-rate (800-1000 ml/min·g). A severe calcination procedure (heating rate: 5 °C/min) as often applied to Fe/ZSM-5 samples studied in the literature leads to a significant agglomeration of the iron complexes towards the formation of iron-oxide clusters at the outer surface of the zeolite crystals.

The autoreduction ability of iron in Fe/ZSM-5 is observed by several authors[7,15-18] and has been investigated by our group for mildly calcined Fe/ZSM-5 using Fe K-edge X-ray absorption spectroscopy (XAS)[19]. In the previous chapter of this thesis we have shown that *in situ* soft X-ray absorption spectroscopy can be applied to determine the structural and electronic properties of the Fe species present in zeolites.[20] The Fe $L_{2,3}$ XAS spectral shape can be simulated in detail, using a charge transfer multiplet code.[21,22] This yields precise information on the electronic ground state of iron, including its number of 3d-electrons, (i.e. its valence state), its spin state, crystal field value, local geometry and degree of covalence. In chapter 3 it has been shown that, by optimizing the procedure applied for the collection of the $L_{2,3}$-edge XAS spectrua, a precise determination of the iron valence can be obtained with a time resolution of approximately one minute.[20]

The objective of this work is to study the reduction and oxidation properties of the iron species present in Fe/ZSM-5, calcined via both the mild and severe calcination procedures. The changes in the iron oxidation state, related to the reactivity of the weakly bound oxygen is of particular interest since it represents the key-step for the decomposition of N_2O, as well as for the HC-SCR of NO.[23] The oxidation state of iron and its local environment in calcined Fe/ZSM-5 samples have been followed during heating treatments in helium by *in situ* soft X-ray absorption spectroscopy measurements at the iron $L_{2,3}$ edge and the oxygen K-edge.

4.2. Experimental

4.2.1. Catalyst preparation and characterization

Overexchanged Fe/ZSM-5 was prepared following the $FeCl_3$ sublimation technique (also called chemical vapour deposition (CVD)), proposed by Chen and Sachtler,[5] and described in more detail in a previous publication.[14] The H^+ removal efficiency (98 %), determined by HCl titration, indicated that during the Fe-exchange procedure nearly all the Brønsted acid sites were removed from the H/ZSM-5.

Particular attention was paid to the calcination procedure. Fe/ZSM-5 was calcined in two different ways. In the case of the *mild calcination* procedure (further denoted by 'mc'), the sample was heated to 200 °C in a PFR-reactor under a specific helium flow of 800 ml/min·g and with a moderate temperature ramp (0.5 °C/min). At this temperature, 200 ml/min·g of O_2 was added to the helium flow while, under the same temperature ramp, heating was continued to 550 °C. After 3 h at 550 °C, the temperature was decreased to 30 °C. The *severely calcined* sample (further denoted by 'sc') was heated under 120 ml/min·g flowing oxygen in a tubular oven using a temperature ramp of 5 °C/min and was calcined at 550 °C for 3 h. The crystalline fingerprint of the zeolitic support was monitored after each synthesis step by XRD. On the basis of these measurements lattice damage or formation of large iron oxides phases could be excluded, even upon calcination. Elemental analysis by Inductively Coupled Plasma (ICP) was carried out to determine the silicon/aluminium ratio (Si/Al = 17.0) and the iron loading (Fe/Al = 0.97) of the obtained Fe/ZSM-5.

4.2.2. *In situ* soft X-ray Absorption Spectroscopy

Samples treatments

Soft X-ray absorption experiments were carried out to investigate the valence of Fe and the nature of the evolving gasses during various chemical and heat treatments. The Fe/ZSM-5 samples investigated in this study and the treatments performed during the collection of the data are indicated in Table 1. All the measurements were performed under dynamic atmospheres (flowing gases). The severely calcined sample (Fe/ZSM-5-sc) was inserted into the chamber, which was subsequently pumped down to vacuum. After approximately 15 min the chamber was brought under 5 % O_2 in helium (O_2-25). After stabilisation at the maximum Fe-valence, the atmosphere was first switched to pure helium (t = 0; He-25) to study the autoreducibility of the sample at room temperature. After 150 min, the temperature was increased from 25 °C to 350 °C with a ramp of 2.7 °C/min at 2 mbar helium. At a time of 280 min the temperature of 350 °C was reached (He-350) and the sample was kept under these conditions for one hour. At a time of 340 min we switched to 5 % O_2 in helium again (O_2-350), to study the reoxidation behavior at 350 °C, followed by switching to helium at a time of 410 min (He-350) in order to study the reversibility of the autoreduction behavior. Fe/ZSM-5-mc and α-FeO(OH) were treated in exactly the

same manner as Fe/ZSM-5-sc. A second Fe/ZSM-5-mc sample (from the same batch) was also investigated. To distinguish between the two samples, the second one has been given a subscript 2 (see Table 1). The same treatment was applied also to this second sample, but upon preheating in helium at 350 °C and cooling to room temperature. In addition, the Fe/ZSM-5-mc_2 sample was measured under DeNOx (HC-SCR) conditions (0.2 vol % NO, 0.2 vol % i-C_4H_{10}, 3 vol % O_2 balanced with He to 100 ml/min; DeNOx-350) instead of under 5 % O_2 in helium. Table 1 outlines the step-by-step treatments of the four samples.

Table 1: Overview of the Fe/ZSM-5 samples

sample	measurement conditions
Fe/ZSM-5–sc	O_2-25 → He-25 → He-ramp to 350 → He-350→ O_2-350 → He-350
Fe/ZSM-5–mc_1	O_2-25 → He-25 → He-ramp to 350 → He-350→ O_2-350 → He-350
Fe/ZSM-5–mc_2	He-25 → He-ramp to 350 → He-350 → He-ramp to 25 →
	O_2-25 → He-25 → ramp to 350 → He-350 → DeNOx-350
α-FeO(OH)	O_2-25 → He-25 → He-ramp to 350 → He-350→ O_2-350 → He-350

O_2-25 indicates 5 % O_2 in helium at 25 °C. The DeNOx (HC-SCR) conditions use 0.2 vol % NO, 0.2 vol % i-C_4H_{10}, 3 vol % O_2 balanced with helium to 100 ml min^{-1}

Data collection

The soft X-ray absorption spectra of the iron $L_{2,3}$ edge (700-730 eV) and the oxygen K edge (525-550 eV) were measured at BESSY (Berlin), beamlines U49/2-PGM-1 and UE56/2-PGM-1. The spectral resolution of the monochromators was approximately 0.2 eV. The instrumentation for *in situ* low energy XAS experiments has been developed by Knop-Gericke and co-workers and is described in detail elsewhere.[24-27] A stainless steel *in situ* cell was used in which the powdered zeolite sample was fixed in a sample holder. The flow rates of helium and of 5 % O_2 in helium were 100 ml/min, of which approximately half entered the *in situ* cell. A homemade gas mixing system regulated the flow and the total pressure at the sample position was about 2 mbar during the experiments. A molecular sieve was used in order to remove traces of oxygen when a pure helium flow was flushed (see Table 1). The temperature was increased from room temperature to the reaction temperature of 350 °C with a heating rate of 2.7 °C/min. The X-ray absorption spectral shape was measured with two collector plates. Both detectors measure the ionised gas due to the created electrons in the X-ray absorption process and the subsequent non-radiative decay of the core hole, that is they measure the ionised-gas-conversion total-electron-yield. Detector A measures the gas phase while a detector B close to the sample surface detects both the gas phase and surface signal. By subtraction of the signal of detector A from detector B, the surface signal can be revealed (see Chapter 1). This ionised-gas-conversion total-electron yield based method has a probing depth of approximately 4 nm.[28]

Data processing

For the determination of the iron valence state and the representation of the changes therein during activation treatments and reaction, we measure the L_3 X-ray absorption spectrum.

Figure 1 shows the $L_{2,3}$ X-ray absorption spectra of the most oxidised (top) and most reduced (bottom) Fe/ZSM-5 sample. The oxidised sample was measured after reoxidation under 5 % O_2 pressure and the reduced sample was measured under 5 % H_2. The spectra can be simulated well with charge transfer multiplet calculations of respectively Fe^{III} and Fe^{II}, which implies that these spectra represent pure Fe^{III} respectively Fe^{II} samples. We estimate that the absolute (maximum) error in this assignment to pure Fe^{III} and Fe^{II} is less than 0.05. A more detailed description of the procedure to determine the average valence of Fe is given in chapter 3, where also the charge transfer multiplet calculations have been discussed; they show that the Fe^{III} site is octahedral with weak bonding between iron and oxygen. The Fe^{II} site is found to be (distorted) tetrahedral. Under the assumption that all the iron sites will be similar to either the oxidised site or the reduced site, each Fe $L_{2,3}$ spectrum is a linear combination of these oxidised Fe^{III} and reduced Fe^{II} samples. Although there will be some variation is iron sites, the calculations show that these are expected to be too small to significantly affect the analysis method. We showed before that the procedure of valence determination can be simplified by employing a procedure that uses the intensity ratio at the peak positions for Fe^{II} (708.0 eV) and Fe^{III} (709.5 eV).[20] This is important since it allows significantly faster measurement times. By using only the energy range between 707 eV and 719 eV, the average valence state can be determined with a time interval of 50 s. Periodically, we recorded the complete Fe $L_{2,3}$ spectral shape to check for potential variations in the background. By applying this analysis method, we have monitored the average valence state of the iron present in Fe/ZSM-5 during treatments at temperatures between 25 and 350 °C and with gas flows of helium, O_2 and under deNOx conditions. The relative uncertainty in the average valence of iron could be established to be ~ 0.02.

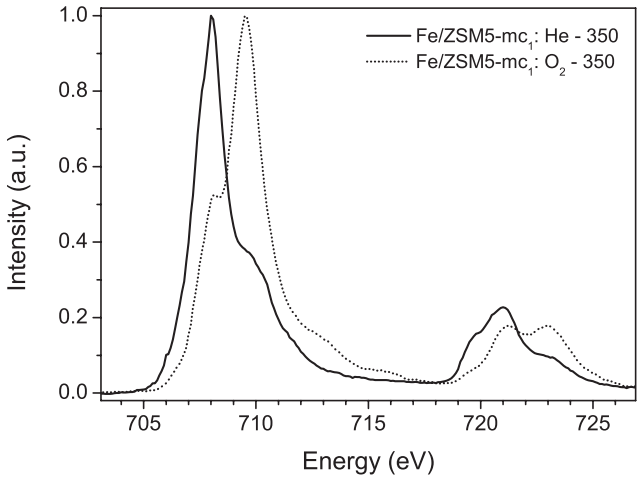

Figure 1: Experimental $L_{2,3}$ X-ray absorption spectra of reduced (solid line) and oxidized (dotted line) mildly calcined Fe/ZSM-5. See Table 2 for details about the samples.

4.3. Results

Figure 2 (up to t = 0 min) shows the variation of the average valence state of iron under an O_2 (5 % in helium) flow of the Fe/ZSM-5–sc and Fe/ZSM-5–mc samples at room temperature and a pressure of 2 mbar. The samples were subsequently exposed to helium for 2 hours. To facilitate the comparison between the redox behavior of the different Fe/ZSM-5 samples the time for switching from O_2 to helium was set to be t = 0 min. The average valence of Fe/ZSM-5–sc under O_2 (5 % in helium) at room temperature shows a value of 2.94 ± 0.01 and stays constant at this value for 50 min. After switching to pure helium the sample reduces in 15 min to a minimum valence of 2.64, followed by a slight reoxidation to a value of approximately 2.67 after 110 min. This slight overshooting behavior has also been observed with hard X-ray absorption,[19] which rules out any specific surface effect (see discussion). The mildly calcined sample, Fe/ZSM-5–mc, shows an oxidation to 2.92, which is less than for the severely calcined sample. It should nevertheless be noted that for this sample the oxidation time was 60 min instead of the 90 min for sample Fe/ZSM-5–sc. The reduction in helium shows a similar behavior to that of Fe/ZSM-5–sc but with a minimum valence of 2.61. It is clear from figure 2 that already at room temperature, both the calcined Fe/ZSM-5 samples are subject to significant autoreduction.

During the experiments depicted in figure 2 the samples were exposed to soft X-rays all the time. To check whether the X-rays may have had an influence on the average Fe-valence, we compared the difference between the X-ray irradiated part of the sample and a fresh spot. In case of the Fe/ZSM-5–sc sample the average valence of the spot that was irradiated for 200 min is 2.67, while a fresh spot turned out to have an average valence of 2.49. Apparently, an irradiated area has a higher average valence.

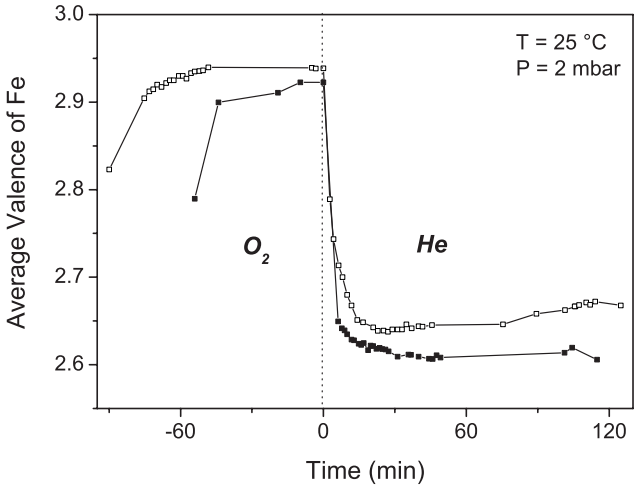

Figure 2: Oxidation in O_2 (5 % in He) and autoreduction in He at room temperature of Fe/ZSM-5, severe (□) and mildly calcined (■).

Table 2: The average valence of iron in the Fe/ZSM-5 samples

	sc	mc_1	mc_2	FeO(OH)	
He - ramp to 350			2.02		
He - 350			2.14		
He - ramp to 25			2.40		
He - 25	2.82	2.78	2.59	2.97	
O_2 - 25	2.94	2.92	2.92	3.00	
He - 25	2.64	2.61	-	3.00	minimum value
	2.67	2.61	-		final value
	2.49	2.44	2.43		fresh spot
He - ramp to 350	2.16	**2.00**	2.16	2.91	
He - 350	2.25	2.10	2.20	2.94	reoxidation
O_2 - 350	2.91	2.89		2.99	
DeNOx - 350			**3.00**		
He - 350	2.54	2.44			

O_2-25 indicates 5 % O_2 in helium at 25 °C, etc. The sample overview of Fe/ZSM-5–sc is indicated with sc, etc.; the mc_2 sample is measured through two temperature ramps as discussed in the text; the boldface valences of 2.00 and 3.00 indicate the spectra that have been used for calibration

Figure 3 shows the changes in the average valence state of iron, while heating the Fe/ZSM-5 samples from 25 °C to 350 °C at 2 mbar helium with a ramp of approximately 2.7 °C/min. A temperature of 350 °C was chosen as it corresponds to the optimal working temperature of Fe/ZSM-5 for the HC-SCR reaction with iso-butane. During heating in helium from room temperature to 350 °C the average valence of the severely calcined sample Fe/ZSM-5–sc reduced from 2.49 to 2.16. The gap between 225 min and 255 min is related to a re-injection of electrons into the storage ring. After reaching the final temperature of 350 °C, we observe a slight reoxidation from 2.16 to 2.25. The average oxidation state of Fe/ZSM-5–mc/s reduced from 2.44 to 2.00 as a result of heating in helium from room temperature to 350 °C. Also in the case of the mildly calcined sample we see a small re-oxidation to a value of 2.10 is observed while keeping the temperature constant at 350 °C.

Figure 4 shows an oxidation/reduction cycle at 350 °C of the previously autoreduced samples (Figure 2). Reoxidation of Fe/ZSM-5–sc in O_2 (5 % in helium) at 350 °C yields a Fe valence above 2.90 after 10 min. The reoxidation with oxygen of the auto reduced Fe/ZSM-5–mc is slower and leads to an average valence of 2.89 only after one hour. For the Fe/ZSM-5–sc sample the rise of the valence upon oxidation with oxygen is much faster than for the mildly calcined sample. After applying an O_2 (5 % in helium) atmosphere to the samples for 70 min, we switched back to helium, inducing a drop of the average iron valence to 2.54 and 2.44 for Fe/ZSM-5–sc and Fe/ZSM-5–mc, respectively. The reduction is more pronounced and occurs faster for the mildly calcined Fe/ZSM-5 sample. Although this reduction (at t = 450 min) is significant, for both the severely and mildly calcined samples the valence state of iron is higher than the minimum valence reached upon autoreduction in helium during the experiments described in Figure 3. Most of this difference is attributed

to the fact that in this case the measurements were interrupted before reaching the steady state.

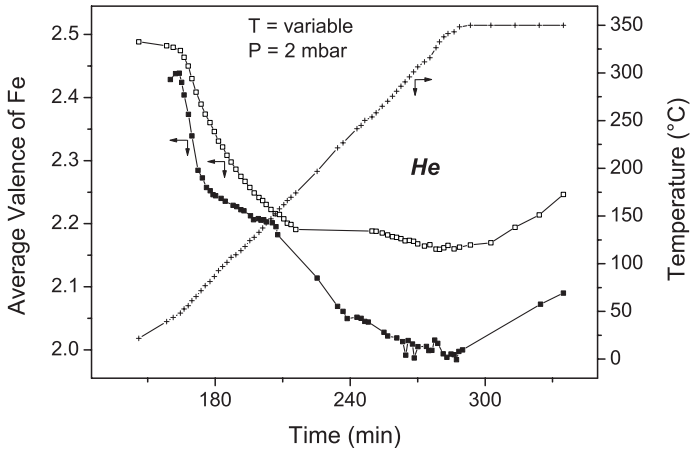

Figure 3: Autoreduction in He from room temperature to 350 °C (+) of Fe/ZSM-5, severe (□) and mildly calcined (■).

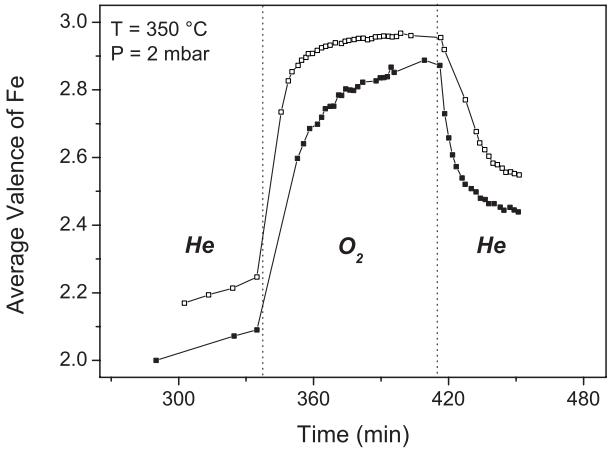

Figure 4: Reversible oxida-tion in O_2 (5 % in He) at 350 °C after autoreduction in He of Fe/ZSM-5, severe (□) and mildly calcined (■).

Figure 5 shows the effect of the temperature on the valence of iron in a continuously flushed helium atmosphere. As already mentioned, this experiment was carried out with a new mildly calcined sample (Fe/ZSM-5–mc_2). During heating in helium the autoreduction of iron follows the same pathway, within a deviation of 0.02, as in the equivalent experiment with sample Fe/ZSM-5–mc_1. Flushing the sample with helium for one hour at 350 °C again results in a reoxidation, from a minimum valence of 2.02 to 2.14. Upon cooling, the sample further reoxidizes to a final valence of 2.59 (room temperature). An almost complete and very fast oxidation is observed upon switching from helium to O_2 (5 % in helium) at room temperature, yielding a final average valence of 2.92, i.e. the same value as obtained during the experiment shown in Figure 3.

After the heating cycle in helium (RT → 350 °C → RT) and subsequent room temperature oxidation with O_2 (5 % in helium) as depicted in Figure 5, the Fe/ZSM-5-mc_2 sample was heated in helium (same gas flow, heating ramp) as shown in Figure 6. The gap between 330 min (Figure 5) and 380 min (Figure 6) is due to re-injection of electrons in the storage ring. The change of the valence is exactly the same as for the first heating ramp shown in Figure 5, but there is a 'delay' and the same average valence is reached at some 50 °C higher. In addition, from 200 to 350 °C the average valence of iron is hardly changing and the minimum valence does not go below 2.16. After the second heating ramp in helium to 350 °C, the (auto)reduced Fe-ZSM-5–mc_2 sample was flushed with a gas mixture with the same composition of that used during DeNOx (HC-SCR) catalytic tests previously performed in our laboratory and described elsewhere.[29] The gas flow contained 0.2 vol % NO, 0.2 vol % i-C_4H_{10}, 3 vol % O_2 balanced with helium to 100 ml/min. Upon switching to the DeNOx gas mixture the valence of iron is rapidly increased to 3.00 (within 15 min).

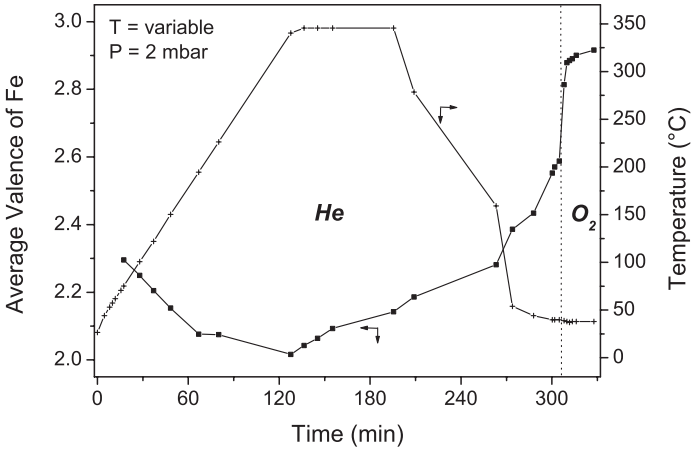

Figure 5: Reversible auto-reduction in He of Fe/ZSM-5, mildly calcined (■), upon heating to 350 °C and cooling down to RT and subsequent oxidation in O_2 (5 % in He) at RT.

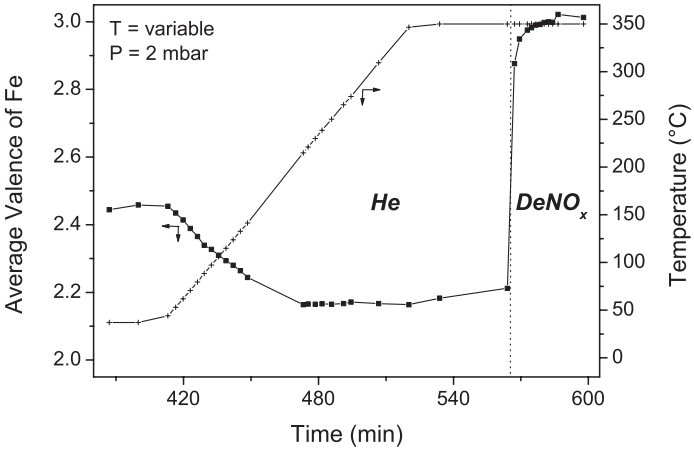

Figure 6: Reversible oxidation in DeNOx (HC-SCR) gas mixture (3% O_2, 0.2% NO and 0.2% i-C_4H_{10} in He) at 350 °C after autoreduction in He of Fe/ZSM-5, mildly calcined (■).

Despite the lower oxygen concentration (3 % vs. 5 %) and notwithstanding the presence of iso-butane the observed reoxidation is faster recorded under HC-SCR conditions than that measured with just oxygen (For this purpose, compare Figures 1 and 3).

In previous studies on the nature of the iron phases in overexchanged Fe/ZSM-5, α-goethite was suggested to be present. Indeed, small Fe-containing particles on the external surface of severely calcined Fe/ZSM-5 samples were investigated by electron microscopy and turned out to contain a crystalline iron oxide phase with a d-spacing similar to α-goethite. However, the d-values were also close[14] to those of both β-goethite and hematite (α-Fe_2O_3).[18] To investigate the redox behavior of goethite, pure α-goethite (FeO(OH)) was treated in the same way as the Fe/ZSM-5 samples. In Figure 7 the changes in the average iron valence state of goethite are shown, while heating in helium from room temperature to 350 °C and subsequent oxidation by O_2 (5 % in helium). Upon heating two neighboring surface iron-hydroxyl groups may condense, resulting in the formation of a water molecule, a single surface iron-oxygen group and a coordinatively unsaturated iron atom. The formation of such coordinatively unsaturated iron species at the surface causes a slight decrease in the average valence state of iron to 2.9 (t = 152 min). Reoxidation by exposure to oxygen yields almost exclusively trivalent iron. We note again that soft X-ray absorption (in the electron-yield mode) probes only a top layer of approximately 4 nm, implying that the valence change from 3.0 to 2.9 reflects a slight reduction of the surface iron species only.

Figure 8 shows the oxygen K edge spectra of goethite at room temperature and at 350 °C in pure helium and of hematite at room temperature in pure helium. The change in the nature of the surface oxygen groups in the iron oxy-hydroxide structure of goethite upon heating is clearly visible in these oxygen K edge spectra. Before the heating cycle the well-known three peaked pre-edge of hydroxyls such as in goethite is visible.[30] After the heating cycle and reoxidation the three-peaked spectrum is modified to a two-peaked spectrum, identical to the spectrum of pure hematite (Fe_2O_3). The complete absence of the third peak indicates that at least the top 10 nm of the goethite sample has been changed into hematite.

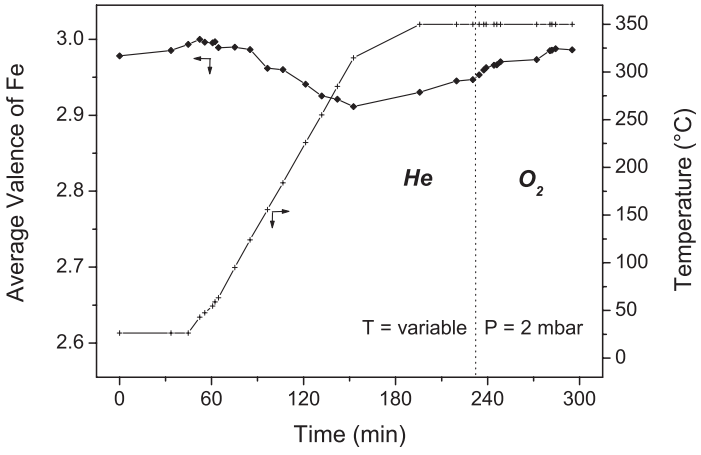

Figure 7: Changes in the average valence state of iron (■) during surface dehydro-xylation of FeO(OH) to Fe_2O_3 while heating in He from RT to 350 °C, and subsequent oxidation of the surface by O_2 (5 % in He) at 350 °C.

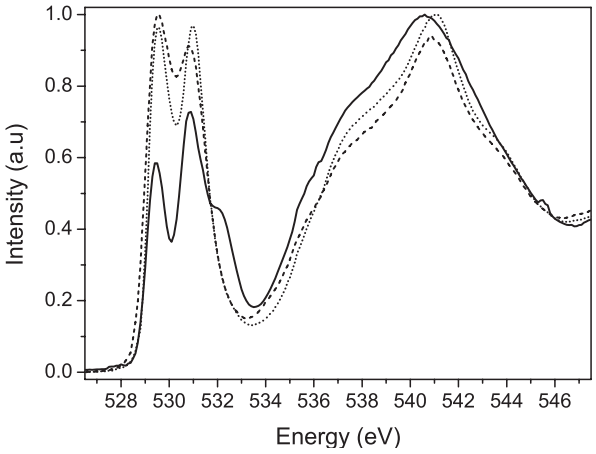

Figure 8: O 1s X-ray absorption spectrum of FeO (OH) at RT in He (solid line), FeO(OH) at 350 °C in He (dashed line) and Fe_2O_3 at RT in He (dotted line).

4.4. Discussion

4.4.1. The oxidation-reduction behavior

Table 2 collects the average valences of the Fe/ZSM-5 samples and goethite measured under various conditions. One can summarize the major features of Table 2 as follows. The valence of all Fe/ZSM-5 samples measured under O_2 (5 % in helium) is approximately 2.9, in other words the Fe/ZSM-5 samples are almost completely oxidised under this condition. Only under DeNOx (HC-SCR) conditions, the average valence reaches its (assumed) maximum value of 3.0 ± 0.1. Note that if the average valence under O_2 (5 % in helium) is set to 3.0, the average valence under DeNOx conditions would reach a value slightly larger than 3.0, thereby suggesting the existence of some Fe^{IV} sites, as will be dwelled upon below in relation to the active site in Fe/ZSM-5. The average valence under helium is depending on the temperature. At 25 °C a value around 2.6 is found for irradiated samples, 2.5 for fresh spots. At 350 °C an average valance of 2.2 is emerging. All these values are almost independent of the sample measurement history. There are however small variations and trends visible that will be discussed below.

At the switching point between Figures 2 and 3 we moved to a fresh spot, in order to test the effects of the X-rays on the average valence. The effects are a reduction in the average value from 2.67 to 2.49 for the Fe/ZSM-5–sc sample and from 2.61 to 2.44 for Fe/ZSM-5–mc. The cause of the lower average valence for the non-irradiated spots is not obvious. On the one hand, one would expect the X-rays to have an *oxidative effect:* due to the ionising Auger decay of the iron sites, i.e. an absorption process at a Fe^{II} ($3d^6$) site creates a Fe^{II} ($2p^53d^7$) site that loses one or more electrons via Auger decay. Although the Auger decay is largely screened by other electrons, one may still expect an effective oxidation. On the other hand, one would expect the temperature at the irradiated spot to be higher than at the non-irradiated spot and as shown above, an increased temperature leads to a decrease of the average valence of iron in Fe/ZSM-5. Apparently this temperature effect

is more important, at least at room temperature. Exactly the opposite effect is observed for the situation with a temperature of 350 °C. In those cases the non-irradiated part of the sample tends to have a higher average valence, in other words in those cases the ionising effect seems to dominate over the temperature effect. This is most likely due to the fact that at 350 °C the temperature effect of the X-rays will be negligible. From this discussion it is clear that upon irradiation the average valence state of iron will be slightly affected, which should be kept in mind for all the results shown.

Next, we would like to focus on the *overshoot* effects. In Figure 2 it can be observed that during treatment in helium at room temperature, the average valence of the Fe/ZSM-5–sc sample goes down to 2.64 after 30 min, before rising again to 2.67. One could imagine that this effect could be due to the surface sensitivity of soft X-ray absorption, i.e. to the fact that the surface of the system reduces more quickly than iron deeper inside the zeolite. When the system then reaches a steady state situation, the surface recovers the average valence of the system. This would be a valid interpretation, however, a similar reoxidation was observed by our group also during hard X-ray absorption experiments.[19] A possible explanation is that the observed phenomenon is due to dynamical effects: depending on the conditions at hand, a steady state situation is often approached via an overshoot situation. The detailed mechanism by which this occurs is difficult to establish, but it will need to increase the iron average valence. Figure 3 shows a much stronger overshoot-situation in that during heating to 350 °C the valence goes down to 2.16 for the Fe/ZSM-5–sc sample (2.00 for Fe/ZSM-5–mc) and after keeping the temperature constant at 350 °C the systems reoxidize again to respectively 2.25 for Fe/ZSM-5–sc and 2.10 for Fe/ZSM-5–mc. In this case the situation is different in the sense that during heating a dynamical situation occurs, with temperature and average valence gradients throughout the sample. In such dynamic situation, it is very likely that the surface reduces more quickly and maintains this reduced state until the temperature becomes constant, thereby allowing also the average valence gradients to establish a steady state situation. Note that this overshoot effect during heating is much larger than in the case when the temperature is not changed at room temperature, i.e. 0.09 respectively 0.03 for the Fe/ZSM-5–sc sample.

Although the redox behavior of the severely and mildly calcined Fe/ZSM-5 samples is similar, by taking a closer look to the path of the curves in the Figures 2 to 4 some important differences can be observed. The Fe/ZSM-5–sc has in all curves a slightly higher average valence than the Fe/ZSM-5–mc samples. This observation is in agreement with the earlier findings[14] that there are larger iron-oxide nanoparticles at the outer surface of the zeolite crystals. These nanoparticles are likely to behave similar to the goethite sample and to have a valence that is close to 3.0 under most conditions. In addition, the reduction in helium is slower for the Fe/ZSM-5–sc sample, while the oxidations of severely calcined samples are faster. Both the slower reduction and faster oxidation indicate the higher affinity for oxygen of severely calcined Fe/ZSM-5. This suggests that the amount of flexible iron complexes in severely calcined samples is less than in the mildly calcined samples. One can also conclude, nevertheless, that even in a severely calcined Fe/ZSM-5 sample the fraction of iron located in inactive species cannot be high. In essence, given that a bulk oxide such as goethite

reaches an average valence of 2.9, a value of 2.2 indicates that this amount must be below 20 %. The difference in average valence between the first (2.02) and second (2.16) heating indicates that some of the iron could not be reduced from Fe^{III} to Fe^{II} in the second heating run. From this observation we conclude that after autoreduction in helium at temperatures up to 350 °C followed by a reoxidation with oxygen, some stable trivalent iron oxide species are formed that are hard to autoreduce.

In order to obtain a reference for the behavior of the most aggregated iron species, we studied iron at the surface of a crystalline iron oxide particle. We showed that heating to 350 °C of pure FeO(OH) results in the dehydroxylation of the surface and the formation of Fe_2O_3. The calcination of overexchanged Fe/ZSM-5 results in the formation of larger iron oxide and/or oxo-hydroxides clusters at the surface. Goethite-like species may be present as intermediates in the formation of stable hematite crystalline structures. However, upon heating to higher temperatures, for instance the DeNOx (HC-SCR) operation temperature of 350 °C, small clusters of goethite will be converted into hematite particles. Although the position of particular features for oxygen-iron bonds in the oxygen K edge spectra are separated from the main edge we were not able to monitor directly the formation of iron oxides as goethite and hematite in calcined Fe/ZSM-5. The abundance of the Fe–O bonds and the changes within them were too small compared to the dominating contribution of the oxygen of the zeolite matrix to the overall intensity.

4.4.2. Implications for the structure and bonding of the active site in Fe/ZSM-5

The precise structure of the iron in overexchanged Fe/ZSM-5 is still under debate. A possible structure is that the hydroxo-bridged Fe atoms are bound via one (or two) oxo-ions to the ZSM-5 framework, where they balance the charge of one (or two) aluminium atom(s).[14,19] Upon calcination (using the temperature ramp of 5 °C/min) agglomeration of the binuclear Fe-complexes towards inactive oxide/hydroxide clusters can be significant. Part of the iron can be present in the form of iron oxide clusters instead of binuclear clusters. We showed, as discussed below, that also upon performing reduction/oxidation cycles at 350 °C additional clustering of binuclear iron complexes to larger agglomerates is likely.

The iron in the oxidised iron oxide clusters is octahedral Fe^{III} and also the binuclear complexes contain octahedral Fe^{III}, bound with one (or two) oxygen atom(s) to the zeolite framework, via two oxo(hydroxo) bridges to each other and by three (or two) hydroxide groups and/or water molecules to make up the five-fold or six-fold coordinated (distorted) octahedral sites.[19] The charge transfer multiplet analysis of the Fe $L_{2,3}$ edge indicates that the crystal field splitting of 1.0 eV is significantly smaller than for Fe_2O_3, implying on average a rather weak iron-oxygen bond. The chemical origin behind this weak bonding is that the structure of the binuclear sites is for a significant part determined by the zeolite structure and the positions of the aluminium atoms therein. In our opinion, the aluminium sites in ZSM-5 can better be understood as randomly distributed than as positioned at special sites,[31] though some site preference might occur. The consequence is that the binuclear iron clusters have to adapt to the different Al locations. This adaptation will lead without

doubt to constraints in the chemical bonding and to coordinatively unsaturated situations, completely different from binary oxides where the structure is essentially determined, and optimised for bonding, by the iron atoms.

We return now to the generation of $Fe^{IV}=O$ (i.e. α-oxygen) states from coordinatively unsaturated Fe^{II} sites. Fe^{II} sites have essentially a S = 2 $3d^6$ ground state and when bound to four neighbors in a distorted tetrahedron, they have an extra spin-down e_g electron in addition to their five spin-up electrons. This spin-down electron is easily accessible to bonding. In contrast Fe^{III} sites have a S = 5/2 $3d^5$ ground state within a distorted octahedron and its five spin-up electrons are strongly bound together. One could imagine that the oxygen atom of N_2O tends to bind to such Fe^{II} site. An isolated Fe^{II} site will not be able to loosen the oxygen from its N_2 counterpart, but the other Fe^{II} site originating from the binuclear iron-cluster can be imagined to bind to the N_2 π-states. The N_2O of the intermediate then breaks its N-O bond neutrally, thereby generating N_2 (bound to an Fe site initially) and O bonded to Fe^{II}. Electronically such intermediate state of Fe^{II} with oxygen couples a $3d^6$ +$3d^7\underline{L}$ configuration with a $\underline{LL}$' configuration of the oxygen atom. These oxygen holes are strongly bonding to iron, thereby creating strong π-bonding, hence short bonds. Effectively, the Fe^{II}–O bond formed as such is able to reorganise to a $3d^4$ + $3d^5\underline{L}$ + $3d^6\underline{LL}$' configuration, where both the σ and π-bonding channels are strong, i.e. there will be large contributions from $3d^5\underline{L}$ and $3d^6\underline{LL}$ into the formally Fe^{IV} $3d^4$ ground state, possibly leaving its actual number of 3d-electrons close to that of the original Fe^{II} site. During this process it possibly helps that the spin state of the Fe^{II} site is not changed in the final state, both being S = 2. The created $Fe^{IV}=O$ state contains the α-oxygen that can act in the oxidation of hydrocarbons. An important difference between iron non-heme enzymes and Fe/ZSM-5 is that the former use O_2 as their α-oxygen source, while Fe/ZSM-5 cannot be activated by O_2, but needs N_2O. A reason could be that O_2 cannot be stabilised on the binuclear iron centres, while the N_2-part of N_2O can use the second iron atom for stabilisation. If the impossibility to use O_2 as a source is further confirmed, this points to a major difference in the oxidation behavior of Fe/ZSM-5 compared with the iron non-heme enzymes.

One could imagine that NO can act similarly to N_2O in the sense that the NO bond gets broken, ending with the $Fe^{IV}=O$ state in combination with a Fe–N site. In case of NO this process needs to be assisted by an activity of the hydrocarbon, for example by stabilising the Fe–N site. If such phenomenon should occur, it would suggest that the average valence of iron could reach a value larger than 3.0, which would imply that the calibration point for the iron valence would be different. The fact that NO + O_2 brings the iron to a valence of 3.0, whereas only O_2 reaches a maximum valence of 2.9, could then also suggest that NO + O_2 brings the system to an average valence slightly larger than 3.0.

In chapter 3, using soft X-ray absorption spectroscopy at the oxygen K edge (probing separately the gas-phase and the surface signal), we showed for Fe/ZSM-5–sc that, at 2 mbar pressure, molecular oxygen and water are released during autoreduction in helium, at room temperature already and during heating to 350 °C.[20] Similar qualitative results are obtained for Fe/ZSM-5–mc. This observation suggests that the bridging oxygen atoms might

have been lost leading to isolated Fe^{II} sites that are spatially close together. As we show in Figure 4 a reoxidation can readily restore the bridging oxygen atoms between these Fe^{II} sites. Reoxidation in O_2 (5 % in helium) at 350 °C creates two (distorted) octahedral Fe^{III} sites within a matter of minutes.

4.4.3. Comparison with Fe K edge XAS

The application of *in situ* soft X-ray absorption spectroscopy is relatively new in the field of catalysis, whereas the hard XAS technique is more often used to determine the valence. The energy position of the (Fe) K edge varies with the valence, at least if the structure and the nature of the neighbours do not vary too much.[32] The procedure to determine the edge position is not uniformly defined and for some systems it is difficult to define the exact edge position. With the use of appropriate references, the edge position can be used to determine the average valence, but because of the complications mentioned above, the quantitative accuracy in valence determination that can be achieved is not good. In addition, the pre-edge region gives valuable information for the determination of the average valence and site symmetry of the iron sites. Wilke *et al.*[33] and Westre *et al.*[34] have proved that the energy position of the centroid and its integrated intensity are good parameters to characterize the pre-edge feature, provided that the pre-edge peak is carefully isolated. The subtraction of the main edge contribution is essential. They showed that the centre-of-gravity of the pre-edge scales with the valence of iron and that the integrated intensity of the pre-edge is related to the site symmetry of the iron, where octahedral sites have the lowest intensity and the tetrahedral sites the highest. Also our group[14,19] and many other groups have employed Fe K edge XAS to study Fe/ZSM-5 and related systems.[15-18,35-37] In these studies the analysis of the pre-edges is, in most cases, only qualitatively and untreated pre-edge peak maxima are used.

The application of soft X-ray absorption spectroscopy for catalysis research benefits from the much higher resolution of soft X-rays together with the relatively large, systematic variation of the spectral features in the – well defined – Fe L_3 edge with the iron oxidation state and the detailed simulation of their spectral shape. It is evident that these factors enable a considerably higher precision in the determination of the average valence of iron, for Fe/ZSM-5 and other (catalytic) systems.

4.5. Conclusions

We have shown that the Fe/ZSM-5 system is an extremely flexible system, with regard to the valence of iron under various conditions. We find that, at a total pressure of 2 mbar, mildly calcined Fe/ZSM-5 has an average valence of 2.9 in O_2 (5 % in helium) – both at room temperature and at 350 °C, of 2.5 under helium at room temperature, and of 2.1 under helium at 350 °C. These values are only slightly depending on the sample measurement history. Severely calcined Fe/ZSM-5 shows values that are approximately

0.03 to 0.05 higher in the (partly) oxidised states, and 0.10 to 0.15 higher in the reduced states. This higher average valence is in agreement with previous observations that part of the iron in this case is positioned in small iron oxide nanoparticles at the outer surface of the zeolite crystals. Such iron oxide nanoparticles, which are more difficult to reduce than the iron clusters inside the Fe/ZSM-5, must nevertheless constitute only a minor part of the total Fe amount, also upon application of a severe calcination procedure.

Changes in the iron valence are accompanied by overshoot effects. During heating in helium, the valence typically reaches a minimum value before slightly rising again (reoxidation), while keeping the temperature constant. A similar, though smaller, effect occurs during autoreduction in helium at a fixed temperature of 25 °C. These overshoot effects are ascribed to local surface-bulk re-equilibration phenomena (kinetic effects) occurring between the iron complexes and the zeolite matrix. Long exposition to soft X-rays can locally affect the average Fe valence by amounts up to 0.10. At room temperature this is essentially due to the heating effects of the X-rays.

The conclusions of this study are in agreement with the model of 'overexchanged' Fe/ZSM-5 as outlined in our previous contributions.[14,19] Iron in the oxidised Fe-complexes is present in a five-fold or six-fold coordinated (distorted) octahedral configuration. Based also on the spectral simulations that were discussed in detail in the previous chapter, we find in the case of the Fe-complexes a ligand field value of only 1.0 eV, i.e. much less than bulk iron oxides. This indicates (on average) a weak bonding between iron and oxygen and is coherent with the low affinity of the Fe-complexes for oxygen. In addition, the spectral simulations imply that the completely reduced Fe/ZSM-5 has lost the bridging oxygen atoms and some of the coordinating water molecules/hydroxide groups and contains almost exclusively Fe in tetrahedral Fe^{II} sites.

References

1. J. Perez-Ramirez, F. Kapteijn, G. Mul and J. A. Moulijn, *Chem. Comm.*, 2001, 693.
2. J. Pérez-Ramírez., F. Kapteijn, G. Mul and J. A. Moulijn, *J. Catal.*, 2002, **208**, 211.
3. G. I. Panov, A. K. Uriarte, M. A. Rodkin and V. I. Sobolev, *Catal. Today*, 1998, **41**, 365.
4. A. Ribera, I. Arends, S. De Vries, J. Perez-Ramirez and R. A. Sheldon, *J. Catal.*, 2000, **195**, 287.
5. H. Y. Chen and W. M. H. Sachtler, *Catal. Today*, 1998, **42**, 73.
6. Q. Zhu, E. J. M. Hensen, B. L. Mojet, J. van Wolput and R. A. van Santen, *Chem. Comm.* 2002, 1232.
7. J. Pérez-Ramírez., G. Mul, F. Kapteijn, J. A. Moulijn, A. R. Overweg, A. Doménech, A. Ribera and I. Arends, *J. Catal.*, 2002, **207**, 113.
8. J. F. Jia, B. Wen and W. M. H. Sachtler, *J. Catal.*, 2002, **210**, 453.
9. T. V. Voskoboinikov, H. Y. Chen and W. M. H. Sachtler, *J. Mol. Catal. A.*, 2000, **155**, 155.
10. J. A. Kovacs, *Science*, 2003, **299**, 1024.
11. J. U. Rohde, J. H. In, M. H. Lim, W. W. Brennessel, M. R. Bukowski, A. Stubna, E. Munck, W.

Nam and L. Que, *Science*, 2003, **299**, 1037.
12. F. Neese and E. I. Solomon, *J. Am. Chem. Soc.*, 1998, **120**, 12829.
13. F. Neese and E. I. Solomon, *J. Inorg. Biochem.*, 1999, **74**, 247.
14. A. A. Battiston, J. H. Bitter, F. M. F. de Groot, A. R. Overweg, O. Stephan, J. A. Van Bokhoven, P. J. Kooyman, C. van der Spek, G. Vanko and D. C. Koningsberger, *J. Catal.*, 2003, **213**, 251.
15. L. J. Lobree, I. C. Hwang, J. A. Reimer and A. T. Bell, *J. Catal.*, 1999, **186**, 242.
16. R. Joyner and M. Stockenhuber, *J. Phys. Chem. B*, 1999, **103**, 5963.
17. P. Marturano, L. Drozdova, A. Kogelbauer and R. Prins, *J. Catal.*, 2000, **192**, 236.
18. P. Marturano, L. Drozdova, G. D. Pirngruber, A. Kogelbauer and R. Prins, *Phys. Chem. Chem. Phys.*, 2001, **3**, 5585.
19. A. A. Battiston, J. H. Bitter, F. M. F. de Groot, Heijboer W. M. and D. C. Koningsberger, *J. Catal.*, 2003, **215**, 279.
20. W. M. Heijboer, A. A. Battiston, A. Knop-Gericke, M. Hävecker, R. Mayer, H. Bluhm, R. Schlögl, B. M. Weckhuysen, D. C. Koningsberger and F. M. F. de Groot, *J. Phys. Chem. B*, 2003, **107**, 13069.
21. F. M. F. de Groot, *J. Elec. Spec.,* 1994, **67**, 529.
22. F. M. F. de Groot, *Chem. Rev.*, 2001, **101**, 1779.
23. T. V. Voskoboinikov, H. Y. Chen and W. M. H. Sachtler, *Appl. Catal. B.*, 1998, **19**, 279.
24. A. Knop-Gericke, M. Hävecker, T. Neisius and T. Schedel-Niedrig, *Nucl. Instrum. Meth. A.*, 1998, **406**, 311.
25. M. Hävecker, A. Knop-Gericke and T. Schedel-Niedrig, *Appl. Surf. Sci.*, 1999, **142**, 438.
26. A. Knop-Gericke, M. Hävecker, T. Schedel-Niedrig and R. Schlögl, *Top. Catal.*, 2000, **10**, 187.
27. A. Knop-Gericke, M. Hävecker, T. Schedel-Niedrig and R. Schlögl, *Catal. Lett.*, 2000, **66**, 215.
28. M. Abbate, J. B. Goedkoop, F. M. F. De Groot, M. Grioni, J. C. Fuggle, S. Hofmann, H. Petersen and M. Sacchi, *Surf. Interf. Anal.*, 1992, **18**, 65.
29. A. A. Battiston, J. H. Bitter and D. C. Koningsberger, *J. Catal.*, 2003, **218**, 163.
30. T. Kendelewicz, P. Liu, C. S. Doyle, G. E. Brown, E. J. Nelson and S. A. Chambers, *Surf. Sci.*, 2000, **453**, 32.
31. E. Theunissen, C. E. A. Kirschhock, S. P. B. Kremer, D. D. Habermacher and J. A. Martens, *Eur. J. Inorg. Chem.*, 2003, 1296.
32. F. M. F. de Groot, A. Knop-Gericke, T. Ressler and J. A. van Bokhoven, *In situ* x-ray absorption spectroscopy in catalysis, in *In situ* Spectroscopy of Catalysts; B.M. Weckhuysen (Ed.), American Scientific Publishers, 2004, 107.
33. M. Wilke, F. Farges, P. E. Petit, G. E. Brown and F. Martin, *Am. Miner.*, 2001, **86**, 714.
34. T. E. Westre, P. Kennepohl, J. G. Dewitt, B. Hedman, K. O. Hodgson and E. I. Solomon, *J. Am. Chem. Soc.*, 1997, **119**, 6297.
35. J. F. Jia, Q. Sun, B. Wen, L. X. Chen and W. M. H. Sachtler, *Catal. Lett.*, 2002, **82**, 7.
36. G. Berlier, G. Spoto, S. Bordiga, G. Ricchiardi, P. Fisicaro, A. Zecchina, I. Rossetti, E. Selli, L. Forni, E. Giamello and C. Lamberti, *J. Catal.*, 2002, **208**, 64.
37. A. Zecchina, S. Bordiga, G. Spoto, A. Damin, G. Berlier, F. Bonino, C. Prestipino and C. Lamberti, *Top. Catal.*, 2002, **21**, 67.

5

X-ray magnetic circular dichroism of FeZSM-5

Abstract

We show that X-ray Magnetic Circular Dichroism (X-MCD) experiments can reveal important new information concerning the active sites in heterogeneous catalysis. We have applied 2p X-ray absorption and its X-MCD to framework-substituted 0.25 wt % FeZSM-5. The results show a pure octahedral Fe^{III} site for the as-made FeZSM-5. Its X-MCD signal indicates that all Fe^{III} sites contribute to the X-MCD, indicating isolated Fe^{III} sites. After calcination, the sample remains mostly mononuclear Fe^{III}, with a minor contribution from aggregated Fe^{II} sites. After steaming half the iron forms aggregates and in addition ~ 20 % changes its valence to Fe^{II}. The metal loading of 0.25 wt % is no obstacle in obtaining the X-MCD signal and it can be concluded that X-MCD provides an important addition to the characterization toolbox of spectroscopists working in the field of heterogeneous catalysis.

5.1. Introduction

X-ray Magnetic Circular Dichroism (X-MCD) has become a major characterization tool for ferromagnetic metals, oxides and their surfaces and for paramagnetic sites in bio-inorganic chemistry and coordination compounds.[1,2] Heterogeneous catalysis also contains transition metal ions that form isolated sites or clusters. As such, it can be expected that much information could be gained from X-MCD experiments. This is the more important because with metal loadings of 0.3 wt % and lower, many other important characterization techniques, for example IR and EXAFS, are difficult.

We showed in the chapters 3 and 4 that soft X-ray absorption at the Fe L edge is an element specific technique that is ideal to study iron catalysts. There, we have successfully applied soft X-ray absorption to overexchanged (5 wt %) Fe-ZSM-5 samples under conditions that allowed pressures up to 10 mbar.[3,4] If the concentration of iron is less than 1 wt % this electron-yield technique reaches its detection limit and we did not succeed in observing a signal for these 0.25 wt % FeZSM-5 samples. Instead of using conversion electron yield, it is more straightforward to measure the soft X-ray absorption spectra with fluorescence yield. An amount of 0.25 wt % Fe inside a zeolite matrix will effectively generate a paramagnetic system. Aligning the paramagnetic sites under an external magnetic field will align the iron moments and as such generate an X-MCD signal if the sample is excited with respectively left and right circularly polarized X-rays.

The activation of low loaded framework-substituted FeZSM-5 yields a heterogeneous system. Heating in a flow of air or oxygen (calcination) especially in the presence of water vapor (steaming) extracts the iron, originally in the tetrahedral sites of the zeolite structure (MFI type), into extra framework positions. Usually a variety of species is formed: isolated extraframework Fe oxo-ions (Fe_1), binuclear oxo-iron complexes (Fe_2) and oligonuclear oxo-iron complexes (Fe_N) located in the zeolite channels in addition to – catalytically inactive – larger iron-oxide nanoparticles in the zeolite pores (nano-FeO_x) and on the external surface of the zeolite (Fe_2O_3 crystallites).[5] Moreover, part of the iron stays in the framework in inverse relation to the severity of the activation treatment (Fe_F). We will use the X-MCD signal in an effort to determine the nature of the isolated iron sites. In addition, we intend to distinguish the behavior of Fe_F, Fe_1, Fe_2, Fe_N and nano-FeO_x. Isolated iron (Fe_F and Fe_1) will be paramagnetic and fully aligned at the experimental conditions. A binuclear Fe^{III} center will be anti-ferromagnetically coupled. This coupling will be maintained in the applied field, hence Fe_2 centers will have no X-MCD signal. Similarly the nearest neighbor couplings in Fe_N will be anti-ferromagnetic and the net X-MCD effect will be zero or small. Larger iron oxide nanoparticles will tend to form anti-ferromagnetic oxides. In principle this yields a zero X-MCD, but because at the edges of the nanoparticles the spin can tilt slightly, a small X-MCD effect might remain.[6] The magnitude of the X-MCD effect is thus an indication for the degree of nucleation and growth of the iron clusters and the largest signal is found for isolated iron atoms. In fact, this signal is expected to be the maximum signal in case the external field aligns their spins completely.

5.2. Experimental

5.2.1. Catalyst preparation and characterization

Framework-substituted FeZSM-5

Framework-substituted FeZSM-5 was prepared via the hydrothermal synthesis method.[7] FeZSM-5, with Si/Al = 36 and Si/Fe = 175 ratios in the starting synthesis mixture, was prepared according to the procedure described below. The synthesis mixture contained tetraethylorthosilicate (TEOS, Aldrich, 99+ %, tetrapropylammonium hydroxide (TPAOH, Alfa Aaeser, 40 % w/w in water), iron (III) sulfate (VWR), aluminum nitrate nonahydrated (Aldrich, 99.99 %), and sodium hydroxide (VWR) in the following nominal molar ratios: H_2O/Si = 45, TPAOH/Si = 0.1, NaOH/Si = 0.2, Si/Al = 36, and Si/Fe = 175.

In a typical synthesis, the silica source (TEOS) was added to the organic template (TPAOH) and sodium hydroxide while vigorously stirring. Drops of this solution were added to a mixture of iron sulfate and aluminum nitrate dissolved in water. The final solution was transferred to a stainless steel autoclave and kept in a static air oven at 190 °C for 5 days. The thus obtained as-made sample, *am*-FeZSM-5, was subject to several activation treatments and so successively were yielded: *tf*-FeZSM-5, *NH_4*-FeZSM-5, *H*-FeZSM-5 and *hs*-FeZSM-5.

From the prepared series three samples have been measured with X-MCD:

am-FeZSM-5: The crystalline material was separated by filtration, washed with ~ 2 liter of deionized water or until the product is color-free and dried at room temperature overnight. The samples were characterized with powder X-ray diffraction (XRD) to confirm the structure and purity of the sample, and elemental analysis by X-ray fluorescence (XRF) for relative ratios of Si, Al and Fe (45.1, 1.17, 0.25 wt % respectively: Si/Fe ~ 360 and Si/Al ~ 37).

H-FeZSM-5: The template was removed carefully from the as-synthesized sample by pyrolysis in a dried nitrogen flow of 50 ml/min at 520 °C (heating rate 1 °C/min) for 2 h and consecutive calcination in a dry airflow of 100 ml/min at 520 °C (2 °C/min) for 2.5 h. The samples were converted into the NH_4-form by exchange with an ammonium nitrate solution (0.1 M) overnight at 70 °C. The sample was filtered and dried for 2 h at 60 °C. Finally, the *H*-form was obtained by calcination in a dry airflow of 100 ml/min at 520 °C (2 °C/min) for 1 h.

hs-FeZSM-5: A (hard) steaming procedure was carried out, according to literature,[7] with a water partial pressure of 300 mbar in a total flow of 30 ml/min nitrogen at high temperature of 600 °C for 5 h.

5.2.2 X-ray absorption and X-MCD experiments

X-MCD measurements were conducted using beam line 4.0.2 at the Advanced Light Source of the Lawrence Berkeley National Laboratory. The beam line is equipped with an elliptically polarizing undulator and a high-resolution monochromator. The photon flux was

10^{12} photons/s and the energy resolution $\Delta E/E$ is better than 4500.[8] The X-ray beam energy was calibrated against the Fe L edge spectrum of Fe_2O_3. The experimental setup consisted of a 6 T superconducting magnet, which hosted a sample stage attached to a separate liquid helium bath pumped cryostat. The sample stage was equipped with a heat shield, which is connected to the liquid helium bath, in order to minimize the sample heating by infrared radiation. We have shown that with our apparatus a temperature of 2.2 K can be obtained.[9,10] Both the X-ray beam and fluorescence radiation pass through 100 nm aluminum plus 100 nm parylene thick windows, mounted in the heat shield. The absorption spectra were measured by collecting the sample fluorescence using a Canberra 30-element germanium detector whose resolution is of 150 eV. The energy of the incident X-ray photons was varied over the Fe absorption edge. For each energy point, a fluorescence spectrum was recorded and the fluorescence lines of the investigated element were integrated. These measurements yield a count rate that is proportional to the absorption cross section. With fluorescence measurements the fluorescence lines from target atoms can be isolated from background lines, considerably increasing the signal to noise ratio in measurements of diluted samples. The fluorescence signal coming from oxygen was used as a control for the incident beam intensity and the Fe signal was normalized by it. The absorption spectra background was corrected by the subtraction of a straight line fitted to the pre-edge region.

5.3. Results

Figure 1 shows the iron 2p X-ray absorption spectrum and its X-MCD of a framework-substituted as-made FeZSM-5 sample (*am*-FeZSM-5). The Fe 2p XAS spectrum is resolved with good statistics, including its X-MCD effect. We have compared the 2p XAS and X-MCD spectra of *am*-FeZSM-5 with charge transfer multiplet simulations, using an octahedral surrounding and an effective cubic crystal field value of 1.2 eV. The theoretical spectra have been broadened with the 2p lifetime broadening and the experimental resolution. The Fe 2p XAS spectrum of *am*-FeZSM-5 is accurately reproduced, where the intensity of the main peak has been normalized to 1.0, both for theory and experiment. Because the calculations are not able to calculate exactly the absolute energy, the energy axis of the theoretical curve has been aligned with experiment. The two peaks of the FeL_3 edge are found at the right distance, where the first smaller peak has a bit lower intensity in the calculations. This has been found for other Fe^{III} oxides as well, in particular the FeL_3 edge of Fe_2O_3 is always calculated with a too small first peak. The agreement between theory and experiment can be improved if one uses a smaller lifetime broadening for the first peak. Although such broadening effect does maybe occur, we will not apply a different broadening in the present paper. Instead of broadening effects, another possibility for extra intensity at this energy is the presence of some Fe^{II}. In Figure 1, we added a second theoretical curve that contains 10 % Fe^{II} in addition to the Fe^{III}. One observes that with 10 % Fe^{II} the leading edge is accurately reproduced and actually 10 % Fe^{II} seems already too much. We did not attempt to optimize the Fe^{II} content, but we conclude that 10 % is the upper limit.

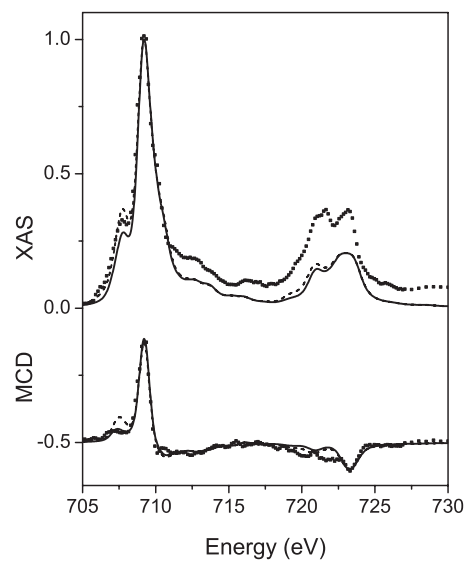

Figure 1: Experimental Fe $L_{2,3}$ edge spectrum (points) and its MCD (points) of a framework-substituted as-made FeZSM-5 sample (*am*-FeZSM-5). The MCD spectra have been offset by −0.5 for clarity. The theoretical curves for octahedral Fe^{III} (solid line) have been calculated with the charge transfer multiplet model with an effective crystal field of 0.9 eV. The dashed line adds a contribution of 10 % Fe^{II}.

Figure 2 shows the theoretical Fe^{II} and Fe^{III} spectra (both in O_h symmetry), where the Fe^{II} spectrum has been calculated using a crystal field multiplet calculation with a crystal field strength of 0.9 eV. The Fe^{III} XAS (top) and MCD (bottom) have been given with a

solid line. The corresponding Fe^{II} spectra have been given with a dashed line. The shift of the peaks has been set to 1.6 eV as is consistently found for FeZSM-5 materials that are 100 % oxidized respectively reduced.[3] At the bottom of Figure 1 we compare the X-MCD spectra, where we did not use any additional shift or normalization. This implies that the magnitude of the calculated X-MCD is exactly equal to the observed X-MCD signal, which indicates that the isolated Fe_F ions have been fully magnetized and in addition that all iron is present as isolated iron. Hereby, the maximal X-MCD as observed in experiment confirms that the synthesis of isolated iron atoms inside the zeolite framework of FeZSM-5 has been successful. The X-MCD spectral shape is also reproduced in great detail. The X-MCD curve where 10 % Fe^{II} has been added (dashed) yields a too large X-MCD effect at 708 eV. The large theoretical X-MCD signal of Fe^{II} at its peak maximum of 708 eV implies that little Fe^{II} is present in the experimental spectrum. This further suggests that the amount of Fe^{II} present is less than 10 % and very likely also less than 5 %, indicating an essentially completely oxidized Fe^{III} system. The same set of samples has been measured also with K edge X-ray absorption and the analysis of the pre-edge structure of these experiment revealed that at 350 °C all the samples were in a pure Fe^{III} state, where the *am*-FeZSM-5 sample has not been measured at 350 °C (chapters 6 and 8). Under O_2 the valence was essentially Fe^{III}, while under He (at 350 °C) less than 10 % was reduced.[11] Soft X-ray absorption experiments on overexchanged Fe/ZSM-5 that contains Fe almost exclusively in extraframework positions revealed a different behavior: these samples show room temperature autoreduction after switching from oxygen to He atmospheres and the average valence changed from 2.95 to 2.65 within minutes (chapters 3 and 4). It should be mentioned that these experiments involve electron-yield detection hence only information from the top 5 nm of the samples can be obtained.[3]

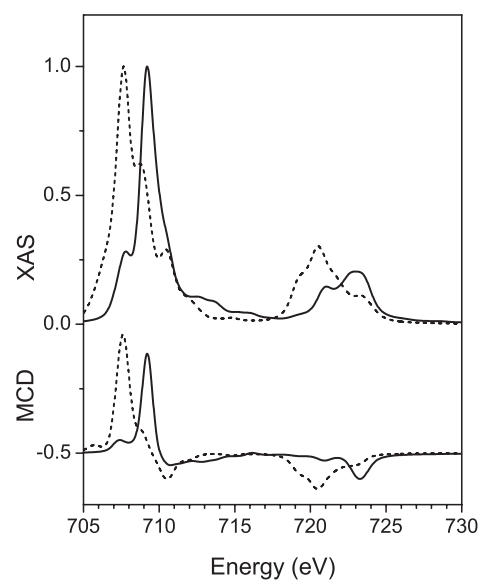

Figure 2: The theoretical Fe $L_{2,3}$ edge XAS (top) and X-MCD (bottom) spectra for Fe^{II} (dashed line) and Fe^{III} (solid line).

Figure 3 shows the comparison of *am*-FeZSM-5 with *H*-FeZSM-5. It can be seen that the 2p XAS spectrum has an increased intensity at 708 eV, suggesting partial reduction to Fe^{II}. In contrast, the X-MCD spectrum is essentially unchanged. This suggests that the reduced Fe^{II} sites have not been magnetized. The magnitude of the X-MCD signal is identical to *am*-FeZSM-5, which indicates that the Fe^{III} sites are still completely magnetized, implying still isolated Fe^{III} sites. The Fe^{II} sites could loose their magnetic orientation because the Fe^{II} sites form an aggregate that couples anti-ferromagnetically, as will be further discussed in section 5.4. It should be noted that under the present conditions, *H*-FeZSM-5 is expected to be sixfold coordinated due to the binding of water at room temperature under ambient conditions. Water is abundantly present in the channels of the zeolites and its removal, even at elevated temperatures, is a slow process. In the following chapter we show – using hard X-ray Fe K edge experiments – that at 350 °C, *H*-FeZSM-5 is a mixture of octahedral and tetrahedral sites and/or contains strongly distorted tetrahedra, where cooling down from 350 °C to room temperature restores the octahedral symmetry. Cooling down from room temperature to 20 K is expected to maintain the local symmetry, though electron yield experiments on overexchanged Fe/ZSM-5 samples showed relatively fast (surface) autoreduction, also at room temperature. Because of the relatively fast cooling (less than 20 minutes during which the pressure is decreasing), we do not expect significant modification of the octahedral site.

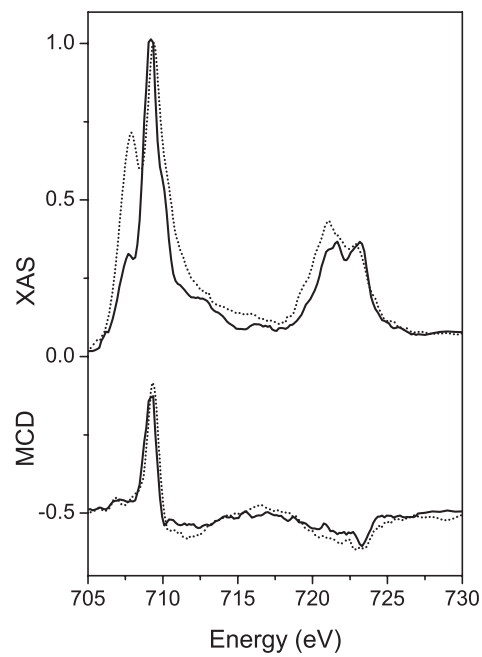

Figure 3: Experimental Fe $L_{2,3}$ edge and X-MCD spectra of *am*-FeZSM-5 (solid line) compared with *H*-FeZSM-5 (dotted line).

Figure 4 shows the comparison of *am*-FeZSM-5 with the hard steamed sample (*hs*-FeZSM-5). It can be seen that the 2p XAS spectrum again has an increased intensity at 708 eV, suggesting partial reduction to Fe^{II}. The X-MCD spectrum has become significantly smaller at the peak position, while the shoulder at 708 eV has increased. The reduced X-MCD intensity at 709.5 eV indicates that approximately half of the Fe^{III} sites do not contribute to the X-MCD signal. This is due to the formation of Fe dimers or oligomers that are antiferromagnetic coupled Fe^{III} (S = 5/2) sites. An antiferromagnetic Fe_2 dimer does have the same XAS spectrum, but its X-MCD will be zero. It can also be seen that there is increases X-MCD of the Fe^{II} sites. This suggests that one creates isolated Fe^{II} sites in the hard steaming treatment. These Fe^{II} sites are different from those in *H*-FeZSM-5 because those did not contribute to the X-MCD. It is not possible to make an accurate quantitative determination of the amount of magnetic Fe^{II} sites, but the signal indicates an amount of the order of 25 % of the overall Fe^{III} sites.

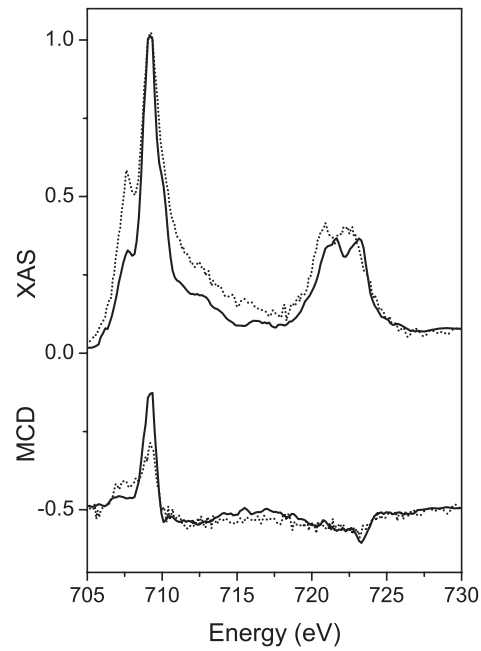

Figure 4: Experimental Fe $L_{2,3}$ edge and X-MCD spectra of *am*-FeZSM-5 (solid line) compared with *hs*-FeZSM-5 (dotted line).

5.4. Discussion

Table 1 summarizes the amount of magnetic Fe^{III} and Fe^{II} sites. It can be concluded that all Fe^{III} sites are paramagnetic and fully magnetized in case of the *am*-FeZSM-5 and *H*-FeZSM-5 samples. This is an important result for *H*-FeZSM-5 because it confirms the EXAFS results as given in chapter 8 that in *H*-FeZSM-5 iron is still in isolated Fe_1 sites. The X-MCD results confirm that all Fe^{III} is surely in isolated sites, though the absence of an X-MCD signal for the Fe^{II} states suggest that the situation is different for the reduced iron as will be discussed below.

The *hs*-FeZSM-5 sample about half of its Fe^{III} X-MCD signal, indicating that ~ 50 % of the Fe^{III} is not in isolated sites, but instead forms Fe_N oligimeric sites and/or Fe_2O_3 nanoparticles. It is noted that Fe_N oligimeric sites and/or Fe_2O_3 nanoparticles will tend to form anti-ferromagnetic coupled structures, but their X-MCD signal is not expected to be zero due to imperfect antiferromagnetism, spin-canting and other finite size effects.[6] The *H*-FeZSM-5 and *hs*-FeZSM-5 samples show reduction to Fe^{II} of respectively 30 % and 20 % of the iron sites. This is most likely due to reduction at room temperature in air. At present there is no procedure to freeze the samples in their active state (at 623 K) and cool down to 20 K within the same chamber.

Table 1: Distribution of magnetic Fe species in low loaded FeZSM-5 samples. The relative amounts of Fe^{III} and Fe^{II} are given in columns 1 and 2, respectively columns 3 and 4. A distinction is made between magnetic and non-magnetic Fe.

	Fe^{III}		Fe^{II}	
	magnetic	non	magnetic	non
am-FeZSM-5	95 ± 5	-	-	5 ± 5
H-FeZSM-5	70 ± 10	-	-	30 ± 10
hs-FeZSM-5	40 ± 10	40 ± 10	10 ± 10	10 ± 10

The Fe^{II} in the *hs*-FeZSM-5 sample is magnetic, which suggests that the Fe^{II} sites are similar to the magnetic Fe^{III} sites. In other words, the non-magnetic Fe_2O_3 nanoparticles contain no Fe^{II}, while the magnetic Fe_1 sites contain a significant amount of Fe^{II}. The X-MCD spectrum seems to rule out the formation of Fe_3O_4 nanoparticles, which has a characteristic X-MCD spectrum that is not visible in the spectra.[12]

A remarkable result is that in contrast to the *hs*-FeZSM-5 sample, all Fe^{II} in the *H*-FeZSM-5 sample seems to be not magnetic, that is as good as no X-MCD signal is observed at the Fe^{II} peak position. This indicates that the Fe^{II} sites are different in *H*-FeZSM-5. We have no convincing explanation for this observation: It could suggests that the *H*-FeZSM-5 sample has its Fe^{II} sites as part of the Fe_N and/or Fe_{Ox} nanoparticles, but then it is remarkable that after steaming the iron becomes magnetic again. It is unlikely that in the *H*-FeZSM-5

sample the Fe^{II} sits in a, distorted, framework position Fe_1 site that is not magnetized at 6 T. An intriguing possibility is that approximately half of the Fe^{II} sites are part of a Fe^{II}-Fe^{III} dimer. Such a dimer will align in a way that the Fe^{III} yields a positive X-MCD signal, while the antiferromagnetically coupled Fe^{II} sites yield a negative X-MCD signal. If there are approximately equal amounts of Fe^{II} in such Fe^{II}-Fe^{III} dimers and in other positions (say as Fe_1 sites), the overall X-MCD of Fe^{II} sites becomes zero, as is observed.

5.5. Conclusions

All iron in *am*-FeZSM-5 is trivalent and occupies dominantly 6-fold sites. These 6-fold sites will be framework sites that are originally tetrahedral, but additional bonding occurs in the *am*-FeZSM-5. The X-MCD signal is exactly equal to its maximum, which implies that all the paramagnetic iron sites have been aligned. This suggests that all iron occupies isolated Fe_1 sites.

After calcination the *H*-FeZSM-5 sample is partly reduced to Fe^{II}. The Fe^{III} sites remain fully magnetized, hence all Fe^{III} remains as isolated Fe_1 sites. The Fe^{II} sites are effectively non-magnetic, suggesting dimers (containing at least one Fe^{II}) or other aggregates.

The *hs*-FeZSM-5 sample shows a ~ 50 % reduced X-MCD signal, indicating that half the iron atoms loose their paramagnetic nature and instead form antiferromagnetic pairs or larger antiferromagnetic aggregates, where ~ 20 % of the iron is reduced to Fe^{II}.

References

(1) de Groot, F. M. F., *J. Electr. Spectr. Rel. Phen.*, **1994**, *67,* 529-622.

(2) Funk, T.; Deb, A.; George, S. J.; Wang, H. and Cramer, S. P., *Coord. Chem Rev.*, **2005**, *249,* 3-30.

(3) Heijboer, W. M.; Battiston, A. A.; Knop-Gericke, A.; Hävecker, M.; Bluhm, H.; Weckhuysen, B. M.; Koningsberger, D. C. and de Groot, F. M. F., *Phys. Chem. Chem. Phys.*, **2003**, *5,* 4484-4491.

(4) Heijboer, W. M.; Battiston, A. A.; Knop-Gericke, A.; Hävecker, M.; Mayer, R.; Bluhm, H.; Schlögl, R.; Weckhuysen, B. M.; Koningsberger, D. C. and de Groot, F. M. F., *J. Phys. Chem. B*, **2003**, *107,* 13069-13075.

(5) Pérez-Ramírez., J.; Mul, G.; Kapteijn, F.; Moulijn, J. A.; Overweg, A. R.; Doménech, A.; Ribera, A. and Arends, I. W. C. E., *J. Catal.*, **2002**, 113-126.

(6) Brice-Profeta, S.; Arrio, M.-A.; Tronc, E.; Menguy, N.; Letard, I.; Cartier dit Moulin, C.; Nogues, M.; Chaneac, C.; Jolivet, J.-P. and Sainctavit, P., *J. Magn. Magn. Mater.*, **2005**, in press.

(7) Ribera, A.; Arends, I.; De Vries, S.; Perez-Ramirez, J. and Sheldon, R. A., *J. Catal.*, **2000**, *195,* 287-297.

(8) Young, A. T.; Feng, J.; Arenholz, E.; Padmore, H. A.; Henderson, T.; Marks, S.; Hoyer, E.; Schlueter, R.; Kortright, J. B.; Martynov, V.; Steier, C. and Portmann, G., *Nuclear Instruments & Methods in Physics Research Section a-Accelerators Spectrometers Detectors and Associated Equipment*, **2001**, *467,* 549-552.

(9) Funk, T.; Friedrich, S.; Young, A.; Arenholz, E. and Cramer, S. P., *Rev. Sci. Instr.*, **2002**, *73,* 1649-1651.

(10) Funk, T.; Kennepohl, P.; Di Bilio, A. J.; Wehbi, W. A.; Young, A. T.; Friedrich, S.; Arenholz, E.; Gray, H. B. and Cramer, S. P., *J. Am. Chem. Soc.*, **2004**, *126,* 5859-5866.

(11) Heijboer, W. M.; Glatzel, P.; Sawant, K. R.; Lobo, R. F.; Bergmann, U.; Barrea, R. A.; Koningsberger, D. C.; Weckhuysen, B. M. and de Groot, F. M. F., *J. Phys. Chem. B*, **2004**, *108,* 10002-10011.

(12) Pattrick, R. A. D.; Van Der Laan, G.; Henderson, C. M. B.; Kuiper, P.; Dudzik, E. and Vaughan, D. J., *Eur. J. Mineral.*, **2002**, *14,* 1095-1102.

6

Kβ-detected XANES of framework-substituted FeZSM-5 zeolites

Based on: W. M. Heijboer, P. Glatzel, K. R. Sawant, R. F. Lobo, U. Bergmann, R. A. Barrea, D. C. Koningsberger, B. M. Weckhuysen and F. M. F. de Groot, *J. Phys. Chem. B*, 2004, **108**, 10002 – 10011

Abstract

The valence and local symmetry of iron in framework-substituted FeZSM-5 with a high Fe dilution (Si/Fe = 360) was studied by means of Kβ-detected X-ray absorption spectroscopy. This technique combines high-resolution ($\Delta E \sim 1$ eV) fluorescence detection of the 3p to 1s (Kβ) transition with the X-ray absorption near edge structure (XANES) at the Fe K edge. An absorption-like spectrum is recorded by detecting the Kβ fluorescence intensity as a function of the incident energy that is scanned through the K absorption edge. Kβ-detected XANES spectra allow for a more precise separation of the weak K pre-edge structure from the main edge as compared to conventional absorption spectroscopy. Subsequent analysis and interpretation of the pre-edge spectral features therefore is more accurate. The pre-edge is sensitive to changes in the local coordination and oxidation state of Fe. Using this technique we were able to quantitatively determine the degree of iron extraction out of a zeolite framework, upon steaming. Based on the use of appropriate reference compounds, the pre-edge analysis was used to monitor the activation of low-loaded, framework-substituted FeZSM-5 (0.3 wt % Fe). Template removal and calcination distort the zeolite framework and induce a deviation from T_d symmetry for incorporated iron. The (deliberate) presence of water at high temperature (T > 500 °C) facilitates the hydrolysis of the Si–O–Fe bonds and increases the formation of extraframework iron species. The amount of Fe^{III} occupying tetrahedral sites in the MFI-type zeolite decreases to 32 % and 19 %, for respectively mild and hard steamed samples.

6.1. Introduction

Oxygen transfer reactions are very important in catalysis, as they are in nature. A wide range of transition metals is able to catalyze such reactions. The activity, selectivity and stability of the catalytically active species strongly depend on their structure and local environment. Zeolites have proven to be good hosts for active species of transition metals. The metal elements can either be introduced during the zeolite synthesis or through post-synthesis treatments. In recent years, FeZSM-5 has attracted much attention because of its ability for selective oxidation of hydrocarbons and its ability for the catalytic conversion of nitrogen oxides.[1] The specific activity for a certain reaction is largely determined by the way in which the FeZSM-5 catalyst is prepared. For example, the activity of framework -substituted FeZSM-5, with a Fe content below 1 wt %, for the catalytic decomposition of nitrous oxide and its use as an oxidant for the one step selective oxidation of benzene to phenol has been shown by Panov and co-workers[2] and by others.[3,4] Conversely, overexchanged Fe/ZSM-5 with much higher concentration of iron, introduced via post-synthesis methods, is an effective catalyst for the reduction of nitrogen oxides by hydrocarbons[5,6] or ammonia.[7] As already indicated in chapter 2, we distinguish the post-synthesis introduction of iron into ZSM-5 by using Fe/ZSM-5 instead of FeZSM-5.

For both types of FeZSM-5 catalysts the specific catalytic activity is well established, but the nature of the active sites involved is still under debate. The exclusive preparation of the active phase on a catalyst is often infeasible, as is the case for FeZSM-5. Unraveling of the structure of the active species becomes therefore a complicated task. Using extended X-ray absorption fine structure (EXAFS) studies it was possible to reveal that in over-exchanged Fe/ZSM-5, prepared by chemical vapor deposition of $FeCl_3$, a fair fraction of the iron is present in active binuclear iron clusters.[8,9] These Fe_2O_2 diamond core structures bear close resemblance to the active site of enzymes as methane mono oxygenase (MMO). Also for Cu-ZSM-5 the existence of such a M_2O_2 diamond core site has been reported.[10]

The activation of low loaded framework-substituted FeZSM-5 mostly yields a very heterogeneous system. Heating in a flow of air or oxygen (calcination) especially in the presence of water vapor (steaming) extracts the iron, originally in the tetrahedral sites of the zeolite structure (MFI type), into extraframework positions. Usually a variety of species is formed: isolated extraframework Fe oxo-ions (Fe_1), binuclear oxo-iron complexes (Fe_2) and oligonuclear oxo-iron complexes (Fe_N) located in the zeolite channels in addition to – catalytically inactive – larger iron oxide nanoparticles (FeO_x), that may also be present on the external surface of the zeolite (as Fe_2O_3).[3] Moreover, part of the iron stays in the framework in inverse relation to the severity of the activation treatment.

However, the current techniques employed for the characterization of FeZSM-5 are not well suited to determine the ratio between iron in tetrahedral (framework) and in octahedral (extraframework) coordination sites. For instance, Mössbauer and EXAFS spectroscopy can prove qualitatively the presence of iron in a specific coordination, but are in general not able to provide a quantitative analysis for mixtures. An exception is a detailed EXAFS study concerning the well-defined case of $CuCl_2/Al_2O_3$ catalysts that

contain mixtures of different phases with known geometry, but with varying mutual ratios depending on the Cu-loading.[11] However, in the present study on Fe-containing zeolites not only the large heterogeneity of the species formed, but moreover, the very low concentration of Fe in framework-substituted Fe/ZSM-5 complicates the use of the above mentioned techniques.

We use Kβ-detected XANES (X-ray absorption near edge structure) to probe quantitatively the local symmetry of Fe. The pre-edge feature of the Fe K edge X-ray absorption spectrum is sensitive to the electronic structure of the iron site. The pre-edge arises from transitions of a Fe 1s electron into the lowest unoccupied electronic states that mainly have Fe 3d character. In a centrosymmetric system those transitions are dipole-forbidden and therefore have in general very low intensity. However, a deviation from a centrosymmetric environment enables the mixing of 3d- with 4p-orbitals. Due to this hybridization some electric dipole allowed 1s → 4p character is added to the 3d-band transitions, resulting in an enhanced intensity of the pre-edge structure. Thus, iron in a non-centrosymmetric tetrahedral symmetry gives rise to a much more intense Fe K edge pre-edge than in a centrosymmetric octahedral symmetry. Therefore, changes in the pre-edge intensity reflect the changes in the local coordination sphere (geometry) of Fe. In addition, the energy position of the pre-edge is related to the oxidation state of Fe, i.e. the occupation of the 3d-band.[12]

The main requirements for a quantitative determination of changes in the coordination of iron based on variations of the pre-edge features are (1) a high resolution of the spectra, so that characteristic features in the pre-edge are well resolved, (2) a precise isolation of the pre-edge structure from the main edge, which requires a proper background subtraction and (3) the choice of relevant parameters to describe the pre-edge characteristics. Lately, several groups have used XANES to study the local coordination of iron in overexchanged Fe/ZSM-5.[9,13-16] Lamberti and co-workers reported on the characterization of – aluminum free – Fe-silicalite, which has the similar MFI zeolite structure as ZSM-5.[17-21] Using Fe K edge XANES they investigated the influence of template removal and calcination on the coordination and oxidation state of iron initially incorporated in Fe-silicalite. The authors described the characteristics of the pre-edge feature by means of peak position and intensity, but did not separate the contribution from the main absorption edge to the pre-edge feature.

In a detailed and extensive XANES study on Fe-bearing minerals Wilke and co-workers[22] presented a correlation of the changes of the Fe K pre-edge with the oxidation state and local symmetry. The pre-edge features of Fe in more than 30 minerals and synthetic compounds were systematically studied. The most useful characteristics of the pre-edge feature were the energy position of the centroid and its integrated intensity. Also Westre and co-workers[12] have proven for ferrous and ferric model compounds that these are the appropriate parameters to unambiguously characterize the pre-edge feature. In previous *in situ* high-resolution XANES studies, Battiston et al.[8,23,24] used the findings of Wilke et al. obtained for binary mixtures of $^{[6]}Fe^{III}/^{[4]}Fe^{II}$ to understand the evolution and reactivity of binuclear Fe-complexes in overexchanged Fe/ZSM-5 upon heating in helium and in O_2.

However, the spectra in the study by Battiston et al. show a lower energy resolution that is essentially the same as for conventional XANES measurements. In addition, it shows rather poor signal to noise ratios at Fe loadings that are by a factor 15 higher than in the present study. Because of the poor energy resolution, the pre-edge analysis utilizes a cubic spline function because of the background, i.e. a tailing contribution of main edge to pre-edge, because the pre-edge is still not well separated from the main edge. The use of a cubic spline function introduces a significant error as we will show below. Due to these experimental limitations the study by Battiston et al. did not allow for a detailed quantitative analysis.

In this work, we present a study of the Fe K pre-edge region in low loaded, framework-substituted FeZSM-5 by means of Kβ-detected XANES spectroscopy. The pre-edge spectral features represent excited electronic states of the Fe ion where a 1s electron has been elevated to a low-lying unoccupied state by an incoming X-ray photon. The Kβ fluorescence is emitted when the hole in the 1s shell is subsequently filled by a 3p electron. A high-resolution Kβ spectrum can be measured using a crystal spectrometer with an energy bandwidth of about 1 eV. The Kβ fluorescence intensity depends on the probability of exciting a 1s electron, i.e. it depends on the absorption cross-section at the K-edge. By detecting the Kβ intensity as a function of the incident energy it is thus possible to record absorption-like spectra.[25-27]

The advantage of high-resolution Kβ-detected XANES spectroscopy is that it shows spectral features that are sharper than in conventional absorption spectroscopy recorded in transmission mode or by fluorescence detection using a solid state detector with medium energy resolution (e.g. Ge: $\Delta E \sim 200$ eV). We show that high-resolution Kβ-detected XANES spectra allow for a more precise background subtraction and consequently a higher accuracy in determining the local geometry and oxidation state of Fe in ZSM-5. The application of this technique enables for a quantitative determination of the degree of iron extraction out of the zeolite matrix which is not possible using other techniques. We point out that in this study X-ray absorption data are presented for the first time on a FeZSM-5 catalyst with a Fe loading fairly below 1 wt %, which was the limit so far, even for a qualitative analysis.[20]

6.2. Experimental

6.2.1. Catalyst preparation and characterization

Framework-substituted FeZSM-5

Framework-substituted FeZSM-5 was prepared via the hydrothermal synthesis method.[4] FeZSM-5, with Si/Al = 36 and Si/Fe = 175 ratios in the starting synthesis mixture, was prepared according to the procedure described below. The synthesis mixture contained tetraethylorthosilicate (TEOS, Aldrich, 99+%), tetrapropylammonium hydroxide (TPAOH, Alfa Aeser, 40 % w/w in water), iron (III) sulfate (VWR), aluminum nitrate nonahydrated (Aldrich, 99.99 %), and sodium hydroxide (VWR) in the following nominal molar ratios: H_2O/Si = 45, TPAOH/Si = 0.1, NaOH/Si = 0.2, Si/Al = 36, and Si/Fe = 175.

In a typical synthesis, the silica source (TEOS) was added to the organic template (TPAOH) and sodium hydroxide while vigorously stirring. Drops of this solution were added to a mixture of iron sulfate and aluminum nitrate dissolved in water. The final solution was transferred to a stainless steel autoclave and kept in a static air oven at 190 °C for 5 days. The crystalline material was separated by filtration, washed with approximately 2 L of deionized water or until the product is color-free and dried at room temperature overnight (denoted as catalyst *am*-FeZSM-5). The samples were characterized with powder X-ray diffraction (XRD) to confirm the structure and purity of the sample, and elemental analysis by X-ray fluorescence (XRF) for relative ratios of Si, Al and Fe (45.1, 1.17, 0.25 wt % respectively: Si/Fe ~ 360 and Si/Al ~ 37).

The template was removed carefully from the as-synthesized sample (*am*) by pyrolysis in a dried nitrogen flow of 50 ml/min at 520 °C (heating rate 1 °C/min) for 2 h and consecutive calcination in a dry airflow of 100 ml/min at 520 °C (2 °C/min) for 2.5 hr *(tf*-FeZSM-5). The samples were converted into the NH_4-form by exchange with an ammonium nitrate solution (0.1 M) overnight at 70 °C. The sample was filtered and dried for 2 h at 60 °C (*NH_4*-FeZSM-5). The H-form was obtained by calcination in a dry airflow of 100 ml/min at 520 °C (2 °C/min) for 1 hr (*H*-FeZSM-5). In the last step, the catalysts were steamed, in two different ways. First a hard steaming procedure was carried out, according to literature,[4] with a water partial pressure of 300 mbar in a total flow of 30 ml/min nitrogen at high temperature of 600 °C for 5 h (*hs*-FeZSM-5). In addition, we performed a mild steaming procedure with a water partial pressure of 200 mbar in a total flow of 200 ml/min nitrogen at high temperature of 550 °C for 4 h (*ms*-FeZSM-5). The samples were stored at room temperature in dry air.

Overexchanged Fe/ZSM-5

Overexchanged Fe/ZSM-5 was prepared following the $FeCl_3$ sublimation technique (also called chemical vapor deposition (CVD)), proposed by Chen and Sachtler,[5] and also described in previous chapters. The H^+ removal efficiency (98 %), determined by HCl titration, indicated that during the Fe-exchange procedure nearly all the Brönsted acid sites were removed from the H/ZSM-5.

Fe/ZSM-5 was calcined by heating to 200 °C in a PFR-reactor under a specific He flow of 800 ml/min·g and with a moderate temperature ramp (0.5 °C/min). At this temperature, 200 ml/min·g of O_2 was added to the He flow while, under the same temperature ramp, heating was continued to 550 °C. After 3 h at 550 °C, the temperature was decreased to 30 °C. The crystalline fingerprint of the zeolitic support was monitored after each synthesis step by XRD. On the basis of these measurements lattice damage or formation of large iron oxides phases could be excluded, even upon calcination. Elemental analysis by Inductively Coupled Plasma (ICP) was carried out to determine the silicon/aluminum ratio (Si/Al = 17.0) and the iron loading (Fe/Al = 0.97, 4.4 wt % Fe) of the obtained Fe/ZSM-5.

6.2.2. Kβ-detected XANES

Experimental setup

The Kβ-detected XANES spectra were measured at beamline 18-ID (BioCAT) at the Advanced Photon Source of the Argonne National Laboratories (Chicago, USA). The energy of the incoming synchrotron beam was selected by means of a Si(111) double-crystal monochromator. The incident beam was guarded by a 0.5 mm vertical by 1 mm horizontal slit in front of the sample. The energy bandwidth of the incident X-ray beam was approximately 1.2 eV at 7100 eV and the (maximum) incident flux was 10^{13} photons/s., as monitored by a helium-filled ionization chamber downstream of the guarding slit. The incident energy was calibrated using tabulated values for the K-edge features of a Fe foil standard. By repeatedly measuring the standard we determined a relative error of 0.1 eV for the incident energy. A focusing mirror rejected higher harmonics.

The fluorescence emission from the sample was collected by a crystal array spectrometer,[28] using six spherically bent Ge(620) crystals. The six-analyzer crystals have a diameter of 44 mm, yielding a solid angle of approximately 0.013 sr. A Ge solid-state detector was placed at the common focus of the six crystals. To avoid unwanted X-ray photons, the energy window of the Ge detector was set to ~ 600 eV and an additional slit was positioned just in front of the detector. The analyzer energy resolution is approximately 0.8 eV at the Fe Kβ emission. The relative energy calibration of the emission spectrometer is sensitive to vertical movements of the synchrotron beam. The energy calibration was repeatedly checked with the Kβ emission of an Fe_2O_3 sample and was found to be constant within 0.1 eV (relative emission energy error). We give an absolute error for the emission energy scale of 1 eV.

High-resolution Kβ-detected XANES spectra were recorded by tuning the emission analyzer energy to the maximum intensity of the Fe Kβ lines of Fe_2O_3 and by scanning the incident energy through the XANES region. This procedure is referred to as a constant emission energy (CEE) scan. In Figure 1 we give a schematic representation of the detection setup as well as a Fe Kβ emission spectrum in which the spectral area is indicated that is selected out of the fluorescence by using the high-resolution detector.

The maximum of the Kβ emission for Fe^{III} (Fe_2O_3) was calibrated at 7059.3 eV and a relative shift of 0.3 eV to lower emission energy was observed for Fe^{II} (Fe_2SiO_4). The same

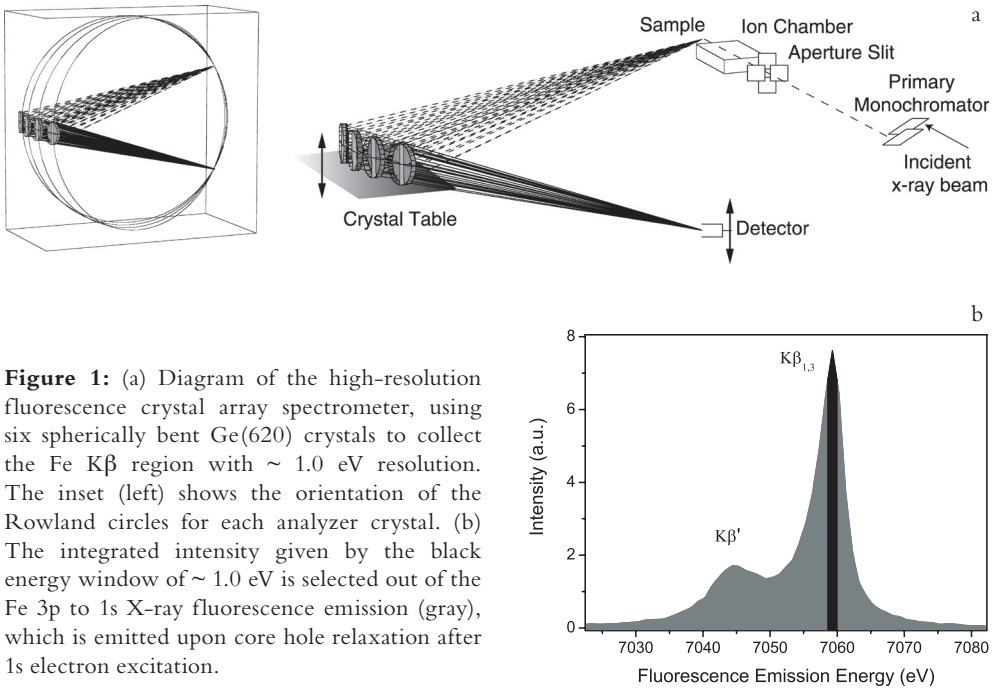

Figure 1: (a) Diagram of the high-resolution fluorescence crystal array spectrometer, using six spherically bent Ge(620) crystals to collect the Fe Kβ region with ~ 1.0 eV resolution. The inset (left) shows the orientation of the Rowland circles for each analyzer crystal. (b) The integrated intensity given by the black energy window of ~ 1.0 eV is selected out of the Fe 3p to 1s X-ray fluorescence emission (gray), which is emitted upon core hole relaxation after 1s electron excitation.

emission energy was used for all FeZSM-5 measurements and the CEE scans were therefore not necessarily taken in the maximum of the Kβ main peak. The Kβ intensity changes by approximately 5 % within 0.3 eV. However, the pre-edge intensity normalized to the main edge will hardly change because the Kβ peak shift affects the pre- and the main edge. The small error introduced by different Kβ peak shifts between pre- and main edge is estimated to be less than 2 %. Conventional absorption spectra were obtained by integrating the Kβ fluorescence over 25 eV. This corresponds to recording the total 3p to 1s fluorescence yield, which gives a good approximation to a conventional absorption spectrum.

Data acquisition

The Fe/ZSM-5 samples were pressed into self-supporting wafers and placed in an in-situ fluorescence cell at 45 degrees scattering angle with respect to the incoming beam.[29] Spectra were recorded at 1 bar during heating treatments from 25 to 350 °C (heating ramp of 5 °C/min). The heating treatments were performed in moderate oxygen atmospheres, i.e., a flowing mixture of 7.7 % O_2 in helium (total flow 100 ml/min). After stabilization at 350 °C XANES spectra were taken. After switching to helium atmosphere this sequence was repeated as was done for some samples in oxygen at room temperature after cooling down. Hematite, Fayalite and Iron(III) phosphate were measured under air at 25 °C as references.

Data processing

The Kβ-detected Fe XANES spectra were normalized by the average absorption intensity, as determined at around 7200 eV. The complete spectrum was modeled by using the software PeakFit4 (AISN Software, 1995). A typical spectrum could be simulated by a Gauss Cumulative Ascending function for the main edge combined with a pseudo-Voigt peak. Voigt profiles combine Lorentzian and Gaussian functions and hence account for respectively lifetime and experimental broadening. The pre-edge spectral shape has been fitted with a good R-squared value ($R^2 > 0.999$) using as few components as possible.

The conventional XANES spectra were also normalized by the average absorption intensity as determined at around 7200 eV. After normalization, the pre-edge feature was isolated by subtraction of the main Fe K absorption edge contribution. The contribution of the main edge was calculated for the whole energy range using a cubic spline function, while the data several eV before and after the energy position of the pre-edge were used to interpolate the main edge at the pre-edge energy position.[22]

The characteristics of the isolated pre-edges, i.e. centroid energy position and integrated intensity were calculated using the peak fitting results of the pre-edge feature. The energy position of the centroid is defined as the center of gravity of the (pseudo-Voigt) components. The contribution from components centered above 7115.0 eV was ignored.[22,23] The obtained centroid positions have been calibrated to the reported values of Wilke and co-workers, which results in a shift to lower energy of 0.77 eV.

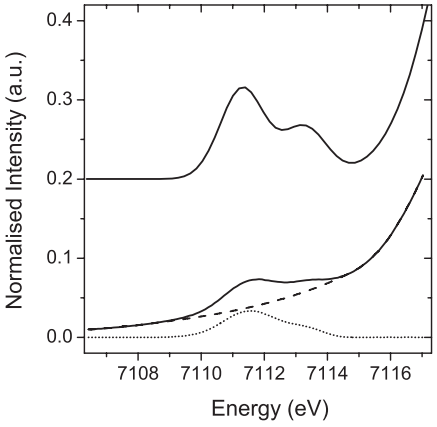

Figure 2: Fe K pre-edge feature of Fe_2SiO_4 (Fayalite: Fe^{II}, O_h). Below: conventional fluorescence XANES spectrum (solid), cubic spline function used to model the background (dash) and the isolated pre-edge (dot), analysis according Wilke et al.[22] On top: Kβ-detected XANES spectrum, no background subtracted. In both spectra the pre-edge is normalized to the average absorption intensity calculated around 7200 eV.

6.3. Results

6.3.1. Fe Kβ-detected XANES versus normal XANES

Pre-edge isolation

Figure 2 shows the pre-edge region of the Fe K edge X-ray absorption spectrum of Fe_2SiO_4 (Fayalite) measured in two different ways. The bottom portion of Figure 2 shows the Fe K pre-edge structure in a conventional absorption spectrum. The contribution of the main Fe K edge in the pre-edge region was determined by using a cubic spline function, obtained by interpolating the data several electron volts before and after the pre-edge (dashed line). The subtraction of the modeled main edge contribution from the XANES spectrum – over the full energy range – yields the isolated pre-edge feature. The pre-edge intensity for the spectra measured by normal XANES strongly depends on the subtracted cubic spline function. We estimated the error of this procedure by performing several cubic spline fits using various energy ranges around the pre-edge energy position. We experienced with a series of cubic spline functions, which in principle were all appropriate to model the background, that the variation in the resulting integrated pre-edge intensity amounts to 20 % for compounds with a weak pre-edge (i.e. with an octahedral oxygen coordination). Reference spectra, which are analyzed in exactly the way, provide a frame for the determination of the variance introduced by the analysis method. However, despite this improvement, we expect this procedure to be still susceptible to a certain lack of reproducibility. To overcome this disadvantage of normal XANES we measured the spectra by means of Kβ-detected XANES.

The top portion of Figure 2 shows the Fe_2SiO_4 spectrum measured by Kβ-detected constant emission energy (CEE) scans, denoted as Kβ-detected XANES. The small fluorescence energy window selected by the high-resolution detector used in this experiment suppresses the background contribution due to lifetime broadening of the main edge. This results in an almost flat signal before the pre-edge. Therefore, no background is subtracted from the Kβ-detected XANES. Figure 2 shows that the peaks in the pre-edge feature measured by Kβ-detected XANES are much better separated from the main edge. Furthermore, we find that the Kβ-detected pre-edge structures show a significantly higher integrated intensity relative to the normalized main edge.

Fe oxide model compounds

Figure 3 shows the Kβ-detected XANES spectra of Fe_2SiO_4 (fayalite: Fe^{II} in O_h), α-Fe_2O_3 (hematite: Fe^{III} in O_h) and $FePO_4$ (iron phosphate: Fe^{III} in T_d). $FePO_4$ exhibits a sharp and strong pre-edge peak – as an almost perfect model for Fe in a tetrahedral coordination of oxygen. The much weaker pre-peaks of α-Fe_2O_3 – Fe in non-perfect octahedral oxygen coordination – are also clearly visible. The low spectral intensity between the pre-edge and the main edge in α-Fe_2O_3 has been attributed to Fe–Fe contributions.[22] Fe_2SiO_4 – as a Fe^{II} model compound with octahedral oxygen coordination – exhibits a different spectral shape of the pre-edge, which is also shifted to lower energy by ~ 1.5 eV relative to the energy

position of α-Fe_2O_3. The position of the main edge shifts by ~ 4 eV relative to the energy position of the Fe^{III} oxide compounds. This difference in the relative energy shifts is in line with the general observations that pre-edges shift less than edges.[12]

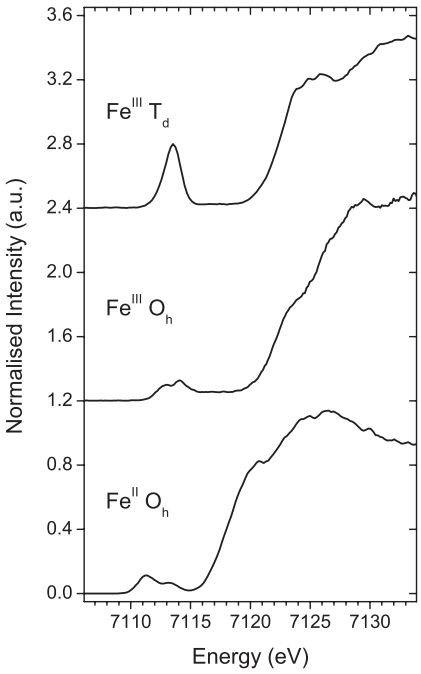

Figure 3: Kβ-detected XANES of selected iron oxide model compounds, from top to bottom: $FePO_4$, iron phosphate (Fe^{III} in tetrahedral oxygen coordination), α-Fe_2O_3, hematite (Fe^{III} in octahedral oxygen coordination) and Fe_2SiO_4, fayalite (Fe^{II} in octahedral oxygen coordination).

Table 1 lists the characteristics of the pre-edge spectral features, i.e. the energy positions of the fitted peaks, the centroid of the pre-edge structure and the integrated intensities. The latter two numbers do not include peaks above 7115 eV, because these peaks are supposedly due to Fe–Fe interactions. For each compound, we show the values as obtained from the Kβ-detected and conventional XANES as well as the numbers reported by Wilke et al.[22] There is good agreement for the numbers obtained from conventional XANES between our data and these results. On the other hand, in the Kβ-detected XANES spectra the intensity (total area) of the pre-edge is approximately three times higher than in the conventional XANES spectra. The systematic increase of the pre-edge intensity with respect to the edge jump is related to the fact that the fluorescence energy selected by the detector is set at the maximum intensity of the Kβ-emission on the pre-edge (using Fe_2O_3). The determination of this setting during resonant excitation at the pre-edge causes an enhanced pre-edge intensity relative to the main edge jump. This accounts for the systematically higher pre-edge to main edge intensity ratio for Kβ-detected XANES compared to conventional XANES.

While the amount and energy position of the different peaks that contribute to the pre-edge feature deviate between the two detection modes, we obtain the same centroid positions. Figure 4 is a graphical summary of the data in Table 1. The dotted vertical lines indicate the average energy position of the centroids representing Fe^{II} and Fe^{III} compounds at 7112.0 and 7113.5 eV respectively.

Table 1: Pre-Edge characteristics for reference compounds, Fe_2SiO_4 (Fe^{II}, O_h), Fe_2O_3 (Fe^{III}, O_h) and $FePO_4$ (Fe^{III}, T_d)

sample – detection[a]	component position (eV)	area	centroid (eV)	total area
Fe_2SiO_4 – Kβ[b]	7111.31	0.2020	7112.02	0.3161
	7113.28	0.1141		
Fe_2SiO_4 – proc Wilke[c]	7110.83	0.0197	7111.85	0.0851
	7111.70	0.0440		
	7113.10	0.0214		
Fe_2SiO_4 – ref Wilke[d]	7111.22	0.0385	7112.04	0.1025
	7111.81	0.0313		
	7113.24	0.0327		
Fe_2O_3 – Kβ	7112.74	0.1239	7113.59	0.2886
	7114.22	0.1647		
	7116.01[e]	0.0581[e]		
	7117.60[e]	0.0418[e]		
Fe_2O_3 – proc Wilke	7112.65	0.0355	7113.50	0.0926
	7114.02	0.0571		
	7115.50[e]	0.0274[e]		
	7116.87[e]	0.0181[e]		
Fe_2O_3 – ref Wilke	7112.68	0.0489	7113.47	0.1236
	7113.98	0.0747		
	7115.22[e]	0.0468[e]		
	7116.68[e]	0.0332[e]		
	7117.83[e]	0.0109[e]		
$FePO_4$ – Kβ	7112.73	0.1561	7113.45	0.8039
	7113.62	0.6478		
$FePO_4$ – proc Wilke	7113.52	0.2500	7113.52	0.2500
$FePO_4$ – ref Wilke	7113.55	0.3423	7113.55	0.3423

[a] Samples measured at 25 °C in air. [b] Spectra measured by Kβ-detected XANES. [c] Spectra measured by conventional fluorescence yield XANES, analysis according Wilke et al.[22] [d] literature data from Wilke et al.[22] [e] Contributions above 7115 eV are not included in centroid.

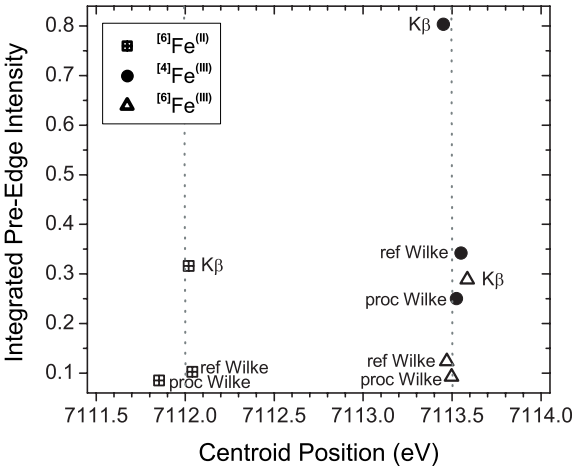

Figure 4: Integrated pre-edge intensity versus centroid position for Fe in selected model compounds, characteristics denoted by $^{[O\text{-coordination}]}Fe^{(formal\ valence)}$: $FePO_4$ = $^{[4]}Fe^{(III)}$, α-Fe_2O_3 = $^{[6]}Fe^{(III)}$ and Fe_2SiO_4 = $^{[6]}Fe^{(II)}$. Dotted vertical lines at respectively 7112.0 and 7113.5 eV indicate the average energy position of the centroid for Fe^{II} and Fe^{III} compounds, respectively. The different methods are (Kβ) Kβ-detected XANES, (proc Wilke) total fluorescence XANES using the edge subtraction procedure outlined by Wilke and co-workers, and (ref Wilke) data as reported by Wilke et al.[22]

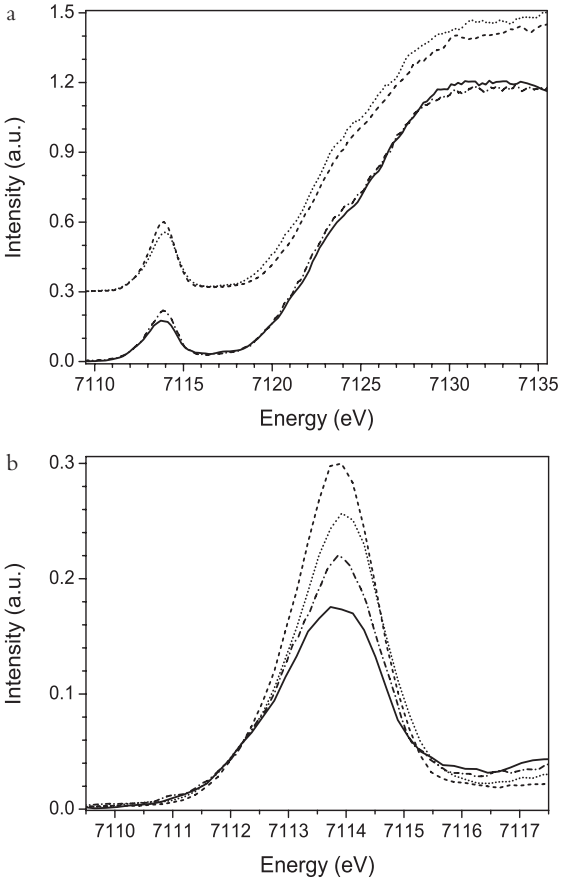

Figure 5: (a) Kβ-detected XANES of framework-substituted FeZSM-5 samples: *tf*-FeZSM-5, after template removal (dashed line); *H*-FeZSM-5, proton form after calcination of ammonium exchanged sample (dotted line); *ms*-FeZSM-5, mild steamed sample (dash-dot line); and *hs*-FeZSM-5, hard steamed sample (solid line). The spectra were measured in a flow of O_2 (7.7 vol % in He) at 350 °C. (b) Zoom of the pre-edge region.

6.3.2. Activation of framework-substituted FeZSM-5

The influence of the activation treatments on the oxidation state and local geometry of iron in framework-substituted FeZSM-5 is probed by Kβ-detected XANES. In Figure 5 the spectra in the energy region 7105-7135 eV are shown for FeZSM-5 samples after template decomposition (*tf*-FeZSM-5), calcination, ion exchange and again calcination (*H*) and steaming (*ms/hs*). The pre-edge region is enlarged to facilitate the comparison of the intensities of the different spectra. The samples were all measured at 350 °C in moderate oxygen atmosphere, i.e. 7.7 % O_2 in helium. No spectra were recorded for as made (*am*) and ammonium-form (NH_4) FeZSM-5 samples. The energy position of the pre-edge does not change. The intensity of the pre-edge peak, however, is clearly influenced by each activation step. We note that after the removal of the template by pyrolysis in dry nitrogen at 520 °C, the sample was calcined in dry air, then ammonium exchanged and finally a second calcination in dry air was conducted to obtain the proton-form (*H*). This treatment results in a decrease of the pre-edge intensity, from 0.64 to 0.55 (see Table 2). A further decline of the pre-edge intensity is observed upon steam treatment. The total area amounts to 0.46 and 0.39 for respectively mildly steamed (*ms*) and hardly steamed samples (*hs*).

Table 2: Pre-edge characteristics for FeZSM-5 samples (Kβ-detected XANES)[a]

sample[b]	treatment	component position (eV)	area	centroid (eV)	total area
am-FeZSM-5	as-synthesized				
tf-FeZSM-5	template free	7112.85	0.1038	7113.74	0.6402
		7113.92	0.5364		
NH_4-FeZSM-5	ammonium exchanged				
H-FeZSM-5	calcined	7112.73	0.0917	7113.78	0.5459
		7114.00	0.4543		
H-FeZSM-5[c]	calcined	7111.89	0.0285	7113.74	0.3383
		7113.91	0.3099		
ms-FeZSM-5	mild steamed	7112.76	0.0935	7113.71	0.4550
		7113.95	0.3615		
hs-FeZSM-5	hard steamed	7112.78	0.0906	7113.68	0.3887
		7113.95	0.2981		
cvd-Fe/ZSM-5	calcined	7112.59	0.0360	7113.58	0.4456
		7113.67	0.4096		
		7116.35[d]	0.0666[d]		
cvd-Fe/ZSM-5[c]	calcined	7112.94	0.0476	7113.64	0.3227
		7113.77	0.2751		
		7116.68[d]	0.0359[d]		

[a] *am*-FeZSM-5 and NH_4-FeZSM-5 are not measured. [b] Measured at 350 °C in O_2 (7.7 % in He) unless stated otherwise. [c] Measured at 25 °C after measurements at 350 °C and cooling down. [d] Contributions above 7115 eV are not included in centroid.

Because of the more uniform preparation way of overexchanged *cvd*-Fe/ZSM-5 its structure and reactivity is much better described in literature. To obtain qualitative information on the behavior of activated framework FeZSM-5 we compare the proton-form (*H*) with extraframework iron containing overexchanged *cvd*-Fe/ZSM-5. Kβ-detected XANES spectra were subsequently taken under O_2 (7.7 % in helium) at 25 °C and at 350 °C. In Figure 6 the spectra in the energy region 7105-7135 eV are shown for *H*-FeZSM-5 and *cvd*-Fe/ZSM-5 (high loaded sample, extraframework iron introduced via the chemical vapor deposition method). Spectra were furthermore taken under pure helium at 350 °C (not shown). The pre-edge peak intensity at 350 °C is higher for framework-substituted *H*-FeZSM-5 indicating the presence of iron in tetrahedral positions, most probably of the zeolite lattice. Extraframework *cvd*-Fe/ZSM-5 does not have iron in the zeolite matrix (apart from small impurities) and the coordination of the iron atoms in the binuclear clusters depends on the chemical environment. At 350 °C, under oxygen atmosphere, the coordination of oxygen around iron is most probably distorted from an octahedral arrangement, regarding the integrated pre-edge intensity, which is intermediate between the tetrahedral and octahedral reference iron oxide compounds (Figure 7).[8] There is a small difference in the height of the pre-edge peak of *H*-FeZSM-5 measured under O_2 in helium and under pure helium. Upon cooling down in the O_2 mixture both the low loaded framework and the high loaded extraframework sample display a lower pre-edge intensity. An additional spectral feature between the pre-edge and the main edge was observed for extraframework *cvd*-Fe/ZSM-5. As noted before, this peak is believed to be due to Fe–Fe interactions.[22]

In Table 2 the pre-edge characteristics for the framework-substituted FeZSM-5 samples are listed. The pre-edge feature could be fitted best by two components. The first component at approximately 7112.8 eV has a smaller area, which remains constant during the treatments. Thus, the changes in the total area are related to the decrease in the integrated intensity of the second component around 7113.9 eV. A theoretical analysis and simulation study of Fe K edge 1s → 3d pre-edge features of iron complexes reveals that for tetrahedral high-spin Fe^{III} compounds two components can be distinguished. The first one at lower energy is related to electric quadrupole transitions and the second component is originating from both quadrupole and dipole transitions.[12] As mentioned before, the enhanced pre-edge intensity for non-centrosymmetric systems is due to the dipole allowed 1s → 4p character added to the 3d-band. The observed changes in the second component therefore clearly point to a change in symmetry. The valence of Fe is hardly affected regarding the unchanged intensities of the first component and rather similar energy positions of the whole centroid for the framework-substituted FeZSM-5 samples.

Figure 7 presents the changes in the centroid position and the integrated pre-edge intensity for framework-substituted (△) and overexchanged samples (●). The characteristics of the reference iron oxide compounds with known valence and local coordination of iron are also plotted in the graph (filled squares). The energy position of the centroid differs not much for the FeZSM-5 samples, but is deviating from the position of the Fe^{III} references by about 0.2 eV to higher energy.

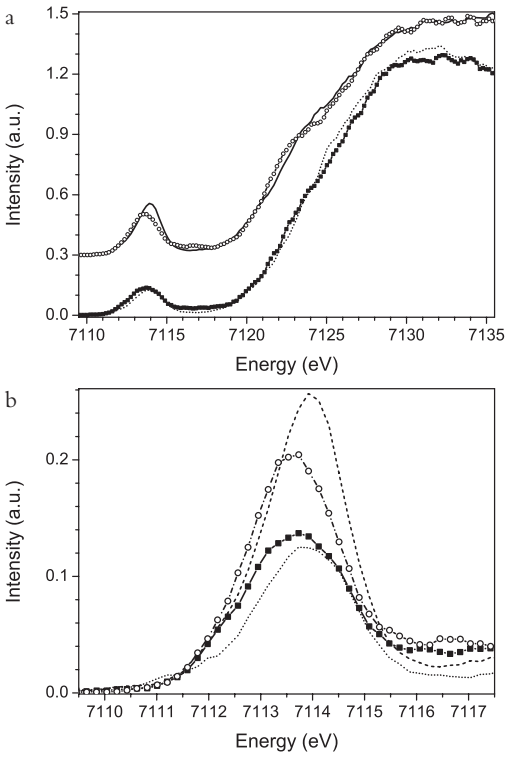

Figure 6: (a) Kβ-detected XANES of framework-substituted FeZSM-5 samples compared with extraframework Fe/ZSM-5 samples: *H*-FeZSM-5 in O_2 (7.7 vol % in He) at 25 °C (dotted line); and 350 °C (solid line); *cvd*-Fe/ZSM-5 in oxygen (7.7 vol % in He) at 25 °C (filled squares) and 350 °C (open circles). (b) Zoom of the pre-edge region.

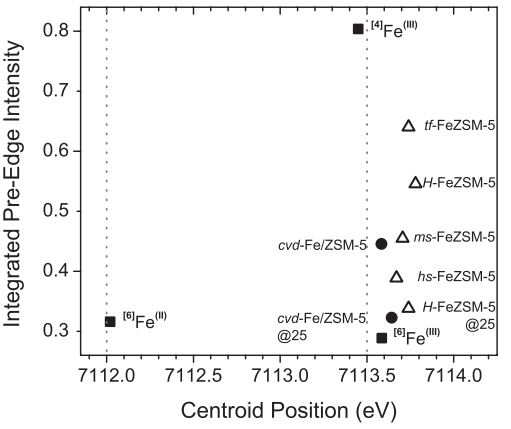

Figure 7: Integrated pre-edge intensity vs centroid position for iron in different FeZSM-5 samples. Framework-substituted FeZSM-5 samples are compared with extraframework *cvd*-Fe/ZSM-5 samples. All iron-containing ZSM-5 samples are measured in a flow of O_2 (7.7 vol % in He) at 350 °C unless indicated by @25, meaning 25 °C: *tf*-FeZSM-5, after template removal; *H*-FeZSM-5, proton form after calcination of ammonium-exchanged sample; *ms*-FeZSM-5, mild-steamed sample; and *hs*-FeZSM-5, hard-steamed sample. The pre-edge characteristics are also given for iron model compounds: $FePO_4$ = $^{[4]}Fe^{(III)}$, α-Fe_2O_3 = $^{[6]}Fe^{(III)}$ and Fe_2SiO_4 = $^{[6]}Fe^{(II)}$.

6.4. Discussion

FeZSM-5 catalysts with a low loading of iron up to 1 wt % are most active and desirable for catalyzing the selective oxidation of benzene to phenol using N_2O as an oxidant.[1] A major reason for the use of framework-substituted iron-containing zeolites over the use of post-synthesis introduced samples is the lack of reproducibility of the latter type of low loaded FeZSM-5. The type of iron species introduced by means of aqueous ion exchange, for instance, strongly depends on the pH of the solution and the nature of the counter anion. A pH close to 7 leads to the formation and precipitation of iron hydroxides and after calcination consequently to iron oxide clustering, most likely on the outer surface of the zeolite crystals. Ion exchange with some particular iron salts also tends to cover preferably the outer surface. Another issue is the stability of the iron anchored on the intrazeolitic cation exchange positions.

To overcome these problems, it was suggested to introduce the active extraframework iron literally from the other side, i.e. transformation of framework Fe into extraframework species. Using the hydrothermal synthesis method Fe can be built in the silica matrix of MFI, yielding Fe-silicalite or – in case of the presence of Al – FeZSM-5. Due to its larger dimensions the incorporation of an Fe atom most likely induces a local stress on the Si–O–Si bonds of the zeolite framework. The well-known hydrolysis of such bonds is probably enhanced for Fe–O–Si bonds. It is known that exposure to water indeed causes the extraction of Fe out of the tetrahedral framework positions. However, up to now, it has been impossible to quantify reliably the fraction of dislodged iron.

6.4.1. Quantitative determination of tetrahedral Fe

From the Kβ-detected XANES spectra the influence of activation treatments on the iron in framework-substituted FeZSM-5 is clearly visible. The maximum intensity of the pre-edge relative to the main edge is continuously decreasing upon progressed treatments from the as-made sample to the final steamed samples, while the peak shape remains rather similar. The integrated pre-edge intensity previously identified as a characteristic of the pre-edge shows the same downward trend. The other defined pre-edge characteristic, the energy position of the centroid, hardly changes for the FeZSM-5 samples from the energy position for Fe^{III} compounds. To make a quantification of the amount of tetrahedral Fe, first the assumption is made that the symmetry of iron in $FePO_4$ and in Fe_2O_3 represent the extremes for the possible coordination of iron species in FeZSM-5, i.e. isomorphous substitution for silicon in the T_d sites of the zeolite framework or fully extracted and hence sixfold coordinated by oxygen. The integrated intensity of FeZSM-5 samples can now be considered as a linear combination of the two Fe^{III} references. We have chosen $FePO_4$ – as a model for Fe^{III} in tetrahedral oxygen coordination – and Fe_2O_3 – Fe^{III} slightly distorted from octahedral oxygen coordination. Hereafter, the changes in the pre-edge will be discussed as modifications in the percentage of Fe^{III} occupying T_d sites, where $FePO_4$ is set to 100 % and Fe_2O_3 to 0 % Fe^{III} in T_d positions. This procedure is possible because the pre-edge

integrated intensity is proportional to the probability of the 1s → 3d transitions, which in turn are related to the degree of distortion from the centro-symmetric coordination of the transition metal element, as is explained before. However, a small modification in the pre-edge intensity may arise from variations in the Fe–O bond distances. In a study on V K pre-edges of selected vanadium compounds Wong et al. found an "empirical relation" between the average bond distance and the product of the normalized peak height and width at half height within each of the geometry types.[30]

6.4.2. Template decomposition and calcination

The use of the hydrothermal synthesis method aims at the incorporation of iron in the ZSM-5 framework structure. The spectrum for the as-synthesized sample at 350 °C was not measured in view of the presence of the carbonaceous template residue in the zeolite channels. We expect that the Fe-coordination remains close to tetrahedral except for positions bound to the template. The next sample, template free *tf*-FeZSM-5, was prepared by pyrolysis in dry nitrogen at 520 °C and a subsequent calcination in dry air at 520 °C. Together with the removal of the template out of the zeolite channels and cages, some iron might be extracted out of the framework as indicated by the decreased integrated pre-edge intensity for *tf*-FeZSM-5. If a low heating ramp (1 °C/min) and dried gases are used, the small extraction of iron should be induced by water produced during the template decomposition. Lamberti et al. reported previously[17-21] that for Fe-silicalite a "large fraction" of Fe migrates to extraframework positions upon template removal at 550 °C and calcination at 600 °C. In our case, most probably, the majority of the iron stays in a fourfold oxygen coordination as derived from the integrated pre-edge intensity of 0.64 for *tf*-FeZSM-5.

The decrease in integrated intensity points to the distortion of the perfect tetrahedral geometry of the zeolite framework rather than to iron migration to extra framework positions. From the previously mentioned study of Wilke and coworkers[22] it is known that iron minerals in a fivefold oxygen coordination display an integrated pre-edge intensity, which is in between that of tetrahedral and octahedral coordination.[22] Distortion of the silicon-oxygen tetrahedrons upon template removal from the zeolite channels is promoted by the isomorphous substitution of silicon by – the larger – iron atoms. As long as the template is present the framework is stabilized, but for *tf*-FeZSM-5 the stress on the framework induced by the incorporated iron results in the apparent lowering of iron in 'pure' T_d sites. An analogous relaxing influence of the synthesis template on the framework of molecular sieves was reported for cobalt atoms incorporated in $AlPO_4$-5.[31] Recently, Lamberti and coworkers presented a study on the template burning inside Fe-MFI using synchrotron based X-ray powder diffraction.[32] Their experiment is somewhat different with respect to the sample (which is Al-free) and the more extreme conditions (the use of a pure oxygen flow and a relatively high heating rate of 7.2 K/min from 300 to 1000 K). Similar to our observations for *tf*-FeZSM-5 they noticed an increased disorder of the framework Si atoms upon template decomposition. This phenomenon is ascribed to rupture of Fe– or Si–O–Si bonds and partial Fe migration from the framework.

The small fraction of Na^+ in *tf*-FeZSM-5 was exchanged for NH_4^+, which subsequently was converted in H^+ by calcination in dry air so that the proton-form (*H*-FeZSM-5) was obtained. Upon ion exchange and calcination, essentially as the result of changing the charge compensating cation from Na^+ to NH_4^+ and finally to H^+, the symmetry of iron in the framework further deviates from T_d geometry. While a flow of dried air was used during the calcination, it is not likely that iron is really extracted from the framework. Most probably the elongation of one of the Fe–O bonds in the FeO_4 unit, causes the distortion of the pure tetrahedral site. The longer Fe–O bond can be attributed to the formation of a bridging hydroxyl bond, Fe–O(H)–Si, due to the association of a proton to oxygen in the Fe–O–Si bond. This phenomenon was earlier observed by using EXAFS for a high-loaded, framework-substituted FeZSM-5 with a Fe content of 3.98 wt % and almost no Al in it.[33] For that catalyst it was also shown that the normal tetrahedral environment could be restored upon introduction of other monovalent ions such as Na^+ or K^+.[34]

6.4.3. Steam treatment

The influence of deliberate disruption of Fe–O–Si bonds by heating in a helium stream containing water vapor (steaming) on the iron coordination was investigated for *H*-FeZSM-5. The method used in the literature[4] is the hard steaming procedure, with a water partial pressure of 300 mbar in a total flow of 30 ml/min nitrogen at high temperature of 600 °C for 5 h. Hard steaming causes considerable extraction of iron out of the framework. Using the above outlined quantification method, based on the integrated pre-edge intensities of the Fe^{III} references, we determined that just 19 % of the iron is left in the tetrahedral positions of the framework.

Separately, we performed a mild steaming procedure with a water partial pressure of 100 mbar in a total flow of 200 ml/min nitrogen at high temperature of 600 °C for 2 h. In that case 32 % of the iron is present in framework positions, compared to 19 % for the hard steamed sample. So, the decrease of the amount of iron in tetrahedral framework positions is related to the duration and severity of the steaming procedure, where the pre-edge intensity is lower for hard steamed (*hs*) compared to mild steamed (*ms*) samples.

It is likely that the effort to extract iron out of the zeolite matrix increases with the decreasing fraction of tetrahedral iron left. Even after a severe steaming treatment a significant fraction of iron stays in the framework (19 %). Although the substitution of Si by Fe is rather low (Si/Fe ratio ~ 360) the presence of extra framework Fe will hinder the extraction of underlying framework iron. Most likely there is a large variety in the extracted iron species based on the nearly symmetric shape of the pre-edge peak. The presence of purely octahedral coordinated iron species would have given rise to a typical shoulder in the pre-edge feature at higher energy (confer Fe_2O_3 in Figure 3). Thus, probably the extracted iron did not fully agglomerate into stable iron oxide species with fixed octahedral coordination.

6.4.4. Stabilization of extraframework Fe

The role of aluminum in the MFI structure on the extraction of iron by steaming is not yet clear. Lamberti and coworkers reported for Fe-silicalite the dislodgement of iron out of the zeolite matrix upon a template removal at 500 °C and activation in vacuum at 700 °C. A significant fraction of iron was supposed to be in extraframework positions and could be reduced. Pirutko et al.[35] investigated the activity of iron centers (α-sites) of several steamed MFI catalysts for the benzene to phenol oxidation and found a non-linear correlation between the total amount of iron and the active part. Catalysts displaying strong Brønsted acidity (containing either Al or Ga) were much more active than others (containing B or Ti). Peréz-Ramírez et al.[36] investigated the evolution of iron species and activity in the direct N_2O decomposition for steam-activated Fe-MFI zeolites. They claimed that the stability of Fe-silicalite is higher than for Fe-AlZSM-5 and Fe-GaZSM-5, due to destabilizing effect of Ga and Al on Fe–O–Si bonds. Their conclusion is based on the lower temperature of the steaming treatment needed for the optimum activity in case of the Al and Ga containing Fe-MFI.

A major problem, however, is the difficulty in determining the degree of extraction of iron. A lower activity not necessarily means a lower extent of extraction but can also point to a higher degree of agglomeration. A statistical analysis of infrared data of NO absorption on Fe-silicalite and FeZSM-5 samples by the group of Lamberti revealed that the presence of framework Al favors the dispersion of extraframework Fe centers.[37,38] In summary, the extraction of Fe from the zeolite framework might be easier in the case of aluminum-containing Fe-MFI samples, but the resistance towards the formation of larger clusters is most likely higher. In this view, it is not surprising that for our framework-substituted FeZSM-5 samples the iron is pulled out of the zeolite lattice to form extraframework iron upon the progressed treatments. On the other hand, we did not see the formation of a significant amount of Fe_2O_3-like iron species even after performing a steaming treatment.

6.4.5. Coordination of water

The presence of Fe^{III} in a distorted octahedral fivefold-coordination by oxygen atoms is observed for binuclear iron clusters in overexchanged *cvd*-Fe/ZSM-5 in O_2 (50 % in helium) at 350 °C.[8] We measured the same sample with Kβ-detected XANES and found also integrated pre-edge intensity corresponding to a Fe-coordination of on average five – in 7.7 % O_2 in helium. This means that most of the iron is present in binuclear clusters and that the oxygen bridge is predominantly intact, where on each Fe atom a water group is missing. On the subsequent lowering of the temperature from 350 to 25 °C the H_2O is again able to coordinate to the iron, making up the octahedral arrangement. The change from mainly tetrahedral coordinated iron to octahedral upon cooling down to room temperature is even more pronounced for calcined framework-substituted *H*-FeZSM-5. In this case, two water molecules may be bonded to one iron atom that is still staying in the zeolite framework. Some water is always present in the zeolite channels and cages and upon lowering the temperature it becomes favorable to bind to the iron species.

6.5. Conclusions

Kβ-detected XANES has been used to study framework-substituted FeZSM-5 zeolites. For the first time a quantitative analysis of XANES data was presented on a FeZSM-5 catalyst with a Fe loading fairly below 1 wt %. This achievement is not only a technical breakthrough in X-ray absorption spectroscopy applied to catalysis, but also it opens new possibilities to study in detail the active site of low loaded, framework-substituted FeZSM-5 zeolites.

The application of this new technique to FeZSM-5 and related iron oxide model compounds revealed that Kβ-detected XANES allows for a quantitative investigation of the oxidation state and local coordination of transition metal ions in catalysis under in-situ conditions. The main improvement is due to high-resolution spectra with a significant smaller background contribution to the pre-edge feature.

The removal of the synthesis template from FeZSM-5 zeolites by heating is practically impossible without introducing minor changes in the elemental composition and local geometry of the framework, although the major structure might not be affected.

The (deliberate) presence of water during heat treatments of framework-substituted FeZSM-5 causes the breaking of Fe–O–Si bond and results in the formation of extraframework Fe species. The degree of iron extraction is dependent on the duration and severity of the steam treatment. No evidence is found for the predominant presence of ordered iron oxide phases.

References

(1) Panov, G. I., *CATTECH*, **2000**, *4,* 18-32.
(2) Panov, G. I.; Uriarte, A. K.; Rodkin, M. A. and Sobolev, V. I., *Catal. Today*, **1998**, *41,* 365-385.
(3) Pérez-Ramírez., J.; Mul, G.; Kapteijn, F.; Moulijn, J. A.; Overweg, A. R.; Doménech, A.; Ribera, A. and Arends, I. W. C. E., *J. Catal.*, **2002**, 113-126.
(4) Ribera, A.; Arends, I.; De Vries, S.; Perez-Ramirez, J. and Sheldon, R. A., *J. Catal.*, **2000**, *195,* 287-297.
(5) Chen, H. Y. and Sachtler, W. M. H., *Catal. Today*, **1998**, *42,* 73-83.
(6) Zhu, Q.; Mojet, B. L.; Janssen, R. A. J.; Hensen, E. J. M.; Van Grondelle, J.; Magusin, P. and Van Santen, R. A., *Catal. Lett.*, **2002**, *81,* 205-212.
(7) Sun, Q.; Gao, Z. X.; Chen, H. Y. and Sachtler, W. M. H., *J. Catal.*, **2001**, *201,* 89-99.
(8) Battiston, A. A.; Bitter, J. H.; De Groot, F. M. F.; Overweg, A. R.; Stephan, O.; Van Bokhoven, J. A.; Kooyman, P. J.; Van Der Spek, C.; Vanko, G. and Koningsberger, D. C., *J. Catal.*, **2003**, *213,* 251-271.
(9) Marturano, P.; Drozdova, L.; Pirngruber, G. D.; Kogelbauer, A. and Prins, R., *Phys. Chem. Chem. Phys.*, **2001**, *3,* 5585-5595.

(10) Groothaert, M. H.; van Bokhoven, J. A.; Battiston, A. A.; Weckhuysen, B. M. and Schoonheydt, R. A., *J. Am. Chem. Soc.*, **2003**, *125,* 7629-7640.
(11) Prestipino, C.; Bordiga, S.; Lamberti, C.; Vidotto, S.; Garilli, M.; Cremaschi, B.; Marsella, A.; Leofanti, G.; Fisicaro, P.; Spoto, G. and Zecchina, A., *J. Phys. Chem. B*, **2003**, *107,* 5022-5030.
(12) Westre, T. E.; Kennepohl, P.; Dewitt, J. G.; Hedman, B.; Hodgson, K. O. and Solomon, E. I., *J. Am. Chem. Soc.*, **1997**, *119,* 6297-6314.
(13) Joyner, R. and Stockenhuber, M., *J. Phys. Chem. B*, **1999**, *103,* 5963-5976.
(14) Heinrich, F.; Schmidt, C.; Loffler, E.; Menzel, M. and Grunert, W., *J. Catal.*, **2002**, *212,* 157-172.
(15) Jia, J. F.; Sun, Q.; Wen, B.; Chen, L. X. and Sachtler, W. M. H., *Catal. Lett.*, **2002**, *82,* 7-11.
(16) Chen, H. Y.; El-Malki, E. M.; Wang, X.; Van Santen, R. A. and Sachtler, W. M. H., *J. Mol. Catal. A*, **2000**, *162,* 159-174.
(17) Bordiga, S.; Buzzoni, R.; Geobaldo, F.; Lamberti, C.; Giamello, E.; Zecchina, A.; Leofanti, G.; Petrini, G.; Tozzola, G. and Vlaic, G., *J. Catal.*, **1996**, *158,* 486-501.
(18) Berlier, G.; Spoto, G.; Bordiga, S.; Ricchiardi, G.; Fisicaro, P.; Zecchina, A.; Rossetti, I.; Selli, E.; Forni, L.; Giamello, E. and Lamberti, C., *J. Catal.*, **2002**, *208,* 64-82.
(19) Ferretti, A. M.; Oliva, C.; Forni, L.; Berlier, G.; Zecchina, A. and Lamberti, C., *J. Catal.*, **2002**, *208,* 83-88.
(20) Berlier, G.; Spoto, G.; Fisicaro, P.; Bordiga, S.; Zecchina, A.; Giamello, E. and Lamberti, C., *Microchem. J.*, **2002**, *71,* 101-116.
(21) Zecchina, A.; Bordiga, S.; Spoto, G.; Damin, A.; Berlier, G.; Bonino, F.; Prestipino, C. and Lamberti, C., *Top. Catal.*, **2002**, *21,* 67-78.
(22) Wilke, M.; Farges, F.; Petit, P. E.; Brown, G. E. and Martin, F., *Am. Miner.*, **2001**, *86,* 714-730.
(23) Battiston, A. A.; Bitter, J. H.; Heijboer, W. M.; De Groot, F. M. F. and Koningsberger, D. C., *J. Catal.*, **2003**, *215,* 279-293.
(24) Battiston, A. A.; Bitter, J. H. and Koningsberger, D. C., *J. Catal.*, **2003**, *218,* 163-177.
(25) Hamalainen, K.; Siddons, D. P.; Hastings, J. B. and Berman, L. E., *Phys. Rev. Lett.*, **1991**, *67,* 2850-2853.
(26) Caliebe, W. A.; Kao, C. C.; Hastings, J. B.; Taguchi, M.; Uozumi, T. and de Groot, F. M. F., *Phys. Rev. B*, **1998**, *58,* 13452-13458.
(27) de Groot, F. M. F., *Chem. Rev.*, **2001**, *101,* 1779-1808.
(28) Bergmann, U. and Cramer, S. P., *SPIE Proc.*, **1998**, *3448,* 198-209.
(29) Vaarkamp, M.; Mojet, B. L.; Kappers, M. J.; Miller, J. T. and Koningsberger, D. C., *J. Phys. Chem.*, **1995**, *99,* 16067-16075.
(30) Wong, J.; Lytle, F. W.; Messmer, R. P. and Maylotte, D. H., *Phys. Rev. B*, **1984**, *30,* 5596.
(31) Verberckmoes, A. A.; Weckhuysen, B. M. and Schoonheydt, R. A., *Micropor. Mesop. Mater.*, **1998**, *22,* 165-178.
(32) Milanesio, M.; Artioli, G.; Gualtieri, A. F.; Palin, L. and Lamberti, C., *J. Am. Chem. Soc.*, **2003**, *125,* 14549-14558.
(33) Axon, S. A.; Fox, K. K.; Carr, S. W. and Klinowski, J., *Chem. Phys. Lett.*, **1992**, *189,* 1-6.
(34) Sankar, G.; Thomas, J. M. and Catlow, C. R. A., *Top. Catal.*, **2000**, *10,* 255-264.

(35) Pirutko, L. V.; Chernyavsky, V. S.; Uriarte, A. K. and Panov, G. I., *Appl. Catal. A*, **2002**, *227,* 143-157.

(36) Perez-Ramirez, J.; Kapteijn, F.; Groen, J. C.; Domenech, A.; Mul, G. and Moulijn, J. A., *J. Catal.*, **2003**, *214,* 33-45.

(37) Berlier, G.; Zecchina, A.; Spoto, G.; Ricchiardi, G.; Bordiga, S. and Lamberti, C., *J. Catal.*, **2003**, *215,* 264-270.

(38) Berlier, G.; Bonino, F.; Zecchina, A.; Bordiga, S. and Lamberti, C., *ChemPhysChem*, **2003**, *4,* 1073-1078.

7

Detection with EXAFS of the Fe–Fe and Fe–Al coordination in Fe/ZSM-5

Abstract

Extended X-ray Absorption Fine Structure (EXAFS) analysis of overexchanged Fe/ZSM-5 has yielded contradictory conclusions over the past years. Studies argue for either a major presence of iron in oligo- or binuclear clusters or a sole presence of iron in the form of mononuclear sites. Previously, we have reported a major presence of Fe in binuclear clusters after mild calcination of the Fe species formed during the synthesis of overexchanged Fe/ZSM-5 obtained by chemical vapor deposition of $FeCl_3$. In this paper the possible detection with EXAFS of a Fe–Al and Fe–Si coordination is investigated. This investigation leads to a detailed comparison with EXAFS of mononuclear iron sites (Fe_1) with binuclear iron sites (Fe_2) and oligomeric species (Fe_N), and also with the presence of larger iron-oxide nanoparticles (Fe_{Ox}). This comparison revealed that before washing and calcination, the coordination of the Fe species in ZSM-5 could (also) be well described by a combination of Al and Si lattice atoms, leading to a model with only Fe_1 sites. These Fe sites are found to remain isolated during washing. Calcination converts part of the isolated species in multinuclear unities with limited size (bi- or oligonuclear clusters). The degree of agglomeration into iron oxide-like phases depends on the severity of the calcination. EXAFS analysis cannot make a statistical distinction between the new model of Fe_1 sites, which are converted to Fe_N sites and the original model with mostly binuclear clusters after mild calcination. However, the fact that after sublimation and washing Fe–Al(Si) coordinations can be detected is very likely. The consequences of the new model for the identification of the catalytic active site will be discussed.

7.1. Introduction

Zeolites containing transition metal ions are promising materials for oxygen transfer reactions such as the conversion of nitrogen oxides and the selective oxidation of hydrocarbons. The research in this field encouraged the development of new preparation routes for FeZSM-5 catalysts. In particular the introduction of the $FeCl_3$ sublimation technique (chemical vapor deposition CVD), by Chen and Sachtler can be considered as a breakthrough.[1] These overexchanged Fe/ZSM-5 (Fe/Al ~ 1) samples prove to be the most reproducible. Because of the enzymatic analog an oxygen bridged binuclear iron complex was proposed as a plausible prototype for the active iron site and several groups endeavored to identify the iron species present in Fe/ZSM-5 by means of a range of characterization techniques.[2-10]

Extended X-ray Absorption Fine Structure (EXAFS) has been a major tool to determine the nature of the sites in Fe/ZSM-5. Battiston and coworkers concluded that the majority of the iron was present in the form of binuclear Fe species upon washing and calcination.[2,11-13] It was suggested that the replacement of the two chlorine atoms for oxygen atoms in the washing step could be accompanied by the formation of binuclear iron units. Evidence was provided by the good agreement between the experimental data and the corresponding fits when a Fe–Fe_1 shell at a distance slightly above 3 Å was included in the fit of the data of the sample after subsequent washing (Fe/ZSM-5–H_2O). The growing intensity of the peaks of the higher coordination shells in the Fourier transform of the EXAFS data obtained after further calcination supported the idea of the presence of Fe–Fe contributions. In the fits of the EXAFS data of the samples after calcination an additional Fe–Fe_2 shell around 3.4 Å was needed related to larger iron oxide particles, in agreement with the observations by TEM/EELS(EDX) and Mössbauer spectroscopy.[2] Concerning the Mössbauer results we note that the assignment of a doublet with a quadrupole splitting (QS) of ~ 1.0 mm/s as evidence for a binuclear site[2] has been put in doubt by the recent results on low loaded framework-substituted Fe ZSM-5 by Taboada and coworkers.[14] They find a single peak at an iron loading of 0.15 wt % and a doublet with a QS of ~ 0.7 mm/s at an iron loading of 0.6 wt %. Extrapolating these numbers to 4.4 wt % overexchanged Fe/ZSM5 samples, a QS value of ~ 1.0 mm/s can as well be explained with a more concentrated uniform iron (Fe_1) loading. The dense distributions of Fe_1 sites yields a further increased spin-relaxation rate, resulting in a QS value of ~ 1.0 mm/s. In other words, in case of high iron loadings, Mössbauer spectroscopy is (also) not able to conclusively distinguish between a uniform distribution of Fe_1 sites and the presence of Fe_2 sites. Marturano and coworkers proposed similar structures for the active site in comparable overexchanged Fe/ZSM-5 samples.[15,16] and Pirngruber and coworkers launched a "hypothetical iron tetramer" that is split into two binuclear clusters upon reduction.[8,17]

Recently, Choi and coworkers questioned the presence of iron in binuclear clusters.[18] They used a combination of EXAFS data analysis in k-space and theoretical simulations of the Fourier Transform (FT) and argued that the peak in the FT at 2.5 Å, appearing as a 'real distance' at 3 Å, should be assigned to Fe–Al backscattering instead of Fe–Fe backscattering.

The authors argue that they are able to "identify" the backscattering element contributing to a given peak by the shape of the imaginary part of the Fourier transform. In our opinion the assumption of a relation between backscattering element and the shape of imaginary part of the Fourier transform is not correct as will be argued in the discussion. However, the question whether Fe–Al and or Fe–Si coordinations can be detected with EXAFS in Fe/ZSM-5 remains to be answered.

In this paper, we will demonstrate that both Fe–Fe and Fe–Al(Si) coordinations can be detected with EXAFS. The crucial aspect of the EXAFS analysis is the occurrence of anti-phase effects in the backscattered waves of Fe–Fe and Fe–Al(Si) contributions. The application of R-space fitting together with the difference file technique makes it possible to unravel the different contributions that are also very close in distance.

7.2. Experimental and EXAFS Data Collection and Analysis

For the sample preparation the $FeCl_3$ sublimation technique – or chemical vapor deposition (CVD) – was used.[1] A full description of the sample preparation is given in an earlier paper.[2] In the exchange procedure Fe is anchored onto Brønsted acid sites in a one to one ratio as indicated by a H^+ removal efficiency of 98 %, determined by HCl titration. After $FeCl_3$ sublimation at 330 °C (sample Fe/ZSM-5–Cl), a washing step was performed (Fe/ZSM-5–H_2O) and two calcination procedures were applied: i) part was severely calcined by calcination in O_2 at 550 °C (Fe/ZSM-5–sc) and ii) part was treated by a milder calcination, i.e. slow heating to 200 °C in helium and after addition of O_2 continuing to 550 °C (Fe/ZSM-5–mc). XRD shows that neither zeolite lattice damage nor formation of large iron oxides phases was occurring, even upon calcination. The Si/Al ratio of 17.0 and the iron loading of 4.4 wt % (Fe/Al = 0.97) were determined by ICP analysis.

The EXAFS data are the same as used for an earlier study.[2] The X-ray absorption spectra of the Fe K edge were collected in transmission mode at Hasylab (Hamburg, Germany) Wiggler Station X1.1, using a Si (111) double crystal monochromator. The edge position was determined for each scan by calibrating the monochromator with a Fe foil. The samples were pressed into self-supporting wafers and placed in a controlled atmosphere cell.[19] Spectra were recorded at liquid nitrogen temperature after flushing with helium at room temperature.

The program XDAP for Windows was used for multiple-shell analysis of the EXAFS data by fitting in R-space.[20] The advantage of R-space fitting compared to the fitting in k-space is discussed elsewhere by Koningsberger and coworkers[21] and Van Bokhoven and coworkers.[22] The different contributions in the EXAFS data were resolved by applying the difference file technique together with phase-corrected Fourier transforms. By using the difference file technique one can survey – during the analysis procedure – the position and intensity of each contribution and the influence of the different contributions on each other. Different k weightings (k = 0 to 3) were used to unravel interference effects of the different coordination shells. Errors in the numerical values obtained by the EXAFS data analysis are estimated to be ± 10 % in the coordination number (N), ± 1 % in the distance (R), ± 5 %

in the Debye Waller factor ($\Delta\sigma^2$) and ± 10 % in the inner potential correction (ΔE_0).

The Fe–O reference used for the EXAFS data analysis was created from experimental EXAFS data of $Fe(acac)_3$. The Fe–Fe phase shifts and backscattering amplitudes were calculated using the software FEFF7.[23] The theoretical Fe–Fe reference was calibrated in a R-space fit on the Fe–Fe shells in the Fourier transform of the EXAFS data obtained from Fe_2O_3. For further details see.[2] The Fe Al/Si reference, based on the structure of hercynite,[24] $FeAl_2O_4$, was calculated with FEFF8 [25] and the input parameters are given in Table 1.

Table 1a: Input parameters[a] for FEFF8 used to produce the EXAFS Fe–Al reference file.

Atom pair	*N*	R (Å)	$\Delta\sigma^2$ (Å^2)	V_r (eV)	V_i (eV)	S_0^2
Fe–Al	1	3.38	0	-7.6	1.0	0.75

[a] The calculated Fe–Al distance is identical to that in the crystallographic structure of iron spinel, $FeAl_2O_4$, space group F_{d3m}, cell parameter a = 8.145 (at 300K) as taken from literature data. [24]

Table 1b: Structural parameters (first Fe–Al shell) as obtained from the R-space fit of Hercynite, $FeAl_2O_4$, using the Fe–Al theoretical reference.

k^1 Fourier Transform		Structural Parameters				Variance	
Δk (Å^{-1})	ΔR (Å)	*N*	*R* (Å)	$\Delta\sigma^2$ (Å^2)	ΔE_0 (eV)	Im.	Abs.
2.5-12.6	1.2-4.0	12.0	3.38	0.0695	0.3	1.46	0.84

7.3. Results and Discussion

7.3.1. Fe oxidation state and characteristics of the Fourier Transform

The positions of the edges in the X-ray absorption near edge structure (XANES) spectra of the Fe/ZSM-5 samples agree with that of Fe_2O_3, the Fe^{III} reference compound. It was concluded that throughout the several synthesis steps, the oxidation state of iron is trivalent.[2] The experimental EXAFS data of all Fe/ZSM-5 samples have been reported earlier.[2] Figure 1a shows as an example the experimental EXAFS data, $\chi(k^0)$, of Fe/ZSM-5–H_2O. The corresponding k^0 Fourier Transform is given in Figure 1b. A broad peak is present in the FT of Fe/ZSM-5–H_2O at values of R between $0.5 < R < 2$ Å. Higher shells are visible up to 4 Å. The same kinds of features are obtained for all four samples (Fe/ZSM-5–Cl, Fe/ZSM-5–H_2O, Fe/ZSM-5–mc and Fe/ZSM-5–sc).

7.3.2. Analysis of first coordination shells

The results for the analysis of the broad peak have been published before and will be briefly summarized below. In the case of the sample after sublimation, Fe/ZSM-5–Cl,

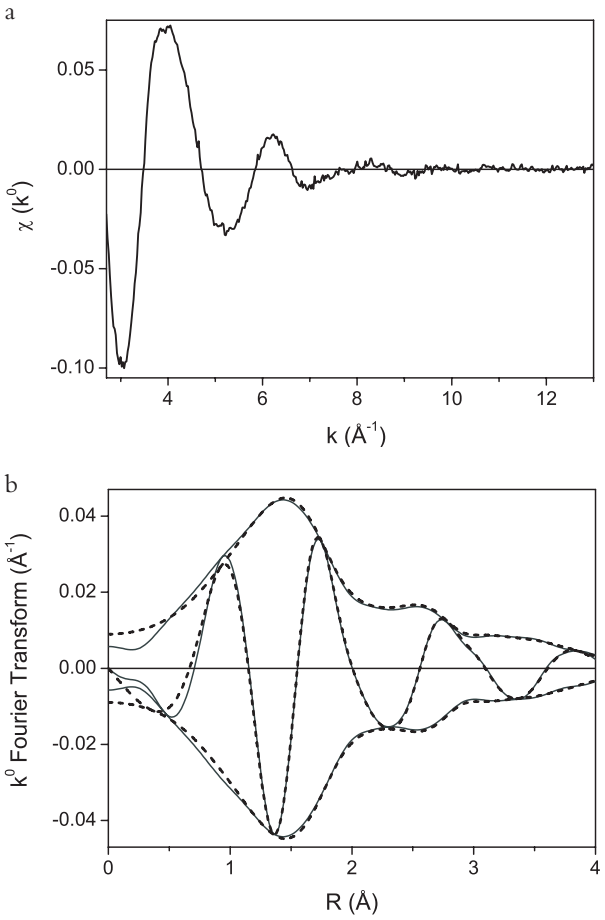

Figure 1: (a) (k^0) experimental data of Fe/ZSM-5–H_2O, measured in helium at 77 K. (b) k^0 Fourier transform (Δk = 2.7–13.0 $Å^{-1}$) of experimental data (solid line) and fit (ΔR = 1–4.5 Å) (dotted line: according to Model I), data of, measured in helium at 77 K.

the broad peak was more asymmetric and positioned at around 1.6 Å. The best fit for the major peak was obtained by using two separate shells: a Fe–Cl and a closer Fe–O shell, each consisting of two atoms. After washing (Fe/ZSM-5–H_2O), no satisfactory fit could be obtained by using a Fe–Cl contribution and the peak at 1.5 Å was entirely fitted with the Fe–O contribution. A total amount of six oxygen neighbors could be fitted using two separate shells with a 3:3 oxygen distribution. The broad FT peak of the mildly calcined sample Fe/ZSM-5–mc resembles very much that of the sample after washing. Again, the best fit could be obtained with a symmetrical distribution of six oxygen atoms in two separate shells. Finally, for the severely calcined sample, Fe/ZSM-5–sc, also no significant differences in the broad peak of the FT were observed and therefore a similar 3:3 model was used to fit the first two oxygen shells. The resulting coordination parameters of the first two coordination shells are summarized in Tables 2 and 3.

7.3.3. Analysis of higher coordination shells, use of difference file

In our previous study[2] we have analyzed for all four samples the higher shell region ($2 < R < 4$ Å) of the FT only in terms of Fe–Fe contributions. This analysis model will be called Model I, and the previously obtained Fe–Fe EXAFS coordination parameters are given in Table 2. Here, we will first provide a detailed inspection of the higher shell region of the FT of the EXAFS data for all four samples by making use of the difference file technique. The strength of the difference file technique is the possibility to zoom in on the weaker contributions by defining a difference file: raw experimental data minus the fit of shell (1) and (2), written as 'RAW-1-2'. The difference file technique provides in this way the opportunity to obtain a FT of the remaining EXAFS that represents the contributions other than the prevailing first two shells, which lead to the intense broad FT peak present at values of R between $0.5 < R < 2$ Å. Moreover, the application of different k-weightings may reveal the presence of heavy scatters. In the FT of EXAFS data having a large contribution of high Z elements the increase in the amplitude in the case of a k^3-weighted FT is more pronounced.[26]

In Figure 2 the FT of the difference file (RAW-1-2) is shown for all four samples using two different k-weightings (k = 0 and 3). The FT's are taken up to k = 10.0 $Å^{-1}$ to suppress the influence of noise; in particular the noise in a k^3 weighted FT is manifested as an oscillation on top of the broad peaks around 2.5 Å. From Figure 2 it is evident that the higher shell contributions can be well resolved in the FT of the difference file (RAW-1-2). It seems that the higher shell contributions are different for all four samples. From comparing Figure 2 (a) and (b) the effect of a different weighting is visible. In Figure 2b for Fe/ZSM-5–sc a clear shoulder appears next to the peak around 2.5 Å when using a k^3 weighting. This feature does not correspond with the relation between the intensity of the different samples in both k-weightings and shows that a high Z element must be present in the higher shells. At least for the severely calcined sample the presence of a significant amount of iron (hydr)oxides is already visible in the FT of the raw data. In our previous paper[2] we have interpreted the increase in intensity of the '2.5 Å peak' between the sample after sublimation and the one after washing to result exclusively from in increase in a Fe–Fe backscattering (model I).

7.3.4. Analysis of higher coordination shells of Fe/ZSM-5–H_2O using Model II

We will use the EXAFS data of the sample after washing (Fe/ZSM-5–H_2O) for a comparison of the previously published model I (Fe–Fe + Fe–O_z) with an alternative model II (Fe–Al/Fe–Si + Fe–$O_{zeolite}$). In our previous paper, it was necessary to include a Fe–$O_{zeolite}$ contribution in order to fit the higher shells up to 4.5 Å. A strong overlap was found to exist between the Fe–O_z and the '2.5 Å peak'. In model I the '2.5 Å peak' was fitted with a Fe–Fe contribution. In model II the '2.5 Å peak' has been fitted with a Fe–Al + Fe–Si contribution. A Fe–Al and Fe–Si coordination was found with N = 1, R = 2.81 Å and N = 2; R = 3.21 Å (Table 3). During the fitting the ΔE_0 values of the Fe–Al and Fe–Si

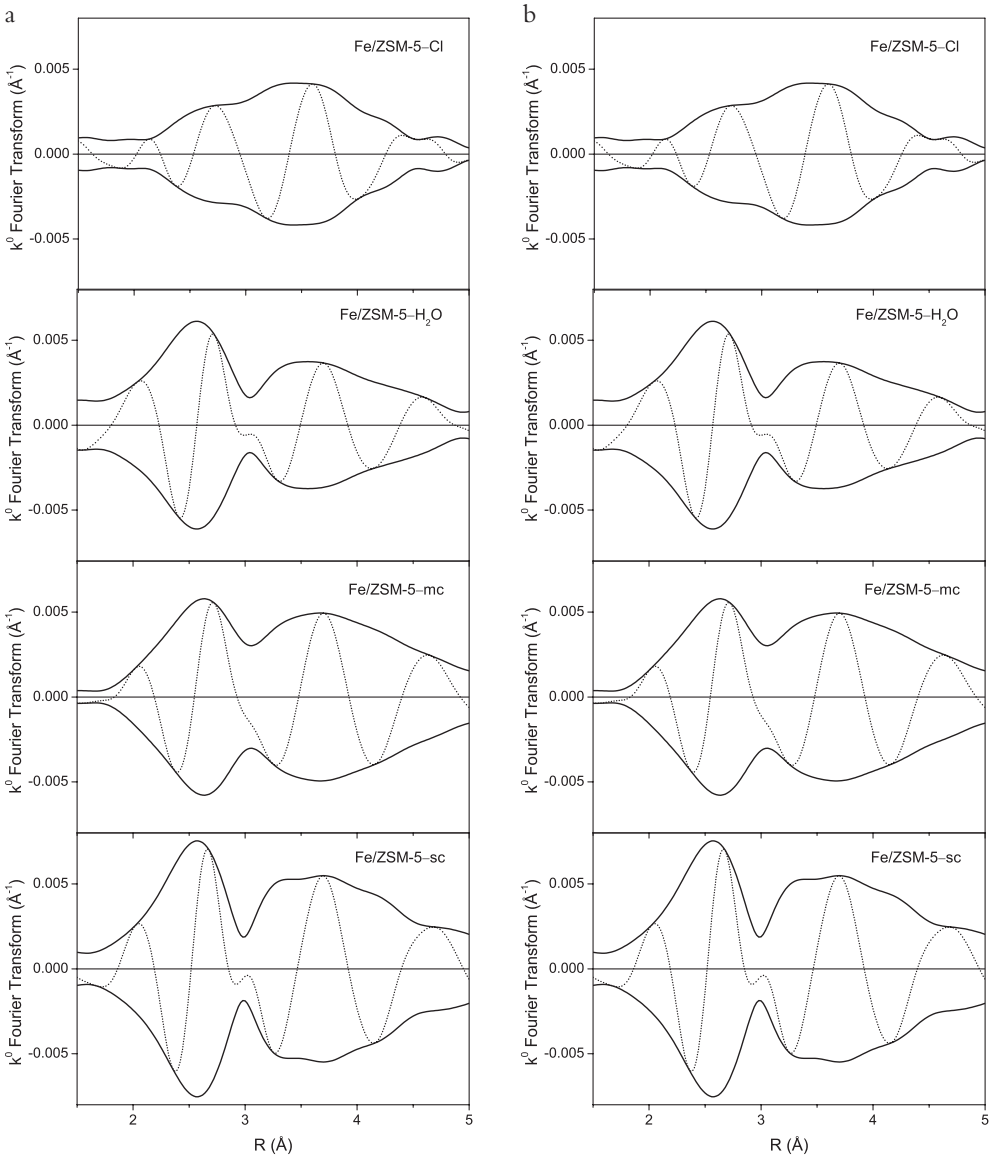

Figure 2: FT (Δk = 2.7–10.0 Å^{-1}) of difference files (RAW data minus (Fe–O_1 + Fe–O_2)) of (top to bottom) Fe/ZSM-5–Cl, Fe/ZSM-5–H_2O, Fe/ZSM-5–mc and Fe/ZSM-5–sc measured in helium at 77 K. (a) k^0-weighted FT, (b) k^3-weighted FT.

contributions were coupled and used as one free fit parameter. This is justified since Al and Si are both distant scatters in contrast to the first shells, in which Fe–O bonds are present which may have different covalences leading to different ΔE_0 values. Moreover, Al and Si are neighbors in the periodic table (respectively Z = 13 and 14) having similar phase shifts and backscattering amplitudes, also justifying the use of the same ΔE_0 value. In Figure 3 the Fourier transform of the difference file (RAW-1-2) of Fe/ZSM-5-H_2O can be compared with the fit according to model I (Fe–Fe) (Figure 3a) and with the fit with Model II (Fe–Al + Fe–Si) (Figure 3b).

Table 2: Fit results for Model I. [a] Best fits obtained by multiple shells analysis of the EXAFS data: Overexchanged Fe/ZSM-5 samples, measured in helium at liquid nitrogen temperature (77 K).

	Shells	N (± 10 %)	R (Å) (± 1 %)	$\Delta\sigma^2$ (10^{-3} Å^2) (± 5 %)	ΔE_0 (eV) (± 10 %)	k^1-variance (%) Im. part	Abs. part
	Fe/ZSM-5–Cl					0.08	0.04
(1)	Fe–O	1.8	1.99	-1.0	-5.9		
(2)	Fe–Cl	2.1	2.20	1.4	4.5		
(3)	Fe–Fe	0.3	2.94	0.0	8.5		
(4)	Fe–O_z	4.4	3.97	10.5	-5.5		
	Fe/ZSM-5–H_2O					0.13	0.08
(1)	Fe–O	3.0	1.91	9.1	12.0		
(2)	Fe–O	3.1	2.05	5.9	-8.1		
(3)	Fe–Fe	1.0	3.05	0.7	-3.0		
(4)	Fe–O_z	4.4	3.99	10.5	-1.9		
	Fe/ZSM-5–mc					0.10	0.06
(1)	Fe–O	3.0	1.89	9.6	12.9		
(2)	Fe–O	3.1	2.05	4.3	-7.3		
(3)	Fe–Fe	1.2	3.06	5.4	-3.6		
(4)	Fe–Fe	0.4	3.40	10.7	-8.0		
(5)	Fe–O_z	4.7	4.11	11.7	-6.6		
	Fe/ZSM-5–sc					0.25	0.12
(1)	Fe–O	3.0	1.90	8.1	12.0		
(2)	Fe–O	3.1	2.04	6.9	-7.2		
(3)	Fe–Fe	1.6	3.03	2.0	-4.3		
(4)	Fe–Fe	1.3	3.42	8.5	-8.5		
(5)	Fe–O_z	4.8	4.18	11.2	-8.9		

[a] Results for model I reproduced from 2.

Table 3: Fit results for Model II. Best fits obtained by multiple shells analysis of the EXAFS data: Overexchanged Fe/ZSM-5 samples, measured in helium at liquid nitrogen temperature (77 K).

	Shells	N (± 10 %)	R (Å) (± 1 %)	$\Delta\sigma^2$ (10^{-3} Å^2) (± 5 %)	ΔE_0 (eV) (± 10 %)	k^1-variance (%) Im. part	Abs. part
	Fe/ZSM-5–Cl					0.09	0.04
(1)	Fe–O [a]	1.8	1.99	-1.0	-5.9		
(2)	Fe–Cl [a]	2.1	2.20	1.4	4.5		
(3)	Fe–Al [b]	1.0	2.75	20.6	12.5		
(4)	Fe–Si [b]	2.3	3.20	24.7	12.5		
(5)	Fe–O_z	5.6	4.00	16.5	-6.7		
	Fe/ZSM-5–H_2O					0.18	0.09
(1)	Fe–O [a]	3.0	1.91	9.1	12.0		
(2)	Fe–O [a]	3.1	2.05	5.9	-8.1		
(3)	Fe–Al [b]	1.0	2.81	22.8	12.7		
(4)	Fe–Si [b]	2.3	3.21	5.6	12.7		
(5)	Fe–O_z	5.2	4.13	16.8	-7.0		
	Fe/ZSM-5–mc					0.07	0.04
(1)	Fe–O [a]	3.0	1.89	9.6	12.9		
(2)	Fe–O [a]	3.1	2.05	4.3	-7.3		
(3)	Fe–Al [b]	0.5	2.81	25.3	5.0		
(4)	Fe–Fe	1.7	3.09	10.1	-2.3		
(5)	Fe–Si [b]	1.2	3.18	10.3	5.0		
(6)	Fe–Fe	0.8 [c]	3.54	9.6	-13.7		
(7)	Fe–O_z	6.0 [d]	4.19	19.7	-7.8		
	Fe/ZSM-5–sc					0.18	0.08
(1)	Fe–O [a]	3.0	1.90	8.1	12.0		
(2)	Fe–O [a]	3.1	2.04	6.9	-7.2		
(3)	Fe–Al [b]	0.3	2.81	21.0	-6.8		
(4)	Fe–Fe	2.6	3.08	4.0	-7.9		
(5)	Fe–Si [b]	0.8	3.17	2.2	-6.8		
(6)	Fe–Fe	3.0 [c]	3.43	16.6	-10.8		
(7)	Fe–O_z	6.0 [d]	4.21	17.5	-8.3		

[a] Parameters of first two shells are set at the values obtained in previous fits, model I in Table II. [b] Fe–Al and Fe–Si shells are coupled during the optimization of the fit with respect to coordination number N (in the ratio 1:2) and regarding the inner potential correction E_0. [c] Error margin in most distant Fe–Fe shell is estimated to be ~ 30 %. [d] Contribution of distant oxygen atoms is fixed.

It can be seen that Model I and Model II both are able to fit the FT of the difference file. Also the k^1-variances for model I and II are similar, respectively 0.13/0.08 and 0.18/0.09 for the Im./Abs. part in %. This indicates that the quality of the fit in both cases is acceptable. Next, we calculated the statistically justified number of independent parameters (N_{ind}) according to the Nyquist theorem: [27]

$$N_{ind} = \frac{2\Delta k \Delta R}{\pi} + 2$$

The value of N_{ind} = 25 is based on the energy and fit range used: Δk = 2.7–13.0 Å^{-1} and ΔR = 1–4.5 Å, respectively. The number of free parameters (N_{free}) used for the fit with model I and model II is 12 and 16, respectively (see Table 2). Therefore both fits are statistically allowed. It can now be concluded that the '2.5 Å peak' can be fitted satisfactorily either as a pure Fe–Fe shell (Model I) or as a combined Fe–Al/Fe–Si shell (Model II). Both models describe the data equally well. Tentative molecular modeling shows that extraframework Fe can be bonded via two oxygen atoms to the aluminum in the framework of the zeolite. Accommodation of these mononuclear Fe_1 sites in close proximity of the ZSM-5 framework with one Al neighbor at 2.81 Å and two Si neighbors at 3.21 Å is therefore very likely.

The question rises how it is possible that EXAFS analysis yields two different results? Hence we take a closer look to the composition of the combined Fe–Al/Fe–Si shell. As summarized in Table 3, shell (3), (4) and (5) accommodate respectively Al (N = 1, R = 2.81 Å), Si (N = 2, R = 3.21 Å), and framework O_z (N = 6, R = 4.13 Å). In Figure 4 both the amplitude (absolute part) and the phase (imaginary part) of the FT's of the fits are shown for the separate shells and also their sum. Figure 4 reveals that the peak at R = 2.5 Å can be described by a combined Fe–Al/Fe–Si backscattering. The Fe–O_z backscattering causes the broad contribution centered around R = 3.7 Å, as can be deduced from the perfect overlap of the imaginary part for the sum (solid line) and shell (5) (dashed-dotted line) at high R. Furthermore, the total phase of the Fe–Al contribution (dotted line) is shifted with respect to the Fe–Si contribution (dashed line) due to the difference in coordination distances and thus leading to destructive wave interference (anti-phase effects) and consequently a lower amplitude of the sum (bold solid line). This example demonstrates that interference effects of waves, that jointly form the total EXAFS function, mask in the first instance the different contributions present and as such strongly complicate the data analysis. Figures 3 and 4 make clear that the EXAFS of a Fe–Fe contribution (N = 1, R = 3.05) over a large range of values of k can be similar to the sum of Fe–Al (N = 1, R = 2.81) and Fe–Si (N = 2, R = 3.21) EXAFS functions.

7.3.5. Analysis of higher coordination shells of Fe/ZSM-5–Cl using Model II

Model II has also been applied to the analysis of the EXAFS data obtained for Fe/ZSM-5–Cl. Also in this case the higher shell difference file can be fitted by a combination of a Fe–Al, Fe–Si and Fe–O_z. The results are given in Table 3. As in the case of Fe/ZSM-5–H_2O the contribution at high R (~ 3.7 Å) originates from distant oxygen neighbors being

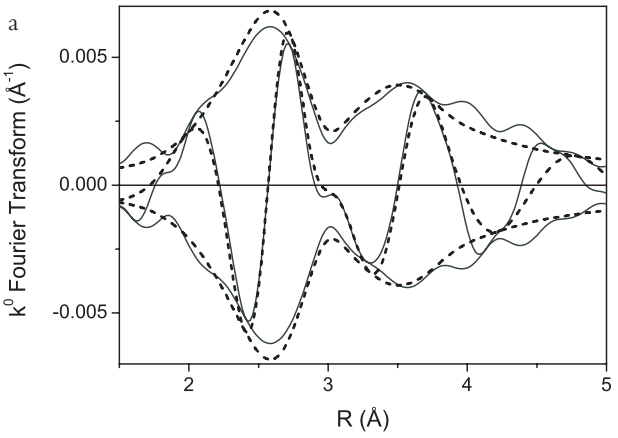

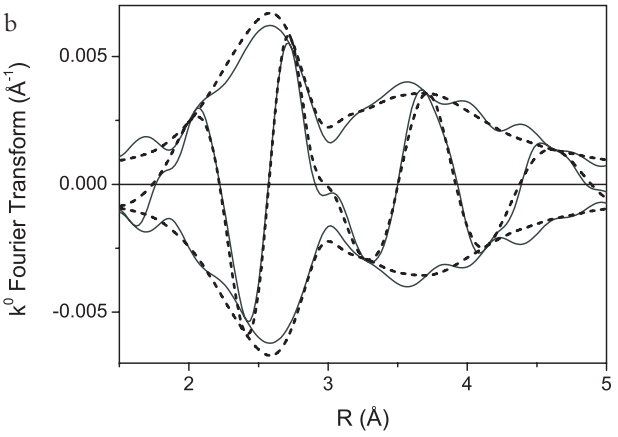

Figure 3: Fourier transform (k^0, Δk = 2.7–13.0 $Å^{-1}$) of difference file (RAW data minus ($Fe–O_1$ + $Fe–O_2$)) (solid lines) and fitted (ΔR = 1–4.5 Å) (dashed lines) higher shells of Fe/ZSM-5–H_2O, measured in He at 77 K. (a) Model I: Fe–Fe + $Fe–O_z$, (b) Model II: Fe–Al + Fe–Si + $Fe–O_z$.

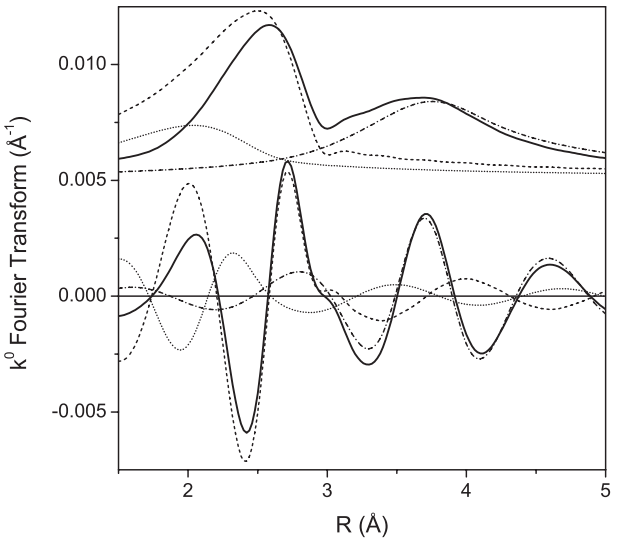

Figure 4: Amplitude (shifted up with 0.005) and phase of Fourier transform (k^0, Δk = 2.7–13.0) for sum of fit (model II) of Fe/ZSM-5–H_2O: Fe–Al + Fe–Si + $Fe–O_z$ (solid line) and individual contributions of Fe–Al (dotted line), Fe–Si (dashed line), $Fe–O_z$ (dashed-dotted line).

part of the zeolite framework. The amount of this oxygen is kept constant at the number of N = 6, because a very distinct determination was not feasible due to an increasing influence of the noise level. The Fe–Al coordination distance is slightly shorter (2.75 versus 2.81 Å) and the disorder in the Fe–Si coordination is 4.4 times higher. The dramatic decrease in the amplitude of the FT of the difference file of Fe/ZSM-5–Cl in comparison with the FT of the corresponding difference file of Fe/ZSM-5–H_2O (Figure 2) can be accounted for by the anti-phase effects of the Fe–Al and Fe–Si contributions induced by the different Fe–Al distance and higher disorder of the Fe–Si coordination.

7.3.6. Perspective of Model II in describing Fe/ZSM-5–Cl and Fe/ZSM-5–H_2O

It can now be concluded that the '2.5 Å peak' can be fitted with only Fe–Al and Fe–Si contributions in the samples after sublimation and after washing. Based on the results of the present EXAFS analysis we can propose for both the Fe/ZSM-5–Cl and Fe/ZSM-5–H_2O samples the presence of a mononuclear Fe_1 species located at a Brønsted acid site. This iron atom is bonded via two oxygen atoms to the aluminum in the framework of the zeolite. The nearest neighbor Al and Si atoms in the ZSM-5 framework are also visible. The slightly shorter Fe–Al distance in Fe/ZSM-5–Cl suggest a stronger attraction of the iron atom. The slightly shorter Fe–Al distance might also result in a larger spread in Fe–Si distances, which can explain the observed higher disorder of the Fe–Si coordination. Most likely, the slightly higher positive charge on iron is due to the presence of chlorine that is able to withdraw electron density. By washing the sublimated sample, the two chlorine atoms are replaced for four oxygen atoms and consequently the geometry around iron is changed from tetrahedral to octahedral. Within the limits of accuracy Model II is not describing the EXAFS better; statistically both Model I and Model II are justified. However, the preference for model II is based upon a more realistic chemical picture, which is also intuitively more appealing. Besides, the newly proposed model agrees with the actual perception in literature of what kind of iron species may be present in Fe/ZSM-5 prepared by sublimation.[28]

7.3.7. Analysis of higher coordination shells of Fe/ZSM-5–mc and –sc using Model II

Assuming that the presence of a mononuclear Fe_1 is correct in describing the structure of Fe/ZSM-5 after washing then a decrease in contribution of this species to the EXAFS data is expected in favor of the growth of binuclear or oligomeric species after mild calcination. The formation of large iron (hydr)oxides species can be expected after more severe calcination. As already shown in Figure 2b a k^3 weighting gives rise to a shoulder next to the FT peak at R = 2.5 Å, which directly points to the presence of heavy scatters as iron in Fe/ZSM-5–sc.

Throughout the fitting procedure of the EXAFS data of the calcined samples the Fe–Al and Fe–Si shells have been coupled during the optimization of the fit both with respect to a ratio in coordination numbers N (1:2) and the inner potential correction ΔE_0

(see discussion above). The coupling with respect to the ratio of the Fe–Al and Fe–Si coordination numbers is based upon the assumption that a fraction of the Fe_1 species is subject to conversion in species with a higher Fe nucleation (Fe_2 and Fe_N). For both calcined samples no reasonable fit could be produced without the inclusion of Fe–Fe contributions. The resulting EXAFS coordination parameters are given in Table 3.

The use of seven coordination shells requires principally 28 free parameters for a statistically justified fit. The octahedral constraint for the first two shells ($N_{1+2} = 6$) and the linking of the Fe–Al and Fe–Si shells (fixed ratio N_{Fe-Al}/N_{Fe-Si}) and the same ΔE_0 lowers N_{free} to 25, which is equal to the allowed value of N_{ind}= 25. Although a comprehensive fit as presented here for the calcined samples may not be covered completely by statistics, the results obtained from fitting Fe/ZSM-5–H_2O with Model II provides in our opinion a validation of the procedure. Because of the very close distances and again the occurrence of interference effects of the Fe–Al, Fe–Si and Fe–Fe shells there is a relatively large uncertainty in the coordination numbers of these shells. On the contrary, the quantity of Fe–Si backscattering, prior to the final linking of N for Al and Si, could be determined independently from variations in the mutual ratio between Fe–Al and Fe–Fe shells.

As already mentioned in the introduction the presence of iron in binuclear clusters has been challenged by Choi and coworkers.[18] Since a different preparation procedure is applied the resulting EXAFS might be different. However, they detected also in the FT of their EXAFS data a higher shell peak at 2.5 Å. The authors used a combination of EXAFS data analysis in k-space and theoretical simulations of the FT. They argue that the peak in the FT at 2.5 Å, appearing as a 'real distance' at 3 Å, should be assigned to Fe–Al backscattering instead of Fe–Fe backscattering. They claim that they are able to "identify" the backscattering element contributing to a given peak by the shape of the imaginary part of the Fourier transform. In our opinion this argument is not correct. The shape of the FT is described by the total phase $\Phi = 2kR+\phi$, where ϕ is the phase shift determined by both the absorber and backscatter. The phase shift, ϕ, is not necessarily the same for the sample under investigation and the theoretical simulated phase. In fact, in the EXAFS data analysis procedure the 'inner potential correction', ΔE_0, is used as a free fit parameter in order to adjust a theoretically calculated phase shift to the phase shift of the experimental EXAFS data. Moreover, as has been shown above interference effects due to anti-phase effects of overlapping shells can severely affect the shape of the imaginary part of the Fourier transform. We therefore cannot support the recent EXAFS conclusions from Choi and coworkers.

7.3.8. Perspective of Model II in describing Fe/ZSM-5–mc and Fe/ZSM-5–sc

Strong arguments in favor of Model II are the systematic changes as observed for the Fe–Al and Fe–Si coordinations as a function of the mild c.q. severe calcination procedures. First of all the fraction Fe_1 species decreases from 100 % to 50 % to 30 %. Also a systematic change in the ΔE_0 values is detected from +12.7 to +5.0 to -6.8 eV. This can be explained by an increase of different iron oxide species with different inner potential values, leading to a

different average inner potential for the sample under investigation. The observed values for the inner potential for the Fe_1 species in comparison to the average inner potential values of the sample can therefore be different. A third important observation is a systematic decrease in the disorder of the Fe–Al and Fe–Si coordination, which can be explained by the fact that Fe_1 entities with the highest disorder will be first converted to Fe_N species.

Moreover, a significant increase in the coordination number is noticed for each of the Fe–Fe shells. We can firmly conclude that the amount of iron that 'sees' the ZSM-5 framework aluminum clearly decreases upon calcination. Already for the mildly calcined sample half of the total amount of iron was not able to stay close to aluminum. That number increases for the severely calcined sample. This observation accounts for the formation of large agglomerates of iron in Fe/ZSM-5–sc, most probably in the form of iron (hydr)oxides, as observed by other techniques.[2] Still, the mildly calcined Fe/ZSM-5–mc is distinguished from Fe/ZSM-5–sc by a different ΔE_0 and a higher degree of disorder, $\Delta\sigma^2$, for the first Fe–Fe shell. Moreover, the mildly calcined sample is characterized by low coordination numbers for both iron shells in contrast with the severely calcined sample and in any case when compared to the higher Fe–Fe coordination shells in Fe_2O_3. The difference between the iron shells of the calcined samples is not only a matter of a decreasing fraction mononuclear Fe_1 (as visualized by the shrinking contribution of Fe–Al and Fe–Si scattering), but reveals first of all the creation of another species with a high diversity in local structure. This can be concluded both from the increase in coordination number of the Fe–Fe_1 and Fe–Fe_2 coordination and the decrease in disorder of the Fe–Fe_1 coordination after severe calcination. In our opinion this might imply that, besides the presence of mononuclear iron units, Fe_1, and agglomerated iron oxide-like phases part, Fe_{Ox}, of the iron is present in multinuclear species, Fe_N. Where a Fe–Fe coordination number equal to unity is typical for binuclear centers, a slightly higher coordination number is expected for oligomeric or chain-like iron species. The anchoring of – either mono or multi nuclear – iron species to framework aluminum is considered to be important to prevent agglomeration and hence inactivity.[29] In the case of steamed samples iron may also be stabilized by extraframework aluminum species.[30-32]

7.3.9. Implication of Model II for the identification of the catalytic active site

We do not intend here to present a more conclusive answer about the species that are active for either or both the selective catalytic reduction of NO (HC-SCR) and the decomposition of N_2O. Despite the clear differences in division of iron over the various species present, see Table 3, no difference in HC-SCR activity was observed between the two calcined samples. This was ascribed to the incomplete participation of all active species for reasons of micropore blocking by aggregated phases.[33] In our earlier studies[2,12,13] we have interpreted the EXAFS data according to Model I. Especially the *in situ* XAFS study of the SCR reaction using the Fe/ZSM-5–mc sample as catalysts[13] led us to assign a binuclear Fe cluster as the catalytic active species. Based upon the statistical evidence of Model I this assignment can still be defended. However, by accepting model II and using literature data

and our earlier *in situ* studies on the Fe/ZSM-5–mc sample a possible closer picture of the catalytic active site can be obtained.

Our *in situ* studies on the Fe/ZSM-5-mc sample made clear that the majority of the Fe species is highly flexible in its oxidation state. We observed a high degree of autoreduction in helium under different conditions. At 1 bar we observe in the temperature range from 150 – 350 °C an ongoing to almost complete autoreduction in helium that is suppressed when O_2 (0.5 bar) is added to the flow.[12] At 2 mbar, still different from ultrahigh vacuum

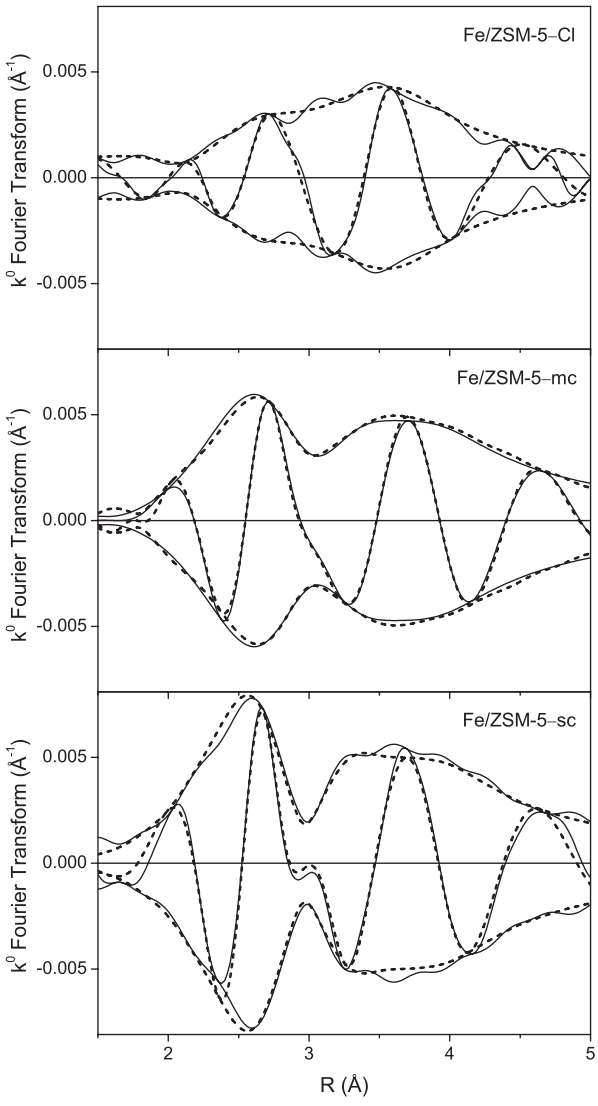

Figure 5: Fourier transform (k^0, Δk = 2.7–13.0 $Å^{-1}$) of difference file (RAW data minus (Fe–O_1 + Fe–O_2)) (solid line) and fitted (ΔR = 1–4.5 Å) (dashed lines) higher shells according to Model II for (top to bottom) Fe/ZSM-5–Cl, Fe/ZSM-5–mc and Fe/ZSM-5–sc, all samples measured in helium at 77 K.

conditions, already at room temperature 30 – 40 % of the Fe is reduced in helium.[34,35] Under these conditions sufficient activation energy for the reduction by organic contaminations in the cell is improbable. Secondly, but not opposite to the first issue, it is known that the average oxidation state of iron measured for Fe/ZSM-5 during the HC-SCR reaction at 1 bar is trivalent.[13] The same average valence was measured by soft X-ray absorption spectroscopy for the catalyst under $DeNO_x$ conditions at 2 mbar.[34] EXAFS studies[2,12,13] of Fe/ZSM-5–mc revealed that the reversible changes in oxidation state from Fe^{III} to ~ 50 % Fe^{II} are connected with the exchange of overall one oxygen in the first two coordination shells around iron.

The assumption of the validity of structural Model II implies directly that almost all octahedral Fe species present in this sample (as mononuclear Fe_1, binuclear Fe_2 and oligomeric multinuclear sites Fe_N) are able to switch oxidation state and can be assigned as possible active sites. Furthermore, it is clear that severe calcination leads to larger FeO_x agglomerates that are inactive. More research is needed to fully establish the structure activity relation for Fe/ZSM-5 catalysts.

7.4. Conclusions

The assumption made by Choi and coworkers to distinguish Fe–Fe from Fe–Al scattering by focusing on the shape of the imaginary part of the Fourier transform cannot be supported. For the analysis of the EXAFS data of complex samples as Fe/ZSM-5, the difference file technique can help to unravel anti-phase effects caused by scattering of coordination shells that are close in distance. We showed that the difference file technique combined with R-space fitting and applying different weightings (k^0, k^3) can be used to analyze both Fe–Fe and Fe–Al/Fe–Si coordinations in the EXAFS data of mild and severe calcined Fe/ZSM-5 samples prepared by the $FeCl_3$ sublimation method.

Two structural models (Model I and II) can describe the EXAFS data and no distinction can be made according to a statistical analysis. In our original Model I the higher coordination shells of the FT of the EXAFS data of the Fe/ZSM-5 samples after sublimation, washing, mild and severe calcination, respectively, are analyzed only in terms of Fe–Fe coordinations. In Model II the higher coordination shells of Fe/ZSM-5 after sublimation and washing can be assigned to a combined Fe–Al and Fe–Si coordination. After calcination also Fe–Fe contributions are observed.

The assumption of Model II implies that in the Fe/ZSM-5 sample after mild calcination the octahedral coordinated Fe species, as mononuclear (Fe_1) and multinuclear ($Fe_{\geq 2}$: binuclear and oligomeric) Fe sites, can be reduced and display activity. After severe calcination also large FeO_x particles are present, which are assumed to be inactive.

References

(1) Chen, H. Y. and Sachtler, W. M. H., *Catal. Today*, **1998**, *42,* 73-83.

(2) Battiston, A. A.; Bitter, J. H.; De Groot, F. M. F.; Overweg, A. R.; Stephan, O.; Van Bokhoven, J. A.; Kooyman, P. J.; Van Der Spek, C.; Vanko, G. and Koningsberger, D. C., *J. Catal.*, **2003**, *213,* 251-271.

(3) El-Malki, E. M.; Van Santen, R. A. and Sachtler, W. M. H., *J. Catal.*, **2000**, *196,* 212-223.

(4) Marturano, P.; Kogelbauer, A. and Prins, R., *J. Catal.*, **2000**, *190,* 460-468.

(5) Heinrich, F.; Schmidt, C.; Loffler, E.; Menzel, M. and Grünert, W., *J. Catal.*, **2002**, *212,* 157-172.

(6) Dubkov, K. A.; Ovanesyan, N. S.; Shteinman, A. A.; Starokon, E. V. and Panov, G. I., *J. Catal.*, **2002**, *207,* 341-352.

(7) Zhu, Q.; van Teeffelen, R. M.; van Santen, R. A. and Hensen, E. J. M., *J. Catal.*, **2004**, *221,* 575-583.

(8) Pirngruber, G. D.; Roy, P. K. and Weiher, N., *J. Phys. Chem. B*, **2004**, *108,* 13746-13754.

(9) Pérez-Ramírez., J.; Santhosh Kumar, M. and Brückner, A., *J. Catal.*, **2004**, 13-27.

(10) Krishna, K.; Seijger, G. B. F.; van den Bleek, C. M.; Makkee, M.; Mul, G. and Calis, H. P. A., *Catal. Lett.*, **2003**, *86,* 121-132.

(11) Battiston, A. A.; Bitter, J. H. and Koningsberger, D. C., *Catal. Lett.*, **2000**, *66,* 75-79.

(12) Battiston, A. A.; Bitter, J. H.; Heijboer, W. M.; De Groot, F. M. F. and Koningsberger, D. C., *J. Catal.*, **2003**, *215,* 279-293.

(13) Battiston, A. A.; Bitter, J. H. and Koningsberger, D. C., *J. Catal.*, **2003**, *218,* 163-177.

(14) Taboada, J. B.; Overweg, A. R.; Craje, M. W. J.; Arends, I. W. C. E.; Mul, G. and Kraan, A. M. v. d., *Micropor. Mesopor. Mater.*, **2004**, *75,* 237-246.

(15) Marturano, P.; Drozdova, L.; Kogelbauer, A. and Prins, R., *J. Catal.*, **2000**, *192,* 236-247.

(16) Marturano, P.; Drozdova, L.; Pirngruber, G. D.; Kogelbauer, A. and Prins, R., *Phys. Chem. Chem. Phys.*, **2001**, *3,* 5585-5595.

(17) Pirngruber, G. D.; Luechinger, M.; Roy, P. K.; Cecchetto, A. and Smirniotis, P., *J. Catal.*, **2004**, *224,* 429-440.

(18) Choi, S. H.; Wood, B. R.; Ryder, J. A. and Bell, A. T., *J. Phys. Chem. B*, **2003**, *107,* 11843-11851.

(19) Vaarkamp, M.; Mojet, B. L.; Kappers, M. J.; Miller, J. T. and Koningsberger, D. C., *J. Phys. Chem.*, **1995**, *99,* 16067-16075.

(20) for the EXAFS analysis program XDAP for Windows of XAFS Services International, see http://www.xsi.nl.

(21) Koningsberger, D. C.; Mojet, B. L.; van Dorssen, G. E. and Ramaker, D. E., *Top. Catal.*, **2000**, *10,* 143-155.

(22) Van Bokhoven, J. A.; Ressler, T.; De Groot, F. M. F. and Knop-Gericke, A., in B.M. Weckhuysen (Ed.), In-situ Spectroscopy of Catalysts, American Scientific Publishers, Stevenson Ranch, CA, USA, **2004**, 123-144.

(23) Ankudinov, A. L. and Rehr, J. J., *Phys. Rev. B*, **1997**, *56,* R1712-R1715.

(24) Harrison, R. J.; Redfern, S. A. T. and O'Neill, H. S. C., *Am. Miner.*, **1998**, *83,* 1092-1099.

(25) Ankudinov, A. L.; Ravel, B.; Rehr, J. J. and Conradson, S. D., *Phys. Rev. B*, **1998**, *58,* 7565-7576.
(26) Koningsberger, D. C. and Prins, R. (Eds.), X-ray Absorption: Principles, Applications, Techniques of EXAFS, SEXAFS and XANES, John Wiley, New York, **1988**.
(27) Stern, E. A., *Phys. Rev. B*, **1993**, *48,* 9825.
(28) Santhosh Kumar, M.; Schwidder, M.; Grünert, W. and Brückner, A., *J. Catal.*, **2004**, *227,* 384-397.
(29) Heijboer, W. M.; Glatzel, P.; Sawant, K. R.; Lobo, R. F.; Bergmann, U.; Barrea, R. A.; Koningsberger, D. C.; Weckhuysen, B. M. and de Groot, F. M. F., *J. Phys. Chem. B*, **2004**, *108,* 10002-10011.
(30) Hensen, E. J. M.; Zhu, Q. and van Santen, R. A., *J. Catal.*, **2003**, *220,* 260-264.
(31) Hensen, E. J. M.; Zhu, Q.; Hendrix, M. M. R. M.; Overweg, A. R.; Kooyman, P. J.; Sychev, M. V. and van Santen, R. A., *J. Catal.*, **2004**, *221,* 560-574.
(32) Hensen, E.; Zhu, Q. J.; Liu, P. H.; Chao, K. J. and van Santen, R., *J. Catal.*, **2004**, *226,* 466-470.
(33) Bitter, J. H.; Battiston, A. A.; van Donk, S.; de Jong, K. P. and Koningsberger, D. C., *Micropor. Mesopor. Mater.*, **2003**, *64,* 175-184.
(34) Heijboer, W. M.; Battiston, A. A.; Knop-Gericke, A.; Hävecker, M.; Bluhm, H.; Weckhuysen, B. M.; Koningsberger, D. C. and de Groot, F. M. F., *Phys. Chem. Chem. Phys.*, **2003**, *5,* 4484-4491.
(35) Heijboer, W. M.; Battiston, A. A.; Knop-Gericke, A.; Hävecker, M.; Mayer, R.; Bluhm, H.; Schlögl, R.; Weckhuysen, B. M.; Koningsberger, D. C. and de Groot, F. M. F., *J. Phys. Chem. B*, **2003**, *107,* 13069-13075.

8

An EXAFS study on the steaming of low loaded FeZSM-5: from framework Fe to oligomeric Fe clusters

Abstract

The changes in the local coordination of Fe upon steaming of framework-substituted FeZSM-5 (Si/Fe = 360, 0.3 wt % Fe) was studied by means of EXAFS. The influence of gas treatments in O_2 and helium at 350 °C was investigated for samples within a series of activated low loaded FeZSM-5. Selective Kα-fluorescence detection was applied to collect high quality *in situ* EXAFS data on 0.3 wt % FeZSM-5 catalysts. The high signal to noise ratio (50) enabled a full EXAFS data-analysis including the higher coordination shells. A structural comparison was made with overexchanged Fe/ZSM-5 (4.4 wt % Fe) prepared by CVD. The activation of low loaded, framework-substituted FeZSM-5 by template removal and calcination distort the zeolite framework and induce a deviation from T_d symmetry for incorporated iron. A 3:1 oxygen distribution was found with Fe–O coordination distances of 1.80 and 1.98 Å, respectively. The introduction of protons leads to a further distortion with a 2:1:1 oxygen distribution with an additional coordination distance at 2.09 Å. Helium treatment at 350 °C of the H-form of FeZSM-5 resulted in a very small release of oxygen (10 %).Steam treatment (T > 500 °C) causes the hydrolysis of the Si–O–Fe bonds and increases the formation of extraframework oligomeric iron species. In the severe steamed sample the extraframework Fe species dominate the EXAFS spectra. The structural properties of the first Fe–O shells of the extraframework Fe species in this sample resemble that of mildly calcined Fe/ZSM-5, including the response of the first oxygen shells to a redox treatment at 350 °C. In addition, the detection with EXAFS of a Fe–Al coordination at 3.1 Å shows that steaming also facilitates the release of framework Al. This Fe–Al coordination is not detected in calcined overexchanged samples. Comparing the intensity of the higher Fe–Fe shells in the most severe steamed sample with those detected in the calcined overexchanged Fe/ZSM-5 leads to the conclusion that the oligomeric extraframework Fe species found after steaming are stabilized by extraframework Al.

8.1. Introduction

The recent research efforts concerning the preparation, testing and characterization of FeZSM-5 catalyst material are tremendous. In the literature review presented in chapter 2 of this thesis we quoted over one hundred research articles of which the majority has appeared in the last five years. FeZSM-5 is a generic name to indicate a large variety of iron-containing zeolites with the ZSM-5 type structure. Besides, several related materials exist based on the structural MFI-analogue without Al in the framework, known as Fe-silicalite. Despite the differences between these FeZSM-5 zeolites almost all of them display to a certain extent activity in the breakdown of nitrogen oxides, being either NO_x or N_2O. This observation may point to the decisive effect of the treatments the catalyst is subject to before use in a catalytic reaction. The various activation treatments as calcination, heating to high temperature and steaming of different FeZSM-5 most likely yields similar sites, but in the distribution between the species is divergent.

The activation of FeZSM-5 materials by performing high temperature treatments (T > 500 °C), as for instance calcinations, heating in helium and steaming, is applied to both synthesis and post-synthesis prepared samples. For post-synthesis prepared Fe/ZSM-5 samples also a beneficial effect of steaming is reported in several studies.[1-3] This increased activity may originate from the formation of more active species, the inhibition of clustering into non-active species, or from the dissolution of transport limitations by for instance mesopore creation.[4-6] For synthesis prepared FeZSM-5 samples steaming or high temperature heating in inert media is profitable since framework Fe sites display almost no activity as they are hampered by a rigid local coordination.[7-9] The anchoring of the created extraframework Fe species is still a matter of debate. In literature three main hypotheses exist to describe the interaction of extraframework Fe with (extra)framework Al: (1) an *electronic* effect on the Fe species, assuming a "chemical difference of iron in Fe-O-Al and Fe-O-Fe adducts".[10] (2) a *structure directing* effect on Fe species, since "the spinel structure of aluminium oxide favors the formation of the inverse spinel structure of an active Fe_3O_4 cluster".[11] (3) an role of (extra)framework aluminum in a *stabilization / anchoring / dispersion* effect.[12]

In chapter 6 the local geometry and oxidation state of Fe in framework-substituted FeZSM-5 samples has been studied using XANES.[13,14] The influence of the various activation steps was examined in O_2 and helium atmosphere at 350 °C. It was found that template removal induced a distortion of the framework FeO_4 tetrahedron. The exchange of the charge-compensating cation associated to the lattice from Na^+, via NH_4^+, to H^+ caused a further deviation from T_d symmetry. However, the lowered intensity of the integrated pre-edge area (the measure used for the site symmetry around Fe[14-16]) may also point to the partial rearrangement of framework iron sites so that additional oxygen atoms are bound. The existence of such flexible framework heteroatoms in H-form zeolites was suggested for Al in zeolites Y, Mordenite and Beta[17,18] and for Fe in ZSM-5.[19] The shrinked integrated pre-edge intensity made clear that the steam treatment brings on the extraction of framework iron and the formation of extraframework species. We noticed the decrease of Fe^{III} in tetrahedral sites to 32 and 19 %, for mild and hard steamed FeZSM-5 respectively

(chapter 6).[14] The decrease in abundance of (magnetic) Fe^{III} in isolated sites was observed also with X-MCD going from the as-made sample, to the H-form and the hard steamed sample (chapter 5).

In literature only few more studies present EXAFS data on FeZSM-5 samples with an iron content below 1 wt %.[3,20,21] However, the quality of the obtained EXAFS data did not allow a full analysis of the data. The analysis of the higher coordination shells turned out to be difficult and contributions – even within a distance of 2 Å from iron – are lumped together.[3]

In this study we used Kα-detected fluorescence detection, using a high-resolution (sub 1 eV) detection system.[22] Apart from low (essentially zero) background, this Kα-detected fluorescence does not alter the EXAFS signal and the EXAFS is equivalent to normal fluorescence EXAFS. It turned out that due to the very low noise, the signal-to-noise ratio of this detection scheme was extremely good. In this work, high quality EXAFS data were collected during *in situ* experiments (O_2/He at 350 °C) on framework substituted FeZSM5 samples with a very low Fe concentration of 0.3 wt %. The high signal to noise ratio allows a full analysis of the EXAFS data including the higher coordination shells. We will study the effects of template removal and proton exchange on the local coordination of the tetrahedral framework sites and the effects of the switch from oxygen to helium. The effects of steaming are studied in oxygen and helium.

8.2. Experimental

8.2.1. Catalyst preparation

Framework-substituted FeZSM-5 was prepared via the hydrothermal synthesis method.[9] The experimental details are described in chapter 6.[14] In short, the silica source (TEOS) was added to the organic template (TPAOH) and sodium hydroxide under vigorous stirring. This solution was added dropwise to a mixed aqueous solution of iron sulfate and aluminum nitrate. The final synthesis gel was transferred to a stainless steel autoclave and kept in a static air oven at 190 °C for 5 days. The crystalline material was separated by filtration, washed with ~ 2 liter of deionized water (till a color-free product was obtained), and dried at room temperature overnight (denoted as catalyst *am*-FeZSM-5). The samples were characterized with powder X-ray diffraction to confirm the MFI-structure and the purity of the sample. The amounts of Si, Al and Fe were determined by elemental analysis using X-ray fluorescence (XRF). The *am*-FeZSM-5 sample contained 45.1 wt % Si, 1.17 wt % Al and 0.25 Fe wt %, corresponding to the ratios Si/Fe ~ 360 and Si/Al ~ 37.

The template was removed carefully from the as-synthesized sample (*am*) by pyrolysis in a dried nitrogen flow of 50 ml/min at 520 °C (heating rate 1 °C/min) for 2 h and consecutive calcination in a dry airflow of 100 ml/min at 520 °C (2 °C/min) for 2.5 hr *(tf*-FeZSM-5). The samples were converted into the NH_4-form by exchange with an ammonium nitrate solution (0.1 M) overnight at 70 °C. The sample was filtered and dried

for 2 h at 60 °C (NH_4-FeZSM-5). The H-form was obtained by calcination in a dry airflow of 100 ml/min at 520 °C (2 °C/min) for 1 hr (*H*-FeZSM-5). In the last step, the catalysts were steamed, in two different ways. First a hard steaming procedure was carried out, according to literature[9], with a water partial pressure of 300 mbar in a total flow of 30 ml/min nitrogen at high temperature of 600 °C for 5 h (*hs*-FeZSM-5). In addition, we performed a mild steaming procedure with a water partial pressure of 200 mbar in a total flow of 200 ml/min nitrogen at high temperature of 550 °C for 4 h (*ms*-FeZSM-5). The samples were stored at room temperature in dry air.

8.2.2. Fe K edge EXAFS Data Collection and Analysis

Experimental setup

We performed the EXAFS experiments at the undulator beamline 18ID BioCAT of the Advanced Photon Source at Argonne National Laboratory (Chicago, USA). The incident energy was selected by means of a liquid nitrogen cooled Si(111) double crystal monochromator. A focusing mirror suppressed higher harmonics and the beam size on the sample was 0.5 mm horizontal and 1.0 mm vertical. The energy bandwidth of the incident X-ray beam was approximately 1.2 eV at 7100 eV and the (maximum) incident flux was 10^{13} photons/s, as monitored by a helium-filled ionization chamber downstream of the guarding slit. The incident energy was calibrated using tabulated values for the K-edge features of a Fe foil standard. By repeatedly measuring the standard we determined a relative calibration error of 0.1 eV for the incident energy.

The Kα fluorescence emission from the sample was collected by a crystal array spectrometer,[23,24] using four spherically bent Ge(440) crystals, specially designed for this experiment. A Ge solid-state detector was placed at the common focus of the four crystals. To avoid unwanted X-ray photons, the energy window of the Ge detector was set to 600 eV and an additional slit was positioned just in front of the detector. The analyzer energy resolution is approximately 0.8 eV at the Fe Kα emission. The relative energy calibration of the emission spectrometer is sensitive to vertical movements of the synchrotron beam. The emission energy calibration was repeatedly checked with the Kα emission of a Fe_2O_3 sample and was found to be constant within 0.1 eV, with a possible absolute error for the emission energy scale of 1 eV. Kα-detected EXAFS spectra were recorded by tuning the emission analyzer energy to the maximum intensity of the Fe Kα lines of Fe_2O_3 and by scanning the incident energy through the XANES and EXAFS region. The scans have been taken up to 700 eV above the edge (E_0 = 7112 eV) and for each catalyst sample at least 90 scans were averaged.

Data acquisition

The FeZSM-5 samples were pressed into self-supporting wafers and placed in an *in situ* fluorescence cell at 45 degrees scattering angle with respect to the incoming beam.[25] To prevent unwanted fluorescence from the *in situ* cell, which for sure would have disturbed the measurement of 0.3 wt % Fe samples, the interior of the reaction chamber including

the furnace and sample holder were coated with a gold layer of ~ 40 μm thickness (For photographs see chapter 1). To remove adsorbed water and eventually organic contaminants the samples were heated 25 to 350 °C (5 °C/min) in a flow of 50 % O_2 in helium (total flow 100 ml/min). After stabilization at 350 °C EXAFS spectra were taken in O_2 atmosphere. After switching to helium atmosphere and stabilization again EXAFS spectra were recorded. EXAFS was measured for the as-made (*am*) sample in a helium flow at room temperature to avoid the decomposition of the template during measurements.

Data analysis

The program XDAP for Windows was used for multiple-shell analysis of the EXAFS data by fitting in R-space.[26] The advantage of R-space fitting compared to the fitting in k-space is discussed elsewhere by Koningsberger and coworkers[27] and Van Bokhoven and coworkers[28] The different contributions in the EXAFS data were resolved by applying the difference file technique together with phase-corrected Fourier transforms. By using the difference file technique one can survey – during the analysis procedure – the position and intensity of each contribution and the influence of the different contributions on each other. Errors in the numerical values obtained by the EXAFS data analysis are estimated to be ± 10 % in the coordination number (N), ± 1 % in the distance (R), ± 5 % in the Debye Waller factor ($\Delta\sigma^2$) and ± 10 % in the inner potential correction (ΔE_0).

The Fe–O reference used for the EXAFS data analysis was created from experimental EXAFS data of $Fe(acac)_3$. The Fe–Fe phase shifts and backscattering amplitudes were calculated using the software FEFF7.[29] The theoretical Fe-Fe reference was calibrated in a R-space fit on the Fe–Fe shells in the Fourier transform of the EXAFS data obtained from Fe_2O_3. For further details see.[30] The Fe–Al/Si reference, based on the structure of hercynite,[31] $FeAl_2O_4$, was calculated with FEFF8.[32] For further details see the previous chapter.[33]

Comparison with overexchanged Fe/ZSM-5

We compared the EXAFS data on low loaded FeZSM-5 samples presented for the first time in this work with previously acquired data on an overexchanged Fe/ZSM-5 sample prepared by chemical vapour deposition of $FeCl_3$ (For the preparation see chapters 3 and 4). This raw EXAFS data concern the mildly calcined Fe/ZSM-5 sample, Fe/ZSM-5–mc, heated in helium to 350 °C and measured in O_2 at the same temperature, and are presented in an earlier publication of our group.[34]

8.3. Results

8.3.1. *tf*-FeZSM-5 (O_2) and *H*-FeZSM-5 (O_2)

Figure 1a shows the raw EXAFS data of *tf*-FeZSM-5 (solid line) and *H*-FeZSM-5 (dotted line) both measured at 350 °C in O_2. The signal to noise ratio is about 50 with the amplitude determined around k = 4 $Å^{-1}$ and the noise at k = at 11 $Å^{-1}$. The data quality is excellent, certainly considering the extremely low Fe loading of 0.3 wt %, and the measurement temperature. The corresponding k^1 weighted Fourier Transforms are given in Figure 1b. A broad peak (first shell region) is present in the Fourier transforms at values of R between 0.5 < R < 1.8 Å. It can be seen in Figure 1b that the amplitude of the FT in the first shell region for the *H*-FeZSM-5 sample is lower. The nodes of the imaginary part of the FT of the EXAFS data of *H*-FeZSM-5 are different form the corresponding FT of *tf*-FeZSM-5 between 1.7 < R < 2.3 Å, pointing to a difference in structure for both samples. For both samples higher shells are visible up to 5 Å.

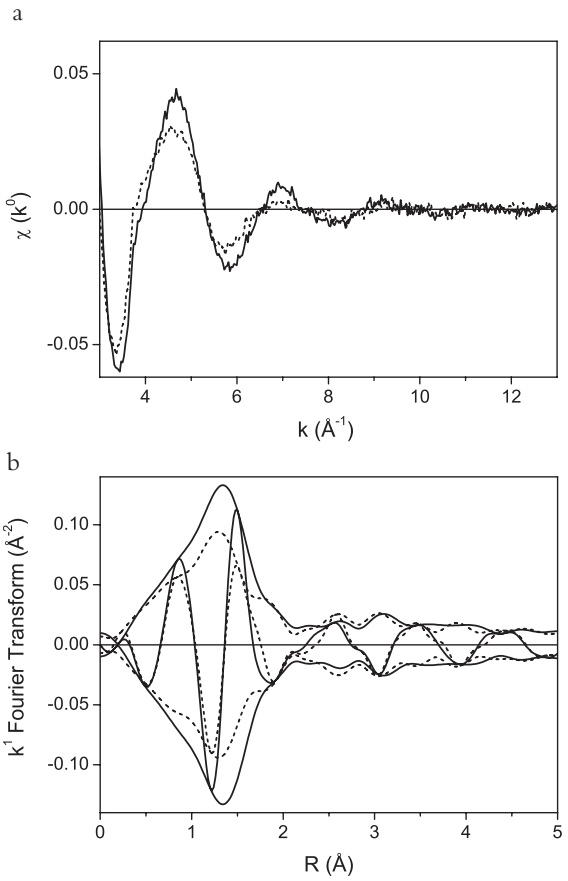

Figure 1: (a) $\chi(k^0)$ experimental EXAFS data of *tf*-FeZSM-5 (black line) and *H*-FeZSM-5 (gray line) both measured in O_2 at 350°C. (b) Corresponding Fourier transforms (k^1, Δk = 3.2 – 11.5 $Å^{-1}$).

The first shell data of *tf*-FeZSM-5 could be fitted by assuming a distorted tetrahedral coordination around Fe with a 3:1 oxygen distribution with distances at 1.80 and 1.97 Å, respectively. For the higher shell region two dominant Fe–Si coordinations at 2.64 and 3.52 Å could be analyzed and two main averaged Fe–O zeolite coordinations at 3.27 and 4.65 Å were detected. The resulting EXAFS coordination parameters are given in Table 1. The results of the R-space fitting procedure for the EXAFS data of the *tf*-FeZSM-5 sample are shown in Figure 2. Figure 2a displays the FT of the raw data (solid line) and the total fit (dotted line). Figure 2b gives the results of the first shell region. The FT of the difference file [RAW data minus ($Fe–Si_1$ + $Fe–Si_2$ + $Fe–O_{z1}$ + $Fe–O_{z2}$)] and the FT of the fitted ($Fe–O_1$ + $Fe–O_2$) contribution are plotted in Figure 2b with a solid and dotted line, respectively. The results for the higher shell region are shown in Figure 2c. The FT of the difference file [RAW data minus ($Fe–O_1$ + $Fe–O_2$)] is indicated with a solid line; the FT of the fitted ($Fe–Si_1$ + $Fe–Si_2$ + $Fe–O_{z1}$ + $Fe–O_{z2}$) is given with a dotted line. The deviations at low values of R are due to the presence of an AXAFS contribution (atomic X-ray absorption fine structure[35-37]).

We were not able to produce a satisfactorily fit of the *am*-FeZSM-5 sample that was measured in helium at room temperature to prevent the decomposition of the synthesis template. However, it became clear from both the pre-edge intensity and the amplitude of the first coordination shells in the FT indicates that besides the presence of four framework oxygen atoms around iron some additional low Z-scatters are present. They are present at relatively short distance and most probably are part of the carbeneous template.

Table 1: Coordination parameters obtained by R-space fit (k^1, $\Delta k = 3.2 – 11.5$ Å^{-1}, $\Delta R = 0.5 – 5.0$ Å) of EXAFS data of *tf*-FeZSM-5, measured in O_2 and next in helium at 350 °C.

Shells	N (± 10 %)	R (Å) (± 1 %)	$\Delta\sigma^2$ (10^{-3} Å^2) (± 5 %)	ΔE_0 (eV) (± 10 %)	k^1-variance (%) FT Im.	FT Abs.
O_2					0.7	0.3
$Fe–O_1$	3	1.80	1.6	2.1		
$Fe–O_2$	1	1.98	12.0	1.8		
$Fe–Si_1$	3	2.69	22.0	3.5		
$Fe–Si_2$	1	3.44	6.0	3.5		
$Fe-O_{z1}$	1	3.26	5.0	7.2		
$Fe-O_{z2}$	4	4.60	8.0	-5.8		
He					0.7	0.2
$Fe–O_1$	3	1.80	2.1	1.6		
$Fe–O_2$	1	1.98	6.8	4.4		
$Fe–Si_1$	3	2.62	22.0	8.2		
$Fe–Si_2$	1	3.41	6.0	8.2		
$Fe-O_{z1}$	1	3.29	5.0	8.1		
$Fe-O_{z2}$	4	4.68	8.0	-7.9		

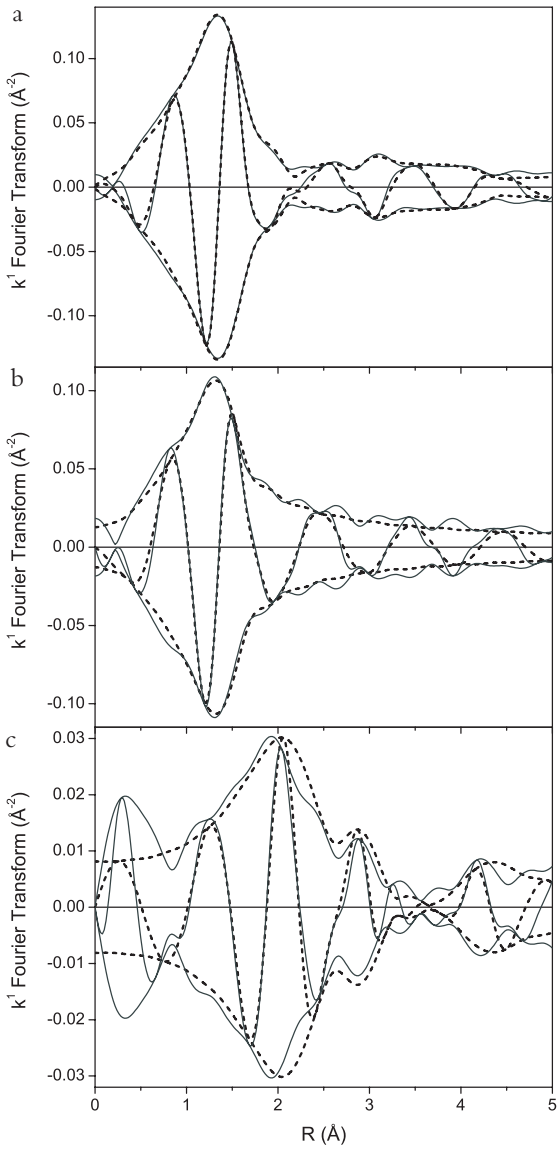

Figure 2: Results of R-space fit of *tf*-FeZSM-5 (O_2). (a) FT (k^1, Δk = 3.2 – 11.5 $Å^{-1}$) of RAW EXAFS data of (solid line) and total fit (ΔR = 0.5 – 5.0 $Å^{-1}$) (dotted line). (b) Same FT of difference file of first oxygen shells [RAW data minus (Fe-Si_1 + Fe-Si_2 + Fe-O_{Z1} + Fe-O_{Z2})] (solid line) and fitted (Fe-O_1 + Fe-O_2) contribution (dotted line). (c) Same FT of difference file of higher shells [RAW data minus (Fe-O_1 + Fe-O_2)] (solid line) and fitted (Fe-Si_1 + Fe-Si_2 + Fe-O_{Z1} + Fe-O_{Z2}) contribution (dotted line).

Introducing acidity in the ZSM-5 zeolite, by the conversion of the *tf*-sample into the *H*-form, leads to a further distortion of the tetrahedron coordination around Fe. The EXAFS data could be fitted with a 2:1:1 distribution. The first shell oxygen coordination distances were detected at 1.79, 1.97 and 2.09 Å, respectively. The higher coordination shells were found at similar distances as for the *tf*-FeZSM-5 sample. The results of the fitting procedure are given in Table 2.

Table 2: Coordination parameters obtained by R-space fit (k^1, Δk = 3.2 – 11.5 $Å^{-1}$, ΔR = 0.5 – 5.0 Å) of EXAFS data of *H*-FeZSM-5, measured in O_2 and next helium at 350 °C.

Shells	N (± 10 %)	R (Å) (± 1 %)	$\Delta\sigma^2$ (10^{-3} $Å^2$) (± 5 %)	ΔE_0 (eV) (± 10 %)	k^1-variance (%) FT Im.	FT Abs.
O_2					2.1	1.1
Fe–O_1	2	1.79	1.6	0.6		
Fe–O_2	1	1.97	6.0	-2.7		
Fe-O_3	1	2.09	8.0	-0.2		
Fe–Si_1	3	2.64	22	10.1		
Fe–Si_2	1	3.52	6	-7.6		
Fe-O_{z1}	1	3.27	5	7.9		
Fe-O_{z2}	4	4.65	16	-2.8		
He					0.9	0.4
Fe–O_1	2	1.79	2.1	2.1		
Fe–O_2	1	1.97	6	5.7		
Fe-O_3	0.9	2.09	8.0	-3.1		
Fe–Si_1	3	2.64	22	12.0		
Fe–Si_2	1	3.52	6	-6.6		
Fe-O_{z1}	1	3.27	5	10.4		
Fe-O_{z2}	4	4.65	16	-4.2		

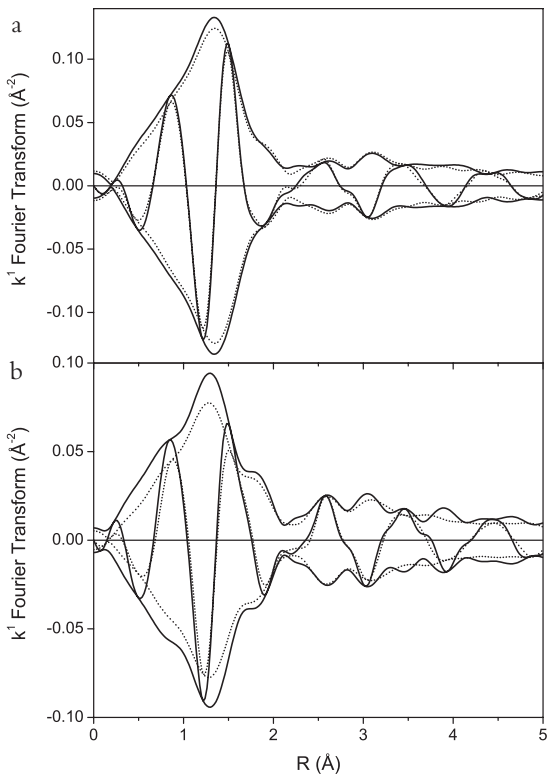

Figure 3: Influence of helium treatment at 350 °C (gray lines), after heating and treatment in O_2 (black lines),. (a) *tf*-FeZSM-5 and (b) *H*-FeZSM-5. FT: (k^1, Δk = 3.2 – 11.5 $Å^{-1}$).

8.3.2. *tf*-FeZSM-5 (He) and *H*-FeZSM-5 (He)

Treatment in helium at 350 °C induces very small changes in the amplitude of the FT of the EXAFS data of *tf*-FeZSM-5. (Figure 3a). The results of the EXAFS data-analysis are given in Table 1. A small increase from 1.6 to 2.1 10^{-3} Å^2 in the disorder of the Fe–O_1 and a decrease in disorder from 12.0 to 6.8 10^{-3} Å^2 of the Fe–O_2 coordination is observed.

Figure 3b shows that helium treatment leads to a decrease in the amplitude and small changes in the nodes of the imaginary part of the FT of the EXAFS data of *H*-FeZSM-5. These effects are caused by a small decrease (10 %) in the oxygen occupation of the Fe–O_3 shell (Table 2).

The quality of the R-space fits of the EXAFS data obtained after helium are similar as obtained for the data of the *tf*-FeZSM-5 sample in O_2. As can be seen, the helium treatment is not influencing the coordination parameters of the higher shells.

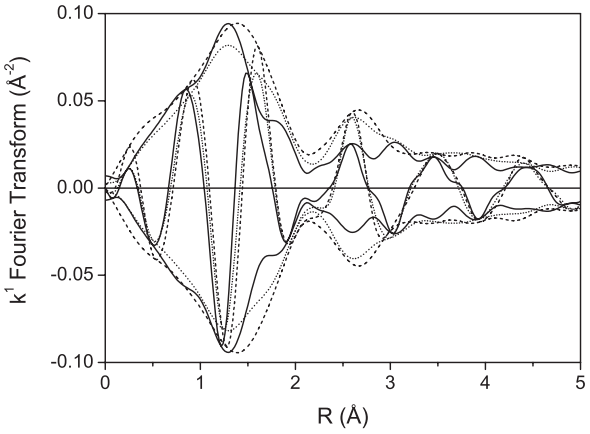

Figure 4: Influence of steaming. (a) FT of *H*-FeZSM-5 (solid line), (b) FT of *ms*-FeZSM-5 (dotted line) and (c) FT of *hs*-FeZSM-5 (dashed line). FT: (k^1, Δk = 3.2 – 11.5 Å^{-1}). All samples measured in O_2 at 350 °C.

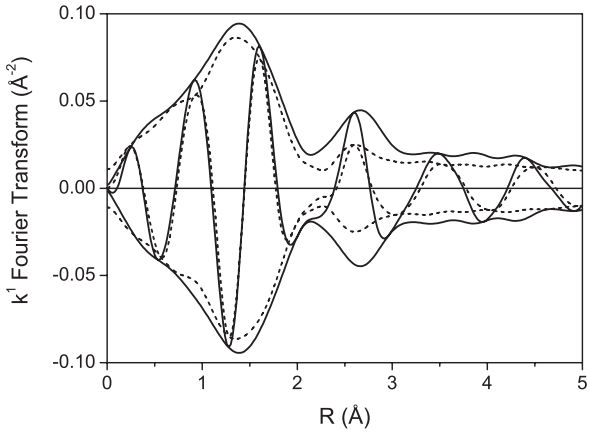

Figure 5: Structural resemblance of low loaded (0.3 wt %) framework-substituted FeZSM-5: high steamed sample, *hs*-FeZSM-5 (black line) with overexchanged (4.4 wt %) CVD-prepared Fe/ZSM-5: mildly calcined sample, Fe/ZSM-5–mc (gray line). FT: k^1, Δk = 3.2 – 11.5 Å^{-1}. Samples measured in O_2 at 350 °C.

8.3.3. Influence of steaming: analysis of *hs*-FeZSM-5 (O_2) and Fe/ZSM-5–mc (O_2)

Steaming of the *H*-FeZSM-5 sample introduces extraframework Fe species (chapter 6). It can be seen that in Figure 4 that mild steaming leads to a strong increase in the amplitude of the FT around R = 1.7 Å with a further increase after hard steaming. The nodes of the imaginary part shift to higher values of R. This points to an increase of the average oxygen coordination around Fe. The higher coordination shells show a strong increase of the amplitude around 2.5 Å.

The amount of Fe in the framework decreases as a function of the severity of the steam treatment. Fe Kβ-detected XANES data obtained on the same set of samples as used in this study (reported in chapter 6) show that a low estimate of the amount of framework Fe in *hs*-FeZSM-5 is about 19 %,[14] implying that the EXAFS spectrum of this sample is dominated by the extraframework Fe species. In order to obtain more information about the structure of the extraframework Fe species it is worthwhile to compare the FT of the EXAFS data of *hs*-FeZSM-5 (hydrothermally synthesized) with overexchanged Fe/ZSM-5–mc (prepared by chemical vapor deposition of $FeCl_3$) also measured in O_2 at 350 °C after a preceding helium treatment from RT to 350 °C.[34] It can be seen in Figure 5 that for $0.5 < R < 2$ Å the FT of the EXAFS data of Fe/ZSM-5–mc (dotted line) is similar to the FT of the *hs*-FeZSM-5 data. A real change can be detected for the higher coordination shells. Especially the intensity of the amplitude around 2.5 Å is much higher for *hs*-FeZSM-5.

Battiston et al.[34] presented a full analysis of the XAFS data (XANES pre-edge and EXAFS analysis) of Fe/ZSM-5–mc obtained after the He/O_2 treatment at 350°C. Fe appeared to be coordinated by 5 oxygen nearest neighbors with a 2:2:1 oxygen distribution. The earlier obtained results for the first 3 oxygen shells are summarized in Table 3. In chapter 7 of this thesis the higher coordination shells of the same Fe/ZSM-5–mc sample, but measured at LN temperatures, have been analyzed applying a different structural model (so-called Model II) as used by Battiston et al.[30] The coordination numbers and distances of the higher coordination shells obtained by using 'Model II' for the analysis of the EXAFS data measured at LN temperatures have been used as fixed input parameters to further fit the higher coordination shells of the same sample now measured after heating in helium to 350 °C and subsequent measurement in O_2 at 350 °C. The final results are given in Table 3. The FT of the raw data (solid line) and the total R-space fit (dotted line) is plotted in Figure 6a. Figure 6b shows the FT's of the difference file [RAW data minus (Fe–O_1 + Fe–O_2 + Fe–O_3)] (solid line) and the fitted contributions (Fe–Fe_1 + Fe–Fe_2 + Fe–Al + Fe–Si + Fe–O_z) (dotted line).

The R-space fit on the EXAFS data of *hs*-FeZSM-5 also resulted in 2:2:1 oxygen distribution with similar distances as found for the high Fe loaded CVD sample (see Table 3). However, the higher coordination shells are very different from the high Fe loaded CVD sample. Besides slightly different Fe–Fe shells with a higher coordination number, a significant Fe–Al contribution was found at a distance of 3.1 Å. The results of the R-space fitting are given in Figure 6c and 6d. The FT of the raw data (solid line) and the total R-space fit (dotted line) is plotted in Figure 6c. Figure 6d shows the FT's of the difference

file [RAW data minus (Fe–O_1 + Fe–O_2 + Fe–O_3)] (solid line) and the fitted contributions (Fe–Fe_1 + Fe–Fe_2 + Fe–Al + Fe–O_z) (dotted line).

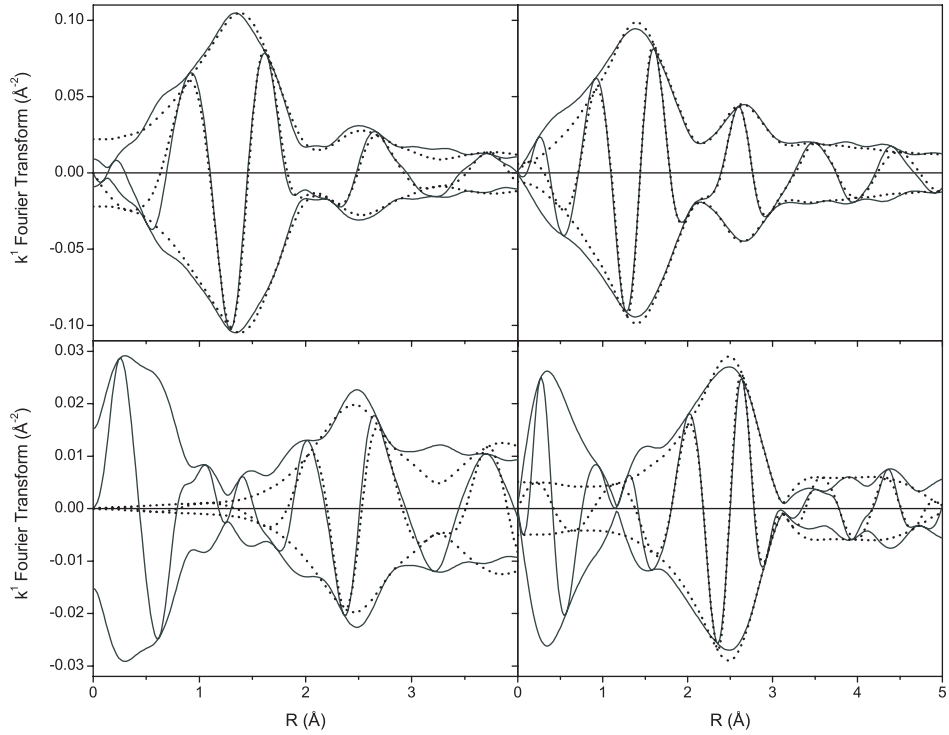

Figure 6: Results of R-space fit of overexchanged Fe/ZSM-5–mc (k^1, Δk = 2.7 – 13.2 $Å^{-1}$, ΔR = 0.7 – 4.2 $Å^{-1}$) (a,b), and low-loaded *hs*-FeZSM-5 (k^1, Δk = 3.2 – 11.5 $Å^{-1}$, ΔR = 0.5 – 5.0 $Å^{-1}$) (c,d). a,c: total fit, b,d: fit higher shells. Solid lines: difference files, dotted lines: fitted contributions. Samples measured in O_2 at 350 °C.

Table 3: Coordination parameters obtained by R-space fit (k^1) of EXAFS data of *hs*-FeZSM-5 and Fe/ZSM-5–mc,[34] measured in O_2 at 350 °C.

Shells	N (± 10 %)	R (Å) (± 1 %)	$\Delta\sigma^2$ (10^{-3} Å^2) (± 5 %)	ΔE_0 (eV) (± 10 %)	k^1-variance (%) FT Im.	FT Abs.
Fe/ZSM-5–mc [a]					1.3	0.5
Fe–O_1	1.9	1.86	2.0	-2.8		
Fe–O_2	2.0	1.99	5.0	12.8		
Fe-O_3	1.0	2.02	1.6	-12.1		
Fe–Fe_1 [c]	1.7	3.09	12	-7.1		
Fe–Fe_2 [c]	0.8	3.54	15	12.5		
Fe-Al [c]	0.5	2.81	13	-4.7		
Fe-Si [c]	1.2	3.18	12	-4.7		
Fe-O_z [c]	6.0	4.19	20	-8.4		
***hs*-FeZSM-5** [b]					1.4	1.1
Fe–O_1	1.9	1.85	0.0	-7.6		
Fe–O_2	2.0	1.99	1.1	0.1		
Fe-O_3	1.0	2.02	3.0	2.8		
Fe–Fe_1	2.2	3.03	3.3	-15.0		
Fe–Fe_2	1.5	3.38	14	7.6		
Fe-Al	4.1	3.10	12	-13.8		
Fe-O_z	6.2	5.11	9.0	4.4		

[a] R-space fit: Δk = 2.7 – 13.2 Å^{-1}, ΔR = 0.7 – 4.2 Å. [b] R-space fit: Δk = 3.2 – 11.5 Å^{-1}, ΔR = 0.5 – 5.0 Å. [c] For this shell the coordination number (N) and the distance (R) were used as fixed input parameters, and obtained in chapter 7 with Model II on the same sample but measured at LN temperature.

8.3.4. *hs*-FeZSM-5 (He) and Fe/ZSM-5–mc (He)

Figure 7 shows that the helium treatment at high temperatures influences both the imaginary part and the amplitude of the FT of the EXAFS data of the high Fe loaded CVD sample. The effects are smaller for the high Fe loaded CVD sample. Battiston et al. showed that the observed changes could be ascribed by a decrease in the Fe–O_1 coordination as a function of the helium treatment.[34] The EXAFS data of Fe/ZSM-5–mc (He) have been re-analyzed using the results of Battiston et al. for the first three oxygen shells. For the higher shells Model II (see chapter 7 of this thesis) has been used. It can be seen in Table 4 that the average oxygen coordination of the Fe–O_1 shell decreases to 1.2, giving a change of 40 %. Applying the same kind of analysis to the low loaded hard steamed sample shows that the effect of the helium treatment could also be ascribed by a change in the average Fe–O_1 coordination. However, the change is smaller (decrease of 15 %).

Table 4: Coordination parameters obtained by R-space fit (k^1) of EXAFS data of *hs*-FeZSM-5 and Fe/ZSM-5–mc,[34] measured in helium at 350 °C.

Shells	N (± 10 %)	R (Å) (± 1 %)	$\Delta\sigma^2$ (10^{-3} Å^2) (± 5 %)	ΔE_0 (eV) (± 10 %)	k^1-variance (%) FT Im.	FT Abs.
Fe/ZSM-5–mc [a]					0.6	0.4
Fe–O_1	1.2	1.88	2.6	-5.5		
Fe–O_2	2.0	1.97	7.2	12.8		
Fe-O_3	1.2	2.08	8.8	-9.9		
Fe–Fe_1 [c]	1.7	3.09	13	-8.5		
Fe–Fe_2 [c]	0.8	3.54	16	14.5		
Fe-Al [c]	0.5	2.81	15	-5.5		
Fe-Si [c]	1.2	3.18	12	-5.5		
Fe-O_z [c]	6.0	4.19	20	-8.6		
***hs*-FeZSM-5** [b]					0.5	0.3
Fe–O_1	1.7	1.83	3.1	0.2		
Fe–O_2	2.0	1.99	5.2	-2.8		
Fe-O_3	1.0	2.02	12	8.4		
Fe–Fe_1	2.2	3.03	4.2	-12.3		
Fe–Fe_2	1.5	3.38	14	11.7		
Fe-Al	4.1	3.10	15	-11.0		
Fe-O_z	6.2	5.11	14	5.7		

[a] R-space fit: Δk = 2.7 – 13.2 Å^{-1}, ΔR = 0.7 – 4.2 Å. [b] R-space fit: Δk = 3.2 – 11.5 Å^{-1}, ΔR = 0.5 – 5.0 Å. [c] For this shell the coordination number (N) and the distance (R) were used as fixed input parameters, and obtained in chapter 7 with Model II on the same sample but measured at LN temperature.

8.4 Discussion

8.4.1 Detection with XAFS spectroscopy of 0.3 wt % Fe

The average signal to noise ratio (S/N) of the EXAFS data on low loaded FeZSM-5 (0.3 wt % Fe) collected at a temperature of 350 °C (Figure 1a), using beamline 18-ID (BioCAT) at the APS equipped with the special high-resolution detection system[23] described in chapter 1, is around 50:1. This relative high S/N ratio made the analysis possible as applied in this chapter. It has to be noted that this S/N ratio is only a factor 2 lower than the data collected at Beamline X.1 of the Hasylab synchrotron on overexchanged Fe/ZSM-5 (4.4 wt % Fe),[34] whereas the loading of the latter is more than 16 times higher. Due to the exceptional properties of the special detection method used at beamline 18-ID of the APS it is possible to measure these low loaded Fe samples that are generally known to be catalytically active in nitrogen oxide decomposition.

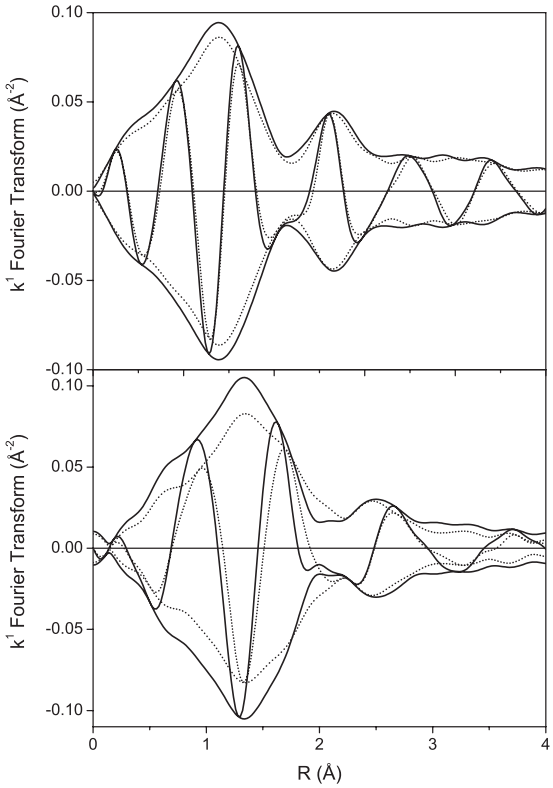

Figure 7: Influence of helium treatment at 350 °C (dotted lines) on (a) low-loaded *hs*-FeZSM-5, FT: (k^1, Δk = 3.2 – 11.5 $Å^{-1}$), and (b) overexchanged Fe/ZSM-5–mc, FT: (k^1, Δk = 2.7 – 13.2 $Å^{-1}$).

8.4.2 Structure of Framework Fe

Comparing the amplitudes of the Fourier transforms displayed in Figure 2a with the FT of Figure 2b, shows that around 2.0 Å the contribution of the first two Fe–O shells (Figure 2b) is higher than the FT of the raw data. This points to a strong anti-phase effect between the EXAFS describing the first shells and the higher shells. It implies that the first shells cannot be analyzed separately and that the higher shells have to be included in a total R-space fit procedure. The EXAFS analysis shows that the structure of framework Fe in the template free ZSM-5 sample is a distorted tetrahedron with a 3:1 oxygen distribution with coordination distances at 1.80 and 1.98 Å, which is in agreement with other studies.[38-40] Molecular modeling shows that Fe–Si coordinations are possible at distances of 2.69 and 3.44 Å as detected with EXAFS. The Fe–O_z distances found at at 3.26 and 4.6 Å are most probably values averaged over different lattice positions and therefore do not necessarily represent real lattice oxygen coordinations. The number of statistically allowed independent parameters, (N_{ind}) according to the Nyquist theorem,[41] is calculated to be 25.7. The number of free fit parameters used for the R-space fit is 24, implying that the fit is statistically allowed.

The comparison of the FT of *tf*- and *H*-ZSM-5 in Figure 1b makes clear that the introduction of protons in the ZSM-5 leads to a further distortion of the symmetry around framework Fe. This can be deduced from the fact that a decrease in the overall amplitude and a change in nodes of the imaginary part of the FT around 1.7 Å is observed for the *H*-ZSM-5 sample. Both phenomena originate from strong anti-phase effects due to the presence of another Fe–O coordination at a higher coordination distance (2.09 Å). The association of a proton to the framework leads to the formation of an OH-group and a rearrangement of electron density, effectuating in the withdrawal of electron density from Fe, and finally resulting in a longer Fe–O bond. It can be seen from Tables 2 and 3 that as expected the structure of the higher coordination shells is not influenced by the introduction of the protons. Actually, to make the fit statistically allowed the coordination numbers of the higher coordination shells was fixed; making the number of free fit parameters 24. This number is lower than the number of allowed independent parameters, which indicates that the fit is statistically allowed.

He treatment at 350 °C leads to small changes in the structure of the *tf*-ZSM-5 sample. The disorder of the Fe–O_1 shell increases with a simultaneous decrease in the disorder of the Fe-O_2 shell. It is possible that is caused by a further dehydroxylation of the ZSM-5 lattice. The influence of the treatment in helium on the structure of framework Fe in the H-form of ZSM-5 is more significant. The disorder of the Fe–O_1 shell increases too, but a reasonable fit could only be obtained by allowing a small decrease in the oxygen coordination of the Fe–O_3 shell. This would imply that under specific conditions (H-form of the zeolite and after removal of water) a small fraction of framework cations are in the threefold oxygen coordination. We mentioned above that similar observations were made for Al in different zeolites with *in situ* XAS spectroscopy at the Al K edge.[17,18]

8.4.3. Influence of steaming

It is well known in literature that steaming of a framework Fe sample results in the presence of extraframework Fe species.[10,14,42-44] Dramatic changes as a function of the severity of the steam treatment can be observed in the Fourier transforms of the steamed samples, *ms*- and *hs*-FeZSM-5 (Figure 4). An increase in the amplitude of the FT is observed which can be explained by an increase in the averaged oxygen coordination (change from 4- to 6-fold). Also the higher coordination shells are completely different from that of *H*-ZSM-5, especially around 2.5 Å large changes are observed.

The similarity of the first shell region of the FT of the low loaded *hs*-FeZSM-5 and of the FT of the mildly calcined, overexchanged Fe/ZSM-5 sample is striking (Figure 5). Analysis of the Fe K XANES pre-edges of the low loaded Fe samples (chapter 6) showed that still at least 19 % framework Fe is present after hard steaming.[14] At present, it is not exactly known how the steam treatment influences the structure of the framework Fe, but it is clear that the spectral contribution by a portion of framework Fe will have some influence on the total FT of the *hs*-FeZSM-5 sample. Despite this probable influence we have analyzed the EXAFS data using the same approach as applied for the overexchanged

Fe/ZSM-5 samples.[34,45] In this way, the first shell region for low loaded *hs*-FeZSM-5 can be described by a 5-fold oxygen coordination with a 2:2:1 distribution (Table 3). Battiston et al. have extensively studied the redox behavior of overexchanged Fe/ZSM-5 samples.[30,34,45] The authors showed that a helium treatment at high temperatures leads to a decrease in both the Fe–O_1 and Fe–O_3 coordinations. After dehydroxylation and measured in O_2 a 5-fold oxygen coordination is detected with a 2:2:1 oxygen distribution. A very resembling type of oxygen coordination with similar Fe–O distances is found here for the 0.3 wt % *hs*-FeZSM-5 (Table 3). These observations comprise favorable arguments to reason that similar Fe oxide species may be present after two totally different preparation (post-synthesis loading trough CVD *versus* framework incorporation by hydrothermal synthesis) and activation procedures (careful calcination *versus* hard steaming) using two totally different Fe loadings (0.3 *versus* 4.4 wt %).

With respect to the higher shells in the Fourier Transforms of the EXAFS data totally different patterns are observed for the two different FeZSM-5 materials (Figure 5). We presented in chapter 7 a way to detect Fe–Al/Si contributions, indicated as 'Model II'. In this work it turned out that 'Model II' is also applicable to describe the higher coordination shells of this overexchanged Fe/ZSM-5–mc sample measured in O_2 after a preceding treatment in helium (Table 3). A smaller fraction of Fe is still close to the framework Al and Si, and a larger fraction is mostly present in the pores of the zeolite as oligomeric Fe oxide species – assuming in the latter case that the Fe is more distant from the framework. In contrast, the low loaded *hs*-FeZSM-5 sample showed an intense contribution of a Fe–Al coordination at 3.10 Å. This can be understood by the fact that steaming not only will lead to the release of framework Fe, but also to the (partial) extraction of framework Al. This extraframework Al can stay in close contact with the formed Fe_N species or can even form some kind of intermediate Fe–Al oxo cluster.[46] The Fe–Fe shells detected in both the synthesis and post-synthesis prepared Fe samples can originate both from these Fe–Al oxide clusters and from some larger Fe_2O_3 particles. However, it is noteworthy to mention that the coordination numbers of the Fe–Fe shells are in the order: mildly calcined < hard steamed < severely calcined (For this purpose see chapter 7). This clearly supports the idea that extraframework Al stabilizes small oligomeric Fe oxide clusters. It has been reported in literature that the presence of Al is beneficial for the catalytic activity of Fe/ZSM-5 samples.[10,11,46] Concerning the low loaded FeZSM-5 samples in this study, it is not yet clear, whether extraframework Al also has an electronic influence on the catalytic active sites of the oligomeric clusters. In the first instance, we consider the effect of Al to be primarily the inhibition of extensive Fe clustering into stable, inactive iron oxide clusters.

The structural similarity between the low loaded *hs*-FeZSM-5 and the overexchanged Fe/ZSM-5–mc sample is further supported by their redox behavior. Battiston et al. have shown that the Fe–O_1 coordination is able to release on average 0.8 oxygen.[34] This is reproduced here using 'Model II' for the description of the higher coordination shells (Table 4). It can be seen in Table 4 that *hs*-FeZSM-5 also has the ability to release oxygen, albeit to a lesser extent (0.3 oxygen).

8.4.4. Implication of this study for the identification of the catalytic active site

The results presented in this work can help to identify the species that are active for either or both the selective catalytic reduction of NO (HC-SCR) and the decomposition of N_2O. The *in situ* XAS study of the SCR reaction using the Fe/ZSM-5–mc sample as catalysts[45] led us to assign a binuclear Fe cluster as the catalytic active species. However, progress in insights concerning the way to analyze the higher shell contributions in EXAFS data ('Model II' in chapter 7) and accumulating proof in literature for the coexistence of multiple species, combined with the results of this study may lead to a better perception of how the catalytic active site may look like.

Our earlier *in situ* studies on the high loaded Fe/ZSM-5-mc sample made clear that a significant part of the Fe species is highly flexible in its oxidation state.[14,34,45,47] In this study, we provide evidence for the hypothesis that hard steaming of low loaded FeZSM-5 samples leads to oligomeric Fe species, stabilized by extraframework Al, with structural and redox properties similar to the oligomeric species present in overexchanged Fe/ZSM-5 samples. It is clear that first shell Fe–O coordinations of the oligomeric Fe oxide species are similar for all Fe ions present. However, only a smaller fraction of atoms – that most probably form the 'chain-ends' are coordinatively unsaturated – is able to switch oxidation state, and are supposed to be the catalytic active site.

A structural model of the active site has been discussed in an earlier study,[34] assuming the presence of binuclear clusters. This structural model explaining the redox behavior of the three different Fe–O first shells can be adapted to the new findings in this study. From this one may conclude that the active site comprises more than one Fe atom and that multinuclear oligomeric Fe clusters display catalytic activity.

In our view, the role of the ZSM-5 zeolite framework is merely to stabilize small, dispersed Fe oxo clusters. The electronic properties of these oligomeric clusters can be very different than the well-known Fe oxide bulk structures. These oligomeric clusters display a remarkable redox behavior. Future studies will learn whether the madelung potential of the zeolite (speaking in terms of metal oxide-support interactions) is also influencing the electronic structure of the small oligomeric clusters.

8.5. Conclusions

EXAFS has been used to study the different stages in the activation of framework-substituted FeZSM-5 zeolites that contain only 0.3 wt % Fe. The data analysis was based on high quality data with a low signal to noise ratio acquired by the utilization of Kα-fluorescence detection. The activation of these low loaded FeZSM-5 samples – that initially contained Fe exclusively in framework positions – by template removal and calcination distort the zeolite framework and induce a deviation from T_d symmetry for incorporated iron in *tf*-FeZSM-5. The introduction of acidity into framework-substituted samples created some flexibility in the coordination of iron that is incorporated in the zeolite and at least causes a further distortion of the tetrahedral symmetry compared to the template free sample. Upon switching to helium we observed for *H*-FeZSM-5 a limited autoreduction of about 10 %, which is hardly visible as a decrease in the oxygen coordination numbers.

Steaming induced the extraction to extraframework positions for most of the iron and part of aluminum. In the most severe steamed sample the extraframework Fe species dominate the EXAFS spectra. The structural properties of the first oxygen coordination shells of the extraframework Fe species in this sample are very similar to the mildly calcined overexchanged high loaded Fe/ZSM-5, including the response of the first oxygen shells to a redox treatment at 350 °C.

In addition, in the steamed samples detection with EXAFS of a Fe–Al coordination at 3.1 Å is observed. This Fe–Al coordination is not detected in calcined overexchanged samples. The intensity of the higher Fe–Fe shells in the hard steamed sample is lower than those detected in the mild calcined overexchanged Fe/ZSM-5. This leads to the conclusion that the oligomeric extraframework Fe species found after steaming are stabilized by extraframework Al.

In this study it has been established that: (1) both for the hard steamed low Fe loaded and the mild calcined high Fe loaded samples the structure of the first Fe–O coordination shells can be described by a 2:2:1 oxygen distribution measured in O_2 after dehydroxylation and (2) the real redox response after dehydroxylation is detected in the Fe–O_1 coordination. From this one may conclude that the active site comprises more than one Fe atom and that highly dispersed multinuclear oligomeric Fe clusters can display catalytic activity.

References

(1) Hensen, E. J. M.; Zhu, Q.; Hendrix, M.; Overweg, A. R.; Kooyman, P. J.; Sychev, M. V. and van Santen, R. A., *J. Catal.*, **2004**, *221,* 560-574.

(2) Perez-Ramirez, J.; Kapteijn, F.; Groen, J. C.; Domenech, A.; Mul, G. and Moulijn, J. A., *J. Catal.*, **2003**, *214,* 33-45.

(3) Pirngruber, G. D.; Luechinger, M.; Roy, P. K.; Cecchetto, A. and Smirniotis, P., *J. Catal.*, **2004**, *224,* 429-440.

(4) Selli, E.; Isernia, A. and Forni, L., *Phys. Chem. Chem. Phys.*, **2000**, *2,* 3301-3305.

(5) Perez-Ramirez, J.; Kapteijn, F.; Mul, G. and Moulijn, J. A., *Chem. Comm.*, **2001**, 693-694.

(6) Jia, J. F.; Pillai, K. S. and Sachtler, W. M. H., *J. Catal.*, **2004**, *221,* 119-126.

(7) Dubkov, K. A.; Ovanesyan, N. S.; Shteinman, A. A.; Starokon, E. V. and Panov, G. I., *J. Catal.*, **2002**, *207,* 341-352.

(8) Wichtelova, B.; Sobalik, Z. and Dedecek, J., *Appl. Catal. B*, **2003**, *41,* 97-114.

(9) Ribera, A.; Arends, I.; De Vries, S.; Perez-Ramirez, J. and Sheldon, R. A., *J. Catal.*, **2000**, *195,* 287-297.

(10) Hensen, E.; Zhu, Q. J.; Liu, P. H.; Chao, K. J. and van Santen, R., *J. Catal.*, **2004**, *226,* 466-470.

(11) Sun, K. Q.; Zhang, H. D.; Xia, H.; Lian, Y. X.; Li, Y.; Feng, Z. C.; Ying, P. L. and Li, C., *Chem. Comm.*, **2004**, 2480-2481.

(12) Berlier, G.; Bonino, F.; Zecchina, A.; Bordiga, S. and Lamberti, C., *ChemPhysChem*, **2003**, *4,* 1073-1078.

(13) chapter 6 of this thesis.

(14) Heijboer, W. M.; Glatzel, P.; Sawant, K. R.; Lobo, R. F.; Bergmann, U.; Barrea, R. A.; Koningsberger, D. C.; Weckhuysen, B. M. and de Groot, F. M. F., *J. Phys. Chem. B*, **2004**, *108,* 10002-10011.

(15) Westre, T. E.; Kennepohl, P.; Dewitt, J. G.; Hedman, B.; Hodgson, K. O. and Solomon, E. I., *J. Am. Chem. Soc.*, **1997**, *119,* 6297-6314.

(16) Wilke, M.; Farges, F.; Petit, P. E.; Brown, G. E. and Martin, F., *Am. Miner.*, **2001**, *86,* 714-730.

(17) van Bokhoven, J. A.; van der Eerden, A. M. J. and Koningsberger, D. C., *Stud. Surf. Sci. Catal.*, **2002**, *142,* 1885-1890.

(18) van Bokhoven, J. A.; van der Eerden, A. M. J. and Koningsberger, D. C., *J. Am. Chem. Soc.*, **2003**, *125,* 7435-7442.

(19) Kubanek, P.; Wichterlova, B. and Sobalik, Z., *J. Catal.*, **2002**, *211,* 109-118.

(20) Choi, S. H.; Wood, B. R.; Ryder, J. A. and Bell, A. T., *J. Phys. Chem. B*, **2003**, *107,* 11843-11851.

(21) Choi, S. H.; Wood, B. R.; Bell, A. T.; Janicke, M. T. and Ott, K. C., *J. Phys. Chem. B*, **2004**, *108,* 8970-8975.

(22) Glatzel, P. and Bergmann, U., *Coord. Chem. Rev.*, **2005**, *249,* 65-95.

(23) Bergmann, U. and Cramer, S. P., *SPIE Proc.*, **1998**, *3448,* 198-209.

(24) Heijboer, W. M.; Glatzel, P.; Sawant, K. R.; Lobo, R. F.; Bergmann, U.; Barrea, R. A.; Koningsberger, D. C.; Weckhuysen, B. M. and de Groot, F. M. F., *J. Phys. Chem. B*, **2004**, *108,* 10002-10011.

(25) Vaarkamp, M.; Mojet, B. L.; Kappers, M. J.; Miller, J. T. and Koningsberger, D. C., *J. Phys. Chem.*, **1995**, *99,* 16067-16075.

(26) for the EXAFS analysis program XDAP for Windows of XAFS Services International, see http://www.xsi.nl.

(27) Koningsberger, D. C.; Mojet, B. L.; van Dorssen, G. E. and Ramaker, D. E., *Top.Catal.*, **2000**, *10,* 143-155.

(28) Van Bokhoven, J. A.; Ressler, T.; De Groot, F. M. F. and Knop-Gericke, A., *in B.M.* Weckhuysen (Ed.), In situ Spectroscopy of Catalysts, American Scientific Publishers, Stevenson Ranch*, CA, USA*, **2004**, 123-144.

(29) Ankudinov, A. L. and Rehr, J. J., *Phys. Rev. B*, **1997**, *56,* R1712-R1715.

(30) Battiston, A. A.; Bitter, J. H.; De Groot, F. M. F.; Overweg, A. R.; Stephan, O.; Van Bokhoven, J. A.; Kooyman, P. J.; Van Der Spek, C.; Vanko, G. and Koningsberger, D. C., *J. Catal.*, **2003**, *213,* 251-271.

(31) Harrison, R. J.; Redfern, S. A. T. and O'Neill, H. S. C., *Am. Miner.*, **1998**, *83,* 1092-1099.

(32) Ankudinov, A. L.; Ravel, B.; Rehr, J. J. and Conradson, S. D., *Phys. Rev. B*, **1998**, *58,* 7565-7576.

(33) chapter 7 of this thesis.

(34) Battiston, A. A.; Bitter, J. H.; Heijboer, W. M.; De Groot, F. M. F. and Koningsberger, D. C., *J. Catal.*, **2003**, *215,* 279-293.

(35) Ramaker, D. E.; Mojet, B. L.; Koningsberger, D. C. and O'Grady, W. E., *J. Phys. Condens. Matter*, **1998**, *10,* 8753-8770.

(36) Ramaker, D. E.; van Dorssen, G. E.; Mojet, B. L. and Koningsberger, D. C., *Top. Catal.*, **2000**, *10,* 157-165.

(37) van Dorssen, G. E.; Koningsberger, D. C. and Ramaker, D. E., *J. Phys. Condens. Matter*, **2002**, *14,* 13529-13541.

(38) Axon, S. A.; Fox, K. K.; Carr, S. W. and Klinowski, J., *Chem. Phys. Lett.*, **1992**, *189,* 1-6.

(39) Sankar, G.; Thomas, J. M. and Catlow, C. R. A., *Top. Catal.*, **2000**, *10,* 255-264.

(40) Lewis, D. W.; Sankar, G.; Richard, C.; Catlow, C. R. A.; Carr, S. W. and Thomas, J. M., *Nucl. Instrum. Methods Phys. Res. B*, **1995**, *97,* 44-49.

(41) Stern, E. A., *Phys. Rev. B*, **1993**, *48,* 9825.

(42) Bulushev, D. A.; Kiwi-Minsker, L. and Renken, A., *J. Catal.*, **2004**, *222,* 389-396.

(43) Perez-Ramirez, J., *J. Catal.*, **2004**, *227,* 512-522.

(44) Starokon, E. V.; Dubkov, K. A.; Pirutko, L. V. and Panov, G. I., *Top. Catal.*, **2003**, *23,* 137-143.

(45) Battiston, A. A.; Bitter, J. H. and Koningsberger, D. C., *J. Catal.*, **2003**, *218,* 163-177.

(46) Hensen, E. J. M.; Zhu, Q. and van Santen, R. A., *J. Catal.*, **2003**, *220,* 260-264.

(47) Heijboer, W. M.; Battiston, A. A.; Knop-Gericke, A.; Hävecker, M.; Mayer, R.; Bluhm, H.; Schlögl, R.; Weckhuysen, B. M.; Koningsberger, D. C. and de Groot, F. M. F., *J. Phys. Chem. B*, **2003**, *107,* 13069-13075.

Summary

The aim of the research described in this work is two fold. Firstly, new techniques based on X-ray spectroscopy have been introduced in the field of heterogeneous catalysis. As a consequence, a more advanced characterization of catalytic solids could be pursued. Secondly, the application of these new methodologies on differently prepared FeZSM-5 zeolites revealed a more detailed understanding of the Fe species present in these important catalytic materials.

This thesis 'New Frontiers in X-ray Spectroscopy of FeZSM-5' intends to contribute to the application of novel X-ray spectroscopic techniques in the study of catalytic solids as well as to the understanding of the structure and function of FeZSM-5 zeolites. Throughout the thesis the description of the 'New Frontiers in X-ray Spectroscopy of FeZSM-5' followed five main themes:

I) The application of in situ soft X-ray Absorption Spectroscopy (XAS) in the study of heterogeneous catalysts and a proposal for the detailed data analysis of transition metal spectra (chapters 3 and 4).
II) The application of X-ray Magnetic Circular Dichroism to heterogeneous catalysts (chapter 5).
III) The exploitation of X-ray Near Edge Absorption Structure (XANES) by benefiting from high quality spectra gathered by selective detection methods in hard XAS (chapter 6).
IV) The push of the detection limits in the Extended X-ray Absorption Fine Structure (EXAFS) to measure low concentrated FeZSM-5 samples by selective detection (chapter 6 and 8).
V) The refinement of the data analysis for EXAFS and XANES (chapters 7 and 8).

It turned out that the knowledge about FeZSM-5 zeolites keeps up with the increasing possibilities afforded by novel X-ray Spectroscopic characterization methods. During the research we concentrated our attention on two types of FeZSM-5 zeolites: overexchanged Fe/ZSM-5 (4.4 wt % Fe in extraframework positions) and framework-substituted FeZSM-5 (0.3 wt % Fe initially in framework positions).

In **Chapter 1** we sketched a general picture of catalyst characterization, a research area of decisive importance for gathering fundamental knowledge about catalyst materials and to fasten progress in the field of catalysis. The characterization tools studied in this thesis have in common the use of X-rays. X-ray spectroscopy is an excellent tool to probe phenomena at the atomic scale. However, the refinement of currently available standard techniques as well as the development of new variants may deliver additional information and hence significantly contribute to a better understanding. A theoretical basis is provided as a background to the next experimental chapters in which the techniques have been introduced. We highlighted *in situ* soft X-ray absorption (together with X-ray Magnetic Circular Dichroism) and *in situ* selective hard X-ray absorption (especially high-resolution Kβ-fluorescence detected XANES and EXAFS).

The advances in X-ray spectroscopy are illustrated by the study of various FeZSM-5 zeolites as an example. These systems can be considered as representative examples of heterogeneous catalysts since the same problems occur as noticed in other transition metal ion containing catalysts: multiple species present in often low concentrations.

Chapter 2 presents a review on the preparation and characterization of FeZSM-5. The main topics in the recent literature on the synthesis, activation procedures and characterization of Fe-containing ZSM-5 zeolites were discussed. It became clear that despite the enormous research efforts still no final answers are provided regarding the nature of the active sites, the best way to prepare and the most effective tools to characterize FeZSM-5.

The first technique we applied to study Fe/ZSM-5 was *in situ* soft X-ray absorption. Both O 1s and Fe 2p XAS experiments were performed. Soft X-ray absorption spectroscopy on 3d metal edges is one of the main techniques in the field of solid state physics, in particular of correlated transition metal oxide systems. In the field of heterogeneous catalysis it has been little used due to the difficulty of in situ measurements. In **Chapter 3** we monitored the Fe oxidation/reduction behavior in overexchanged Fe/ZSM-5, prepared by chemical vapor deposition of $FeCl_3$, as a function of (heat) treatment and gas atmosphere. We developed a fast valence determination method based on the shape and position of the Fe L_3 edge. Charge-transfer multiplet calculations were suitable to simulate the Fe $L_{2,3}$ spectral shapes and provided new information on the geometry and valence of the iron sites. The oxidized form of Fe/ZSM-5 contained Fe^{III} in an octahedral surrounding with a crystal field strength of 1 eV, less than that of bulk oxides. In a helium environment a spontaneous reduction was observed, autoreduction, starting already at room temperature and further taking place during heating to 350 °C, at 2 mbar. Reduced Fe/ZSM-5 had Fe^{II} in tetrahedral oxygen surrounding. From the oxygen spectra, it became clear that the autoreduction was accompanied by the loss of molecular oxygen and water. At high temperature the reoxidation by oxygen of almost completely reduced Fe/ZSM-5 is a matter of minutes.

This study can be taken as an example that demonstrates the power of *in situ* soft X-ray absorption spectroscopy (XAS) in catalyst characterization to study structural and electronic properties. The application benefits from the much higher resolution of soft X-rays together with the relatively large, systematic variation of the spectral features in the – well defined

– Fe L_3 edge with the iron oxidation state and the detailed simulation of their spectral shape. These factors enabled a considerably higher precision in the determination of the average valence of iron. However, because of the use of electron yield detection the technique is surface sensitive and the results reflect only the upper 4 nm of the sample.

A more extended study on the redox behaviour of overexchanged Fe/ZSM-5 zeolites was carried out in **Chapter 4**. The influence of the calcination method on the (auto)reducibility of the iron was investigated. We utilized the soft XAS technique introduced in chapter 3 to compare different Fe/ZSM-5 samples and to follow the average valence of iron during oxidation/reduction cycles as well as during heating and cooling. Severely calcined samples were more resistant to autoreduction in helium than mildly calcined samples and did not reach such a low average oxidation state. This difference in redox behaviour, visible at room temperature switches from oxygen to helium and during heating in helium to 350 °C, was ascribed to the presence of iron oxide nanoparticles after more extreme calcination. Both samples displayed a reversible autoreduction in helium at 350 °C after exposure to oxygen for more than one hour. A similar experiment with FeO(OH), goethite, revealed that bulk iron hydroxo species does not display autoreduction upon heating in helium, but undergo surface reorganisation (dehydroxylation) to iron oxide-like structures. A side effect of probing the local structure of iron in Fe/ZSM-5 by soft X-ray absorption was the occurrence of overshoot effects in the iron valence. Besides kinetic effects due to local surface-bulk equilibrium settling also the heating by X-rays temporarily affected the Fe valence in the order of 0.10.

Our work on the use of Fe 2p X-ray absorption in the characterization of FeZSM-5 samples has been expanded in **Chapter 5** by making use of the polarization of X-ray light. Paramagnetic samples are sensitive to the application of a magnetic field. The extent of Magnetic Circular Dichroism, MCD, depends on the nature of the iron (oxide) species that are present. In this way, information could be obtained about the size and structure of the Fe sites in framework-substituted FeZSM-5 samples. Besides the XMCD-effect also the 'normal' 2p XAS spectrum was obtained for these low loaded samples (0.3 wt % Fe). Earlier characterization attempts by means of the *in situ* soft XAS measurements as reported in the previous chapters failed for reasons of too low count rates in the total electron yield mode. Here, we have used bulk-sensitive fluorescence detected soft XAS instead of surface sensitive TEY detection. However, these measurements were performed in vacuum and at liquid He conditions (4 K) instead of reaction temperature and at mbar-pressures. We showed that X-ray Magnetic Circular Dichroism (XMCD) experiments could reveal important new information concerning the sites in FeZSM-5. All the iron sites in as-made FeZSM-5 were Fe^{III}, had pure O_h symmetry and were isolated, as deduced from the X-MCD signal since all Fe^{III} sites contributed to this effect. After calcination, the sample remained mostly single Fe^{III}, with a minor contribution from aggregated Fe^{II} sites (having no XMCD-effect). Severe steaming turned half of the iron in aggregates and in addition one third of the remaining single sites changed its valence to Fe^{II}. The metal loading of 0.3 wt % was no obstacle in obtaining the XMCD signal. We can conclude that XMCD provides an important addition

to the characterization tools for heterogeneous catalysts containing a low concentration of transition metal ions and should be generally applicable in the field of heterogeneous catalysts containing low amounts of active sites.

In the next part of this work the study of (framework-substituted) FeZSM-5 and the development of – selective – hard X-ray absorption techniques for catalysis research go hand in hand. In **Chapter 6** we showed that the use of a sophisticated fluorescence detector allows for the acquisition of well-resolved Fe K edge XANES spectra with minimal background signal. The technical basis for this achievement was the measurement of the fluorescent 3p to 1s (Kβ) transition with a high-resolution ($\Delta E \sim 1$ eV) by a spectrometer utilizing Bragg reflection. The high quality spectra enabled a refined analysis of in particular the pre-edge feature. Thus detailed information on the local coordination and oxidation state of an absorbing transition metal ion was obtained for both bulk iron oxide model compounds and FeZSM-5 with a low concentration. The measurements for FeZSM-5 were performed at 350 °C in an O_2 and/or helium flow. We found that template removal and calcination caused a distortion of the zeolite framework, while a steaming treatments induces the dislodgement of iron out of the lattice. The application of 'Kβ-detected XANES' made it possible to quantify the degree of iron extraction out of the zeolite framework as a function of the steaming treatment.

We undertook a closer look to the nature of the iron species present at the different stages in the preparation of framework-substituted FeZSM-5 by using Kα-detected EXAFS. Before we investigated the possible detection by EXAFS of Fe–Al and Fe–Si backscattering in **Chapter 7**. As stated in chapters 3 and 4, Fe/ZSM-5 samples prepared by the chemical vapor deposition method were supposed to have mostly iron in binuclear clusters. A renewed analysis of the EXAFS data has led to a comparison of mononuclear (Fe_1) and multinuclear oxo-bridged (Fe_2) iron species. The coordination of Fe in Fe/ZSM-5 after sublimation could also be described by a combination of Al and Si framework atoms. In the subsequent washing step these Fe_1 sites turned out to be still isolated. A mild calcination converted part of the mononuclear iron into small multinuclear species (binuclear and oligonuclear). More severe calcinations induced the formation of larger agglomerates resembling iron oxide phases. The fit quality of this alternative model was similar to the previous analysis, while the obtained chemical picture was intuitively more attractive.

The experience gained from this re-analysis of overexchanged Fe/ZSM-5 was adopted for the analysis of the EXAFS data of framework-substituted FeZSM-5. In analogy to the selective hard X-ray absorption detection setup used in chapter 6 we measured the EXAFS by high resolution Kα-fluorescence detection (2p to 1s transition). In **Chapter 8** we presented the results obtained for low loaded FeZSM-5 (0.3 wt %) at 350 °C in both an O_2 and helium atmosphere. Selective Kα-fluorescence detection was applied to collect high quality in situ EXAFS data. The high signal to noise ratio enabled a full EXAFS data-analysis including the higher coordination shells. Template removal followed by calcinations distorted the framework iron sites from T_d symmetry and yielded a 3:1 oxygen distribution with Fe–O coordination distances of 1.80 and 1.98 Å, respectively. The introduction of protons led to a

further distortion with a 2:1:1 oxygen distribution with an additional coordination distance at 2.09 Å. Helium treatment at 350 °C of the H-form of FeZSM-5 resulted in a very small release of oxygen (10 %). Also the analysis of the pre-edge revealed that the amount of autoreduction in helium of the Fe sites in framework-substituted FeZSM-5 samples ranged from 10 to 20 %. This extent of autoreduction is less than for overexchanged Fe/ZSM-5 samples. Upon steaming extraframework iron species were formed. The structural properties of the first Fe–O shells of the extraframework Fe species in severely steamed FeZSM-5 resembled that of mildly calcined Fe/ZSM-5, including the response of the first oxygen shells to a redox treatment at 350 °C. In addition, the detection with EXAFS of a Fe–Al coordination at 3.1 Å shows that steaming also facilitates the release of framework Al. This Fe–Al coordination is not detected in calcined overexchanged samples. Comparing the intensity of the higher Fe–Fe shells in the most severe steamed sample with those detected in the calcined overexchanged Fe/ZSM-5 leads to the conclusion that the oligomeric extraframework Fe species found after steaming are stabilized by extraframework Al.

We demonstrated that the precise, quantitative measurements of key characteristics as valence and local symmetry of transition metal ions in catalysts is made possible by both (in situ) soft XAS and selective hard XAS techniques. Even for measurements performed at high temperature and for low concentrated samples we present higher accuracy data and more detailed analysis procedures.

However, some limitations for certain systems are still present. Future developments comprise among others a combination of techniques, named Resonant Inelastic X-ray Scattering (RIXS). RIXS unites some benefits from soft and hard X-ray absorption: a higher spectral resolution and experimentally more feasible measurement conditions. Over the next years experiments with 0.3 eV resolution with hard X-rays will become feasible under reaction conditions. Preliminary experiments on FeZSM-5, with 1.0 eV resolution, show that additional information may be gained. Although, progress is made for several iron oxide model compounds, a proper and unambiguous interpretation of the observed features is still ahead. Another set of experiments that will become possible is valence- and site-specific X-ray absorption so that the spectra can be determined independently for different valences present and that no longer the averages are measured. Actually, this research was initiated to contribute to this topic. Although advances are made for model compounds the application for real catalytic systems exceeds the current experimental status.

In summary, the results that we described in this thesis show that the characterization of heterogeneous catalysts clearly benefits from the continuous developments in X-ray spectroscopy. In particular for the study of complex catalytic systems, as FeZSM-5, one should exploit the possibilities offered by advanced spectroscopic techniques to unravel the active site structures and reaction mechanisms. Also other fields engaged in the study of chemical and biological systems will take advantage of new X-ray spectroscopic techniques and methods. The frontiers as emerged in this work are today's limits, but will certainly contribute to that of tomorrow. An exciting field of spectroscopy is therefore just ahead of us.

Samenvatting

Het doel van het in dit proefschrift beschreven onderzoek is tweeledig. In de eerste plaats worden nieuwe Röntgenspectroscopie technieken geïntroduceerd op het gebied van de heterogene katalyse. Daardoor wordt een meer geavanceerde karakterisering van katalytisch actieve vaste stoffen mogelijk gemaakt. In de tweede plaats gaf de toepassing van deze nieuwe methoden op FeZSM-5 zeolieten aanleiding tot een meer gedetailleerd begrip van de soorten van ijzer verbindingen die aanwezig zijn.

De intentie van dit proefschrift 'Grensverleggend onderzoek betreffende Röntgenspectroscopie van FeZSM-5' is om bij te dragen aan de toepassing van nieuwe Röntgenspectroscopie technieken voor de bestudering van katalytisch actieve vaste stoffen, alsmede aan het begrip van de structuur en functie van FeZSM-5 zeolieten. De beschrijving van het 'Grensverleggend onderzoek betreffende Röntgenspectroscopie van FeZSM-5' kan onderverdeeld worden in vijf hoofdthema's:

I) De toepassing van *in situ* zachte Röntgenabsorptie-spectroscopie (XAS) voor de bestudering van heterogene katalysatoren en een voorstel voor de gedetailleerde data-analyse van de spectra van overgangsmetalen (hoofdstuk 3 en 4)
II) Het gebruik van Röntgen magnetisch circulair dichroisme voor heterogene katalysatoren (hoofdstuk 5)
III) Het beter benutten van Röntgen nabije stap absorptie structuur (XANES) door gebruik te maken van hoge resolutie spectra vergaard door selectieve detectiemethodes in de harde Röntgenspectroscopie (hoofdstuk 6)
IV) Het oprekken van de detectielimieten in de verderstrekkende Röntgenabsorptie fijnstructuur (EXAFS) om FeZSM-5 monsters met een lage ijzerconcentratie te meten met behulp van selectieve detectie (hoofdstuk 6 en 8)
V) De verfijning van de data-analyse voor EXAFS en XANES technieken (hoofdstuk 7 en 8).

Het is gebleken dat de kennis aangaande FeZSM-5 zeolieten gelijk opgaat met de toenemende mogelijkheden die geboden worden door nieuwe Röntgenspectroscopische karakteriseringmethoden. Gedurende het onderzoek hebben we ons geconcentreerd op twee typen FeZSM-5 zeolieten: overbeladen Fe/ZSM-5 (4,4 gew. % Fe in extra-rooster posities) en rooster-gesubstitueerd FeZSM-5 (0,3 gew. % Fe initieel in rooster posities).

Hoofdstuk 1 geeft een algemeen beeld van katalysatorkarakterisering, een onderzoeksgebied dat van doorslaggevend belang is om fundamentele kennis te vergaren over katalysatormaterialen, en om de voortgang in het veld van de katalyse te bespoedigen. De karakteriseringgereedschappen die we bestudeerd hebben in dit proefschrift hebben alle het gebruik van Röntgenstraling gemeen. Röntgenspectroscopie is een uitstekend middel om verschijnselen op atomaire schaal te onderzoeken. Echter, de verfijning van de op dit moment beschikbare standaardtechnieken alsmede de ontwikkeling van nieuwe varianten zouden aanvullende informatie op kunnen leveren en zo aanzienlijk kunnen bijdragen aan een beter moleculair begrip van katalysatoren en hun werking. Er wordt een theoretische basis gelegd voor de volgende experimentele hoofdstukken waarin de technieken zijn geïntroduceerd. We hebben bijzondere aandacht besteed aan in situ zachte Röntgenspectroscopie (tegelijkertijd met Röntgen magnetisch circulair dichroisme) en in situ selectieve harde Röntgenspectroscopie (in het bijzonder hoge-resolutie Kβ-fluorescentie gedetecteerde XANES en EXAFS).

Bij de voortschrijdende ontwikkelingen in de Röntgenspectroscopie wordt de bestudering van verschillende FeZSM-5 zeolieten gebruikt als voorbeeld. Deze materialen kunnen worden beschouwd als representatieve voorbeelden voor heterogene katalysatoren omdat vergelijkbare problemen optreden als bij andere katalysatoren die overgangsmetaal-ionen bevatten: de aanwezigheid van meerdere moleculaire structuren, vaak in lage concentraties.

Hoofdstuk 2 geeft een overzicht van de bereiding en karakterisering van FeZSM-5. De belangrijkste onderwerpen in de literatuur met betrekking tot de synthese, activeringsprocedures en karakterisering van ijzerhoudende ZSM-5 zeolieten worden bediscussieerd. Het is duidelijk geworden dat ondanks de enorme onderzoeksinspanningen nog steeds geen definitieve antwoorden geleverd zijn over de aard van de actieve plaatsen, de beste bereidingswijze en de meest effectieve karakteriseringsmethoden voor FeZSM-5.

De eerste techniek die we hebben gebruikt om Fe/ZSM-5 te bestuderen was zachte Röntgenspectroscopie. Röntgenabsorptie experimenten werden uitgevoerd voor zowel de zuurstof 1s schil als voor het ijzer 2p niveau. Zachte Röntgenspectroscopie voor 3d metaal absorptieniveaus is een van de belangrijkste technieken in het gebied van de vaste stof fysica, in het bijzonder voor de verwante overgangsmetaal oxide systemen. In het veld van de heterogene katalyse is het weinig gebruikt vanwege de moeilijkheid van *in situ* metingen. In **hoofdstuk 3** hebben we het Fe oxidatie/reductie gedrag gevolgd in overbeladen Fe/ZSM-5, bereid volgens de chemische damp afzetting (sublimatie) van $FeCl_3$, als een functie van (verwarmings/warmte)behandeling en gas-atmosfeer. We hebben een methode ontwikkeld om snel de valentie te bepalen, gebaseerd op de vorm en positie van de Fe L_3 absorptiestap. Ladings-overdracht multiplet berekeningen waren geschikt om de spectraalvorm van de Fe $L_{2,3}$ absorptiestap te simuleren en op deze wijze werd nieuwe informatie verkregen over de geometrie en valentie van de ijzerplaatsen. De geoxideerde vorm van Fe/ZSM5 bevatte Fe^{III} in een octaëder omringing met een kristalveldsterkte van 1 eV, wat minder is dan die voor bulk oxides. In een helium omgeving werd een spontane reductie waargenomen, autoreductie, die al begon op kamertemperatuur en verder plaatsvond gedurende verwarming

naar 350 °C, op 2 mbar. Gereduceerd Fe/ZSM-5 had Fe^{II} in een tetraëder omringing. Uit de zuurstofspectra werd duidelijk dat de autoreductie vergezeld werd door het verlies van moleculair zuurstof en water. Op hoge temperatuur is de re-oxidatie door zuurstof van bijna-volledig gereduceerd Fe/ZSM-5 een kwestie van minuten.

Deze studie mag opgevat worden als een voorbeeld om de kracht van *in situ* zachte Röntgenspectroscopie (XAS) te demonstreren voor de bestudering van structurele en electronische eigenschappen. De toepassing profiteert van de veel hogere resolutie van zachte Röntgenstralen tegelijkertijd met de relatief grote, systematische variatie van de spectrale kenmerken in de – goedgedefinieerde – Fe L_3 absorptiestap met de oxidatietoestand van ijzer en de gedetailleerde simulatie van de spectraalvorm. Deze factoren maken een aanzienlijk hogere precisie in de bepaling van de gemiddelde valentie van ijzer mogelijk. Vanwege het gebruik van de electron-opbrengst detectie is de techniek echter oppervlaktegevoelig en reflecteren de resultaten slechts de bovenste 4 nm van het monster.

Een uitgebreidere studie naar het redox-gedrag van overbeladen Fe/ZSM-5 zeolieten is uitgevoerd in **hoofdstuk 4**. De invloed van de calcinatiemethode op de (auto)reduceerbaarheid van het ijzer werd nagegaan. We maakten gebruiken van de zachte Röntgenspectroscopie-techniek die geïntroduceerd was in hoofdstuk 3 om verschillende Fe/ZSM-5 monsters te vergelijken en de gemiddelde valentie van ijzer te volgen tijdens de oxidatie/reductie cycli alsook gedurende verwarmen en afkoelen. Zwaar gecalcineerde monsters waren ongevoeliger voor autoreductie in helium dan milder gecalcineerde monsters en bereikten niet zulke lage gemiddelde oxidatietoestanden. Dit verschil in redox-gedrag, zichtbaar na omschakeling op kamertemperatuur van zuurstof naar helium en tijdens verwarming in helium naar 350 °C, werd toegeschreven aan de aanwezigheid van ijzeroxide nanodeeltjes na zwaardere calcinatie. Beide monsters vertoonden een omkeerbare autoreductie in helium op 350 °C na blootstelling aan zuurstof voor langer dan een uur. Een vergelijkbaar experiment met FeO(OH), goethiet, maakte duidelijk dat bulk ijzer hydroxides geen autoreductie vertonen als ze verwarmd worden in helium, maar dat ze een oppervlakte-reorganisatie (dehydroxylatie/ontwatering) ondergaan tot ijzeroxide structuren. Een neveneffect van het bepalen van de lokale structuur van ijzer in Fe/ZSM-5 met zachte Röntgenabsorptie was het optreden van voorbijschiet-effecten van de ijzervalentie. Naast kinetische effecten als gevolg van lokale oppervlakte-bulk evenwichtsinstelling was er ook een tijdelijk effect van de Röntgenstralen op de ijzervalentie in de ordegrootte van 0.10.

Ons werk over het gebruik van Fe 2p Röntgenabsorptie voor de karakterisering van FeZSM-5 monsters is met een dimensie uitgebreid in **hoofdstuk 5** door gebruik te maken van de polarisatie van Röntgenlicht. Paramagnetische monsters reageren op het aanleggen van een magnetisch veld. De mate van optreden van het magnetisch circulair dichroisme, MCD, is afhankelijk van het karakter van de aanwezige ijzer(oxide) deeltjes. Op deze manier kan informatie verkregen worden over de afmetingen en structuur van de Fe plaatsen in rooster-gesubstitueerde FeZSM-5 monsters. Naast het XMCD effect werd ook het 'normale' 2p Röntgenabsorptiespectrum verkregen voor deze laag beladen monsters (0,3 gew. % Fe). Eerdere pogingen om deze monsters te karakteriseren met behulp van *in*

situ zachte Röntgenspectroscopie-metingen, zoals vermeld in de voorgaande hoofdstukken, mislukten vanwege een te zwak signaal bij het gebruik van totale-electron-opbrengst detectie. Hier hebben we bulk-gevoelige fluorescentie gedetecteerde zachte Röntgenspectroscopie gebruikt in plaats van de oppervlakte-gevoelige totale-electron-opbrengst detectie. Echter, deze metingen werden uitgevoerd in vacuüm en onder vloeibaar helium condities (4 K) in plaats van op de reactietemperatuur en op mbar-drukken. We hebben laten zien dat Röntgen magnetisch circulair dichroisme (XMCD) experimenten nieuwe informatie aan het licht brengen over de aanwezige ijzerstructuren in FeZSM-5. Alle ijzerplaatsen in gesynthetiseerd, onbehandeld FeZSM-5 waren Fe^{III}, hadden een niet-verstoorde O_h symmetrie en bevonden zich in geïsoleerde posities, zoals afgeleid werd uit het XMCD signaal omdat alle Fe^{III} plaatsen bijdroegen aan het effect. Na calcinatie bleven de plaatsen in het monster voornamelijk afzonderlijk Fe^{III}, met een kleine bijdrage van geaggregeerde Fe^{II} plaatsen (die geen XMCD effect vertonen). Een zware stoombehandeling zorgde ervoor dat de helft van het ijzer bijeenklonterde en dat daarnaast eenderde van de overgebleven afzonderlijke plaatsen haar valentie veranderde in Fe^{II}. De metaalbelading van slechts 0,3 % op gewichtsbasis was geen obstakel voor het kunnen meten van het XMCD signaal. De conclusie is gerechtvaardigd dat XMCD een belangrijke aanvulling vormt op de karakteri seringgereedschappen voor heterogene katalysatoren die overgangsmetalen bevatten in een lage concentratie. Deze techniek zou algemeen gebruikt moeten gaan worden in het gebied van heterogene katalysatoren met slechts een lage concentratie van actieve structuren.

In het volgende deel van dit proefschrift gaan de bestudering van (rooster-gesubstitueerd) FeZSM-5 en de ontwikkeling van – selectieve – harde Röntgenabsorptie-technieken voor katalysatoronderzoek hand in hand. In **hoofdstuk 6** hebben we laten zien dat het gebruik van een verfijnde fluorescentiedetector het mogelijk maakt om goed-opgeloste Fe K absorptiestap XANES spectra te kunnen meten met een minimale bijdrage van een achtergrondsignaal. De technische basis voor deze prestatie is het meten van de fluorescente 3p naar 1s ($K\beta$) overgang met een hoge resolutie ($\Delta E \sim 1$ eV) door middel van een spectrometer die gebruik maakt van Bragg reflectie. Deze spectra van hoge kwaliteit maakten een nauwkeuriger analyse mogelijk van de spectrale kenmerken net voor de absorptiestap. Zo kon gedetailleerde informatie verkregen worden over de lokale coördinatie en oxidatietoestand van een absorberend overgangsmetaal-ion in zowel bulk ijzeroxide verbindingen als FeZSM-5 met een lage concentratie. De metingen voor FeZSM-5 werden uitgevoerd op 350 °C in een stroom van zuurstof en/of helium. We vonden dat de verwijdering van de mal uit het zeolietkanaal en calcinatie ervoor zorgden dat het zeolietrooster werd vervormd en dat stoombehandelingen het uitlogen van ijzer uit het rooster veroorzaakten. De toepassing van $K\beta$-gedetecteerde XANES' maakte het mogelijk om de mate van ijzerextractie uit het zeolietrooster te quantificeren als een functie van de stoombehandeling.

We hebben gedetailleerder gekeken naar de aard van de aanwezige ijzerverbindingen in de verschillende stadia van de bereiding van rooster-gesubstitueerd FeZSM-5 met behulp $K\alpha$-gedetecteerde EXAFS. Hieraan voorafgaand gingen we in **hoofdstuk 7** na of het

mogelijk was om met EXAFS de verstrooiing door Fe–Al en Fe–Si te detecteren. Zoals we gezegd hebben in hoofdstuk 3 en 4 was de veronderstelling dat Fe/ZSM-5 monsters die bereid waren middels chemische damp afzetting het ijzer voornamelijk bevat als binucleaire clusters. Een hernieuwde analyse van de EXAFS meetgegevens heeft geleid tot een vergelijking tussen mononucleair (Fe_1) en multinucleaire zuurstof-gebrugde (Fe_2) ijzerstructuren. De coördinatie van ijzer in FeZSM-5 na sublimatie kan ook beschreven worden door een combinatie van aluminium- en silicium-roosteratomen. In de daaropvolgende was-stap blijken deze Fe_1 plaatsen nog steeds geïsoleerd te zijn. Een milde calcinatiebehandeling zette een gedeelte van het mononucleaire ijzer om in multinucleaire ijzerstructuren (binucleaire en oligomere structuren). Een zwaardere calcinatiebehandeling induceerde de vorming van grotere agglomeraten die erg lijken op ijzeroxide fasen. De kwaliteit van de EXAFS fit voor dit alternatieve model was vergelijkbaar met die van de vorige analyse, terwijl het verkregen chemische 'plaatje' intuïtief aantrekkelijker is.

De kennis die werd opgedaan van het opnieuw analyseren van data van overbeladen Fe/ZSM-5 werd aangewend voor de analyse van EXAFS data van rooster-gesubstitueerd FeZSM-5. Analoog aan de detectie-opstelling voor selectieve harde Röntgenabsorptie-experimenten die we gebruikt hebben in hoofdstuk 6, hebben we hier de EXAFS gemeten door middel van hoge resolutie Kα-fluorescentiedetectie (2p naar 1s overgang). In **hoofdstuk 8** hebben we de resultaten gepresenteerd die we verkregen hebben voor laag beladen FeZSM-5 (0,3 gew. %) op 350 °C in zowel een zuurstof als in een helium gas-atmosfeer. Selectieve Kα-fluorescentiedetectie zorgde ervoor dat de kwaliteit van de in situ EXAFS erg goed was. De hoge signaal/ruis verhouding maakte een volledige EXAFS data-analyse mogelijk, zelfs voor de hogere coördinatieschillen. De verwijdering van de mal uit de zeolietkanalen van de FeZSM-5 monsters en de daaropvolgende calcinatiebehandeling zorgen ervoor dat ijzeratomen in het zeolietrooster een vervorming ondergaan zodat ze afwijken van een ideale tetraëdische symmetrie. Deze viervoudige omringing door zuurstof was in een 3:1 verhouding met Fe–O coördinatieafstanden van respectievelijk 1,80 en 1,98 Å. Het introduceren van protonen leidde ertoe dat een verdere vervorming optrad en dat er een 2:1:1 zuurstofverdeling ontstond met een aanvullende coördinatieafstand van 2,09 Å. De behandeling in helium op 350 °C van deze H-vorm van Fe/ZSM-5 resulteerde in het vrijkomen van een erg kleine hoeveelheid zuurstof (10 %). Ook uit de analyse van de spectrale kenmerken net voor de absorptiestap bleek dat de mate van autoreductie in helium van Fe plaatsen in rooster-gesubstitueerde FeZSM-5 monsters beperkt bleef tot 10 á 20 %. Deze mate van autoreductie is veel minder dan waargenomen voor overbeladen FeZSM-5 monsters. Door een stoombehandeling werden geëxtraheerde, buiten-rooster ijzerverbindingen gevormd. De structurele eigenschappen van de eerste Fe–O coördinatieschillen van buiten-rooster Fe structuren in zwaar gestoomd FeZSM-5 lijken op die van mild gecalcineerd Fe/ZSM-5, ook als gekeken wordt naar de respons van de eerste zuurstofschillen op een redox behandeling op 350 °C. Daarnaast maakt de detectie met EXAFS van een Fe–Al coördinatie op een afstand van 3,1 Å duidelijk dat een stoombehandeling ook het vrijkomen van rooster Al-atomen faciliteert. Deze Fe–Al coördinatie werd niet waargenomen bij gecalcineerde overbeladen monsters. De vergelijking van de intensiteit van de hogere Fe–Fe schillen in

het zwaarst gestoomde monster met die waargenomen in de gecalcineerde overbeladen Fe/ZSM-5 leidt tot de conclusie dat de oligomere buiten-rooster Fe verbindingen gevormd door stomen, worden gestabiliseerd door buiten-rooster Al-atomen.

We hebben laten zien dat de precieze, kwantitatieve bepaling van sleuteleigenschappen als de valentie en de lokale symmetrie van overgangsmetaal-ionen in katalysatoren mogelijk wordt gemaakt door zowel (*in situ*) zachte Röntgenspectroscopie als door selectieve harde Röntgenabsorptie-technieken. Zelfs voor metingen die uitgevoerd werden op hoge temperatuur en voor monsters met een lage concentratie hebben we data gepresenteerd met een hoge nauwkeurigheid en hebben we meer gedetailleerde analyse procedures voorgesteld. Voor sommige systemen blijven er echter beperkingen bestaan. Ontwikkelingen in de toekomst zullen zich onder andere richten op een combinatie van technieken, ook wel resonante inelastische Röntgenverstrooiing (RIXS) genoemd. RIXS verenigt voordelen van zachte en harde Röntgenabsorptie: een hoge resolutie van de spectra en meetcondities die experimenteel beter te behappen zijn. In de komende jaren zullen experimenten met een resolutie van 0,3 eV voor harde Röntgenstralen uitvoerbaar zijn voor metingen onder reactiecondities. Testexperimenten met FeZSM-5, met een resolutie van 1,0 eV, toonden al aan dat er extra informatie te behalen valt. Ondanks dat er voortgang is geboekt voor diverse ijzeroxide modelverbindingen (mineralen) laat een ondubbelzinnige interpretatie van de waargenomen kenmerken nog op zich wachten. Een ander soort van experimenten dat beschikbaar zal komen is valentie- en plaatsspecifieke Röntgenabsorptie zodat de spectra onafhankelijk bepaald kunnen worden voor de aanwezige valenties en niet langer een gemiddelde wordt gemeten. Eigenlijk was dit onderzoek geïnitieerd om aan dit onderwerp bij te dragen. Ondanks de vorderingen voor modelverbindingen ligt de toepassing voor reële katalytische systemen niet binnen het bereik van de huidige stand van de techniek.

Samenvattend, de resultaten die we beschreven hebben in deze dissertatie laten zien dat de karakterisering van heterogene katalysatoren duidelijk baat heeft van de voortdurende ontwikkelingen in de Röntgenspectroscopie. In het bijzonder voor de bestudering van complexe katalytische systemen, zoals FeZSM-5, zouden de mogelijkheden die worden geboden door geavanceerde spectroscopische technieken uitgebuit moeten worden om de structuur van actieve plaatsen en reactiemechanismen te ontrafelen. Ook ander gebieden die betrokken zijn bij de bestudering van chemische en biologische systemen zullen voordeel hebben van nieuwe Röntgenspectroscopische technieken en methoden. Uit dit onderzoek is gebleken waar de grenzen van vandaag liggen, maar ongetwijfeld zullen die bijdragen aan de nieuwe grenzen van morgen. Een enerverend gebied van spectroscopie ligt voor ons.

List of publications and presentations

Publications

Reactivity of Fe-binuclear complexes in over-exchanged Fe/ZSM-5, studied by in situ XAFS spectroscopy. Part 1: Heat treatment in He and O_2
A. A. Battiston, J. H. Bitter, W. M. Heijboer, F. M. F. De Groot and D. C. Koningsberger, *J. Catal.*, **2003**, *215*, 279-293

In-Situ Soft X-ray Absorption of Over-exchanged Fe/ZSM-5
W. M. Heijboer, A. A. Battiston, A. Knop-Gericke, M. Hävecker, R. Mayer, H. Bluhm, R. Schlögl, B. M. Weckhuysen, D. C. Koningsberger and F. M. F. de Groot, *J. Phys. Chem. B*, **2003**, *107*, 13069-13075

Redox behaviour of over-exchanged Fe/ZSM-5 zeolites studied with in-situ soft X-ray absorption spectroscopy
W. M. Heijboer, A. A. Battiston, A. Knop-Gericke, M. Hävecker, H. Bluhm, B. M. Weckhuysen, D. C. Koningsberger and F. M. F. de Groot, *Phys. Chem. Chem. Phys.*, **2003**, *5*, 4484-4491

Kβ-Detected XANES of Framework-Substituted FeZSM-5 Zeolites
W. M. Heijboer, P. Glatzel, K. R. Sawant, R. F. Lobo, U. Bergmann, R. A. Barrea, D. C. Koningsberger, B. M. Weckhuysen and F. M. F. de Groot, *J. Phys. Chem. B*, **2004**, *108,* 10002-10011

Detection with EXAFS of the Fe–Fe and Fe–Al coordination in Fe/ZSM-5
W. M. Heijboer, F. M. F. de Groot, A. A. Battiston, B. M. Weckhuysen, and D. C. Koningsberger, *J. Phys. Chem. B*, **2005**, submitted

An EXAFS study on the steaming of low loaded FeZSM-5: from framework Fe to oligomeric Fe clusters
W. M. Heijboer, F.M.F. de Groot, P. Glatzel, R. F. Lobo, R. A. Barrea, B. M. Weckhuysen, and D. C. Koningsberger, *J. Catal.,* **2005**, submitted

1s2p Resonant Inelastic X-ray Scattering of iron oxides
F. M. F. de Groot , P. Glatzel, W. M. Heijboer, U. Bergmann, R. A. Barrea, and B. M. Weckhuysen, J. *Phys. Chem. B.*, **2005**, submitted

X-ray Magnetic Circular Dichroism of catalytic nanoparticles in FeZSM-5 zeolites
F. M. F. de Groot , W. M. Heijboer, C. Piamonteze, S. George, S. P. Cramer, R. F. Lobo, A. J. M. van der Eerden and B. M. Weckhuysen, J. *Phys. Chem. B.*, **2005**, submitted

New Frontiers in X-ray Spectroscopy of FeZSM-5
W. M. Heijboer, D. C. Koningsberger, B. M. Weckhuysen, and F. M. F. de Groot, *Catal. Today*, **2005**, in preparation

Iron and Copper Binuclear Complexes in Zeolites and their relation with Oxygenation Enzymes
W. M. Heijboer, M. H. Groothaert, F. M. F. de Groot, R. A. Schoonheydt and B. M. Weckhuysen, *Chem. Rev.*, **2005**, proposal accepted, manuscript in preparation

Oral presentations

F. M. F. de Groot, W. M. Heijboer, P. Glatzel, D. C. Koningsberger, and B. M. Weckhuysen 'Selective X-ray Absorption Spectroscopy', North American Catalysis Society (NACS) Conference, Toronto, Canada, June 2001

F. M. F. de Groot, W. M. Heijboer, P. Glatzel, D. C. Koningsberger, and B. M. Weckhuysen 'Selective X-ray Absorption of Fe/ZSM-5', Eurocat-7 Conference, Limerick, Ireland, September 2001

W. M. Heijboer, A. A. Battiston, A. Knop-Gericke, D. C. Koningsberger and F. M. F. de Groot, 'Soft X-ray Absorption Spectroscopy of Fe/ZSM5', National Research School Combination Catalysis – Workshop – Probing catalytic events, Utrecht, The Netherlands, November 2001

W. M. Heijboer, A.A. Battiston, A. Knop-Gericke, B.M. Weckhuysen, D.C. Koningsberger and F.M.F. de Groot , 'In-situ soft X-ray absorption spectroscopy of Fe/ZSM5', International Congress on Operando Congress, Lunteren, The Netherlands, March 2003

W. M. Heijboer, A.A. Battiston, A. Knop-Gericke, B.M. Weckhuysen, D.C. Koningsberger and F.M.F. de Groot, 'In-situ soft X-ray absorption spectroscopy of Fe/ZSM5', Netherlands' Catalysis and Chemistry Conference IV, Noordwijkerhout, The Netherlands, March 2003

W. M. Heijboer, 'Redox behaviour of Fe/ZSM5 studied by in-situ soft X-ray Absorption Spectroscopy', Universiteit Utrecht Debye Ontmoetingsdagen, Noordwijkerhout, Netherlands, March 2003

W. M. Heijboer, P. Glatzel, R. F. Lobo, D. C. Koningsberger, B. M. Weckhuysen and F. M. F. de Groot, 'The valence and symmetry of iron in framework substituted FeZSM-5', Netherlands' Catalysis and Chemistry Conference V, Noordwijkerhout, The Netherlands, March 2004

W. M. Heijboer, P. Glatzel, U. Bergmann, A. Knop-Gericke, D. C. Koningsberger, B. M. Weckhuysen and F. M. F. de Groot, 'FeZSM-5 catalysts and related systems studied with various X-ray Spectroscopic Techniques', NWO/CW – studiedag sectie Kristal & Structuuronderzoek, Lunteren, The Netherlands, March 2004

Poster presentations

W. M. Heijboer and F. M. F. de Groot, 'Selective X-ray Absorption Spectroscopy', Netherlands' Catalysis and Chemistry Conference II, Noordwijkerhout, The Netherlands, March, 2001

W. M. Heijboer, F. M. F. de Groot, A. A. Battiston, B. M. Weckhuysen, A. Knop-Gericke and D. C. Koningsberger, 'In-situ soft X-ray Absorption Spectroscopy of Fe/ZSM-5', Netherlands' Catalysis and Chemistry Conference III, Noordwijkerhout, The Netherlands, March, 2002

W. M. Heijboer, A. A. Battiston, A. Knop-Gericke, B. M. Weckhuysen, D. C. Koningsberger and F.M.F. de Groot, 'In-situ soft X-ray absorption spectroscopy of Fe/ZSM-5', 6th European Congress on Catalysis, Innsbruck, Austria, August/September 2003

W. M. Heijboer, P. Glatzel, R. F. Lobo, D. C. Koningsberger, B. M. Weckhuysen and F. M. F. de Groot, 'The valence and symmetry of iron in framework substituted FeZSM-5', 13th International Congress on Catalysis, Paris, France, July 12, 2004

F. M. F. de Groot, W. M. Heijboer, A. A. Battiston, A. Knop-Gericke, D. C. Koningsberger and B. M. Weckhuysen, 'Redox behaviour of over-exchanged FeZSM-5 studied by in-situ soft XAS', 13th International Congress on Catalysis, Paris, France, July 13, 2004

Dankwoord

Met een variant op een christendemocratische leuze zeg ik 'Promoveren doe je niet alleen!' Iedereen die me geholpen heeft wil ik hartelijk danken, sommigen in het bijzonder.

Allereerst is daar Frank de Groot, copromotor. Frank, als aanvrager en begeleider van mijn onderzoeksproject was je de intellectuele kracht achter veel van onze nieuwigheden op het gebied van de Röntgenspectroscopie in de heterogene katalyse. Ik heb je dagelijkse bijstand en gesprekken erg gewaardeerd. Bedankt.

Van het begin is er ook Diek Koningsberger, eerste promotor. Diek, we hebben een goede samenwerking gehad. De intensiteit mocht van tijd tot tijd verschillen, als het moest was je er. Bedankt voor je aanstekelijke enthousiasme.

Halverwege kwam Bert Weckhuysen erbij, tweede promotor. Bert, met jouw komst veranderde de tandem in een driewieler. De rol van derde wiel heb je met verve vervuld: je nam een middenpositie in, stuurde waar nodig, zorgde voor stabiliteit en liep niet zelden aan kop. Dankjewel.

Pieter Glatzel, danke! Je bijdrage is in grote delen van dit boekje terug te vinden. Andrea Battiston wil ik ook bedanken voor de samenwerking de afgelopen jaren. Jullie stelden me vaak goede en terechte vragen.

I would like to thank Axel Knop-Gericke, Michael Hävecker and Hendrik Bluhm for the pleasant collaboration on soft X-ray absorption spectroscopy. I enjoyed Berlin, vielen Dank!

Uwe Bergmann and Raul Barrea, many thanks for the nice and fruitful work together on selective hard X-ray spectroscopy. Uwe, die Unterhaltungen mit dir habe ich genossen.

Thanks to everybody who assisted me during the synchrotron experiments.

Raul Lobo and Kaveri Sawant are thanked for the synthesis of the framework-substituted samples and the discussions about the treatments.

Stephan Klemme and Peter van Aken are gratefully acknowledged for kindly providing me some iron mineral samples.

Het samen denken en schrijven met Marijke Groothaert en Robert Schoonheydt is een fijne bezigheid, er komt vast een mooi overzichtsartikel.

Ad van der Eerden en Ad Mens wil ik bedanken voor hun ondersteunende bijdrage op velerlei gebied. Jullie inzichten hebben me er vaak toe gebracht om het net iets anders te doen dan ik eigenlijk van plan was. Daniel Radu, thanks for our work together.

Mijn studenten Kees Baldé, Kees Visser en Volkert de Villeneuve wil ik hartelijk danken voor al het werk dat ze verricht hebben, hetzij in het lab of achter de computer. Jullie bijdrage is reeds of zal nog worden verwerkt in experimentele dan wel overzichtsartikelen.

De kamer heb ik lange tijd gedeeld met Cristina (altijd in voor een aanvulling op het vocabulaire Nederlands) en Stan (altijd in voor een nieuwtje). Dank voor jullie gezelligheid.

Meer in het algemeen geldt dat ook voor de andere collega's: bedankt voor de dagelijkse praatjes en hulp bij van alles en nog wat. Wat mij betreft is de richting van de koffietafelgesprekken onomkeerbaar veranderd…

Het secretariaat verdient een afzonderlijke vermelding. Dymph, Monique en Thea, bedankt!

De mensen van de werkplaats, glasblazerij en de audiovisuele dienst wil ik hartelijk danken voor alle ondersteuning die ze me geboden hebben. Jan den Boesterd, je grafische oog geeft dit boekje een extra uitstraling.

Mijn collega's in de organisatiecommissie van NCCC wil ik vriendelijk bedanken voor de prettige contacten en goede sfeer. Ik heb ervan genoten.

Pa en ma, broers, zus en aanhang wil ik bedanken voor de nodige realiteitszin buiten de wetenschappelijke wereld.

Erika, lieve vrouw van me, we hebben samen al het een en ander meegemaakt. In alle drukke en moeilijke tijden heb je me gesteund en verdragen. Bedankt voor je liefde!

Bovenal komt God de eer en lof toe voor de kracht en het verstand aan ons geschonken om dit werk te kunnen doen.

Curriculum Vitae

Willem Matthijs Heijboer werd geboren op 5 juni 1977 in Sint Annaland. In 1995 behaalde hij het VWO diploma aan het Calvijn College te Goes. Aansluitend startte hij met de studie Scheikunde aan de Universiteit Utrecht en in 1996 verkreeg hij het propaedeuse diploma met genoegen. Na universitaire stages bij de vakgroep Chemiedidactiek en de vakgroep Anorganische Chemie en Katalyse en een industriële eindstage bij het Shell Research and Technology Center, Amsterdam (SRTCA) werd in 2000 het doctoraal diploma behaald met genoegen.

Willem Heijboer was secretaris van de organisatiecommissie van het 'Netherlands' Catalysis and Chemistry Conference' gedurende de eerste drie jaar (NCCC 2000, NCCC II en NCCC III).

Vanaf 2000 was Willem Heijboer werkzaam als Onderzoeker in Opleiding bij de faculteit Scheikunde aan de Universiteit Utrecht. In de vakgroep Anorganische Chemie en Katalyse voerde hij onderzoek uit onder begeleiding van Dr. F.M.F. de Groot in het kader van het project 'Site specific XAFS of active centres, probing catalytic events', gefinancierd door de Nederlandse Organisatie voor Wetenschappelijk Onderzoek, NWO (projectnummer 700.98.036). De supervisie van het promotietraject lag bij Prof. Dr. Ir. D.C. Koningsberger en Prof. Dr. Ir. B.M. Weckhuysen.